Diptoindonesin G is an HSP90 middle domain modulator

by

Kristine Donahue

A dissertation submitted in partial fulfillment of the requirements for the degree of

Doctor of Philosophy

(Cancer Biology)

At the UNIVERSITY OF WISCONSIN-MADISON 2022

Date of final oral examination: September 30th, 2022

The dissertation is approved by the following members of the Final Oral Committee:

Wei Xu, Professor, Oncology

Bill Sugden, Professor, Oncology

James Shull, Professor, Oncology

Mark Burkard, Professor, Medicine

Vincent Cryns, Professor, Medicine

Diptoindonesin G is an HSP90 middle domain modulator

Kristine Donahue

Under the supervision of Professor Wei Xu at the University of Wisconsin-Madison

DISSERTATION ABSTRACT

HSP90 inhibitors can target many oncoproteins simultaneously, but none have made it through clinical trials due to dose-limiting toxicity and induction of heat shock response, leading to clinical resistance. We identified diptoindonesin G (dip G) as an HSP90 modulator that can promote degradation of HSP90 clients by binding to the middle domain of HSP90 (K_d = 0.13 ± 0.02 μM) without inducing heat shock response. We found that binding of dip G to HSP90 promotes degradation of HSP90 client protein estrogen receptor α (ER), a major oncogenic driver protein in most breast cancers. Mutations in the ER ligand-binding domain (LBD) are an established mechanism of endocrine resistance and decrease the binding affinity of mainstay endocrine therapies targeting ER, reducing their ability to promote ER degradation or transcriptionally silence ER. Because dip G binds to HSP90 and does not bind to the LBD of ER, unlike mainstay endocrine therapies, it is insensitive to ER LBD mutations that drive endocrine resistance. Additionally, we determined that dip G promoted degradation of WT and mutant ER with similar efficacy, downregulated ER- and mutant ER-regulated gene expression, and inhibited WT and mutant cell proliferation. Our data suggest that dip G is not only a molecular probe to study HSP90 biology and the HSP90 conformation

cycle, but also a new therapeutic avenue for various cancers, particularly endocrine-resistant breast cancer harboring ER LBD mutations.

TABLE OF CONTENTS

LIST OF FIGURES

LIST OF TABLES

ACKNOWLEDGEMENTS

Dear reader,

Before diving into what I am *sure* you will find an enthralling read, I must ask that you to read this section first, as it is the most important one. There are so many people who made this work possible, both directly, by conducting experiments and participating in scientific discussions, as well as indirectly, through supporting this author in more ways than one. This was the most difficult section to write because currently there is not a good assay available to quantify or properly summarize gratitude and how I feel about the many people who contributed to this work.

To my advisor Wei, thanks for all the guidance, insight, and advice over the years, as well as the encouragement and all the opportunities you threw my way. I always felt better about the trajectory of the project after leaving your office. I admired and appreciated your ability to break down complicated concepts into bite size pieces anyone could understand, and tried to implement that in my own personal and scientific communication.

I also must acknowledge all my lab mates. Eui-Jun and Gui, thank you for always being kind and patient teachers. Yidan, thank you for laughing at my bad jokes, teaching me most of lab techniques used in this work, keeping the lab running, and providing critical emotional support through many mouse studies. A special thank you to my “lab besties” Shengjie, Ang, and Megan. Shengjie, you are supremely funny and stylish, and always make me laugh. Thank you for caring for me, and making sure I was

nourished on my busiest, most stressful days. Ang, you are the best dumpling maker in the world. Your friendliness makes the lab a better place to be, and I always appreciated our chats and your advice. Megan, thanks for keeping me young. It was so refreshing to have you around, especially during my latter years, where I was tired and crotchety. It was really sharing snacks, stories, triumphs, failures, and gossip with you all that motivated me to go to lab.

I am indebted to my committee members Drs. Bill Sugden, Jim Shull, Vincent Cryns, and Mark Burkard. I really appreciate the excellent questions, guidance, time, and support over the years, and my science is better for it. I genuinely enjoyed my committee meetings and hearing your thoughts. I must give a special thank you to Bill, for always believing in me, and giving me a chance, especially because I never did. I am also grateful for all the pre-presentation pep talks, the invaluable advice and insight, and general support though the years. Another special thank you goes to Jim, who not only served as another excellent mentor, but is also a fellow bike fanatic. Thank you both for also reading through this thesis line by line, which was not a trivial undertaking. Elaine, though you were not on my committee, you still gave me valuable insight and feedback, included me in your lab meetings, and were another wonderful mentor too.

I could write a book about the gratitude I have for the Tran clan, including my grandma Anh, my aunts Phuong, Oanh, Trinh, and Linh, my uncles Tuan, Tuan, Thai, Doug, and Mike, and my cousins. I always keep them in mind with everything that I do. I am grateful for all of the support and encouragement over the years, even from afar. Thanks to the Donahue's, especially my uncles Steve, Al, and Joe, my aunts Julie, Lori,

DeeAnn, and Mary, and my cousins, who welcomed me to Wisconsin, helped me get settled, and hosted me for many happy summers as a little girl. I am grateful to have had the opportunity to reconnect with my Wisconsin “roots”.

To my mom Man, thank you for teaching me how to care for others. Dad, thanks for giving me what little sense of adventure I have. You both provided countless opportunities, and gave me safe homes in which to grow, play, and learn, perhaps sometimes at the cost of your own happiness. Tiffany, you are the best gift I have ever received, even though I didn’t know it at the time. I consider myself very lucky to have such a wonderful sister. Even though you are the younger sibling, recently I have found that I have been learning a lot from you.

To my cohort, Genevra and Christina (and by the transitive property, Nathan), I am deeply indebted to you for reminding me when we had homework due, for giving your HONEST feedback during my practice talks, and generally supporting me. I will never forget all the fun we had together cooking dinner, rock climbing, road tripping, watching movies, and biking to forget about our woes. I don’t think we ever really thought the day would come where we would all graduate and go our separate ways. I am excited to see what you all will do next, but it is terrifying to begin this next chapter without you all close by.

Siri and Daniel. You are both are just the best. Your friendship got me through some tough times, and continues to sustain me. Thanks for teaching me so much about myself, being excellent listeners, and letting me be a part of your lives. You know me

better than I know myself, and make me feel like I am the best thing since sliced bread. You are the most thoughtful and insightful people I know, and I try (unsuccessfully) to emulate you both in every way.

Squawww (Megan, River, Kaitlyn, and Jessica), thank you for the countless years of friendship. I am thankful to have people who have been with me through every stage of my life and have willingly been in a long-distance friendship for 12 years. Thanks for making a space where we can just be ourselves and easily pick up where we left off.

Ben (and Oscar), you both played an extremely important role in this process. Thanks for taking care of things when I had no bandwidth or time, for the reassurance, the support, the tip-top memes, and the long days traveling so we could have a few days together, despite also being a grad student. Finally, thanks for dealing with my general nonsense on the daily. I am very grateful.

To the friends I made along the way, including Luis and Katie, Jonas, Zach, Max, Ashley, Nate and Molly, Grace, Ben G, Oliva, and Jeff, thanks for being wonderful friends. This all would not have been possible without you.

Last, but not least, thank you to my collaborators in the Li and Tang labs, the UWCCC Flow Cytometry lab, the Experimental Animal Pathology lab, and the faculty and staff at McArdle Lab for their help, advice, and expertise.

ABBREVIATIONS

°C	Degrees Celcius
µg	Microgram
µL	Microliter
µM	Micromolar
^{18}F-FES	16α-18F-fluoro-17β-estradiol
18srRNA	18 Svedberg Unit Ribosomal RNA
ACI	August Copenhagen Irish Rat
ACN	Acetonitrile
AF-1	Activation fuction 1
AF-2	Activation fuction 2
AGC	Automatic gain control
AI	Aromatase inhibitor
AIB1	Amplified in Breast Cancer 1
ALL	Acute Lymphocytic Leukemia
AML	Acute Myeloid Leukemia
AP-1	Activator Protein 1

APL	Acute Promyelocytic Leukemia
AR	Androgen Receptor
ARv7	AR variant 7
ATP	Adenine Triphosphate
ATRA	All-Trans Retinoic Acid
BARD1	BRCA1 Associated RING Domain 1
BOLERO2	Breast Cancer Trials of Oral Everolimus-2
bp	Base Pair
BRCA1	Breast Cancer Gene 1
BSA	Bovine Serum Albumin
B-SERDs	Benzothiophene SERDs
BuOH	Butanol
CaCl2	Calcium Chloride
CAK	CDK Activating Kinase
CDK	Cyclin-Dependent Kinase
CHCl3	Chloroform
ChIP	Chromatin Immunoprecipitation

CHIP	C-terminus of HSC-70 Interacting Protein
ChIP-seq	Chromatin Immunoprecipitation Sequencing
CO_2	Carbon Dioxide
Cq	Quantification Cycle
CRISPR	Clustered Regularly Interspaced Short Palindromic Repeats
CTC	Circulating Tumor Cell
C-terminus	Carboxy-terminus
D538G	Aspartic Acid 537S Glycine
DAB	3,3′-Diaminobenzidine
DBD	DNA-Binding Domain
DES	Diethylstilbestrerol
Dip G	Diptoindonesin G
DMEM	Dulbecco's Modified Eagle Medium
DMSO	Dimethylsulfoxide
DNA	Deoxyribonucleic acid
DPBS	Dulbecco's Phosphate Buffered Saline
DTT	Dithiothreitol

E2	17 β-estradiol
E380Q	Glutamic Acid 380 Glutamine Missense mutation
E6AP	E6-Associated Protein
ECL	Enhanced Chemiluminescence
EDTA	Ethylenediaminetetraacetic acid
EGF	Epiderminal Growth Factor
EGFR	Epidermal Growth Factor Receptor
ELISA	Enzyme-Linked Immunosorbent Assay
EMT	Epithelial Mesenchymal Transition
ER	Estrogen Receptor α
ERE	Estrogen Response Element
ERK	Extracellular Signal-Regulated Kinase
FA	Formic acid
FAD	Flavin adenine dinucleotide
FBS	Fetal Bovine Serum
FDA	Food and Drug Administration
FDR	False Discovery Rate

FGF	Fibroblast Growth Factor
FLIM	Fluorescence Lifetime Imaging
FOXA1	Fork Head Box Protein A1
FULV	Fulvestrant
g	Gram
GATA3	GATA binding protein 3
GFP	Green Fluorescent Protein
GREB1	Growth Regulating Estrogen Receptor Binding 1
GRHL2	Grainy Head Like 2
gRNA	Guide RNA
GSEA	Gene Set Enrichment Analysis
GST	Glutathione S-Transferase
H&E	Hematoxylin and Eosin
H_2O	Water
H3K27Ac	Histone 3 Lysine 27 Acetylation
HA	Human Influenza Hemagglutinin
HCD	Higher-energy collision dissociation

HCl	Hydrochloric Acid
HEPES	2-[4-(2-Hydroxyethyl)piperazin-1-yl]ethane-1-sulfonic acid
HER2	Human Epidermal Growth Factor Receptor 2
HIF	Hypoxia Induced Factor
HPLC	High Performance Liquid Chromatography
HRP	Horse Radish Peroxidase
HSC	Heat Shock Cognate
HSF1	Heat Shock Factor 1
HSP	Heat Shock Protein
HSR	Heat Shock Response
IC_{50}	Half Maximal Inhibitory Concentration
ICI	Imperial Chemical Company
IDC	Invasive Ductal Carcinoma
IGF1R	Insulin Growth Factor-Like 1 Receptor
ILC	Invasive Lobular Carcinoma
IP	Immunoprecipitation
IPTG	Isopropyl β-D-1-thiogalactopyranoside

K302	Lysine 303 Arginine Missense Mutation
K303R	Lysine 303 Arginine Missense Mutation
K_d	Equilibrium Dissociation Constant
KD	Knock Down
Ki67	Kiel 67
KMT2C	Lysine Methyltransferase 2C
KMT2D	Lysine Methyltransferase 2D
KO	Knock Out
L	Liter
LB	Lauria Broth
LBD	Ligand-binding domain
LC	Liquid Chromatography
LC-MS/MS	Liquid chromatography-tandem mass spectrometry
LFQ	Label-free protein quantification
LXXLL	Leucine-Any Amino Acid-Any Amino Acid-Leucine-Leucine
M	Molar
M/Z	Mass-To-Charge Ratio

MAPK	Mitogen-Activated Protein Kinase
MDM2	Mouse Double Minute 2 Homolog
MEEVD	Methionine-Glutamic Acid-Glutamic Acid-Valine-Aspartic Acid Peptide at C-terminus of HSP90. Binds tetratricopeptide repeat-containing proteins
MEF	Mouse Embryonic Fibroblast
MeOH	Methanol
mg	Milligram
mL	Milliliter
mM	Millimolar
mP	Millipolarization
MS	Mass Spectrometry
MS/MS	Tandem Mass Spectrometry
MTS	[3-(4,5-dimethylthiazol-2-yl)-5-(3-carboxymethoxyphenyl)-2-(4-sulfophenyl)-2H-tetrazolium]
NAC	N-Acetyl-L-cysteine
NaCl	Sodium Chloride
NADH	Nicotinamide Adenine Dinucleotide

NCE	Normalized collision energy
NF-κB	Nuclear Factor Kappa B
ng	Nanogram
NLS	Nuclear Localization Signal
nM	Nanomolar
NSG	Non-Obese Diabetes-Severe Combined Immunodeficient Interleukin 2 Receptor Gamma Null Mouse
N-terminus	Amino-terminus
OD	Optical Density
OHT	Tamoxifen
PALOMA2	Palbociclib: Ongoing Trials in the Management of Breast Cancer
PBS	Phosphate Buffered Saline
PBST	Phosphate Buffered Saline Tween 20
PCR	Polymerase Chain Reaction
PDX	Patient-Derived Xenograft
PDXO	Patient-Derived Xenograft Organoid
PEG	Polyethylene Glycol
PFS	Progression-Free Survival

pg	Picogram
PGR	Progesterone Receptor (transcript or gene)
PI3K	Phosphoinositide 3-kinase
PROTAC	Proteolysis Targeting Chimera
pS118	Phosphorylated Serine 118
PSM	Peptide-spectrum matches
PR	Progesterone Receptor
R	Correlation Coefficient
RAF	Rapidly Accelerated Fibrosarcoma
RNA	Ribonucleic Acid
RNAseq	RNA Sequencing
RPM	Revolutions Per Minute
RTqPCR	Reverse Transcriptase Quantitative PCR
S118	Serine 118
S432L	Serine 432 Leucine Missense Mutation
SDS	Sodium Docecyl Sulfate
SDS-PAGE	Sodium Docecyl Sulfate Polyacrylamide Electrophoresis

Seq	Sequencing
SERCA	Selective Estrogen Receptor Covalent Antagonist
SERD	Selective Estrogen Receptor Degrader
SERM	Selective Estrogen Receptor Modulator
SKP2	S-Phase Kinase Associated Protein 2
SP-1	Specificity Protein 1
SRC	Steroid Receptor Coactivator
STCA	Sulphoxythiocarbamate Alkyne
TAMRA	Tetramethylrhodamine azide
TAN	Tanespimycin
TBTA	Tris (benzyltriazolylmethyl)amine
TCEP	Tris(2-carboxyethyl)phosphine HCl
TFF1	Trefoil Factor 1
Th	Thompson Unit
TNBC	Triple Negative Breast Cancer
TPR	Tetratricopeptide repeat
TRIS	Tris(hydroxymethyl)aminomethane

UPS	Ubiquitin Proteasome System
UV	Ultra Violet
UW	University of Wisconsin-Madison
V534E	Valine 534 Glutamic Acid Missense Mutation
WT	Wild-type
X	Times
X g	Times Gravity
Y537F	Tyrosine 537 Phenylalanine Missense Mutation
Y537N	Tyrosine Y537 Asparagine Missense Mutation
Y537S	Tyrosine Y537 Serine Missense Mutation
α	Alpha
β	Beta
γ	Gamma

CHAPTER 1: Introduction

Portions of this chapter have been previously published in the following book chapter:

Donahue K, and Xu W. “Therapeutic Strategies to Target Activating Estrogen Receptor α Mutations.” *Nuclear Receptors: The Art and Science of Modulator Design and Discovery*, Springer Nature, 2021. DOI: 10.1007/978-3-030-78315-0

Abstract

Despite great strides, estrogen receptor α (ER) positive breast cancer remains a challenging disease. About 60-70% of breast cancers express estrogen receptor, which is predictive of response to endocrine therapies, including selective estrogen receptor modulators (SERMs), and selective estrogen receptor degraders (SERDs). However, many patients will still develop therapeutic resistance. One mechanism of resistance is the development of gain-of-function mutations in the ligand-binding domain (LBD) of ER. Mutant ER exhibits ligand-independent, pro-metastatic activity, and higher concentrations of anti-estrogens are required to inhibit its activity. Fulvestrant, currently the only FDA-approved SERD, possesses dose-limiting pharmacological properties, must be administered intramuscularly, and promotes only partial degradation of ER. New orally bioavailable SERMs and SERDs are being developed to overcome the shortcomings of current mainstay treatments, but are challenging classes of drug to develop. Taking a ligand-binding domain-independent approach by modulating molecular chaperones and E3 ligases that control ER stability could circumvent endocrine resistance, and target additional drivers in mutant ER tumors.

Introduction

In 2019, breast cancer was the most commonly diagnosed cancer in the US[1]. It is a heterogeneous disease, and can be subclassified based on expression, or lack of expression, of different classes of receptors. About 60-70% of breast cancers are luminal tumors, which arise from luminal cells of the mammary duct. They express estrogen receptor α (ERα or ER), and can be subgrouped into luminal A and luminal B tumors. Luminal B tumors express high levels of Ki67, and can also express human epidermal growth factor receptor 2 (HER2). In luminal A tumors, tumor growth is driven primarily by estrogen and ER. Even before the discovery of estrogenic hormones produced in the ovary (1923)[2] and ER (1958)[3,4], as well as the cloning of ER (1986)[5,6], it was recognized that endocrine ablation through oophorectomy, first performed in 1895, could lead to regression of some breast tumors[7]. ER is a nuclear receptor and a ligand-activated transcription factor encoded by *ESR1* and is responsible for sensing and mediating the effects of its ligand, estrogen. In humans, estrogens are produced throughout life, with 17β-estradiol (E2) being the predominant and most potent circulating estrogen, particularly during reproductive years. Estrogen signaling and ER are important regulators of diverse functions, including normal development of mammary glands and reproductive tissues, as well as inflammation, bone density, cognitive function, and cholesterol homeostasis. As a result, dysregulation can lead to a variety of disease states.

Estrogen Receptor α and Breast Cancer

ER structure

The full length ER protein weighs ~66KDa, and has several domains. The intrinsically disordered N-terminal activation functional domain 1 (AF-1) is involved in ligand-independent activation[8,9]. The structure of AF-1 remained elusive until recently due to its flexible and intrinsically-disordered nature[10]. Phosphorylation in the AF-1 domain represents a major mechanism of ER activation[11]. Most notably, residue serine 118 (S118) can be phosphorylated[11] by cyclin- dependent kinase 7 (CDK7) in response to E2 stimulation[12] and by mitogen-activated protein kinase (MAPK) in response to activation of growth factors[13–15].

The DNA binding domain (DBD) of ER contains two zinc finger motifs, allowing it to bind to estrogen response elements (EREs) within the genes it regulates[16,17], as well as a dimerization interface[18]. The hinge region of ER connects the DBD and ligand-binding domain (LBD), and contains a nuclear localization signal (NLS)[19] responsible for nuclear translocation. This region is subjected to a variety of post-translational modifications. For example, lysine residues in the hinge domain can be acetylated, which fine tunes and regulates hormone and ligand responsiveness[20], as well as sumoylated[21]. In addition, K302 and K303 can be polyubiquitinated, which is important for regulating receptor stability[22]. In addition, amino acids required for stable DNA binding and interaction of ER with accessory proteins are also found in the hinge domain[17,23]. The LBD, which resides in the activation functional domain 2 (AF-2) is

required for interaction with endogenous estrogens, synthetic ligands, and coactivators[24,25].

ER signaling pathways

Ligand-Dependent Genomic Functions of ER

The canonical or genomic action of ER as a transcription factor involves binding of an endogenous ligand, such as E2, or synthetic ligands, to the LBD. This binding induces the C-terminal helix 12 to change to the agonistic conformation[24], leading to dissociation of ER from the HSP90 chaperone complex[26], dimerization[27], and association with DNA motifs, such as ERE found in the promoter, enhancer, and intergenic regions of target genes[28]. Though the ERE consensus sequence is 5′-GGTCAnnnTGACC-3′ [29], where n is any nucleotide, the actual sequence of many EREs can differ, resulting in changes to the binding affinity of the receptor to an ERE[30]. Some genes regulated by ER do not contain EREs at all.

Once bound to an ERE, the complex interacts with co-regulators, including co-repressors and co-activators which interact via their LXXLL motif[31], and epigenetic enzymes, to regulate the transcription of estrogen-responsive genes, some of which are important in tumor growth and survival. Post-translational regulation promotes the dissociation of the complex, and finally, ubiquitylation of ER induces its degradation by the 26S proteasome, and results in either further transcriptional activation or silencing[32–34]. ER-coregulatory complexes can also be recruited by other transcription factors, such as AP-1[35], SP-1[36], and NF-κB[37,38], to regulate transcription.

Ligand-Independent Genomic Functions of ER

Ligand-independent activation of ER is also well documented. One mechanism is through receptor tyrosine kinases. Membrane receptor tyrosine kinases such as EGFR, HER2, and IGF1R can activate kinase cascades that phosphorylate serine and tyrosine residues in the AF-1 domain of ER. For example, HER2 can trigger activation of MAP kinase ERK which can phosphorylate ER at S118, resulting in ER transcriptional activation[39,40].

Non-genomic functions of ER

Many effects of estrogen that take place within seconds to minutes are too rapid to be explained by transcriptional and translational mechanisms, which can take hours to days. This rapid signaling can be mediated by membrane-associated ERs, which account for ~5-10% of the total cellular ER[41], depending on the cell type. Palmitoylation of serine 522 and cysteine 447 on ER allows for association with caveolin 1, and for ER to be transported to the plasma membrane where ER can modulate signaling cascades, including PI3K/AKT, MAPK/ERK[41].

A brief history of breast cancer treatment and the discovery of the estrogen receptor

In 1882, William Halstead began pioneering the radical mastectomy for breast cancer patients, which involved removal of cancerous breast tissue, as well as the surrounding tissue where cancer may have spread, including the pectoralis major and minor, and axillary lymph nodes[42]. This surgery significantly improved local recurrence,

but was horribly disfiguring and brutal procedure, and ignored estrogen produced by the ovaries, a major contributor to breast cancer growth. Endocrine ablation through oophorectomy, first performed by George Beatson in 1895, had a significant advantage over radical mastectomy alone as it could lead to regression of some breast tumors, even those that were metastatic[7]. This is considered one of the earliest forms of endocrine therapy. However, Stanley Boyd observed that only one-third of patients responded to ovarian ablation[43], indicating that not all breast tumors were equally dependent on an unknown factor secreted from ovaries that drove growth of tumors. This factor was later identified as estrogen[2].

Despite variable responses to oophorectomy, it was part of the standard of care until advances were made in surgery, radiotherapy, and chemotherapy. It was unclear how estrogens functioned, and what mediated their effects until Elwood Jensen's laboratory discovered the estrogen receptor in 1958. His lab demonstrated that tritiated estrogen was bound and retained in estrogen-sensitive tissues such as the uterus and vagina in immature rats[3,4]. Along with Elwood Jensen's lab, Jack Gorski's lab was also working to address this question, and was able to isolate and characterize the estrogen receptor from rat uterine tissue[44]. These discoveries were particularly notable given that the prevailing hypothesis at the time was that estrogens participated in enzymatic reactions to exert their effects[3,4]. Unlike an enzyme, which fundamentally changes its substrates, steroid hormone receptors leave their ligands unaltered. It would take another 20 years before ER would be cloned and sequenced by Chambon and colleagues[5], Shine and colleagues[45], as well as Waterfield and colleagues[6].

Collectively, these discoveries laid the foundation for the idea that if some tumors are indeed dependent on estrogen, and ER is necessary for estrogen stimulated growth, then detection of ER may be predictive of clinical outcomes. This idea would revolutionize breast cancer treatment.

Jensen and colleagues showed in 1971 that breast cancers expressing high levels of ER were more likely to respond to endocrine ablation than those expressing low-levels of ER[46]. Breast cancer task force data would corroborate this observation, showing 60% of ER-positive patients responded to endocrine ablation, whereas only 8% of ER-negative patients responded to the same treatment[3]. These findings established ER as a predictive biomarker for response to endocrine therapy. However, even then, it was recognized that ER+ breast tumors were very heterogenous, with some cells expressing ER while others did not, as seen by immunocytochemistry[47,48]. Around this time, Harper and Walpole at the Imperial Chemical Company (ICI) were investigating anti-estrogens, not as anti-cancer agents, but rather as modulators of the reproductive system[49]. ICI 46,474, now known as tamoxifen, was one of the more notable molecules developed because of its tolerability, and potent anti-fertility properties in rats[3,49]. Walpole encouraged V. Craig Jordan to investigate tamoxifen's anti-cancer properties because tamoxifen had been shown to inhibit the binding of tritiated estradiol to mouse and rat estrogen-sensitive tissues[3,50]. Jordan and colleagues showed that indeed, tamoxifen could not only inhibit binding of tritiated estradiol to rat and mouse tumors[50,51], and human tumors[52], but also inhibit tumor growth and initiation of DMBA-induced rat mammary carcinogenesis, establishing that tamoxifen not only has anti-neoplastic

effects, but also chemopreventative effects in ER+ breast cancer[53]. This discovery laid the foundation for the approval of tamoxifen as a chemopreventative drug for breast cancer by FDA.

ER-based therapy

Because luminal A tumors are highly dependent on ER for growth, methods that either inhibit production of its ligand, such as aromatase inhibitors (AI), or antagonize the receptor directly, such as selective ER modulators (SERMs), are highly effective therapies in the adjuvant setting. E2, a potent ER agonist, binds ER via the LBD. SERMs like tamoxifen often compete with E2 for binding to the LBD, forcing ER into an antagonistic conformation and blocking ER-mediated transcription[24,34]. Tamoxifen, the first clinically approved SERM used in the adjuvant setting, is now primarily used to treat premenopausal breast cancer patients at low-risk for recurrence with, or without, interventions to achieve ovarian suppression. Though tamoxifen competes with E2 and inhibits LBD-mediated co-activator recruitment, it can also promote activation of the AF-1 domain[54–56]. This results in weak agonist activity in some tissues (e.g. uterus), increasing the risk for other kinds of cancer, and incomplete ablation of ER transcriptional activity. Fulvestrant, a selective ER degrader (SERD), also directly antagonizes ER. Fulvestrant has the advantage of being a pure anti-estrogen with no agonist activity, and can promote degradation of ER through the 26S proteasome[57]. Fulvestrant is used as a second line therapy in the recurrent, and metastatic setting. Aromatase inhibitors, such as exemestane, anastrozole, and letrozole stop estrogen biosynthesis, thereby preventing ER-mediated transcription. AIs in the adjuvant setting

are used as the frontline endocrine therapy in postmenopausal patients, or in high-risk premenopausal patients when combined with ovarian suppression. Recently, cyclin dependent kinase (CDK) 4/6 inhibitors such as palbociclib have been approved for treating metastatic ER+ breast cancer in combination with letrozole for advanced or metastatic breast cancer, or in combination with fulvestrant in those previously treated with endocrine therapy[58].

ESR1 mutations

ER+ tumors are typically associated with the most favorable prognosis, and expression of ER indicates a more differentiated and luminal state. In addition, expression of ER predicts response to endocrine therapies. However, approximately 25% of patients with primary disease, and almost all patients with metastatic disease, will eventually develop resistance to these therapies[59].

Several mechanisms of resistance have been reported, including loss of ER, increases in ER expression, gene fusions, bidirectional crosstalk between ER and growth factor receptors, as well as aberrant activation of growth factor receptors and their downstream signaling cascades[60,61]. One recently established mechanism of resistance in breast cancer patients treated previously with endocrine therapies is the development of hotspot missense mutations in the LBD of *ESR1*. These mutations were originally identified in the late 90's, but because they were rarely found in primary tumors, they were largely ignored until ER mutations were identified by deep sequencing of metastatic tumors[62–66]. These experiments identified "hotspot" *ESR1* mutations in ~ 20-50% of metastatic breast cancers following endocrine therapy,

depending on the study, cohort, and sequencing technology used[62–66]. Some hotspot mutations found in metastatic sites include the Y537S, Y537N, and D538G mutations[62–66].

The D538G mutation results in increased migratory capacity in MCF7 cell models in 2D cell culture [62], and the D538G and Y537S mutations are associated with increased metastatic potential in vivo[67]. Moreover, the *ESR1* mutations are prognostic of poor outcomes in patients with metastatic disease[68,69]. *ESR1* LBD mutations result in a constitutively active receptor. In addition, they have reduced ligand binding, including to E2 and fulvestrant[70–72,]. Therefore, higher concentrations of anti-estrogens are required to inhibit its activity [70–72]. Interestingly, not all LBD mutations are involved in hormone insensitivity. K303R (though technically at the interface of the LBD and hinge region) and E380Q result in estrogen hypersensitivity[73,74], and S432L and V534E are neutral mutations[74]. However, there are still many LBD missense mutations that have yet to be functionally characterized. Though ER mutations are not the primary drivers of carcinogenesis, under selective pressure, such as long-term anti-estrogen therapy in a post-menopausal breast cancer patient, clonal expansion of rare mutants, or acquisition of *de novo* mutations, can lead to resistance[59].

Phenotypically, the wild type (WT) and mutant ER are distinct, and their structures help to explain their respective phenotypes. In WT ER-expressing cells, binding of agonists, such as E2, to ER changes the C-terminal helix 12 to the agonistic conformation[38,75]. However, in ER LBD mutants, the helix 12 is maintained in the agonistic conformation, mimicking ER bound to estrogen[65,70], even in the absence of

ligand. This may explain the hormone-independent activity of mutated receptors, and reduced efficacy of antiestrogens and ER antagonists.

Indeed, Martin et al. discovered naturally occurring *ESR1* mutations in SUM44 cells following long-term estrogen deprivation, and showed that *ESR1* mutations are sufficient for driving acquired resistance[76]. Expression of these mutations has also been shown to be sufficient to drive metastasis. Jeselsohn et al also demonstrated that the Y537S mutation drives metastasis using in vivo orthotopic xenografts with doxycycline (dox)-inducible ER Y537S and ER D538G cells in ovariectomized mice with no E2 supplementation. These metastases were dependent on expression of mutant ER, as removal of the dox diet resulted in regression of the Y537S tumors[67]. Using CRISPR-Cas9 engineered homozygous knock in ER Y537S xenograft models, Fuqua et al also reported that the *ESR1 Y537S* mutation drives spontaneous, distant metastasis in vivo [77].

Despite structural similarities, the mutant ER does not simply behave like constitutively active ligand-bound WT ER, but instead has its own unique phenotype. Further, not all mutations are equivalent, and each mutation is distinct, and displays varying degrees of anti-estrogen resistance. Several reports have shown that ER residue Y537 (S and N) mutations are more resistant to anti-estrogens than mutations at D538[67,71] and S463[73]. This is also evidenced by co-regulators with mutant selectivity for the Y537S mutant over the D538G mutant, and vice versa[78]

Mutant ER Coregulators

Because of mutant ER's ligand independent activity, many groups have found that co-activator recruitment is constitutive. Gates et al. found co-activators such as SRC1, SRC3, AIB1, p300, RNA polymerase II, KMT2C, and KMT2D were recruited by mutant ER, even in the absence of hormones[78]. Fanning et al found that SRC3 did not bind to the WT ER α LBD in the absence of hormone[7170]. However, the ER Y537S and ER D538G bound SRC3 in the absence of E2, albeit with reduced affinity as compared to E2-bound WT receptor[70]. Toy et al. found that compared to WT ER, the D538G mutant co-immunoprecipitated with a much higher amount of AIB1[63], indicating that, in addition to constitutive coactivator recruitment, coactivator recruitment to mutant ER is enhanced compared to WT ER.

ER mutant transcriptome and cistrome

Jeselsohn et al. compared the transcriptomes of dox-inducible ER mutants Y537S, Y537N, and D538G in the absence of E2 with WT ER cells stimulated with E2 using RNAseq[67]. Based on the structural similarities between E2-bound WT ER and the ER mutant proteins, one would hypothesize that there would be large overlaps in their respective transcriptomes. However, only 18% of the Y537S-induced genes, and 33% of the D538G-induced genes overlapped with the E2-induced genes in WT ER cells[67], indicating that many mutant ER-regulated genes in hormone-deprived conditions were unique. In addition, each mutant exhibits differing degrees of E2 independence. When examining the E2-regulated genes in the ER mutant cells, only 12 genes were upregulated by E2 in the Y537S mutant cells. In the D538G mutant cells, 416 genes were upregulated in response to E2, and 64% of these genes overlapped with the E2-

induced genes in WT ER-expressing cells[67]. Analysis of patient derived xenograft (PDX) RNAseq data and patient RNAseq data confirmed the relevance of the cell line data, and the two data sets were highly correlated[67]. This indicates several points. The transcriptional activity of these mutants is more E2-independent compared to the WT ER. Further, each ER mutant drives a unique transcriptional program, and even ER Y537S and ER D538G elicit distinct transcriptional differences[67].

Jeselsohn et al also found that the mutant cistrome is indeed E2-independent using ChIP-seq, with the number of binding sites in the Y537S, Y537N, and D538G mutants correlating to the known resistance phenotype of each[67]. The Y537S mutant cells had the greatest number of binding sites, and D538G mutant cells had the fewest[67]. In addition, the ER binding sites gained in the presence of the mutations occurred at transcriptionally active regions, and >30% of the super enhancers detected in the Y537S mutant cells, marked by acetylation of histone 3 lysine 27 (H3K27ac), overlapped with the mutant gained binding sites[67]. However, no specific pioneer factors co-occupied these sites[67]. Motif analysis showed that the ERE motif was the most significantly enriched of all of the binding sites, indicative of direct ER binding among all receptors and treatment conditions[67]. There were many enriched motifs common to WT and mutant ER, including FOXA1, AP-1, and GRHL2[67]. FOXA1 was the second most enriched motif in the WT ER-selective binding sites, whereas ERE motifs were enriched in the Y537S and D538G selective motif sites[67]. The FOXA1 motif was not significantly enriched in the mutant-selective binding sites, suggesting that FOXA1 may be less essential for mutant-specific ER DNA binding[67]. Knockdown of FOXA1 did not

significantly affect growth of mutant ER-expressing cells in hormone-depleted conditions[67]. Fu et al. showed that FOXA1 overexpression in ER^+ breast cancer cells drives genome-wide enhancer reprogramming to activate pro-metastatic transcriptional programs, and, using clinical $ER^+/HER2^-$ metastatic breast cancer datasets, that the aberrant FOXA1/HIF-2α transcriptional axis is largely non-concurrent with the *ESR1* mutations[79], implying different mechanisms are employed to drive endocrine resistance.

Using a CRISPR knock-in model, results from Harrod et al confirm that there was a greater magnitude of ER binding in absence of estrogen in MCF7 Y537S cells compared to WT cells[80]. In the mutant ER transcriptome, estrogen-regulated gene expression was still a dominant feature. GSEA hallmark gene sets such as “estrogen response early” and “estrogen response late” were among the most upregulated gene sets compared to MCF7 vehicle treatment[80]. However, in the unstimulated Y537S knock-in model where only one ER allele was mutated, most of the peaks found were shared with estrogen-treated Y537S cells, as well as MCF7 WT cells[80], which does not agree with Jeselsohn et al[67]. In addition, motif analysis showed that the Y537S mutation does not cause ER binding to new unique sites[80]. In all conditions, ERE, FOXA1, AP-1, and GATA3 were the most enriched binding motifs[80]. To complicate things further, Martin et al performed rapid immunoprecipitation with tandem mass spectrometry of endogenous proteins to delineate the WT and mutant ER interactomes[76]. These analyses demonstrated that, though many of the proteins bound by mutant ER were also bound by WT ER, there were increased interactions between ER and

transcriptional regulators like GREB1 and FOXA1[76]. ChIP-Seq analyses also demonstrated a ligand-independent enrichment of FOXA1 motifs in mutant ER-expressing cells[76]. Targeted knockdown of *FOXA1* in WT and mutant cells resulted in a greater growth inhibition in mutant ER-expressing cells compared with WT ER-expressing cells, suggesting a role for FOXA1 in mutant-specific biology[76], which directly contradicts the results from Jeselsohn et al[67].

One explanation for the discrepancy between these studies is the differences in models used, with one study using an MCF7 inducible overexpression approach[67], one using an MCF7 knock-in approach[80], and the last using long term estrogen-deprived SUM44 cells with a naturally occurring *ESR1* mutation[76] . Indeed, Andreano et al. showed that response to ligands was not dictated simply by the presence of a mutant allele, but rather by the relative WT ER levels co-expressed in cells[81]. Specifically, dysregulated response to anti-estrogens was only evident in cells in which the mutants were overexpressed relative to the ligand-activated WT ER[81]. This finding underlines the importance of using multiple models, as well as paying specific attention to "allelism".

ER mutant phosphorylation

Phosphorylation may also contribute to the constitutive activity of mutant ER. Serine 118 (S118) is a major phosphorylation site within the AF-1 domain. S118 is phosphorylated in response to many stimuli, but most notably by E2[11,82]. S118 phosphorylation (pS118) is important for receptor stability, and is required for

proteasome-dependent degradation of ER, which is often coupled to transactivation[83]. Mutations in this site were shown to impair ER transactivation[11]. Helzer et al. performed ChIP-seq to define the pS118-ER and ER cistomes in MCF-7 cells treated with estrogen, and found that pS118 promotes direct DNA binding at active enhancers, which is associated with increased transcriptional activity[82]. In addition, pS118-ER sites were enriched in GRHL2 DNA binding motifs[82]. E2 treatment enhanced GRHL2 recruitment to pS118-ER-occupied sites[82]. Interestingly, mutant ER is constitutively phosphorylated at S118[84]. CDK7 functions as a CDK-activating kinase (CAK) for CDK1, 2, 4, and 6, but has also been shown to modulate ER activity through S118[12]. CRISPR-Cas9 gRNA-mediated silencing of CDK7 resulted in suppressed proliferation in both WT ER cells in full medium, and mutant ER cells in estrogen-deprived conditions[67], demonstrating CDK7's importance in regulating WT and mutant ER transcription. Normally, WT ER is rapidly phosphorylated within a matter of minutes in response to E2 treatment[82]. However, even in cells expressing HA-tagged ER D538G, the endogenous WT ER could be phosphorylated in hormone starved conditions, whereas this effect was not seen in the Y537S mutant-expressing cells, perhaps suggesting that the D538G mutant has a greater propensity to heterodimerize with WT ER[67]. This propensity may also explain some of the phenotypic differences observed between the two mutants. In addition to phosphorylation of S118, phosphorylation on residue Y537 by SRC kinase increases E6AP recruitment, and is involved in ER proteolysis and transcriptional activation[85]. When this residue is mutated to a residue

that cannot be phosphorylated (e.g. Y537F), fails to undergo ligand-dependent proteolysis, stabilizing the receptor[85]

Clinical significance of mutant ER

Despite many pre-clinical studies demonstrating that mutant ER-expressing cells are are resistant to fulvestrant treatment, ER-positive metastatic breast cancer patients are not currently stratified based on *ESR1* mutational status. A recent retrospective analyses of the PALOMA-2 clinical trial published by O'Leary showed that patients continued to acquire the Y537S *ESR1* mutation during fulvestrant monotherapy, or fulvestrant and palbociclib treatment[86]. Analysis of the BOLERO2 clinical trial suggested that patients with the Y537S mutant allele may have worse outcomes compared with patients whose tumors harbor the D538G mutation[68]. Mutant alleles are also associated with shorter progression-free survival[68,87,88] Even in early-stage local recurrence and metastatic lesions, mutant alleles are associated with worse prognosis[89]. *ESR1* mutations occur at a higher incidence rate in patients previously treated with AI compared to those whose treatments did not include AI[89]. Though there is evidence from several studies that *ESR1* mutations are associated with worse progression free and overall survival[68,87,88,90], the authors of one particular meta-analysis observed that when inspecting specific mutations, the D538G, but not the Y537S mutation, was associated with a worse prognosis and shorter progression free survival (PFS), regardless of what treatment was administered[88,90]. Additionally, *ESR1* mutations were predictive of resistance to aromatase inhibitors, but were not predictive of resistance to other endocrine therapies[88,90], which disagrees with the conclusions and observations of

many in vitro and in vivo studies. However, additional studies with larger cohorts harboring these ER mutations will be needed to conclusively determine the clinical differences among the various mutant alleles, including responses to specific endocrine treatments, and prognosis.

PET imaging with 16α-^{18}F-fluoro-17β-estradiol (^{18}F-FES) is a common imaging modality that can be used to measure ER in metastatic sites, optimize doses for endocrine therapies, and predict therapeutic response in breast cancer patients[91]. Despite reduced ligand binding ability of mutant ER, as well as the structural similarities between E2 and ^{18}F-FES, surprisingly, Kumar et al found that tumoral uptake of ^{18}F-FES in MDA-MB-231 cells stably expressing either WT ER, ER Y537S, or ER Y537C was not found to be significantly impacted by the Y537S or Y537C mutations[93]. This indicates that ^{18}F-FES PET imaging may be used for breast cancer patients, regardless of ER mutational status[92].

Organotropism of ER Mutants

Frequent metastatic sites for ER+ breast cancer include the bone, liver, lymph nodes, and brain. Toy et al found that *ESR1* mutations were most frequently detected in the liver liver and bone, and were not found in brain biopsies[73]. Zundelevicet al., however, was able to detect one brain metastasis expressing an *ESR1* mutation in their cohort. Jeselsohn et al[67] was able to confirm their findings from Merenbakh-Lamin et al[62] that the D538G mutant allele has a liver organotropism.

Methods to Target Mutant ER

Selective estrogen receptor modulators and degraders

Because ER is constitutively active in these tumors, it remains an important therapeutic target. Several approaches are being pursued to target mutant ER. One notable class of drugs being used to directly antagonize mutant ER is selective estrogen receptor degraders, or SERDs. Fulvestrant is currently the only FDA-approved SERD, and was shown to signficantly downregulate ER Y537S and ER D538G expression, but at very high doses[63,65]. Though fulvestrant has been shown to be effective in the metastatic setting, fulvestrant possesses dose-limiting pharmacological properties, such as low bioavailability[93–96]. Further, fulvestrant is administered intramuscularly, and it is unclear whether fulvestrant occupies the receptor at saturating levels at the current clinical dosages[93–96]. Therefore, there is strong rationale for developing more potent, orally bioavailable, pure antiestrogens that are insensitive to *ESR1* mutations.

The SERM, lasofoxifene, which was originally developed for the treatment of vulvovaginal atrophy and osteoporosis, has been shown to not be impacted by mutant *ESR1* status[81]. In addition, it has been shown to be efficacious in mammary intraductal mouse models, where MCF7, or MCF7 expressing the Y537S or D538G mutations were introduced[97]. It was more effective than fulvestrant (250mg/kg 1/week SQ) at inhibiting primary tumor growth (5 and 10 mg/kg SQ)[97]. Lasofoxifene also inhibited the Y537S and D538G mutants from metastasizing to the lung and liver, whereas fulvestrant only inhibited the D538G mutant[97]. It is now in phase 3 clinical trials for osteoporosis, and is

being clinically evaluated as a treatment for patients with advanced ER-positive breast cancer whose tumors harbor *ESR1* mutations (Table 1-1).

Bazedoxifene is a unique antiestrogen that possesses both SERM and SERD properties. It has been studied extensively clinically, and is approved for use in combination with conjugated equine estrogens for hormone replacement therapy in postmenopausal women, as well as a single agent for the prevention of osteoporosis[98,99]. It has strong antagonist and SERD profiles in breast, agonist properties in bone, and, unlike many SERMs and SERDs, did not stimulate endometrial tissue in preclinical studies[98,100,101]. In addition, bazedoxifene showed good oral bioavailability and improved pharmacokinetics compared with fulvestrant[98]. Preclinical studies found bazedoxifene possesses antitumor activity not only in several models of endocrine resistance, including AI, SERM resistant tumors[98], as well as ER mutants, though the Y537S mutant was found to be relatively resistant to degradation[102]. Bazedoxifene was also found to have anti-tumor activity in multiple ER+ PDX models, including those expressing WT ER, the ER Y537S mutation, as well as PI3K mutations[102]. However, some data suggest that at low concentrations, bazedoxifene may behave more like a SERM than a SERD, with mixed agonist/antagonist activity[102].

New orally bioavailable nonsteroidal SERDs, such as AZD9496, GDC-0810 (also known as brilacestrant), and GDC-0927 have been evaluated in pre-clinical models, and were found to be effective in mutant ER-expressing models[73,103–107]. In addition, they all have improved pharmacokinetics, are orally bioavailable, and do not exhibit the dose

limitations of fulvestrant [73,103–107]. Although exhibiting desirable mechanistic features over fulvestrant and GDC-0810, GDC-0927 still suffers from suboptimal drug-like properties[103]. In addition, both GDC-0810 and GDC-9027 are not pure antiestrogens, and showed some weak agonistic activity[103]. GDC-0810 and AZD9496, in endometrial cells and rat models, both exhibited uterotrophic effects, raising the concern that these drugs may have agonistic activity in reproductive tissues[104,105]. Though Genentech is no longer actively investigating GDC-0810 and GDC-0927, both have proven to be useful tools in SERD development, and for understanding ER biology.

GDC-9545 is the replacement molecule for GDC-0927, and touts major improvements over both GDC-0927 and fulvestrant[108]. GDC-9545 has high binding potency, and an improved DMPK profile when compared to GDC-0927 and fulvestrant[108]. GDC-9545's increased oral bioavailability, reduced metabolism, and improved oral exposure in multiple species means that the same degree of anti-tumor activity can be achieved but at 100-fold lower doses in the HCI-013 patient-derived xenograft (PDX) model compared to GDC-0927[108]. In addition, GDC-9545 can achieve full suppression of ER signaling, resulting in robust anti-proliferative activity, which may indicate a lack of detectable agonist activity, as was seen in GDC-0810 and GDC-0927[103,108]. A Study of GDC-9545 alone or in combination with Palbociclib and/or Luteinizing Hormone-Releasing Hormone agonist in locally advanced or metastatic ER+ breast cancer is currently recruiting patients for a phase I clinical trial (Table 1-1).

Elacestrant (RAD1901), developed by Radius, is currently the only next generation non-steroidal, orally bioavailable SERD to make it through phase III clinical

trials[109], underlining the difficulty of developing this class of drugs. Elacestrant has demonstrated evidence of single agent activity, with confirmed partial responses in heavily pre-treated patients with advanced ER+ breast cancer, including those with *ESR1* mutations[109]. It displayed potent anti-tumour activity in multiple ER-expressing tumor models, including PDX models originating from patients who previously received multiple lines of endocrine therapy, those harboring *ESR1* mutations, and those with *de novo* or acquired resistance to CDK4/6 inhibitors[110–112]. Elacestrant is also unique in that it can pass the blood brain barrier[112]. Phase III clinical trials were recently completed and showed that elacestrant doubled the percentage of patients with 12 month progression-free survival. If approved, elacestrant would be the first clinically approved oral SERDs that may also be useful for patients with *ESR1* mutations.

Many new SERDs have improved ER-targeting and drug-like properties compared to fulvestrant, but lack the ability to penetrate the blood–brain barrier[113]. One recently developed class of SERDs, benzothiophene SERDs (B-SERDs), contains a basic amino side arm [113]. Though its efficacy is comparable to that of fulvestrant in models of endocrine resistance, including *ESR1* LBD mutants, in vitro and in vivo, B-SERDs possess both oral and brain bioavailability, an advantage over acidic SERDs and fulvestrant[113]. Currently, there are other numerous new ER modulators under evaluation in the clinic listed in Table 1-1, though relatively little pre-clinical data is available.

One consideration for identifying and characterizing SERDs in vitro moving forward suggested by Guan et al. indicates that during development of GDC-0810 and

GDC-0927, they found that ER degradation alone is not sufficient for choosing lead molecules that consistently and fully antagonize ER and its transcriptional activity, particularly with a heavy reliance on MCF7 cells[103]. Many ER+ models should be used when evaluating new SERDS, as they showed that ER+ breast cancer cell lines had variable responses to GDC-0810 and GDC-0927, even though GDC-0810 and GDC-0927 demonstrated potent ER degradation in MCF7[103]. Sreekumar et al. showed that though in invasive ductal carcinoma (IDC), AZD9496 and fulvestrant behaved equivalently in terms of ER turnover and cell growth, in invasive lobular carcinoma (ILC) cell lines, AZD9496 behaved as a partial agonist, and was not as potent of an ER degrader[114]. In addition, ER mobility should be considered, rather than potency of degradation alone[114]. Fulvestrant and other SERDs do not act simply by depleting the receptor, but rather through slowing and immobilizing the receptor. Indeed, in 2006, Long et al. recognized this feature, and showed that fulvestrant immobilizes ER at the nuclear matrix, followed by receptor degradation through the ubiquitin proteasome system (UPS)[57]. This immobilization is mediated by cytokeratins 8 and 18, and helix 12 of ER is essential for association with cytokeratin 8 and 18[57]. These cytokeratins are essential for fulvestrant's mechanism of action, as siRNAs targeting cytokeratin 8 and 18 partially blocked fulvestrant's effects[57]. This finding suggests that fulvestrant induces ER to interact with CK8 and CK18, drawing the receptor into close proximity to nuclear matrix-associated proteasomes that facilitate ER turnover[57]. Receptor turnover is a result of receptor immobilization, which distinguishes full antagonists from partial agonists[57]. While the capacity to degrade ER may be a key feature of SERDs, it is not

sufficient for their function. This agrees with previous work by Wardell et al that demonstrated that fulvestrant-mediated degradation of ER indeed varies between cell models[115], as found by Guan et al[103]. However, the efficacy of fulvestrant as an inhibitor of ER transcriptional activity was similar in all cells under saturating conditions, and was neither influenced by the extent of ER degradation, nor the ER expression levels[115]. Although fulvestrant binding partially denatures ER, it can be reactivated by competing off bound drug with estradiol[115]. Collectively, competitive inhibition of ER, and not degradation, is a more important consideration[115]. One way to measure receptor mobility is live-cell imaging, which was performed in Guan et al[103]. Live-cell imaging can capture the highly dynamic and transient nature of transcription factors and transcription complexes, and could be incorporated into drug characterization pipelines to measure receptor mobility, and receptor antagonism[103], in addition to the typical measurements of ER target gene expression, proliferation, tumor growth, as well as ER degradation.

Another consideration for developing and evaluating SERDs in vivo is the dose of fulvestrant used as a benchmark. Wardell et al. demonstrated that a 25 mg/kg dose of fulvestrant is a more accurate and clinically relevant dose of fulvestrant for a mouse model[93]. 25 mg/kg of fulvestrant exhibited antitumor efficacy comparable to the historically used 200 mg/kg dose, but at this lower dose, it did not result in robust ER downregulation[93]. The antitumor efficacy of the lower dose of fulvestrant was comparable to that observed for other oral SERDs currently in development[94]. Using clinically unachievable doses of fulvestrant as a benchmark may undermine SERD development[93]. These studies suggest that receptor immobilization and antagonist

efficacy, as opposed to ER degrading activity, is likely to be the primary driver of clinical response. In the future, using these parameters could improve selection of lead ER antagonists.

SERCAs and Novel ER-targeting Agents

In addition to SERDs, other approaches being used to directly antagonize ER include selective estrogen receptor covalent antagonists (SERCAs), specifically, H3B-5942, that covalently binds the C530 residue of both WT and mutant ER, enforcing an irreversible antagonist conformation[116]. This residue is not conserved among other steroid hormone receptors, rendering SERCAs very specific to ER[116] H3B-5942 demonstrated better antagonistic properties in mutant overexpressing models, and growth inhibition properties than fulvestrant in vivo using cell line-derived xenografts and a PDX model expressing the Y537S mutation[116]. Like some SERMs and SERDs, H3B-5942 exhibits uterotrophic activity in immature rat models[116]. In addition, because of its high dependence on covalent engagement specific to residue C530, it is not impossibile that a mutation at C530 could be one mechanism of resistance[116]. A related compound, H3B-6545[117,118], is now in phase I/II clinical trials.

Finally, Zhao et al. developed a series of structurally novel anti-estrogens[71]. They had demonstrated efficacy in vitro and in vivo against ER D538G and Y537S mutant-expressing cells, as well as their respective cell-line derived xenografts, with compound K-07 being the most effective against WT, Y537S and D538G mutant tumor growth, and having the best pharmacokinetic profile[72]. K-07 is also orally bioavailable[71].

Additional targets and combination treatments

Though *ESR1* mutations are sufficient for driving acquired resistance, other drivers can coexist in many of these tumors, and justifies combination treatment. Toy et al. observed that the CTC-174 PDX model that expresses the D538G mutation used in their studies was only partially inhibited by AZD9496 treatment, indicating that this mutant tumor model is not exclusively dependent on ER signaling for its growth[73]. When this model was sequenced, an activating PIK3CA^{N345K} and two inactivating ARID1A truncation mutations E1776* and S705fs were found[73].

Tumor genotyping of *ESR1*-mutant breast cancers also revealed recurrent alterations in the PI3K/AKT pathway, cyclin D1, and FGFR[63]. These alterations likely reduce tumor dependence on ER signaling, and may benefit from combinations of antiestrogens with inhibitors of these pathways[73]. Despite decreased dependence on ER signaling, tumors under a single selection agent can restore ER dependence, and combinatory anti-estrogen treatment still remains important as, interestingly, inhibition of growth signals such as PI3K/AKT restored ER signaling activation and dependence[86] .

Furthermore, a more recent retrospective, correlative analysis of the PALMOA-3 trial evaluated whether early changes in *ESR1* or *PIK3CA* mutations measured using ddPCR of ctDNA were predictive of response to therapy[86]. Although total *ESR1* mutant abundance was shown to decrease in both treatment arms, these changes were not predictive of response to fulvestrant[86]. In contrast, *PIK3CA* mutation frequency was lower in the fulvestrant and palbociclib-treated group, and was significantly predictive of

PFS[86]. This study suggests that truncated mutations, such as *PIK3CA*, may be more useful to predict treatment responses than *ESR1* mutation status[86]. Differences in the predictive value of these two genetic biomarkers may be due to the clinical resistance of selected *ESR1* mutant cells to fulvestrant, and the truncational nature of PIK3CA mutations that are shared by all subclones in the metastatic tumor[86]. O'Leary et al also showed that other driver mutations in RB1, growth factor receptors, TP53, and PIK3CA were acquired over the course of treatment[86]. The acquisition of these mutations was associated with a longer time of treatment, and acquired mutations at the end of treatment correlated with a longer PFS[86]. These data support the conclusion that driver mutations may be acquired later in therapy as a consequence of therapeutic pressures, but perhaps not always in the early treatment setting. These studies also suggest there may be limited clinical utility to stratify patients to treatment based on *ESR1* mutation status alone, and that concurrent acquisition of other driver mutations should be considered when designing therapeutic regimens to overcome resistance.

Jeselsohn et al performed a genome-wide CRISPR-cas9 KO screening to determine what genes were essential for E2-independent growth of ER mutant-expressing breast cancer cells[67]. As these ER mutants are constitutively active, it is not surprising that many of the negatively selected genes, or essential genes, identified in the screen are known drivers of ER^+ breast cancers such as *GATA3, TFAP2C*, *MTOR*, *MYC* , and *ESR1* itself, as well as ER co-regulators, such as NCOA3, EP300, MED1, and MEN1[67]. *CCND1* and *CDK4* remained essential genes in the mutant cells also[67], which is consistent with a retrospective clinical study in which patients with ER

mutations remained sensitive to CDK4/6 inhibitors[119] and Jelselsohn et al confirmed that mutant-ER expressing cells retain sensitivity to palbociclib, a CDK4/6 inhibitor.

Wardell et al. tested the activity of the cyclin-dependent kinase 4/6 (CDK 4/6) inhibitor palbociclib, administered as both monotherapy or in combination with the SERM bazedoxifene, in PDX models derived from patients with ER+ endocrine-resistant breast cancer[120]. Palbociclib monotherapy was effective in a PDX expressing WT *ESR1*, and in a PDX with amplification of *ESR1*, but was ineffective in a PDX with the *ESR1* D538G mutation[120]. However, this observation may be explained by the concurrent loss of Rb expression in this model, a well-described mechanism of resistance to CDK4/6 inhibitors[120]. Conversely, in an ER Y537S mutant PDX model, palbociclib alone or in combination with bazedoxifene similarly inhibited tumor growth, but the combination proved more effective in decreasing Ki67 expression than either agent alone[120]. This observation further demonstrates that *ESR1* status, including the specific mutation, is important, but is not sufficient for stratifying and predicting responses to therapy, and other co-occuring mutations and alterations should be taken into consideration.

As mentioned previously, CDK7 was shown to modulate ER activity through S118 phosphorylation[12], as well as contribute to WT and mutant ER-expressing cell growth[67]. Therapeutic inhibition of CDK7 using THZ1 resulted in a dose- and time-dependent inhibition of Y537S and D538G S118 phosphorylation in vitro[67]. THZ1 treatment of ER Y537S cells downregulated pathways enriched by ER mutations related to ERBB2, PI3K and MTOR, implying that THZ1 may be targeting ER mutant

transcription, as well as other components of mutant ER's transcriptional network[67]. The combination of THZ1 with fulvestrant showed significant synergism in MCF7 and T47D dox-inducible cell lines expressing WT ER and ER Y537S, as well as the Y537S ER mutant knock-in cell line. Orthotopic xenografts of MCF7 cells expressing the Y537S mutant demonstrated that the combination of THZ1 with fulvestrant had improved efficacy in inhibiting tumor growth compared with either single agent[67]. These results support the potential of this combination as a therapeutic strategy to overcome endocrine resistance caused by the ER mutants. Harrod et al. also confirmed this strategy in vitro, showing that THZ1 itself can inhibit MCF7 and MCF7 Y537S cell growth, and co-treatment of THZ1 with fulvestrant significantly augmented the growth inhibition of MCF7 Y537S cells compared to either agent alone[80]. However, the differences in sensitivity to THZ1 by mutant ER and WT ER-expressing cell were not statistically significant[80].

An additional target shown to be involved in tamoxifen resistance in *ESR1* mutant models by Gelsomino et al is insulin growth factor 1 receptor (IGF1R) signaling[121]. IGF1R and mutant ER showed enhanced crosstalk and co-localization, as shown by ER immunoprecipitation and proximity ligation assays [121]. Treatment with IGF-1R pathway inhibitors sensitized mutant-ER-expressing cells to tamoxifen[121]. Using similar mutant models, Li et al also demonstrated that the IGF1R pathway contributes to endocrine resistance[122]. The mutant ER-expressing models had an enhanced IGF gene signature compared to the WT ER-expressing models, based on RNAseq analyses[122]. In addition to an enhanced IGF gene signature, mutant ER-expressing cells, tamoxifen

resistant cells, and long-term estrogen-deprived cells all showed enhanced growth in response to IGF1 stimulation[122], indicating that IGF1R-mediated endocrine resistance may be shared among many models of endocrine resistance, and is not specific only to mutant ER-expressing models. Using inhibitors or small interfering RNA knockdown to target the IGF1R pathway sensitized mutant ER-expressing cells to endocrine therapy[122], confirming the results from Gelsomino et al[121]. Despite promising results from these pre-clinical studies, IGF1R inhibitors do not yet have demonstrated efficacy in the clinic in the context of metastatic breast cancer.

Though mutations in growth factor receptors are known to contribute to endocrine resistance, it appears that *ESR1* mutations and growth factor receptor mutations, including those in *ERBB2*, *FGFR1*, *FGFR2*, and *FGFR3*, are mutually exclusive, meaning it is extremely rare that a tumor cell would have both an *ESR1* mutation and growth factor receptor mutation [123,124].

HSP90, E3 Ligases, and the Ubiquitin-Proteasome System

One of the primary strategies for targeting ER in breast cancer is small-molecule-mediated receptor degradation. However, as mentioned previously, degradation can be coupled to both transcriptional activation, as well as transcriptional repression, and can be explained by ER being regulated by two different ubiquitin proteasome pathways, depending on the ligand[125]. As a result, it is important to understand the mechanisms that regulate ER stability in order to develop effective ER-targeting therapies.

HSP90 Structure and Function

Members of the HSP90 family are conserved molecular chaperones responsible for the folding, maturation, and activation, but also stabilization of over 200 clients, including ER[126], and have a molecular weight of approximately 90 kilodaltons. HSP90 proteins can account for ~ 2% of cytosolic proteins in an unstressed cell[127]. Low levels of HSP90 or HSP90 inactivating mutations result in hypersensitivity to stress and HSP90 inhibitors[128–130]. HSP90 has four isoforms in humans. Expression of HSP90 α, encoded by *HSPC1*, is inducible. Expression of HSP90 β, encoded by *HSPC3,* is constitutive. Both isoforms are cytoplasmic[131]. HSP90 α knock out mice are viable, but male mice are sterile[132]. HSP90 β knock out mice do not survive past nine days[133]. In this thesis, HSP90 refers primarily to the α isoform, though the antibody used for western blotting in this work cannot distinguish between the two isoforms. Glucose-related protein 94 (GRP94) is specific to the endoplasmic reticulum, and tumor necrosis factor (TNF) receptor-associated protein 1 (TRAP1) is specific to mitochondrial matrix[131].

HSP90 is composed of three domains. The N-terminal domain is responsible for ATP hydrolysis, and is also where some co-chaperones bind, including p23, and CDC37[134]. The N-terminus also contains a druggable ATP binding pocket. ATPase activity is essential for HSP90's chaperone functions[135,136]. The N-terminus and middle (M) domain are connected by an unstructured, charged linker region. The M-domain is responsible for assembling unfolded client proteins and is also where the co-chaperone AHA1 binds[137]. The M-domain also modulates the ATPase activity of the N-terminus[138]

as it binds the γ-phosphate of ATP, the phosphate furthest from the adenine rings, promoting ATP hydrolysis. The C-terminal domain is primarily involved in the dimerization of HSP90, and also contains a highly conserved MEEVD peptide where co-chaperones containing a tetratricopeptide repeat (TPR) domain bind [139,140].

The HSP90 chaperone cycle is highly dynamic in nature. HSP90 is just one component of a multi-component chaperone complex. Co-chaperones regulate and define the conformational dynamics and states of HSP90 and are required for optimal chaperoning activity. ATP binding and hydrolysis are coupled to the “opening” and “closing” of HSP90 protomers[141–143] and these structural rearrangements regulate interactions with co-chaperones and client proteins[144].

In normal cells, heat shock response (HSR) is a reaction to common physiological stressors such as increased temperature, infection, and reactive oxygen species, and helps to maintain homeostasis. HSR is orchestrated primarily by transcription factors called heat shock factors. Heat shock factor 1 (HSF1) is a master regulator of HSR. Under unstressed conditions, HSF1 is sequestered in the cytoplasm by HSP90 and HSP70. Stress induces HSPs to dissociate from HSF1, derepressing HSF1, which then trimerizes and translocates to the nucleus. In the nucleus, HSF1 binds to heat shock response elements, cis-acting sequences found in the promoter region of target genes, and recruits RNA polymerase, driving transcription of HSPs[145]. Subsequently, heat shock proteins like HSP27, HSP40, HSP70, and HSP90 are upregulated[146–148]. This upregulation protects proteins from misfolding and aggregation, and promotes cell survival in conditions that would otherwise be lethal. However, there

are some HSPs, sometimes called heat shock protein cognates (HSCs), that do not require HSR for expression, and are usually constitutively expressed[149]. In addition, there is some controversy surrounding this simple model of HSF1-mediated HSR, as HSF1 can be activated independently of chaperones, and transcriptional regulation of heat shock proteins does not rely solely on HSF1, but is also regulated by other transcription factors, including NF- κB, AP-1, and NRF1[150].

Targeting HSP90 in Cancer

Cancer cells often are in a chronically stressful hypoxic, acidic, and nutrient-deprived microenvironment, and, in response, upregulate HSP90. HSP90 and other chaperones likely allow cancer cells to survive, and even thrive, in an environment that normal cells would not tolerate. HSP90 client proteins and co-chaperones have roles that span every hallmark of cancer, including sustained proliferative signaling, modified metabolism, immortalization, angiogenesis, metastasis and invasion, inflammation, as well as evasion of apoptosis, immune surveillance, and growth suppression (Table 1-2). As a result, cancer cells become “addicted” to HSP90 because HSP90 facilitates the folding, maturation, and stabilization of overexpressed and mutated oncoproteins that contribute to carcinogenesis[126]. Indeed, increased expression of HSP90 is a commonly observed feature in breast cancer and is associated with decreased survival[151–153]. In tumor cells, knocking out HSP90 α using CRISPR-cas9 reduced cell migration, invasion, and metastasis, but had no effect on growth and survival, and knocking out HSP90 β in tumor cells resulted in cell death, further emphasizing the importance of HSP90 in sustaining cancer[154,155].

HSP90 inhibitors in general have a higher affinity for HSP90 in tumors than in normal cells, and accumulate selectivity in tumors[156]. One explanation for this phenomenon is that soluble HSP90 in tumor cells is present in assembled multi-chaperone complexes that are more active than HSP90 in normal cells, which is in a non-complexed inactive form[156]. In addition, HSP90, as well as many of its oncogenic client proteins, are expressed at higher levels in cancer cells compared to normal cells[157,158]. Because HSP90 client proteins span every cancer hallmark, HSP90 inhibition can potentially target multiple oncogenic pathways simultaneously.

N-terminal HSP90 Inhibitors

Many specific HSP90 inhibitors have been developed over the last two decades. One of the first small molecule inhibitors identified, geldanamycin, belongs to the benzoquinone ansamycin antibiotic family. Geldanamycin is a natural compound derived from *Streptomyces hygroscopicus*[159]. Geldanamycin binds to the N-terminal ATP binding pocket, inhibiting HSP90's chaperoning cycle[141–143], leading to recruitment of E3 ligases, and the degradation of client proteins by the 26S proteasome[33,160]. Though geldanamycin performed well in in vitro and in vivo assays, these results were never translated to the clinic, due to hepatotoxicity[161] . Geldanamycin's quinone group possesses toxicity that is independent of HSP90 inhibition as it produces superoxide radicals that cause cell death[162]. Despite the initial lack of success seen with the first-generation benzoquinone ansamycin inhibitors, geldanamycin has served as an important molecular probe for better understanding HSP90 biology, and is often used as a bench mark for HSP90 inhibition. Geldanamycin has also served as an important

scaffold from which two analogs with improved solubility and decreased toxicity were developed: tanespimycin and alvespimycin. However, neither drug has progressed past phase II clinical trials.

Radicicol is another first generation HSP90 inhibitor derived from *Monosporium bonorden* [163]. Like geldanamycin, it is a natural compound that competitively binds to the N-terminal ATP binding pocket[164,165], and also suffers from structural instability[166]. Second generation derivatives of radicicol have had the most success in the clinic of all the classes of HSP90 inhibitors. Inhibitors in this class include liminespib, ganetespib, onalespib, and KW-2478. Ganetespib is the most clinically studied, and is the only inhibitor to have progressed to phase III clinical trials. Ganetaspib has the advantage of being smaller than the ansamycin analogs, and can bind to the ATP binding pocket even when the pocket lid is closed, which may partially explain its more potent effects in vitro[167]. It may also bind to HSP90 with a higher affinity compared to the ansamycin analogs[168]. Ganetespib also has a favorable safety profile, and has minimal hepatotoxicity, and ocular toxicity, which has hindered the previous generations of HSP90 inhibitors from progressing in the clinic[167].

Another class of HSP90 inhibitors that targets the N-terminus are purine-based inhibitors. These inhibitors are fully synthetic, and defined by a purine or purine-like scaffold. The first of these was PU-3[169]. From there, additional analogs were generated. Five purine scaffold inhibitors, PU-H71[170], BIIB021[171,172], BIIB028[173], and Debio0932[174] have been tested in clinical trials, but have not progressed past phase II.

All the inhibitors described thus far indiscriminately target the N-terminus of all isoforms of HSP90. TAS-116[175] and gambogic acid[176] are unique in that they are isoform-selective inhibitors. TAS-116 is selective for the cytosolic HSP90 α and HSP90 β[175]. Isoform specificity has been proposed as a way to circumvent heat shock response (HSR), an important mechanism of resistance to HSP90 inhibition.

C-terminal HSP90 Inhibitors

Thus far, only N-terminal inhibitors have been evaluated in the clinic. However, targeting other domains of HSP90 can circumvent challenges associated with N-terminal inhibition. C-terminal targeting inhibitors bind to the cryptic ATP pocket at HSP90's C-terminus[139], and disrupt the interaction of HSP90 with co-chaperones possessing a TPR domain, ultimately resulting in client protein downregulation and apoptosis due to dysregulated chaperone function without inducing heat shock response[139]. Coumarin antibiotics, like novobiocin, were among the first described C-terminal inhibitors. Since then, more potent analogs, such as KU-174[177], have been developed. (−)-Epigallocatechin-3-gallate (EGCG)[178,179] as well as cisplatin are also reported C-terminal inhibitors[180].

Middle domain inhibitors

The M-domain is arguably the least studied, and least targeted of the three HSP90 domains. Thus far, only a handful of middle domain inhibitors have been identified. Kongensin A binds covalently to the middle domain of HSP90 at cysteine 420[181]. Binding to C420 disrupts the association between HSP90 and CDC37, a co-

chaperone of HSP90 that not only provides specificity for HSP90's interactions with client proteins, but also activation of kinase clients[181]. This residue is essential for kongensin A's mechanism as the interaction between HSP90 and CDC37 was restored when C420 was mutated to an alanine[181]. Kongensin A can also promote degradation of HSP90 client proteins such as HER2, AKT, and B-RAF[181]. Another HSP90 M-domain ligand triptolide is selective for the HSP90 β isoform, and blocks the interaction of HSP90 and CDC37, but through binding to C366[182]. Gambogic acid has also been reported as selective for the middle domain of the HSP90 β isoform[182].

Finally, sulphoxythiocarbamate alkyne (STCA) has been shown to selectively target cysteines 412, 564, and either Cys589 or Cys590 in the middle domain of HSP90β [183]. STCA forms stable thiocarbamate adducts, which likely causes HSP90 β's conformation to change such that it interferes with its chaperoning function without affecting its ATP-binding ability [183]. STCA has been shown to decrease breast cancer cell proliferation and promote degradation of HSP90 clients RAF1, HER2, CDK1, CHK1, and mutant p53, but also upregulate HSP70 in an HSF-1 dependent manner [183].

Mechanisms of Resistance to HSP90 Inhibitors

Though N-terminal targeting inhibitors have been tested in over 170 clinical trials as a single agent, or in combination with other drugs, in a variety of cancer types, more than half of these trials did not progress past phase I, and no HSP90 inhibitors have been FDA-approved to date. In addition to ocular and liver toxicity, drug resistance is also a significant challenge. Heat shock response is one of the major mechanisms of resistance, especially in response to N-terminal inhibition. One way chaperones

regulated by HSF1, particularly HSP70 and HSP27, confer chemoprotective and pro-survival effects is through evasion of apoptosis by inhibiting cytochrome c and TNF-mediated cell death[146,184]. Silencing HSP70 in cancer cells can induce client degradation and, even in cells rendered resistant to in geldanamycin and tanespimycin, silencing HSP27 and HSP70 re-sensitizes cells to tanespimycin[146,184].

Another major resistance mechanism specific to benzoquinone asamycins is the overexpression of multidrug resistance pump 1 (MRP-1) efflux pump and p-glycoprotein[185]. However, cells resistant to benzoquinone asamycins are still sensitive to synthetic purine inhibitors because they are not p-glycoprotein substrates[171]. Decreased expression of quinone-metabolizing enzyme NAD(P)H: quinone oxidoreductase 1 (NQO1) has also been implicated in resistance to benzoquinone asamycins[186]. NQO1 is responsible for reducing this class of compounds into hydroquinone, which is a more potent HSP90 inhibitor. Treatment of cells with an NQO1 inhibitor recapitulated the drug resistance phenotype observed in cells with low expression of NQO1, indicating that low NQO1 expression is not just correlative, but causative[186].

Resistance to resorcinol-based inhibitors such as ganetespib and luminespib has been attributed to elevated levels of UDP glycuronosyltransferase 1 A (UGT1A)[187]. Gene expression analysis of sensitive and resistant colorectal and bladder cancer cell lines treated with HSP90 inhibitors showed that upregulation of UGT1A was a primary distinguishing feature[187]. As a result, there is a need to develop better tolerated and mechanistically distinct HSP90 inhibitors.

The Ubiquitin Proteasome System and ER

HSP90 collaborates with the ubiquitin proteasome system (UPS), another primary regulator of ER stability that is critical for maintaining protein homeostasis, and unfolded protein turnover[188]**.** There are many players involved in the UPS. Three enzymes, ubiquitin activating enzyme (E1), ubiquitin conjugating enzyme (E2), and ubiquitin ligase (E3) catalyze the covalent binding of ubiquitin to protein lysine residues[188]. In humans, though there is only one major E1, and approximately 40 E2s in humans, E3 ligases help impart substrate specificity to E1 and E2, and there are estimated to be between 500-1000 E3 ligases[189]. Some of the most well-known E3 ligases that regulate ER stability include MDM2[190151], C-terminus of HSC70 interacting protein (CHIP)[33], BARD1[191]/ BRCA1[192], SKP2[154], and E6AP[85]. Residues K302 and K303 are essential for ER ubiquitination and subsequent degradation by the 26S proteasome[22].

E3 Ligase Modulators

One way to circumvent HSP90-dependence is to directly modulate E3 ligases to target proteins for degradation. There are several molecules that have been reported as E3 ligases modulators. The most notorious small molecule E3 modulator is thalidomide. Despite its teratogenicity, it has since been shown to bind directly to cereblon, and to be an effective treatment in the refractory multiple myeloma setting[193,194]. Once bound to thalidomide or related compounds such as lenolidomide and pomalidomide, cereblon can promote degradation of the IKAROS family of transcription factors, which results in downregulation of IKAROS targets that regulate cell death[195]. One study reported the

use of novel cereblon modulator CC-92480 to treat multiple myeloma in the relapse, refractory, and lenalidomide-resistant setting by targeting AIOLOS and IKAROS for degradation by the 26S proteasome[196]. CC-92480 had superior degradation efficiency and kinetics compared to lenolidomide and pomalidomide. CC-92480 is reported to act as a molecular glue, allowing cereblon to interact with proteins it would not normally bind[196]. Further experiments would be needed to know if CC-92480 would be useful in the context of mutant ER in breast cancer.

A new emerging class of drug, proteolysis targeting chimera technology (PROTAC), can link ER ligands to a small molecule that binds an E3 ligase, leading to ubiquitination and proteasomal degradation of ER. Arvinas' PROTAC was effective against mutant ER, and thus far has shown no agonist activity[197]. Preclinical studies showed that the ER PROTAC ARV-471 promoted potent degradation of ER in multiple ER-positive cell line models[197]. Furthermore, ARV471 showed robust growth inhibition of WT and mutant ER xenograft models[197]. Clinical development of ARV471 is ongoing and, if successful, will represent a novel class of ER protein degraders that can also be applied to targeting other proteins in breast and other cancers. Gonzales et al. developed a series of ER-targeting degraders based on PROTAC, including ERD-148[198]. Likely because of its ligand-dependent mechanism, ER mutants exhibit resistance to ERD-148 to the same degree as fulvestrant as measured by cell proliferation and downregulation of GREB1[198]. Though its biological activity in vitro is comparable to that of fulvestrant, it has the advantage of potentially being orally bioavailable[198]. Roberts et al. reported a two-stage strategy to develop PROTACs

against ER[199]. A promising molecule generated, AM-A3, elicits potent ER degradation activity, and decreased the proliferation of MCF7[199]. This approach can significantly simplify, as well as increase the throughput of PROTAC development, and could theoretically be expanded to other targets of interest[199]. However, PROTAC is still based on a ligand-dependent mechanism, and its large bulky size (~700-1000 Da) may restrict cell permeability. In addition, it is unknown how PROTACs may affect the endogenous substrates of the E3 ligases they modulate.

Conclusions

Despite great strides in understanding the biology of estrogen signaling and breast cancer, as well as treating breast cancer in the last century, ER positive breast cancer remains a challenging disease. Most mortality is related to metastatic disease and the development of resistance to mainstay therapies. One recently established mechanism of resistance is caused by *ESR1* hot spot mutations, and drug candidates specifically targeting mutant-ER-expressing breast cancers are needed. *ESR1* mutations have a unique biology, and do not simply recapitulate the phenotype of WT ER in the agonist conformation. In addition, *ESR1* mutations at different residues do not have identical phenotypes. The *ESR1* mutants have their own distinct cistromes, transcriptomes, and resistance phenotypes. New orally bioavailable SERDs are being developed to overcome the shortcomings of aromatase inhibitors, fulvestrant, and tamoxifen. However, SERDs have been a challenging class of drug to develop. New SERDs and SERMs still rely on the ligand-binding domain for their mechanisms of action, and many of them also exhibit tissue-specific mixed agonist-antagonist activity. This may explain

why many SERDs have failed in development. Currently, elacestrant is the only SERD that has completed phase III clinical trials. One way to improve lead molecule selection in the future is considering receptor mobility in addition to ER degradation. Several studies have proposed that fulvestrant's antagonistic effects are not driven by receptor degradation. Instead, antagonism is driven by receptor immobilization to the nuclear matrix, and degradation occurs in response to immobilization. In addition, optimizing for ER degradation does not necessarily result in pure antagonism, and can lead to the selection of molecules with a range of effects on downstream ER transcriptional activity and cell proliferation. Using assays that measure receptor mobility in a high throughput manner, rather than ER degradation, may increase the tractability of targeting ER and the likelihood of finding a successful ER antagonist. To circumvent challenges associated with drugging the *ESR1* LBD, modulating molecular chaperones like HSP90 and E3 ligases that control ER stability could also be a promising approach to skirt endocrine resistance, and could also be used to target additional drivers in mutant ER tumors. However, the efficacy of HSP90 inhibitors and E3 ligase modulators in the context of *ESR1* mutations requires further investigation.

Figure 1-1

Estrogen Receptor Protein Domains and *ESR1* Mutations. Schematic of ER's protein domains, as well as the relative position of selected *ESR1* point mutations found in clinical samples. The majority of *ESR1* point mutations occur within the ligand-binding domain.

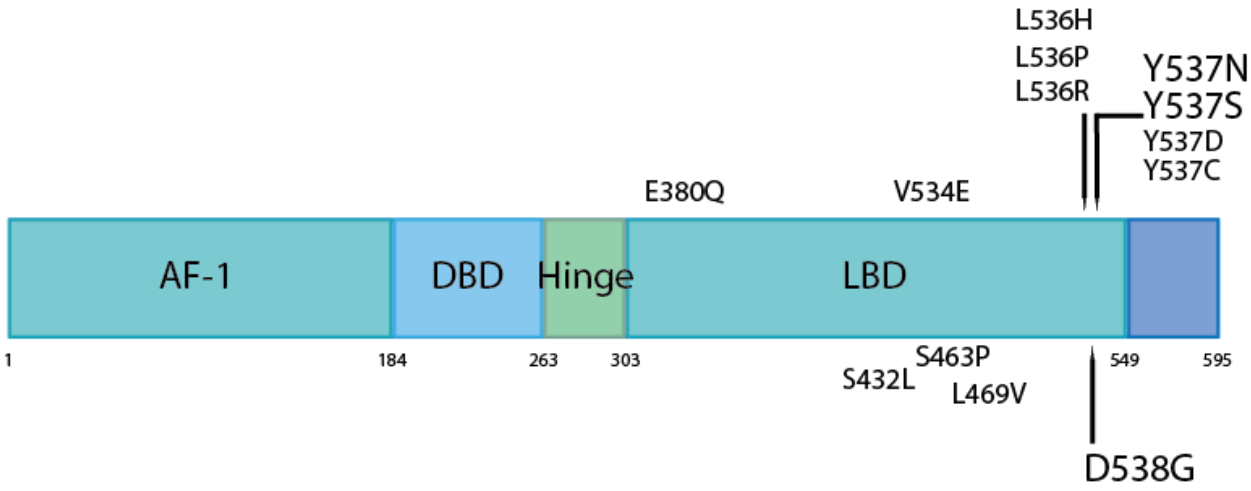

Figure 1-2

Selected major milestones in endocrine therapy development

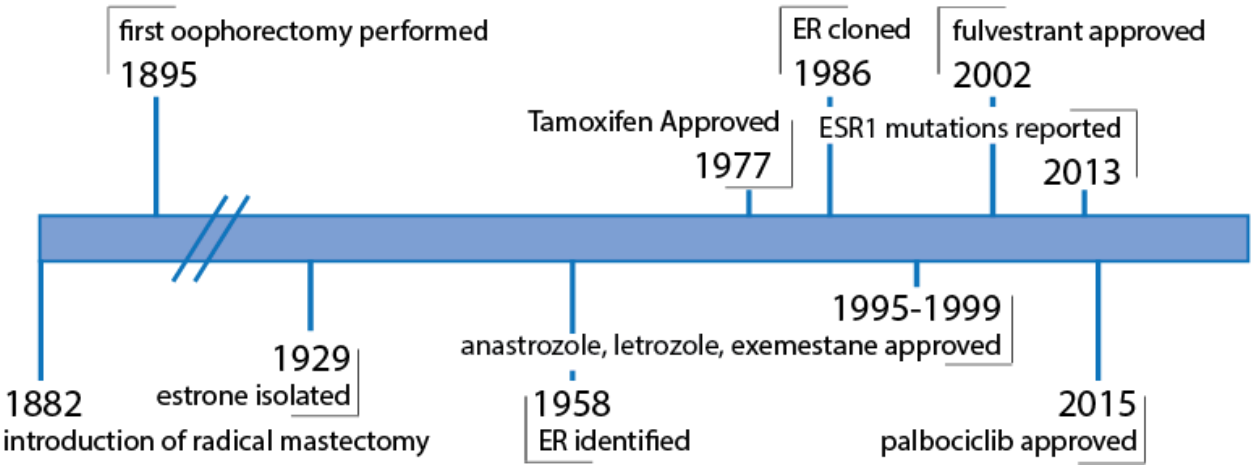

Figure 1-3

Summary of the mechanism of action of various ER ligands. Binding of estrogen to ER's ligand-binding domain releases ER from its chaperone protein. ER can then homo- or hetero-dimerize and bind to EREs, and recruit co-regulators to regulate the transcription of ER-target genes. Tamoxifen also binds to ER via the ligand-binding domain. Tamoxifen transcriptionally represses ER, and prevents the recruitment of coactivators. Fulvestrant and other SERDs also bind to the ligand-binding domain, but slow receptor mobilization, and ER is eventually degraded by the 26S proteasome. PROTACs link a moiety to recruit an E3 ligases as well as an ER ligand. When the ER ligand on the PROTAC binds ER, it brings ER into close proximity of the recruited E3 ligase. ER can then be polyubiquitinated and targeted for degradation by the 26S proteasome.

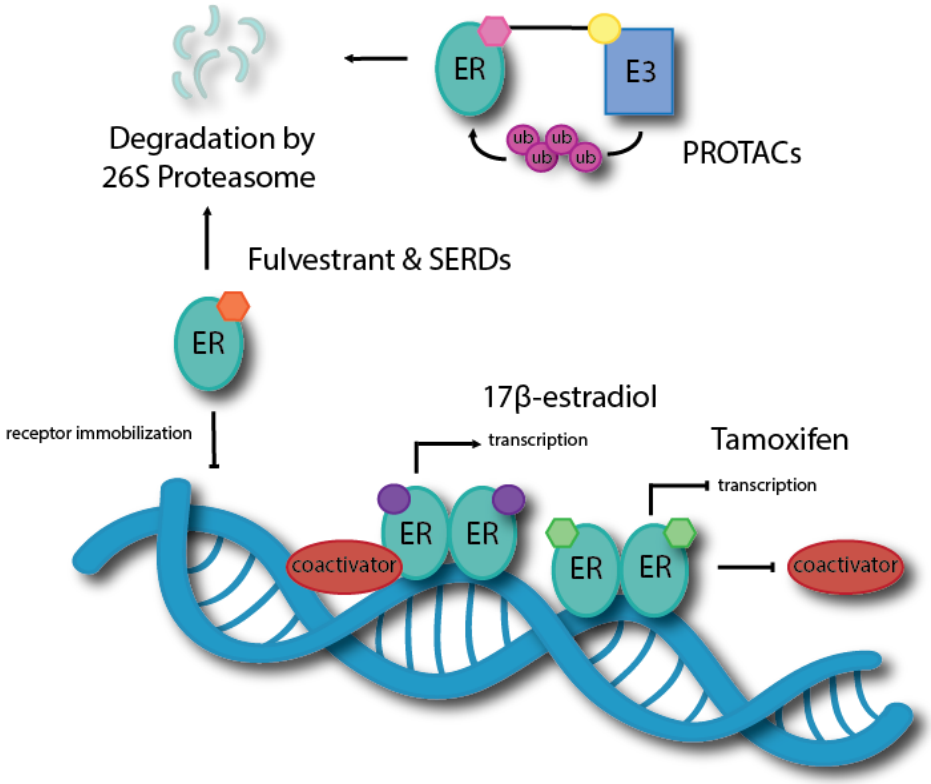

Figure 1-4

Comparison of wildtype ER and mutant ER transcription. In the presence of E2, ER can homodimerize and bind to chromatin to regulate the expression of estrogen-regulated genes, including *GREB1*, *PGR*, and *MYC*, some of which are important for normal development, as well as tumor growth and survival. However, mutant ER can initiate transcription of estrogen-regulated genes, even in the absence of ligand, as well as ER mutant-specific regulated genes, which results in drug resistance and metastasis.

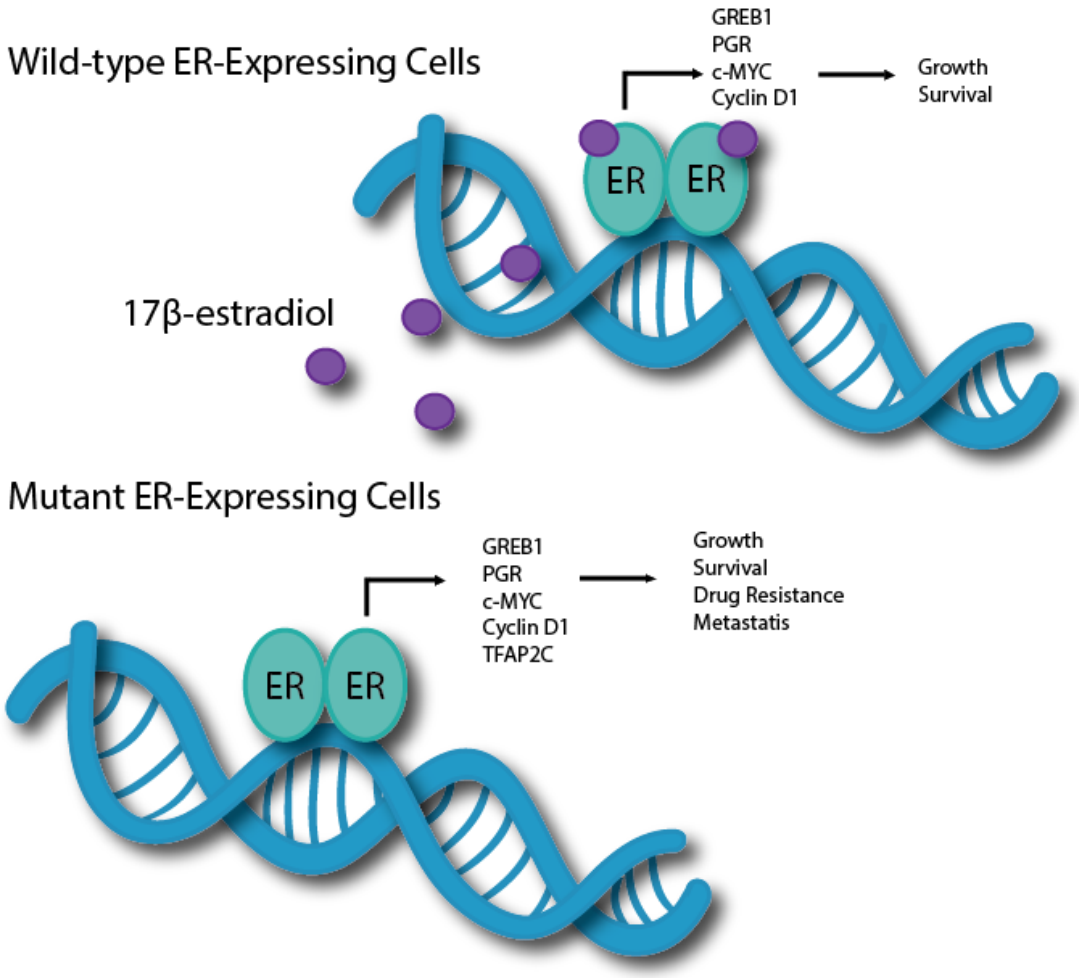

Figure 1-5

Schematic of the domains of HSP90 α protein

Table 1-1

Summary of therapies targeting mutant ER, and their related publications and clinical trials, if applicable

Class	Therapy Name	Citation	Clinical Trial
SERM	Lasofoxifene	Andreano et al. 2020[82], Laine et al. 2019 [98]	NCT03781063
SERM/SERD	Bazedoxifene	Fanning et al. 2018[103], Wardell et al. 2013[99], Wardell et al 2015[123]	NCT02448771
SERD	AZD9496	Toy et al. 2017[74], Nardone A et al. 2019[108], Weir et al 2016[105]	NCT02248090, NCT03236874
SERD	AZD9833	Hamilton et al. 2020[163]	NCT03616587, NCT04214288
SERD	B-SERDs	Lu et al. 2019[115]	
SERD	D-0502	Zhang et al. 2019[164]	NCT03471663
SERD	G1T48	Andreano et al. 2020[165]	NCT03455270
SERD	GDC-9545	Metcalfe et al. 2019[109]	NCT03332797, NCT03916744
SERD	GDC-0810/ Brilacestrant	Guan et al. 2019[104], Joseph et al 2016[106], Lai et al. 2015[107]	NCT01823835
SERD	GDC-0927	Guan et al. 2019[104]	NCT02316509
SERD	LSZ102	Tria GS et al. 2018[166]	NCT202734615
SERD	RAD1901/ Elacestrant	Bihani et al. 2017[112], Patel et al. 2019[113], Garner et al.2015[167], Wardell et al. 2015[114]	NCT02338349, NCT03778931
SERD	SAR439859	Campone et al. 2020[168], Shomali et al 2017[169]	NCT03284957
SERD	SHR9549	Bardia et al. 2019[170]	NCT03596658
SERCA	H3B-5942	Puyang et al. 2018[118]	
SERCA	H3B-6545	Hamilton et al. 2019[119], Rioux et al 2018[120]	NCT03250676, NCT04288089
Novel	K-07	Zhao et al.[72]	
PROTAC	AM-A3	Roberts et al.[161]	
PROTAC	ARV-471	Flanagan et al. 2019[159]	NCT04072952
PROTAC	ERD-148	Gonzalez et al.2020[160]	

Table 1-2

Summary of selected HSP90 interacting proteins and their contributions to the hallmarks of cancer

Cancer Hallmark	HSP90 Interacting Protein
Sustained Proliferative Signaling	Steroid hormone receptors (Estrogen receptor, Androgen receptor), receptor tyrosine kinases (ERBB2, 3, 4), Serine/threonine kinases (mitogen-activated protein kinases), PI3K/AKT, mTOR
Altered Metabolism	c-MYC, HIF1 a, PKM2
Immortalization	Telomerase
Angiogenesis	FGFR, VEGFR, TGF-β, TNF-α
Metastasis and Invasion	MMP-2, 3, 9
Inflammation	NF-κB, IL-6, IL-8, STING
Apoptosis Evasion	Survivin, BAG family proteins
Immune Evasion	IRAK3
Growth Suppressor Evasion	WEE1, PLK, CDK4/6

CHAPTER 2: Dip G is an HSP90 middle domain modulator

Dr. Ang Gao performed the CLICK chemistry-related experiments

Dr. Haibo Xie performed the medicial chemistry and binding assays

Miyang Li performed the mass spectrometry experiments

Portions of this chapter were adapted from the following:

Donahue K, Xie H, Li M, Gao A, Ma M, Wang Y, Tipton R, Semanik N, Primeau T, Li S, Li L, Tang W, Xu W. Diptoindonesin G is a middle domain HSP90 modulator for cancer treatment. J Biol Chem. 2022 Nov 14:102700. doi: 10.1016/j.jbc.2022.102700. PMID: 36395883.

Abstract

HSP90 inhibitors can target many oncoproteins and tumorigenic pathways simultaneously. However, few HSP90 inhibitors have successfully made it through clinical trials due to dose-limiting toxicity and induction of heat shock response, leading to clinical resistance. We identified diptoindonesin G (dip G) as an HSP90 modulator that can promote degradation of HSP90 clients, including estrogen receptor α (ER), by binding to the middle domain of HSP90 without inducing heat shock response, which is one mechanism of clinical resistance to HSP90 inhibitors. Our data suggest that dip G is not only a molecular probe for HSP90 biology, but also a new therapeutic avenue for various cancers, and circumvents some obstacles associated with HSP90 inhibition.

Introduction

Estrogen receptor α (ER) positive tumors are typically associated with the most favorable prognosis, and expression of ER indicates a more differentiated and luminal state. In addition, expression of ER predicts response to endocrine therapies. ER stability is known to be affected by multiple factors. Heat shock protein 90 (HSP90) is a molecular chaperone that is responsible for the folding, maturation, and activation, but also stabilization of its over 200 clients, including ER (https://www.picard.ch/downloads/Hsp90interactors.pdf)[126]. It accounts for 2% of cytosolic protein under unstressed conditions[127]. Many of these clients include steroid hormone receptors[143,200]. HSP90 maintains ER in a ligand binding conformation, and also protects it from proteasomal degradation[201]. HSP90 is composed of three domains. The N-terminal domain is responsible for ATP hydrolysis, and is also where some co-chaperones bind, and contains a druggable ATP binding pocket. The middle (M) domain is responsible for assembling unfolded client proteins. The C-terminal domain is primarily involved in homodimerization of HSP90 and contains a highly conserved MEEVD peptide where co-chaperones bind. HSP90 in cancer behaves very differently from HSP90 in normal cells, and protects overexpressed and mutated oncoproteins, mediating oncoprotein addiction[126]. Interestingly, HSP90 inhibitors in general have a higher affinity for HSP90 in tumors than in normal cells and accumulate selectively in tumors[156]. One explanation for this phenomenon is that soluble HSP90 in tumor cells is present in assembled multi-chaperone complexes that are more active than HSP90 in normal cells, which is in a

non-complexed inactive form[156], making it an attractive and highly sought-after cancer target.

HSP90 can be pharmacologically inhibited using HSP90 inhibitors that belong to the benzoquinone antibiotic family. Geldanamycin, and its analogs tanespimycin and alvespimycin, bind to the N-terminal ATP binding pocket, inhibiting its ATPase activity essential for performing its chaperone functions[135,136]. ATP binding and hydrolysis are coupled to the “opening” and “closing” of HSP90 protomers[141–143] and these structural rearrangements regulate the interactions with co-chaperones and client proteins[136]. Inhibition of HSP90 results in inhibition of this chaperoning cycle [141–143], recruitment of E3 ligases, and the degradation of client proteins by the 26S proteasome[33,160].

Unfortunately, though amino-terminal targeting HSP90 inhibitors have been tested in over 40 clinical trials as a single agent, or in combination with other drugs, in a variety of cancer types, the toxicity, particularly to hepatocytes in the context of benzoquinone ansamycin derivatives[202], and lack of clinical response observed have so far precluded their FDA approval. HSP90 inhibitors that target the N-terminus, have very potent antiproliferative effects initially[203], but often become ineffective over time due to induction of heat shock response. This is because N-terminal inhibitors induce derepression of HSF1, which subsequently upregulates HSP27, HSP40, HSP70, and HSP90[146–148]. This leads to undesirable chemoprotective effects, and clinical resistance, and has limited the use of HSP90 inhibitors as single agents. As a result, there is a need to develop better tolerated and mechanistically distinct HSP90 inhibitors.

HSP90 collaborates with the ubiquitin proteasome system (UPS), another primary regulator of ER stability that is critical for maintaining protein homeostasis and unfolded protein turnover[188]. There are many players involved in UPS. Ubiquitin ligases (E3) catalyze the covalent binding of the protein ubiquitin to lysine residues[188] to target substrates for degradation by the 26S proteasome. There are estimated to be between 500-1000 E3 ligases[189]. Some of the most well-known E3 ligases that regulate ER stability include MDM2[151], C-terminus of HSC70 interacting protein (CHIP)[33], BARD1[191]/ BRCA1[192], SKP2[204], and E6AP[85].

Diptoindonesin G (dip G) was originally reported by our group to be a modulator of the E3 ligase CHIP, and has been studied in the context of ER+ breast cancer[205,206], as well as AML[207], triple negative breast cancer[208], and prostate cancer. Mao et al demonstrated that dip G could induce AR degradation in a CHIP-dependent manner in human prostate cancer cells and manipulating CHIP expression affected dip G sensitivity[209]. Zhao et al showed that dip G could promote degradation of ERα, but also reciprocally stabilize ERβ, implicating a commonly shared E3 ligase, CHIP[205]. When CHIP was knocked down using shRNA, dip G-mediated ERα degradation and ERβ stabilization was abrogated, indicating that CHIP is essential for dip G's mechanism of action[205]. In addition, Zhao et al also showed that dip G increased proximity of CHIP and ER. However, it remains unclear whether CHIP is truly the direct target of dip G, or whether dip G perhaps modulates another component of the HSP90-ER-CHIP ternary complex, or acts as a molecular glue[205]. Herein we determined that dip G does not directly regulate CHIP activity, as previously hypothesized, but rather, is a novel HSP90

modulator which, unlike previously described amino and carboxy-terminal targeting inhibitors, targets the middle domain of HSP90. To our knowledge, a handful of other compounds, all of which are natural products, are known to bind to the middle domain. Unlike tanespimycin, dip G does not upregulate HSPs to the same extent, and only affects a subset of the proteins affected by tanespimycin, which may indicate it may be more tolerable to normal cells.

Results

Diptoindonesin G and its analog deoxy-diptoindonesin G promote ER degradation

We first compared diptoindonesin G's (dip G) ability to promote estrogen receptor α (ER) degradation to that of other known ER ligands by treating MCF7 cells with 10 nM 17-β estradiol (E2), 1μM 4-hydroxytamoxifen (OHT), 100 nM fulvestrant, 1μM tanespimycin, as well as 10 μM dip G. Cells were treated after three days of hormone starvation in phenol red-free medium containing 6X charcoal-stripped fetal bovine serum to exclude the effects of hormones, and study each drug's effect in isolation. As expected, E2 induced significant degradation of ER. OHT treatment stabilized ER, and resulted in accumulation of ER levels that were even higher than that of DMSO treatment (Fig. 2-1). Fulvestrant, tanespimycin, and dip G resulted in similar levels of degradation to that of E2 (Fig. 2-1). To quantitatively measure the ability of dip G to induce ER degradation, following hormone starvation, we treated MCF7 cells with increasing concentrations of dip G (0.1-10 μM), fulvestrant (1-1000 nM), or tanespimycin (0.25-4 μM), for 24 hours. ER levels were evaluated using an ER ELISA. Fulvestrant, dip G, and tanespimycin induced dose-dependent degradation of ER. Treatment with 1 μM fulvestrant, the highest non-physiologically relevant dose used in this experiment, 10 μM dip G, and 4 μM tanespimycin resulted in a 64.8%, 72.8%, and 58.3%, reduction in ER, respectively, as compared to vehicle treatment (Fig. 2-2). These results were validated for dip G by western blot (Fig. 2-3). In addition, a modified dip G analog, deoxy-dip G, which is missing a hydroxyl group, and has been shown to

have increased efficacy to degrade ER α and stabilize ER β[206], results in similar dose-dependent degradation of ER (Fig. 2-4).

Diptoindonesin G mediates ER degradation through the 26S proteasome independently of CHIP

To test whether dip G promotes ER degradation through the 26S proteasome, MCF7 cells that were hormone starved for three days were treated with 10 μM dip G, 0.5 μM bortezomib, a proteasome inhibitor, or a combination of dip G and bortezomib for 6 hours. Dip G promoted ER degradation alone. Treatment with bortezomib slightly decreased ER levels, but also resulted in accumulation of ubiquitinated proteins. MG132 treatment abrogated dip G-mediated ER degradation, indicating that dip G promotes ER degradation through the 26S proteasome (Fig. 2-5).

Previously, our group showed that CHIP was required for dip G-induced ER degradation using ER-negative cell line Hs578T overexpressing flag-tagged ER. When CHIP was knocked down with shRNA, ER degradation was abrogated[205]. To test what proteins are affected by dip G treatment in the presence and absence of CHIP, we performed mass spectrometry analysis of LCC2 shControl and MCF7 LCC2 shCHIP cells treated with 10 μM dip G. LCC2 is a tamoxifen-resistant clone of MCF7[210]. We found that 245 proteins were downregulated and 233 proteins were upregulated in the shControl cells, and 297 proteins were downregulated and 334 proteins were upregulated in the shCHIP cells in response to dip G treatment (Supplementary Table 1). To our surprise, we saw significant downregulation of ER protein in both cell lines (Fig. 2-6). 27.3% of the downregulated proteins overlapped in the two groups, and

35.8% of the downregulated proteins were shared. 55% of the total changed proteins in the shControl group were shared with the changed proteins in the shCHIP group, indicating that more than half of the total significantly changed proteins are regulated by dip G in a CHIP-independent manner (Fig. 2-7). We validated this effect in MCF7 shControl and MCF7 shCHIP cells[205] by western blot. In agreement with the mass spectrometry results, a 24-hour treatment with 10 μM dip G decreased ER levels by 54% in the presence and 53% in the absence of CHIP (Fig. 2-8). In addition, basal ER levels appeared to be higher in the MCF7 shCHIP cells, indicating that CHIP does indeed regulate ER stability in these cells (Fig. 2-8). To eliminate the possibility that residual levels of CHIP were mediating dip G's effects, we designed gRNAs targeting the second exon of *STUB1,* encoding CHIP, and generated two CHIP KO cell lines in MCF7 using CRISPRcas9[211]. Absence of full-length CHIP protein was confirmed using western blot, as well as mass spectrometry, where CHIP was the most downregulated protein in the dataset (Fig. 2-9). Actin filament binding, actin binding, cadherin binding, and cell adhesion molecule binding were the top affected functions upregulated by CHIP KO according to our mass spectrometry results. To test whether dip G could promote degradation of ER in a CHIP-dependent manner in CHIP KO cell lines, parental MCF7, as well as both MCF7 CHIP KO clones were treated with 10 μM dip G for 24 hours following hormone starvation. In parental MCF7, ER was degraded in response to dip G. In both MCF7 CHIP KO clones, ER was also degraded in response to dip G treatment (Fig. 2-10). In MCF7 CHIP KO clones 1 and 2, dip G significantly decreased ER levels to a similar extent by 57% and 52%, respectively, compared to a

49% decrease in the presence of CHIP (Fig. 2-10). This effect was also observed using deoxy-dip G (Fig. 2-11), suggesting that CHIP is dispensable for dip G-induced ER degradation, at least in MCF7 cells. In addition, ER was degraded in response to E2 treatment (Fig. 2-12) in both the presence and absence of CHIP, validating what has been reported previously, supporting that liganded and unliganded ER is regulated by two different proteolytic pathways. In addition, we found that ER could be degraded in response to tanespimycin in the presence and absence of CHIP (Fig. 2-13).

E3 ligase expression is variable across breast cancer cell lines and subtypes

To better understand the discrepancy between the results from Hs578T-ER-LUC cells, MCF7, and LCC2, we measured expression of E3 ligases that regulate ER stability, including MDM2, CHIP, and E6AP in 13 different ER +, HER+, and triple negative breast cancer cell lines by western blot. Expression levels of these proteins varied across cell lines, even within the same molecular subtype. MCF7 had higher expression of all E3 ligases known to regulate ER compared to HS578T (Fig. 2-14), implying that other E3 ligases may regulate ER stability, and compensate for CHIP's absence in MCF7.

Determining the diptoindonesin G interactome using CLICK chemistry

To further investigate dip G's direct target, as well as interrogate the dip G interactome, we synthesized an analog of dip G containing an alkyne handle (Figure 2-15). This terminal alkyne handle is reactive with biotin azide via a copper-catalyzed CLICK chemistry reaction. This then results in triazole formation linking biotin to alkyne

dip G (2-16). Modification of dip G at this position only marginally affects dip G's ability to induce ER degradation (Figure 2-17). This biotinylated dip G analog can be subsequently pulled down with streptavidin Dynabeads. BT474 cells were treated with vehicle or 20 μM alkyne dip G for 1 hour. Cells were then UV crosslinked at 365 nM for 20 minutes, and then lysed. CLICK chemistry was then performed, followed by a pull down with a magnetic streptavidin Dynabeads. We then subjected these lysates to mass spectrometry to use an unbiased approach to identify potential dip G interactors (Figure 2-16). We identified HSP90, along with many HSP90-interacting proteins, including HSP27, ATPA, and GRP75 (Supplementary Table 2). Though HSP90 was detected in the DMSO control samples, HSP90 was strongly enriched in the alkyne dip G samples. In addition, when these lysates were probed by western blot, we found HSP90, as well as CHIP, indicating that CHIP may be the primary E3 ligase regulating ER stability in response to dip G treatment (Figure 2-17). However, we cannot distinguish between direct and indirect dip G binding partners using this methodology.

Diptoindonesin G analog deoxy-diptoindonesin G binds to the middle domain of HSP90

We used dip G analog deoxy-dip G, as well as compounds known to interact with different domains of HSP90 in fluorescence polarization assays to further probe dip G's direct target, and measure the interaction of deoxy-dip G with CHIP, ER, and HSP90. Deoxy-dip G was used instead of dip G because deoxy-dip G has a fluorescence emission between 485-520 nm, and can be a used as a fluorescent tracer (Fig. 2-18). The N-terminus of HSP90 is specific to adenosine nucleotides with an intact adenine

ring, such as ATP, as well as compounds that are structurally similar to ATP, like geldanamycin. The C-terminus can bind to Novobiocin and (-)-epigallocatechin gallate (EGCE). The C-terminus of HSP90 is more promiscuous with the kind of nucleotides it can interact with, and binds both ATP as well as GTP. The K_d of deoxy-dip G to HSP90 was 310 nM, while the K_d of deoxy-dip G to CHIP and ER was 9.6 μM and 3.1 μM, respectively, indicating that HSP90 is more likely to be deoxy-dip G's direct target (Fig. 2-20). The MEEVD peptide is found at the C-terminus of HSP90, and binds to co-chaperones with a tetratricopeptide repeat (TPR) domain, like CHIP. As a positive control, we measured the K_d of CHIP to an 5FAM-MEEVD peptide, which was 1.60 μM (Fig. 2-19). In addition, the literature values of 17-β estradiol binding to ER is 0.21 nM[70]. By comparison, we found the K_d of geldanamycin-FITC, an HSP90 inhibitor known to bind the N-terminus of HSP90, was 509 nM, which is similar to literature values (Fig. 2-19)[212]. This indicates that deoxy-dip G binds to HSP90 with a similar affinity as geldanamycin. We found that deoxy-dip G could be competed off by ATP. However, deoxy-dip G could neither be competed off by geldanamycin, nor radicicol[164,165], implying that deoxy-dip G does not bind to HSP90's N-terminus (Fig. 2-21). Deoxy-dip G also could neither be competed off by novobiocin[139], GTP[213], nor EGCE[178], indicating that it is unlikely that deoxy-dip G binds to the C-terminus (Fig. 2-21).

Next, we determined the domain of HSP90 to which deoxy-dip G binds by expressing and purifying GST-tagged HSP90 protein fragments from plasmids corresponding to the N-terminus (AA 9-236), M-domain (AA 272-617), and C-terminus (AA 626-732)[214]. The GST tag was cleaved using thrombin, and these fragments were

used for fluorescence polarization assays (Fig. 2-22). We found that deoxy-dip G bound to the N fragment with a K_d of 13.8 μM. In comparison, deoxy-dip G's K_d to the middle domain was 250 nM (Fig. 2-23), equivalent to the K_d of deoxy-dip G to full-length HSP90 (349 nM). In contrast, deoxy-dip G's K_d to the C fragment was 8 μM (Fig. 2-23). However, even known C-terminal inhibitors, such as cisplatin and novobiocin are not known to bind with high affinity to the C-terminal domain of HSP90[180]. Our results indicate the dip G likely binds to the middle domain of HSP90.

Tanespimycin and diptoindonesin G have distinct mechanisms for targeting HSP90

Fan et al. established that CHIP is required for geldanamycin-induced ER degradation [33]. ER ligands, such as E2, OHT, can promote ER-HSP90 complex disassembly, which completely abolishes geldanamycin-induced ER degradation[33]. We wondered if ligand binding would disrupt dip G-induced ER degradation, as has been previously reported for geldanamycin.

To test this, MCF7 cells were pretreated with vehicle, HSP90 inhibitor tanespimycin (tan), or dip G for 30 min, followed by a five-and-a-half-hour treatment with ER ligands, including E2, 4-hydroxytamoxifen (OHT), or fulvestrant (Fulv). Though E2 is an ER agonist, transcriptional activation of ER is coupled with ER degradation. This degradation mechanism is distinct from that of tanespimycin and dip G, where degradation is coupled to target gene downregulation. Our results (Fig. 2-24) showed that dip G and tanespimycin alone promoted ER degradation. Co-treatment of either dip G or tanespimycin with OHT stabilized ER, and abolished both tanespimycin's and dip

G's ability to promote ER degradation. The effect of fulvestrant with either tanespimycin or dip G was additive, and induced ER degradation. However, co-treatment with E2 and tanespimycin stabilized ER compared to tanespimycin alone. This is likely because ER is already bound to E2, and is no longer complexed with HSP90. With E2 and dip G co-treatment, the combination was additive. In addition, tanespimycin and dip G co-treatment abrogated dip G's effects on ER degradation, indicating that they both target HSP90, and that HSP90 cannot engage the proteasome to degrade ER when it is occupied by both compounds (Fig. 2-24). We also saw that co-treatment with deoxy-dip G and tanespimycin had a similar effect on ER degradation (Fig. 2-25).

Many N-terminal HSP90 inhibitors can derepress HSF1, leading to induction of heat shock response (HSR), a major mechanism of resistance to HSP90 inhibitors. We evaluated dip G's ability to induce heat shock response by incubating MCF7 cells with dip G, tanespimycin, or novobiocin for 24 hours, and measuring expression of HSP27, HSP40, HSP70, and HSP90 by RT-qPCR, all of which are upregulated in response to heat shock and protect cells from proteotoxic stress. Dip G had no significant effect on the expression of the HSPs tested. Novobiocin, a C-terminal HSP90 inhibitor that is known to have no effect on HSR, did not significantly change HSP levels[180,216] (Fig. 2-26). Tanespimycin was the only compound to significantly upregulate all HSPs, consistent with what has been previously reported[215] (Fig. 2-26). Collectively, these findings indicate that dip G does not induce HSR, which circumvents a major hurdle limiting the therapeutic utility of N-terminal HSP90 inhibitors.

Towards further distinguishing tanespimycin and dip G, we measured their effects on the proteome. MCF7 cells were treated with tanespimycin and dip G concentrations that resulted in comparable ER downregulation (Fig. 2-27). Using label-free MS, over 450 proteins were affected by tanespimycin, but less than 200 proteins were affected by dip G treatment. Specifically, 225 proteins were downregulated and 239 proteins were up-regulated by tanespimycin, respectively, and 92 proteins were downregulated and 79 proteins were upregulated by dip G (Fig. 2-28). When examining the top up and down-regulated processes in response to dip G, DNA N-glycosylase activity was significantly downregulated, as well as short chain fatty acid metabolic process, indicating that perhaps dip G affects fatty acid metabolism in cancer cells, linking HSP90 and metabolism. When comparing the proteins downregulated by tanespimycin and dip G, 29% of the dip G downregulated proteins fall within the tanespimycin downregulated proteins, and 48% of the dip G upregulated proteins fall within the tanespimycin upregulated proteins (Fig. 2-29) (Supplementary Table 3). Proteins affected by tanespimycin include known HSP90 clients and co-chaperones, such as ERBB2, DDR1, and BAG1. Dip G regulates a subset of tanespimycin-affected proteins, but also regulates a unique set of proteins.

Discussion

In this study, we uncovered that dip G is a small molecule modulator of HSP90 that directly acts on the middle domain of HSP90, rather than the E3 ligase CHIP, as originally hypothesized.

CHIP is not required for dip G's mechanism of action

Though CHIP may be one of the primary E3 ligases that mediates dip G-induced ER degradation, it is not required for dip G's mechanism of action. When CHIP was knocked out, ER was still degraded in response to dip G (Fig. 2-10). One explanation for the discrepancy between our current hypothesis and the model proposed by Zhao et al. are the cell lines used. ER is endogenously expressed in MCF7, whereas HS578T-ER-LUC cells are a triple negative breast cancer cell line that expresses exogenously introduced expresses ER. This may be why depletion of CHIP abrogates dip G-induced ER degradation, as the protein degradation machinery present in MCF7 for degrading ER does not exist in HS578T. We found that expression of CHIP, MDM2, and E6AP, three well-known E3 ligases involved in regulating ER stability, was low in HS578T, but high in MCF7 (Fig. 2-14). Perhaps other E3 ligases can compensate in the absence of CHIP in MCF7, but not in HS578T. Results from Mao et al showed that manipulating CHIP levels affected prostate cancer cell's sensitivity to dip G [209]. This further emphasizes that reliance on CHIP varies between cell lines and cancer types. Our results agree with the results from Fan et al [33]. Using MCF7, they observed ER degradation in response to geldanamycin treatment when CHIP is knocked down, but the rate of degradation was decreased[33]. We found using geldanamycin analog tanespimycin, dip G, and deoxy-dip G that ER is degraded in response to tanespimycin treatment in the presence and absence of CHIP, but we did not test this as a function over time (Fig. 2-10,11,12,13). Functional redundancy is expected, as E3 ligases are important for regulating proteostasis[217]. Though CHIP appears to be an important E3 ligase that is recruited to promote degradation of mature ER in response to HSP90

inhibition, and geldanamycin has been shown to stimulate the interaction between CHIP and ER [33], CHIP does not play an exclusive role in regulating the turnover of HSP90 client signaling proteins. Morishima et al. have shown that HSP70-dependent E3 ligase Parkin acts redundantly to CHIP on some substrates[217]. Others have shown that in CHIP null mouse embryonic fibroblasts, HSP90 client glucocorticoid receptor could still be degraded at the same rate in response to geldanamycin treatment, indicating that other redundant E3 ligases are likely involved in client stability in the absence of CHIP[217]. In agreement with this hypothesis, Fan et al showed that multiple E3 ligases co-localize with CHIP at poly Q-expanded AR[33].

Dip G is a middle domain modulator of HSP90

Our data support that dip G is an HSP90 modulator (Fig. 2-20, 2-23). Fluorescence polarization assays confirmed that deoxy-dip G indeed directly binds to HSP90 with an affinity comparable to geldanamycin, an amino-terminal HSP90 inhibitor (Fig. 2-20). We also found that tanespimycin interferes with dip G and deoxy-dip G's ability to induce ER degradation, indicating that they share protein targets (Fig. 2-24). However, we also found that deoxy-dip G could neither be competed off of HSP90 by geldanamycin, nor GTP (Fig. 2-21). This supports that dip G is a middle domain modulator, as it neither competitively binds to the same pocket as geldanamycin, nor GTP. The nucleotide specificity of the C-terminus of HSP90 differs from that of the N-terminus, and GTP and UTP are C-terminal-specific nucleotides[213]. However, ATP could compete off deoxy-dip G (Fig. 2-21). HSP90 is reported to have two ATP binding sites localized in the N- and C-domains. It is possible that ATP induces conformational

changes of HSP90 by binding to the N or C domains, masking the deoxy-dip G binding site in the M-domain.

Nevertheless, when comparing dip G with HSP90 N-terminal inhibitors like tanespimycin and geldanamycin, there were many similarities. For example, they both bind to HSP90 with high affinity. In addition, both dip G and tanespimycin affect a variety of proteins, many of which are known HSP90 clients. However, when comparing their respective affected proteomes, we found that, though there was some overlap between tanespimycin and dip G-affected proteins, about 51% of the proteins upregulated by dip G and 70% of the proteins down-regulated by dip G were unique, indicating that dip G has a distinct mechanism of action from tanespimycin even though the compounds share some targets (Fig. 2-28). The distinction between dip G and HSP90 inhibitors is further emphasized by dip G, tanespimycin, and novobiocin's effects on heat shock response, where tanespimycin was the only compound to significantly increase expression levels of all HSPs tested, consistent with what has been previously reported (Fig. 2-26).

HSP90 is required for transcription coupled ER degradation. However, as mentioned previously, degradation can be coupled to transcriptional activation, as well as transcriptional repression, and can be explained by ER being regulated by two different ubiquitin proteasome pathways, depending on whether ER is liganded[125]. One proteasome is responsible for the transactivation of ER, while the other proteasome is responsible for ER quality control[125]. Tateishi *et al* showed using mouse embryonic fibroblasts (MEFs) that under thermally stressed conditions, unliganded ER was

degraded in CHIP-expressing MEFs, but not in CHIP null MEFs, whereas in both CHIP expressing and CHIP null MEFs, ER was degraded in the presence of estrogen[125]. We were able to replicate these results using our CHIP KO cells, and found E2 treatment induced ER degradation in the absence of CHIP (Fig. 2-12). Although both dip G and tanespimycin promote ER degradation engaging HSP90, their mechanisms of action differ. Dip G appears to stabilize the HSP90/E3/ER complex, promoting ER degradation, whereas tanespimycin binding to HSP90 promotes dissociation of ER and causes ER misfolding and subsequent degradation. When cells were treated with tanespimycin and dip G in the presence of E2, tanespimycin and E2 stabilized receptor levels compared to tanespimycin alone, which promoted ER degradation (Fig. 2-24). This is likely because some ER is already bound to ligand and is no longer complexed with HSP90, and some HSP90 is bound to tanespimycin, inhibiting ER's hormone binding ability. Dip G and E2 have an additive effect on ER degradation, indicating that dip G can promote degradation of activated ligand-bound ER, and that dip G likely engages a similar proteolytic pathway as E2-treatment. In addition, dip G can promote degradation of activated ER, unlike tanespimycin, which could not promote degradation of ligand-bound ER (Fig. 2-24). Dip G can promote degradation of certain ligand-stabilized ERs, such as E2 treated, but not OHT-treated ER (Fig. 2-24). This would support a mechanism where dip G can only promote degradation of HSP90-bound ER, and cannot degrade chromatin-bound ER, which is why residual levels of ER are still observed by WB. However, tanespimycin and dip G do not affect fulvestrant-mediated degradation, where degradation is independent of ER transcription (Fig. 2-24). Instead,

fulvestrant immobilizes ER to the nuclear matrix, where it can then be degraded[57]. When cells are treated with dip G and tanespimycin together, dip G offsets the effect of tanespimycin, and less HSP90/E3/ER complex can form. Even though these two compounds do not compete for the same sites on HSP90, they compete for the same pool of HSP90, and binding of one may prohibit the binding of the other, resulting in the higher amount of ER observed compared to either treatment alone. Another explanation is that, rather than competing for sites on HSP90, both compounds can bind to HSP90 simultaneously, but antagonistic each gother, resulting in ER stabilization rather than additive ER degradation. Our most striking evidence supporting dip G as an M-domain modulator is that deoxy-dip G bound with highest affinity to a fragment corresponding to the middle domain of HSP90 to a much greater extent than either the N or C fragments of HSP90 (Fig. 2-23). To our knowledge, only a handful of middle domain inhibitors have been reported. Kongensin A binds covalently to the middle domain of HSP90 at cysteine 420. Binding to C420 disrupts the association between HSP90 and CDC37, a co-chaperone of HSP90 that not only provides specificity for HSP90's interactions with client proteins, but also activation of kinase clients[181]. This residue is essential for kongensin A's mechanism as the interaction between HSP90 and CDC37 was restored when C420 was mutated to an alanine[181]. The methods we used in our study can only pinpoint dip G's binding between AA 272-617. Kongensin A can also promote degradation of HSP90 client proteins such as HER2, AKT, and B-RAF[181]. Another HSP90 M-domain ligand triptolide also blocks the interaction of HSP90 and CDC37, but through binding to C366. Other HSP90 inhibitors have been reported to allosterically

inhibit HSP90-co-chaperone interactions, such as withaferin A[218], celastrol[219], derrubone[220], but they have not been reported to bind to the M-domain of HSP90.

This thesis proposes a new hypothesis for dip G-induced ER degradation, implicating HSP90 as dip G's direct target. We demonstrate that dip G can bind to the middle domain, but not the N nor C-terminus of HSP90. Binding to the middle domain results in degradation of ER, an HSP90 client protein, but does not upregulate proteins involved in heat shock response, which contribute to resistance to HSP90 inhibitors. We also provide additional insight on the biology of HSP90 inhibition.

Figure 2-1

(A) Western blot of ER levels in MCF7 cells treated with DMSO, 10 nM 17β-estradiol (E2), 1μM 4-hydroxytamoxifen (OHT), 100 nM fulvestrant, 1μM tanespimycin, or 10 μM dip G for 6 hours. MCF7 cells were hormone starved for 3 days prior to treatment. Actin was used as a loading control. Three independent experiments with 3 biological replicates. One representative blot is shown. (B) Quantification is shown as the mean ± SD. Individual biological replicates are plotted.

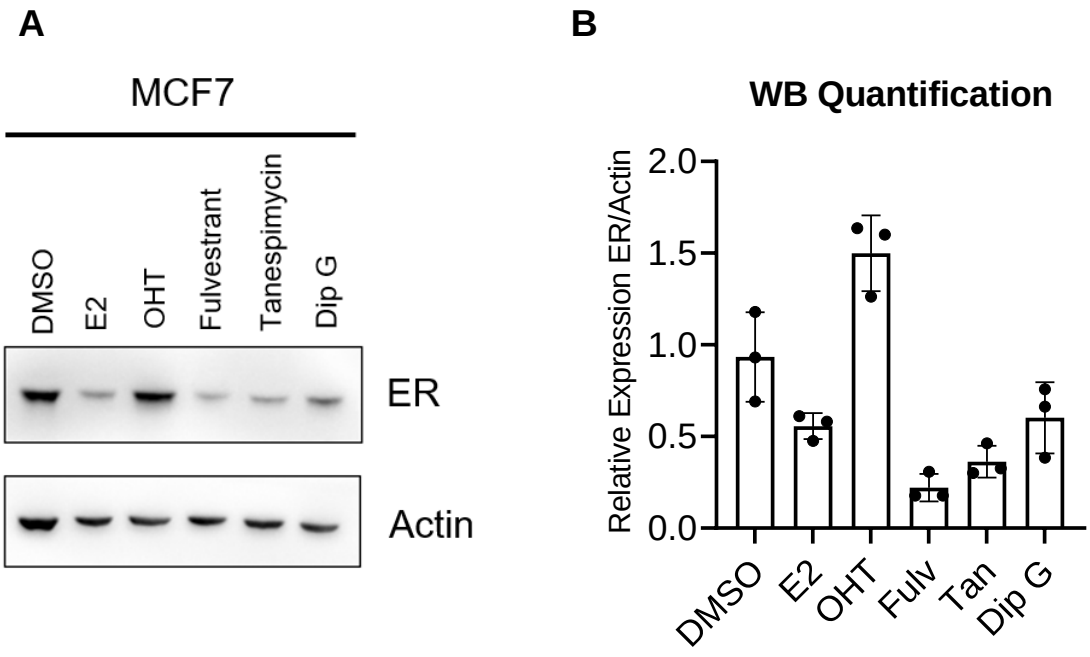

Figure 2-2

ELISA assay of ER levels in MCF7 cells following treatment with (A) DMSO, 1, 10, 50, 100, and 1000 nM of fulvestrant, or (B) 0.1, 1, 5, 7.5, and 10 μM dip G or (C) 0, 0.25, 0.5, 1, 2, and 4 μM tanespimycin for 24 hours. MCF7 cells were hormone starved for 3 days prior to treatment. ER protein levels were normalized to either $1x10^7$ cells (fulvestrant and dip G) or total protein concentration (tanespimycin). Two independent experiments with three biological replicates and two technical replicates (fulvestrant and dip G). Three independent experiments with three biological replicates and two technical replicates (tanespimycin).

A

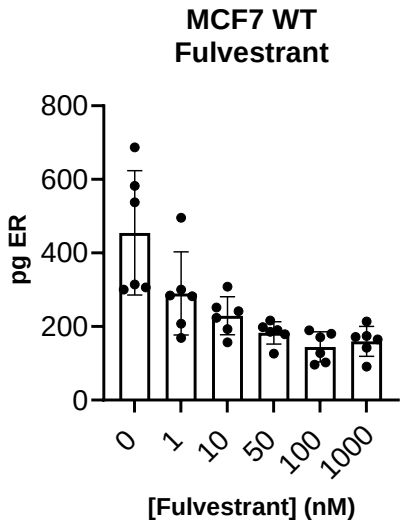
MCF7 WT
Fulvestrant
pg ER
800
600
400
200
0
0
1
10
50
100
1000
[Fulvestrant] (nM)

B

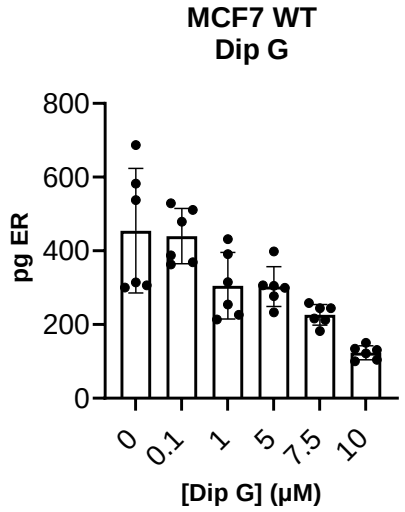
MCF7 WT
Dip G
pg ER
800
600
400
200
0
0
0.1
1
5
7.5
10
[Dip G] (µM)

C

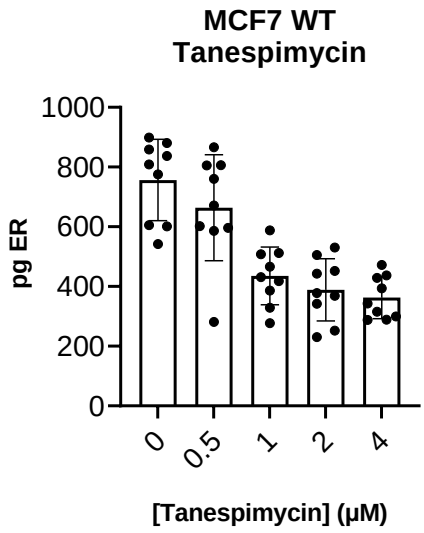
MCF7 WT
Tanespimycin
pg ER
1000
800
600
400
200
0
0
0.5
1
2
4
[Tanespimycin] (µM)

Figure 2-3

(Upper) Molecular structure of diptoindonesin G. (Lower) Western blot of ER levels in MCF7 cells treated with DMSO, 1, 5, or 10 μM dip G for 24 hours. MCF7 cells were hormone starved for 3 days prior to treatment. Actin was used as a loading control. Three independent experiments with three biological replicates. One representative blot is shown.

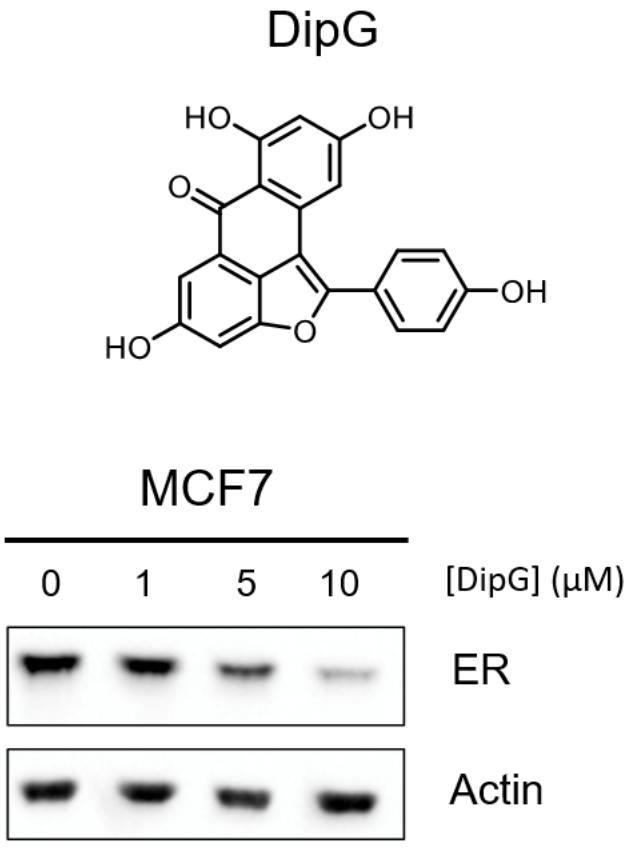

Figure 2-4

(Upper) Molecular structure of deoxy-diptoindonesin G. (Lower) Western blot of ER levels in MCF7 cells treated with DMSO, 1, 2.5, 5, or 10 μM deoxy-dip G for 24 hours. MCF7 cells were hormone starved for 3 days prior to treatment. Actin was used as a loading control. Three independent experiments with three biological replicates. One representative blot is shown.

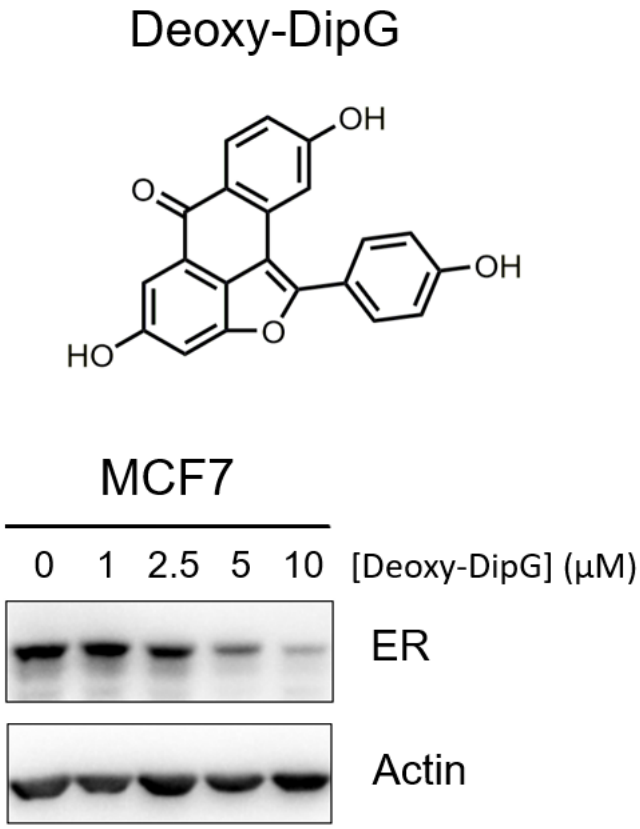

Figure 2-5

(A) Western blot of ER and ubiquitin levels in MCF7 cells treated with DMSO, 10 μM dip G, 0.5 μM bortezomib (BORT), or a combination of the two compounds for 6 hours. MCF7 cells were hormone starved for 3 days prior to treatment. Actin was used as a loading control. Four independent experiments with four biological replicates. One representative blot is shown. (B) Quantification is shown as the mean ± SD. Individual biological replicates are plotted. Significance was determined using an unpaired Welch's t-test.

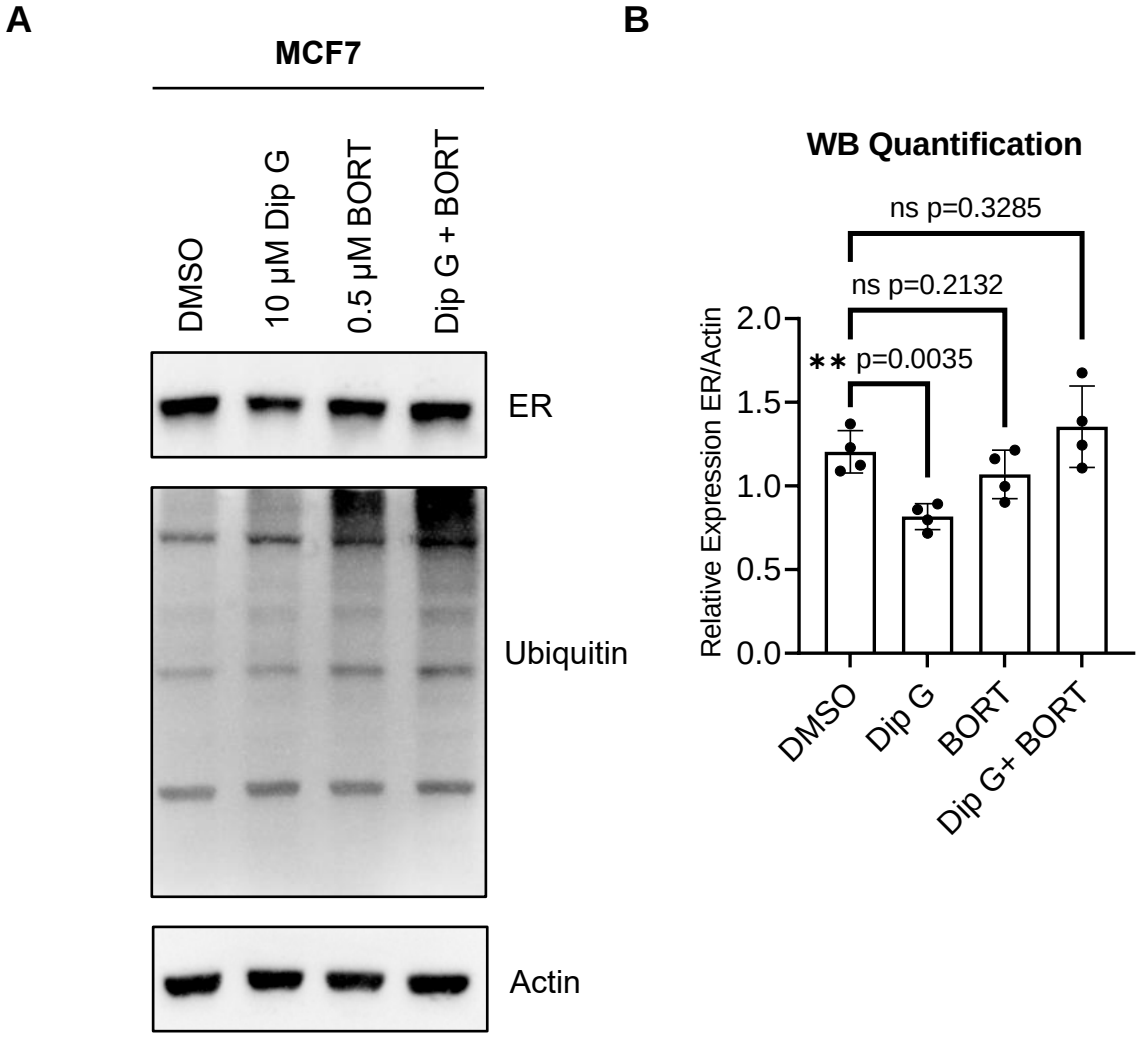

Figure 2-6

Volcano plot of proteins significantly down- (green) and upregulated (red) in MCF7 LCC2 shControl (left) and LCC2 shCHIP (right) cells in response to 10 μM dip G 10 μM dip G for 24 hours. Log_2 (fold change) is plotted on the x-axis and significance, or the $-log_{10}$(P-value) is plotted on the y-axis. Proteins not significantly changed are indicated in black. ESR1 (ER), highlighted in cyan, was significantly decreased by dip G treatment in both cell lines. One independent experiment with three biological replicates with three technical replicates.

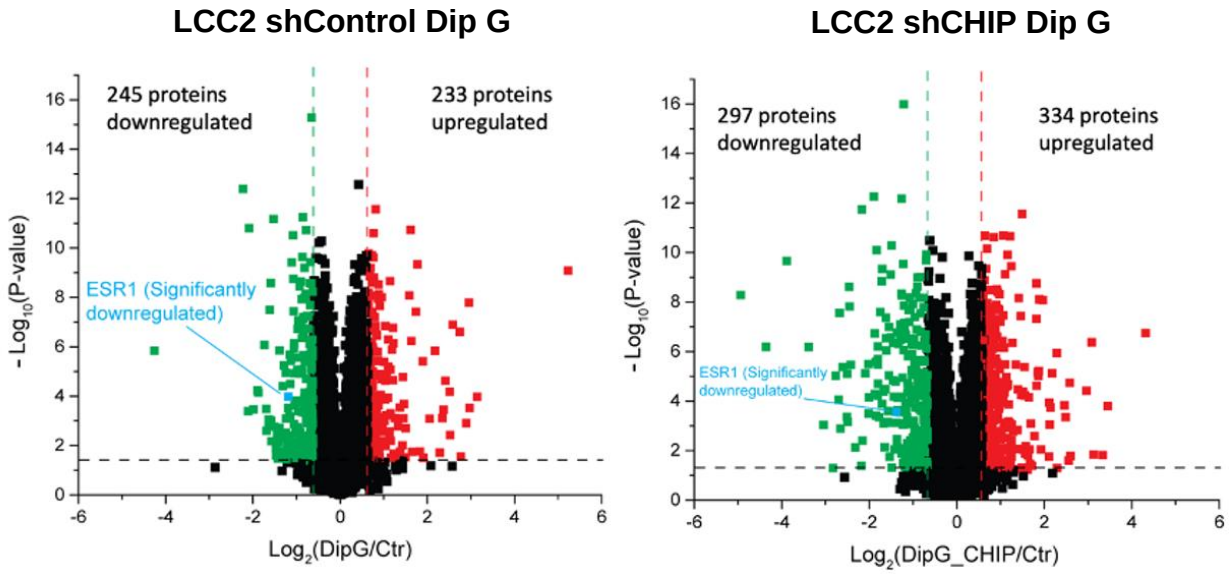

Figure 2-7

Venn diagrams of the (A) total proteins significantly changed by 10 µM dip G in LCC2 shControl and shCHIP cells (B) proteins significantly upregulated by 10 µM dip G in LCC2 shControl and shCHIP cell and upregulated and (C) proteins significantly downregulated by 10 µM dip G in LCC2 shControl and shCHIP cells.

A

Total Proteins Changed by Dip

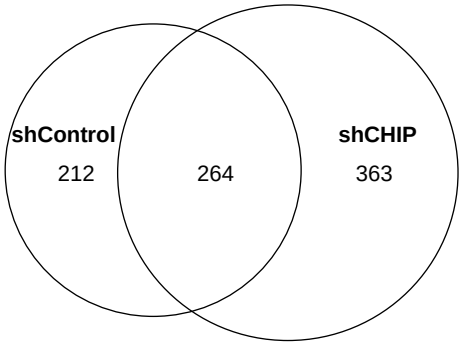

B

Proteins Upregulated by Dip G

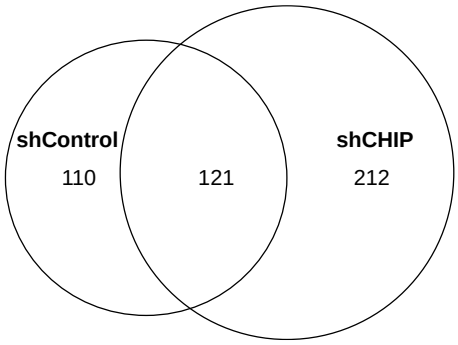

C

Proteins Downregulated by Dip G

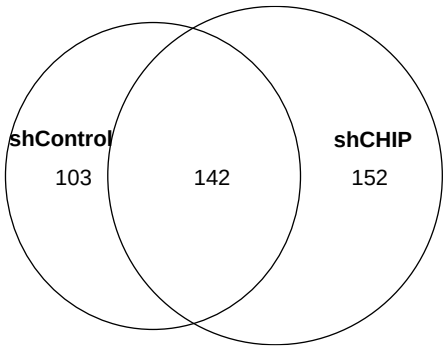

Figure 2-8

Western blot of ER and CHIP levels in MCF7 shControl and MCF7 shCHIP cells treated with DMSO or 10 μM dip G for 24 hours. MCF7 cells were hormone starved for 3 days prior to treatment. Actin was used as a loading control. Three independent experiments with three biological replicates. One representative blot is shown. (B) Quantification is shown as the mean ± SD. Individual biological replicates are plotted. Significance was determined using an unpaired Welch's t-test.

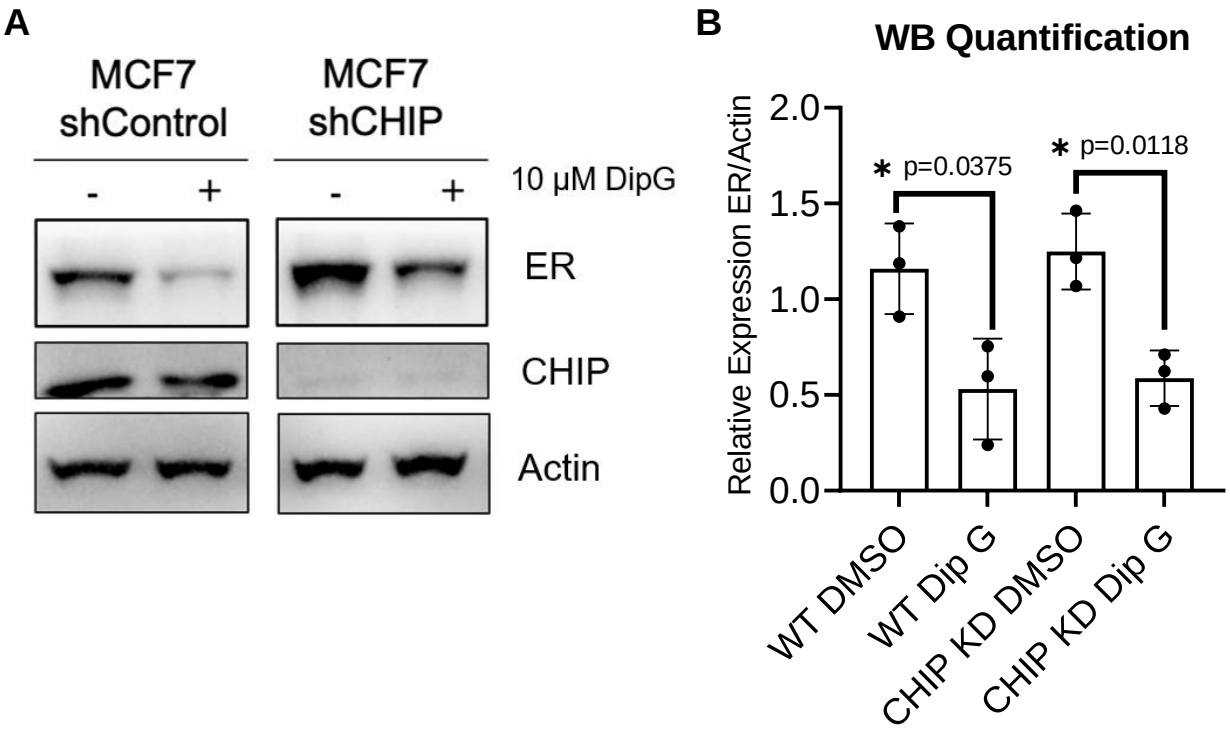

Figure 2-9

(A) Western blot of CHIP levels in MCF7 CHIP KO clones #1 and #2 cells. Actin was used as a loading control. Three independent experiments with three biological replicates. One representative blot is shown. (B) Volcano plot of proteins significantly downregulated (blue) and upregulated (red) in MCF7 CHIP KO cells Log_2 (fold change) is plotted on the x-axis and significance, or the $-log_{10}$(P-value) is plotted on the y-axis. CHIP was the most significantly downregulated protein in the entire dataset. One independent experiment with three biological replicates with three technical replicates.

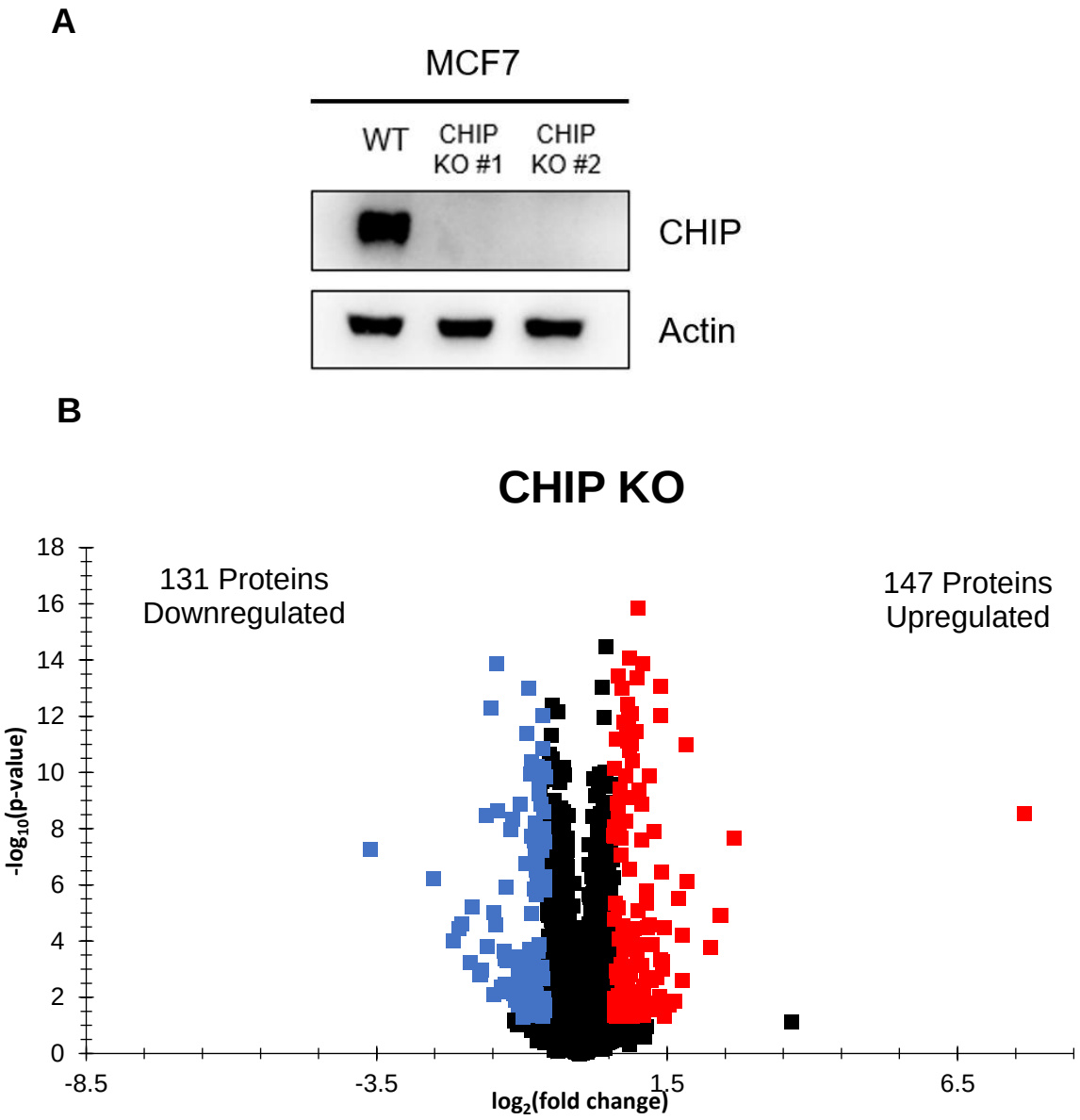

Figure 2-10

(A) Western blot of ER and CHIP levels in MCF7 parental and CHIP KO clone #1 and #2 cells treated with DMSO or 10 μM dip G for 24 hours. Cells were hormone starved for 3 days prior to treatment. Actin was used as a loading control. Five independent experiments with five biological replicates. One representative blot is shown. (B) Quantification is shown below as the mean ± SD. Individual biological replicates are plotted. Significance was determined using an unpaired Welch's t-test.

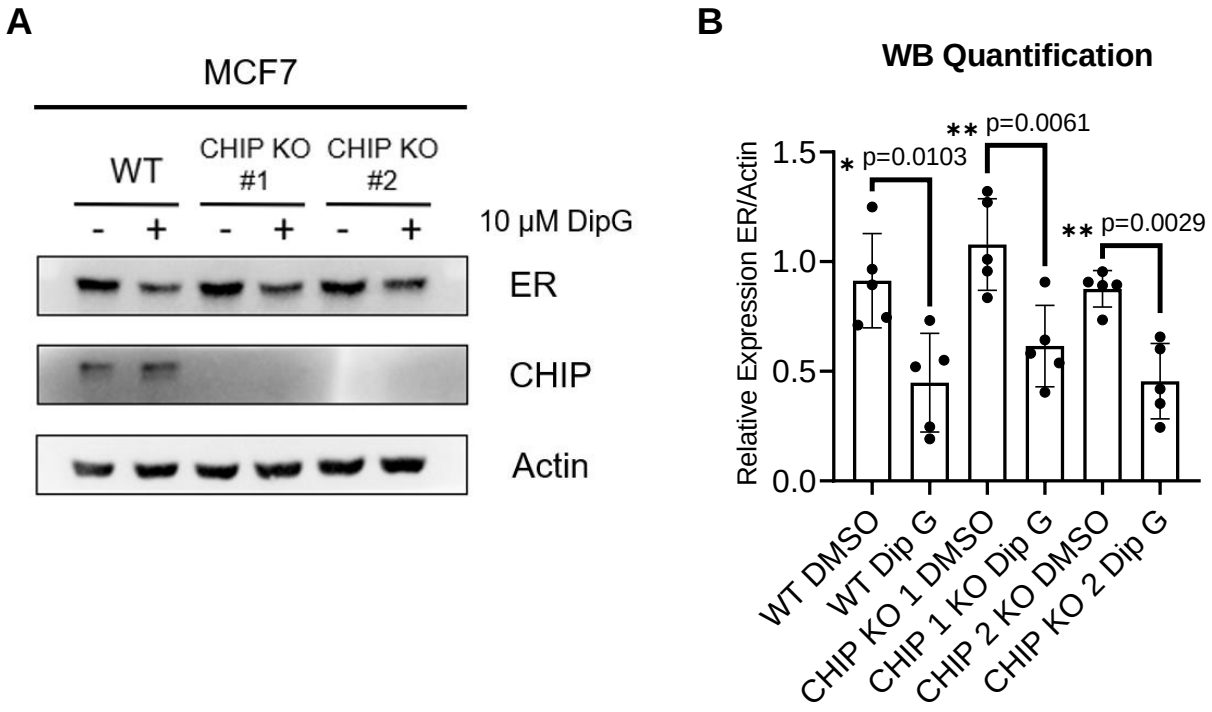

Figure 2-11

Western blot of ER and CHIP levels in MCF7 parental and CHIP KO clone #1 cells treated with DMSO or 10 μM deoxy-dip G for 24 hours. Cells were hormone starved for 3 days prior to treatment. Actin was used as a loading control. Five independent experiments with five biological replicates. One representative blot is shown. Quantification is shown below as the mean ± SD. Individual biological replicates are plotted. Significance was determined using an unpaired Mann-Whitney test.

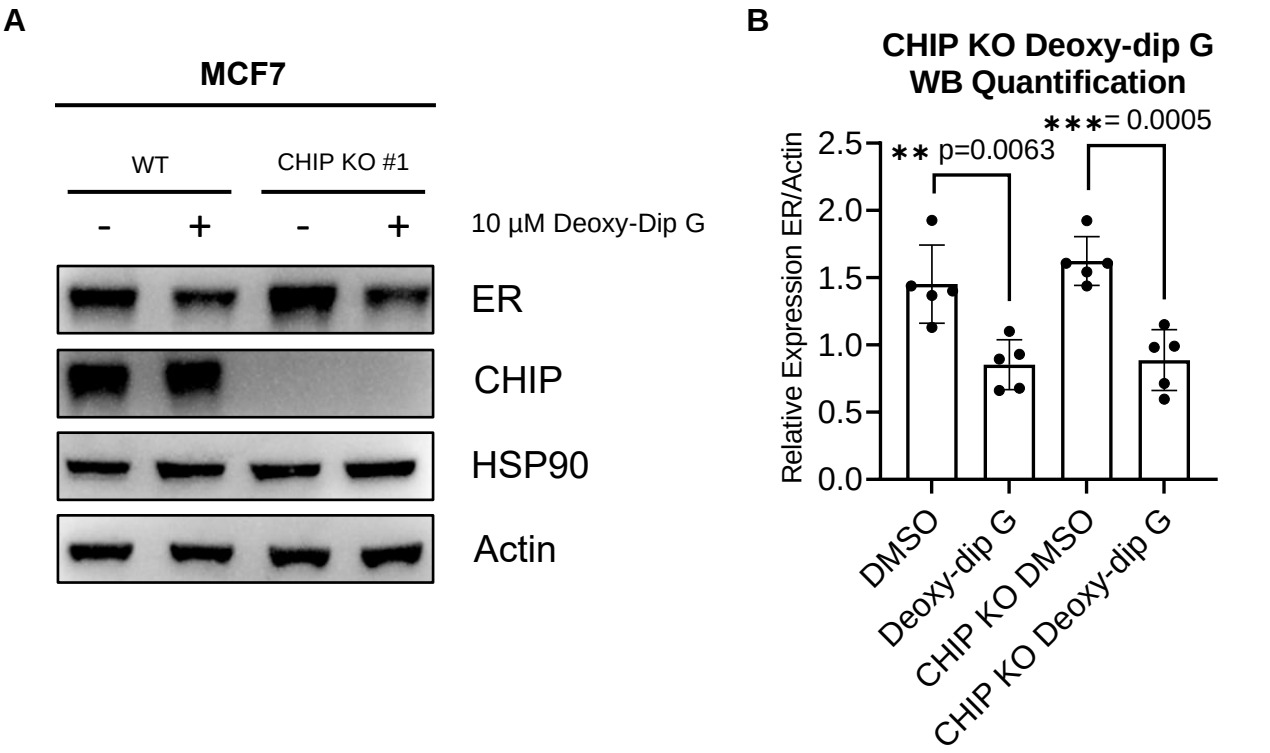

Figure 2-12

(A) Western blot of ER levels in MCF7 parental and CHIP KO clones #1 and 2 cells treated with DMSO or 10 nM E2 for 6 hours. Cells were hormone starved for 3 days prior to treatment. Actin was used as a loading control. Four independent experiments with one four biological replicates. One representative blot is shown. (B) Quantification is shown below as the mean ± SD. Individual biological replicates are plotted.

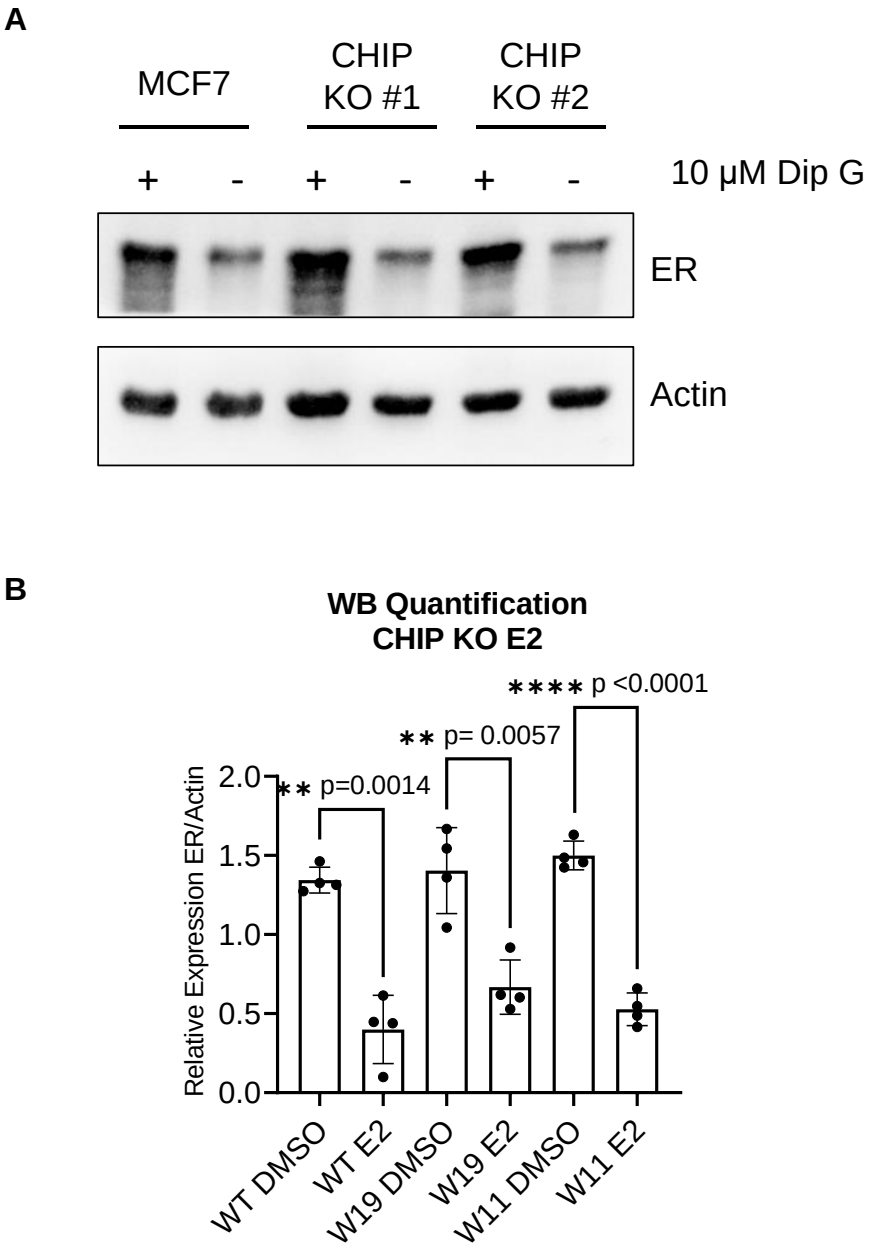

Figure 2-13

(A) Western blot of ER levels in MCF7 parental and CHIP KO clones #1 and 2 cells treated with DMSO or 2 µM tanespimycin for 6 hours. Cells were hormone starved for 3 days prior to treatment. Actin was used as a loading control. Four independent experiments with four biological replicates. One representative blot is shown. (B) Quantification is shown as the mean ± SD. Individual biological replicates are plotted. Significance was determined using an unpaired Welch's t-test.

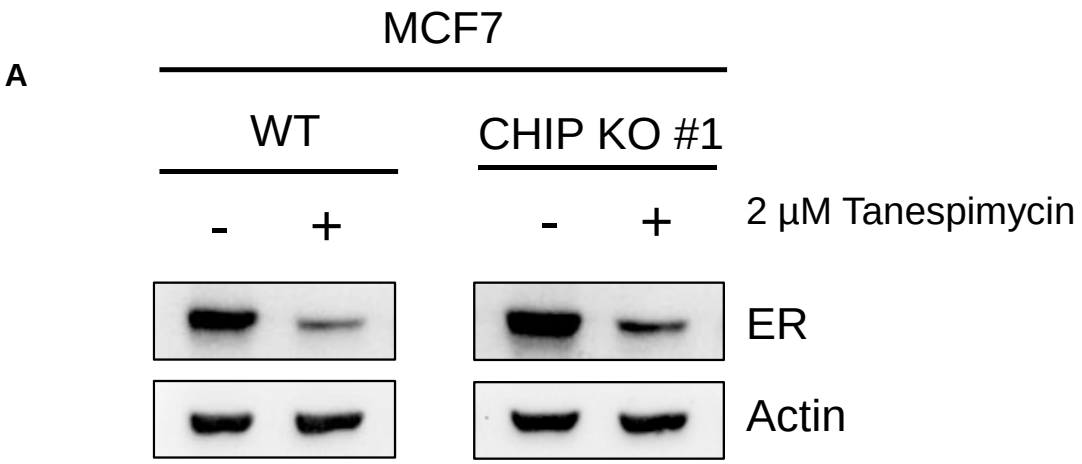

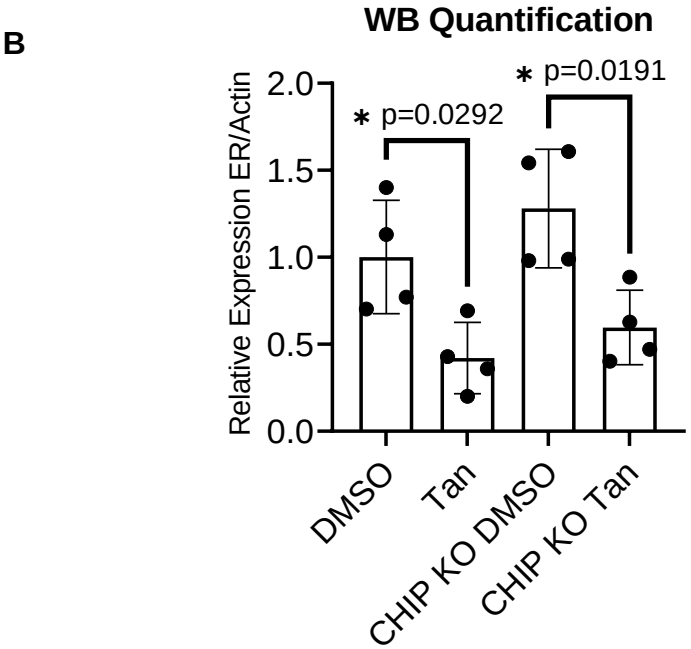

Figure 2-14

Western blot of ER, HER2, MDM2, CHIP, E6AP, and actin in 13 different breast cancer cell lines, characterized by either ER expression, HER2 expression, or no expression of either receptor. Actin was used as a loading control. One representative blot is shown.

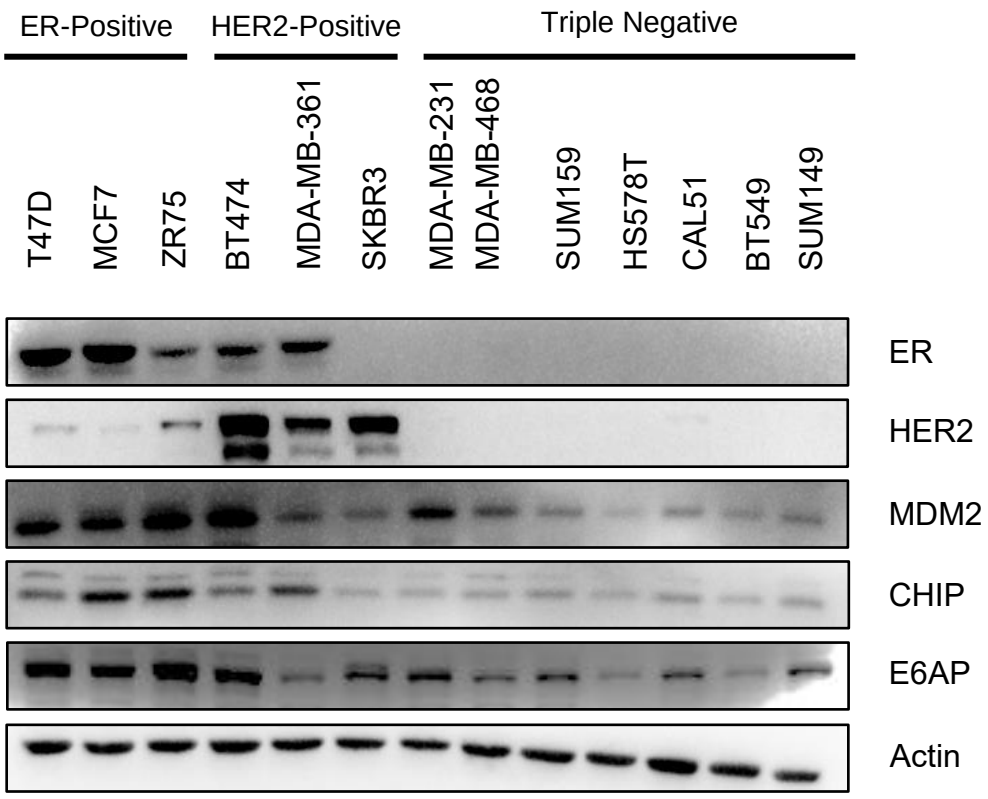

Figure 2-15

Molecular structure of diptoindonesin G (left) and dip G alkyne (right)

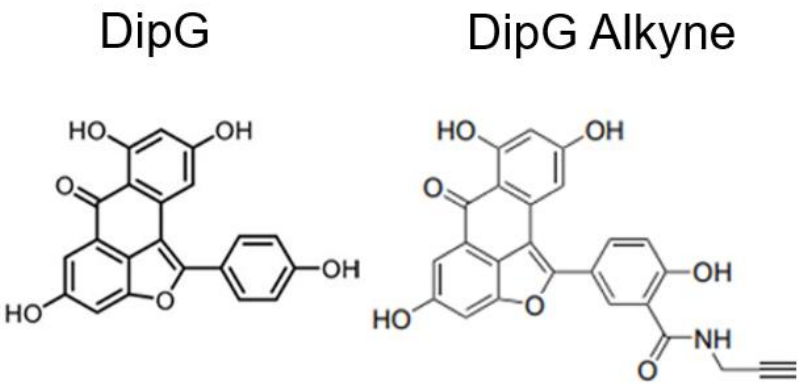

Figure 2-16

Schematic of CLICK chemistry workflow and identification of the dip G interactome

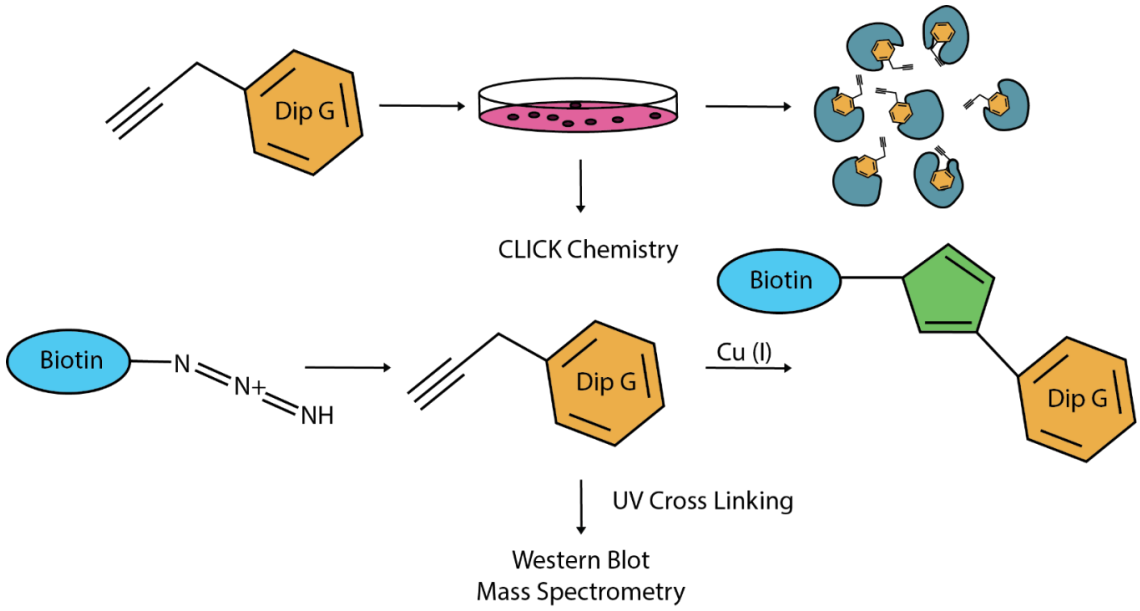

Figure 2-17

Western blot of HSP90 and CHIP in BT474 cells treated with DMSO or 20 μM alkyne dip G and subjected to CLICK chemistry.

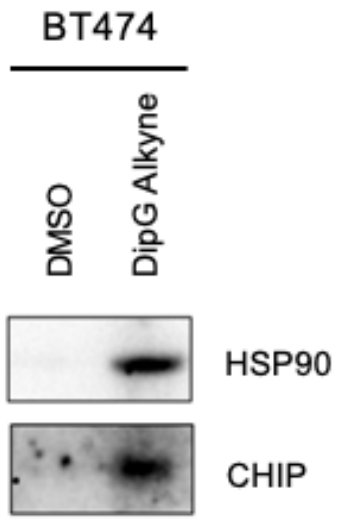

Figure 2-18

Excitation and emission spectrum of deoxy-dip G (nm).

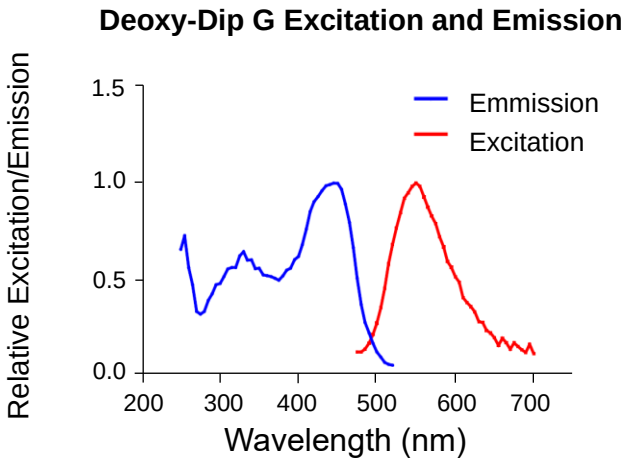

Figure 2-19

(A) Fluorescence polarization competition assays of ER and fluormone ES2 competed against 17β-estradiol. Fluorescence polarization (in units of mP) is plotted on the y-axis (linear scale) and the competitor molecule concentration is plotted on the x-axis (logarithmic scale). The concentration of Fluromone ES2 Green was 4.5 nM. The concentration of ER was 80 nM. Fluorescence polarization plots measuring the K_d (bottom right corner of each plot) of (B) HSP90 and geldanamycin-FITC and (C) CHIP and 5-FAM-MEEVD. Fluorescence polarization (in units of mP) is plotted on the y-axis (linear scale) and the protein concentration is plotted on the x-axis (logarithmic scale). The concentration of geldanamycin-FITC used was 20 nM. The concentration of 5FAM-MEEVD was 20 nM.

A

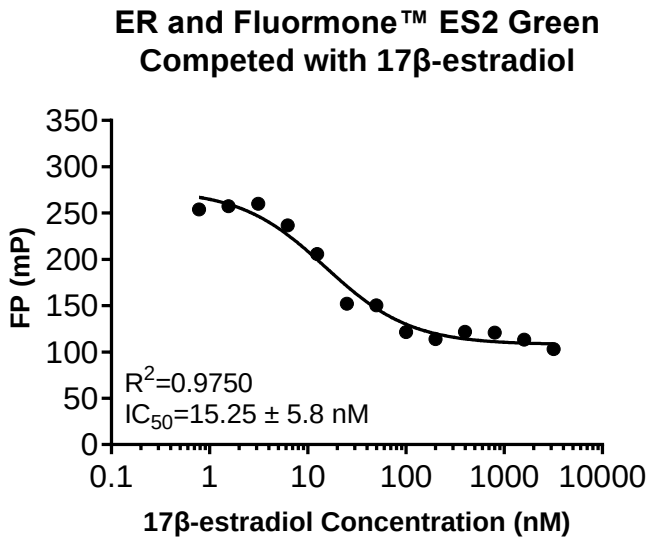
ER and Fluormone™ ES2 Green
Competed with 17β-estradiol
FP (mP)
350
300
250
200
150
100
50
0
0.1
1
10
100
1000
10000
R2=0.9750
IC50=15.25 ± 5.8 nM
17β-estradiol Concentration (nM)

B

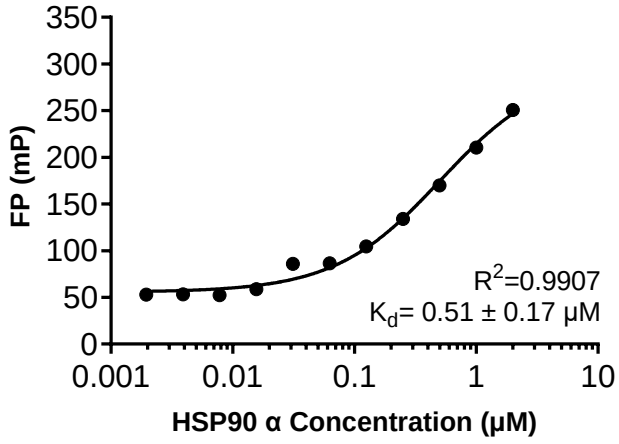
HSP90 α and Geldanamycin-FITC
FP (mP)
350
300
250
200
150
100
50
0
0.001
0.01
0.1
1
10
R2=0.9907
Kd= 0.51 ± 0.17 μM
HSP90 α Concentration (μM)

C

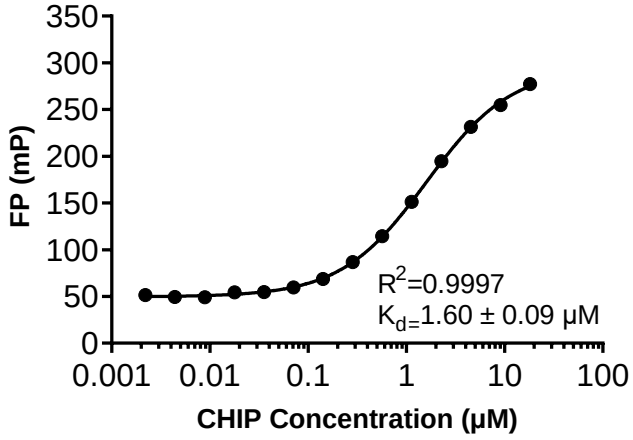
CHIP and 5FAM-MEEVD
FP (mP)
350
300
250
200
150
100
50
0
0.001
0.01
0.1
1
10
100
R2=0.9997
Kd=1.60 ± 0.09 μM
CHIP Concentration (μM)

Figure 2-20

Fluorescence polarization plots measuring the K_d (bottom right corner of each plot) of deoxy-dip G to (A) ER, (B) HSP90 and (C) CHIP. Fluorescence polarization (in units of mP) is plotted on the y-axis (linear scale) and the protein concentration is plotted on the x-axis (logarithmic scale). The concentration of deoxy-dip G used was 1 μM.

A

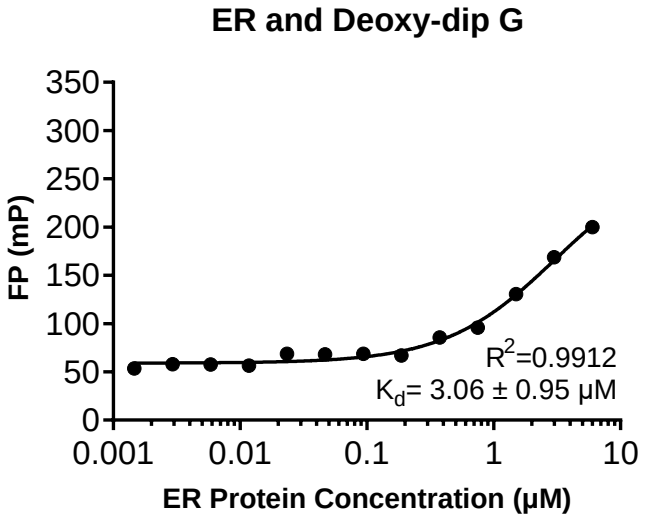
ER and Deoxy-dip G
FP (mP)
350
300
250
200
150
100
50
0
0.001
0.01
0.1
1
10
ER Protein Concentration (μM)
R2=0.9912
Kd= 3.06 ± 0.95 μM

B

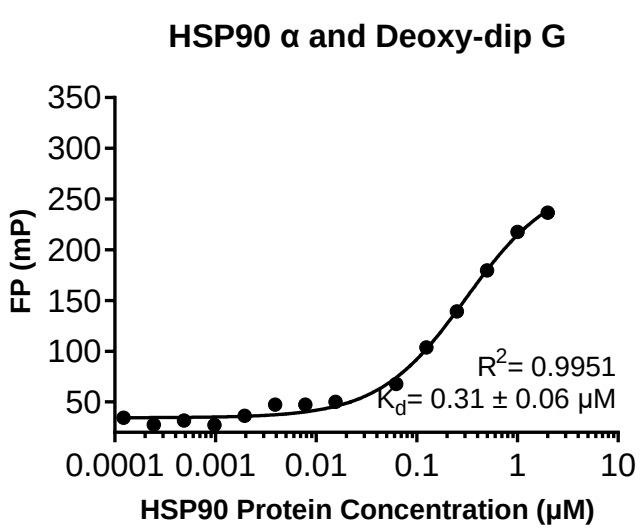
HSP90 α and Deoxy-dip G
FP (mP)
350
300
250
200
150
100
50
0.0001
0.001
0.01
0.1
1
10
HSP90 Protein Concentration (μM)
R2= 0.9951
Kd= 0.31 ± 0.06 μM

C

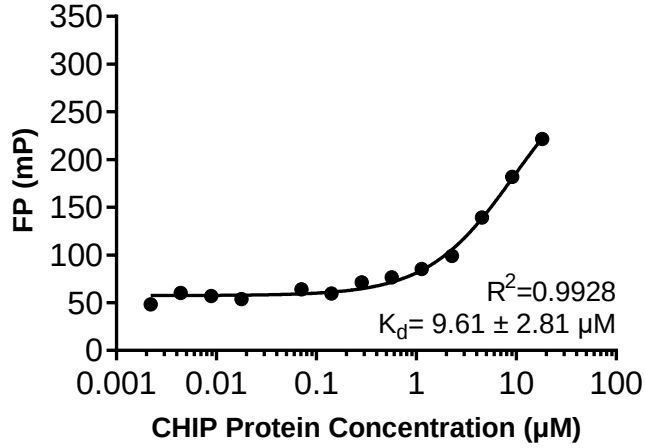
CHIP and Deoxy-dip G
FP (mP)
350
300
250
200
150
100
50
0
0.001
0.01
0.1
1
10
100
CHIP Protein Concentration (μM)
R2=0.9928
Kd= 9.61 ± 2.81 μM

Figure 2-21

Fluorescence polarization competition assays of (A) geldanamycin, (B) radicicol (C) ATP, (D) novobiocin, (E) GTP, or (E) EGCG against deoxy-dip G and HSP90. Fluorescence polarization (in units of mP) is plotted on the y-axis (linear scale) and the competitor molecule concentration is plotted on the x-axis (logarithmic scale). The concentration of deoxy-dip G used was 1 μM.

A

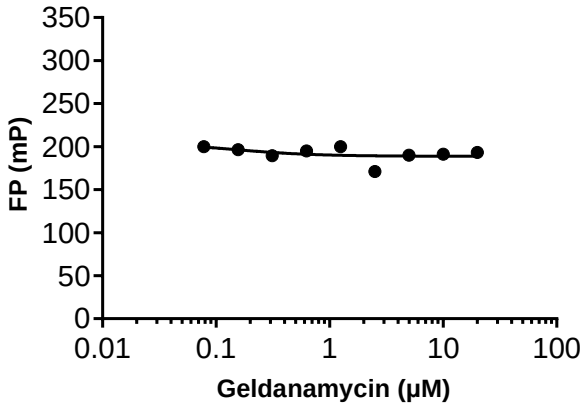
HSP90 and Deoxy-dip G
Competed With Geldanamycin
FP (mP)
350
300
250
200
150
100
50
0
0.01
0.1
1
10
100
Geldanamycin (μM)

D

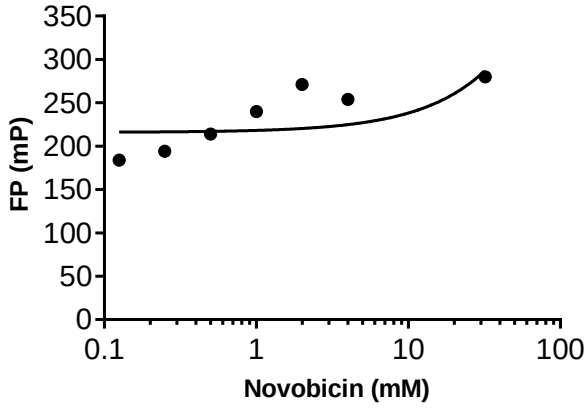
HSP90 and Deoxy-dip G
Competed With Novobiocin
FP (mP)
350
300
250
200
150
100
50
0
0.1
1
10
100
Novobicin (mM)

B

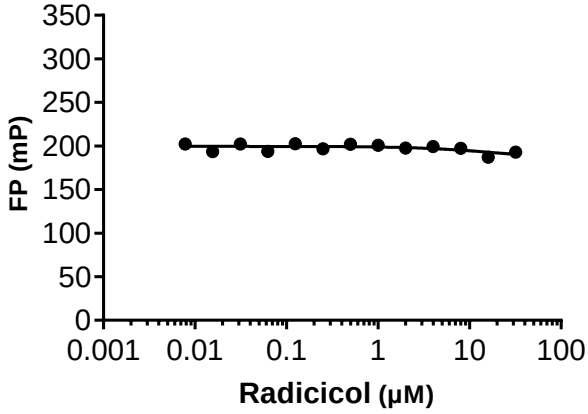
HSP90 and Deoxy- Dip G
Competed With Radicicol
FP (mP)
350
300
250
200
150
100
50
0
0.001
0.01
0.1
1
10
100
Radicicol (μM)

E

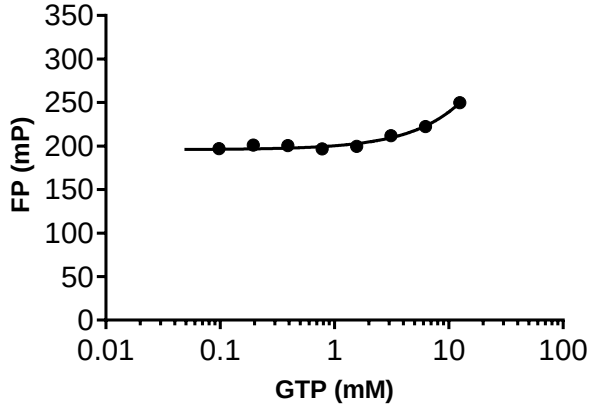
HSP90 and Deoxy-dip G
Competed With GTP
FP (mP)
350
300
250
200
150
100
50
0
0.01
0.1
1
10
100
GTP (mM)

C

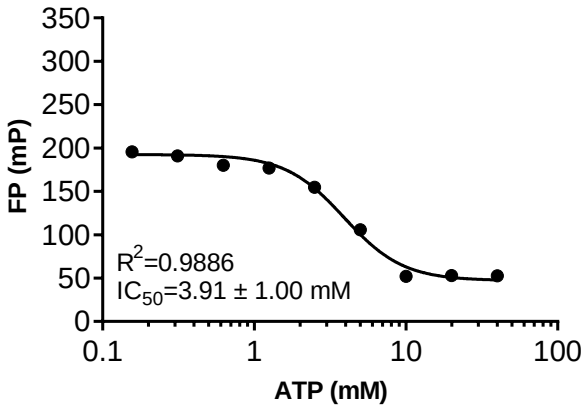
HSP90 and Deoxy-dip G
Competed With ATP
FP (mP)
350
300
250
200
150
100
50
0
R2=0.9886
IC50=3.91 ± 1.00 mM
0.1
1
10
100
ATP (mM)

E

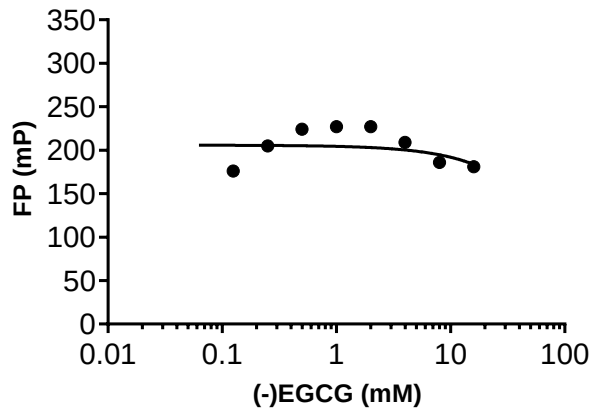
HSP90 and Deoxy-dip G
Competed With EGCG
FP (mP)
350
300
250
200
150
100
50
0
0.01
0.1
1
10
100
(-)EGCG (mM)

Figure 2-22

Coomassie stained SDS-PAGE gel of full length HSP90 (FL-HSP90), purified HSP90 N-domain (N), HSP90 middle domain (M), and HSP90 C domain (C). The expected molecular weights are as follows: FL-HSP90- 90 KDa, GST-HSP90 N (AA 9-236)-55KDa, HSP90 N- 26 KDa, GST-HSP90 M (AA 272-617)-62 KDa, HSP90 M- 41 KDa, GST-HSP90 C (AA 626-732)-38 KDa, HSP90 C-11.91 KDa, GST- 26 KDa

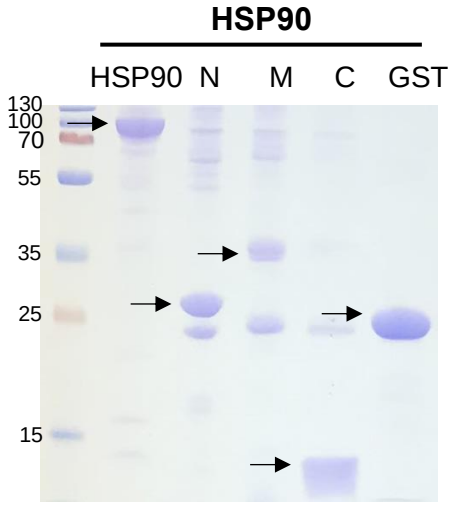

Figure 2-23

Fluorescence polarization plots measuring the K_d (bottom right corner of each plot) of deoxy-dip G to (A) HSP90 M domain, (B) HSP90 N-terminus and (C) HSP90 C-terminus. Fluorescence polarization (in units of mP) is plotted on the y-axis (linear scale) and the protein concentration is plotted on the x-axis (logarithmic scale). The concentration of deoxy-dip G used was 1 μM.

A

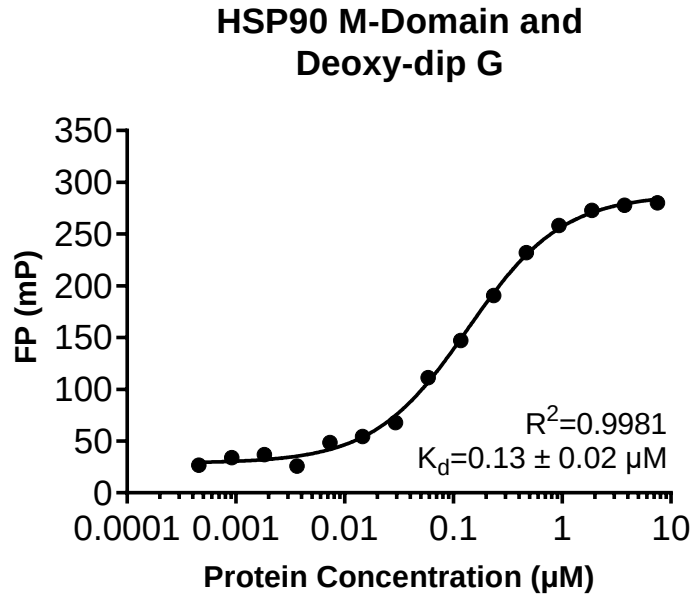
HSP90 M-Domain and
Deoxy-dip G
FP (mP)
350
300
250
200
150
100
50
0
0.0001 0.001 0.01 0.1 1 10
Protein Concentration (μM)
R2=0.9981
Kd=0.13 ± 0.02 μM

B

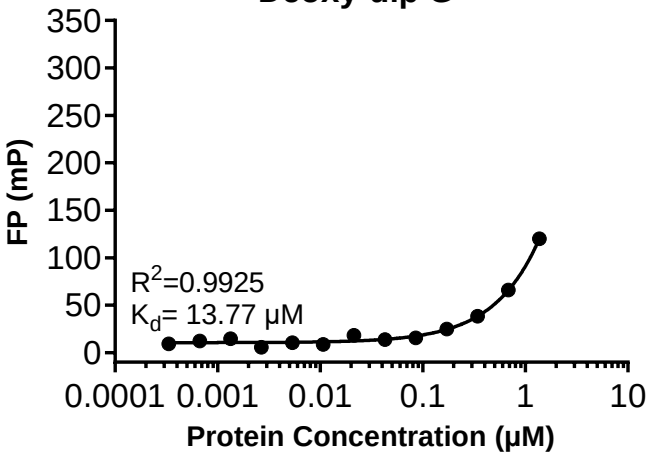
HSP90 N-Domain and
Deoxy-dip G
FP (mP)
350
300
250
200
150
100
50
0
0.0001 0.001 0.01 0.1 1 10
Protein Concentration (μM)
R2=0.9925
Kd= 13.77 μM

C

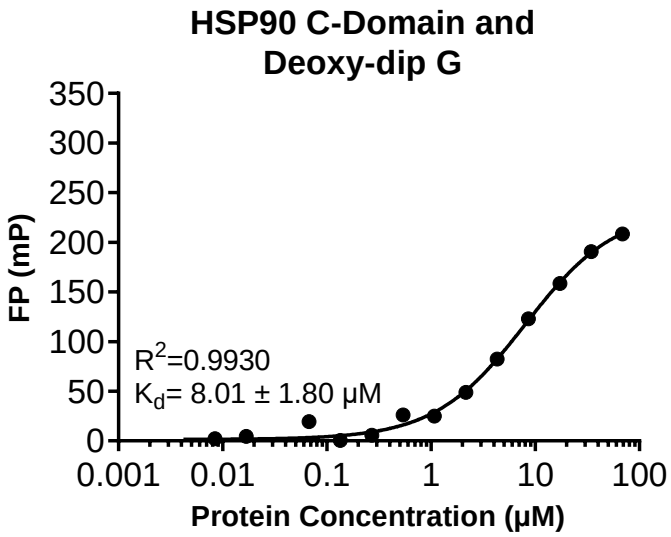
HSP90 C-Domain and
Deoxy-dip G
FP (mP)
350
300
250
200
150
100
50
0
0.001 0.01 0.1 1 10 100
Protein Concentration (μM)
R2=0.9930
Kd= 8.01 ± 1.80 μM

Figure 2-24

(A) Western blot of ER levels in MCF7 cells pre-treated with 10 μM dip G or 1 μM tanespimycin for 0.5 hours and then treated with DMSO, 10 nM 17-β estradiol (E2), 1μM 4-hydroxytamoxifen (OHT), 100 nM fulvestrant, 1μM tanespimycin, or 10 μM dip G for 5.5 hours. MCF7 cells were hormone starved for 3 days prior to treatment. Actin was used as a loading control. Three independent experiments with three biological replicates (B) Quantification is shown as the mean ± SD. Individual biological replicates are plotted. Significance was determined using a Welch's t-test.

A

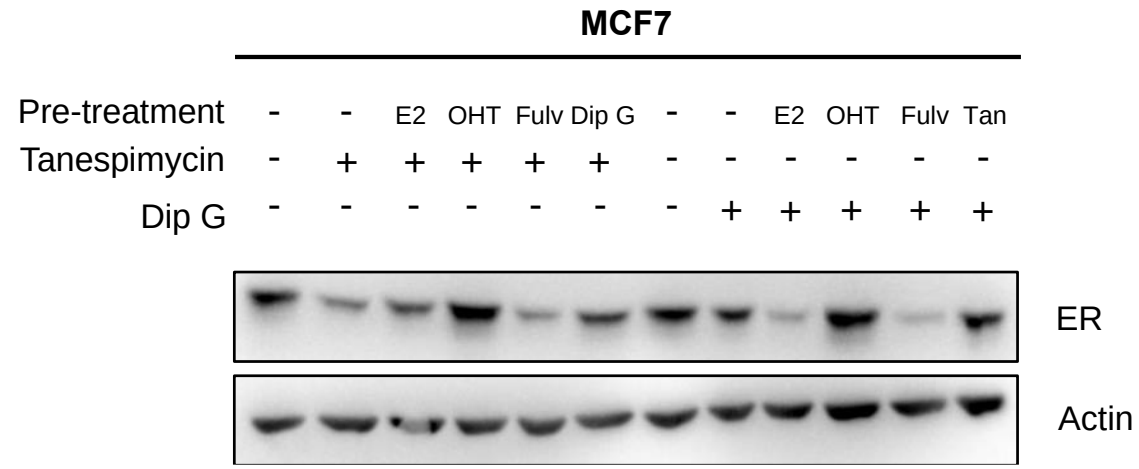
MCF7
Pre-treatment - - E2 OHT Fulv Dip G - - E2 OHT Fulv Tan
Tanespimycin - + + + + + - - - - - -
Dip G - - - - - - - + + + + +
ER
Actin

B

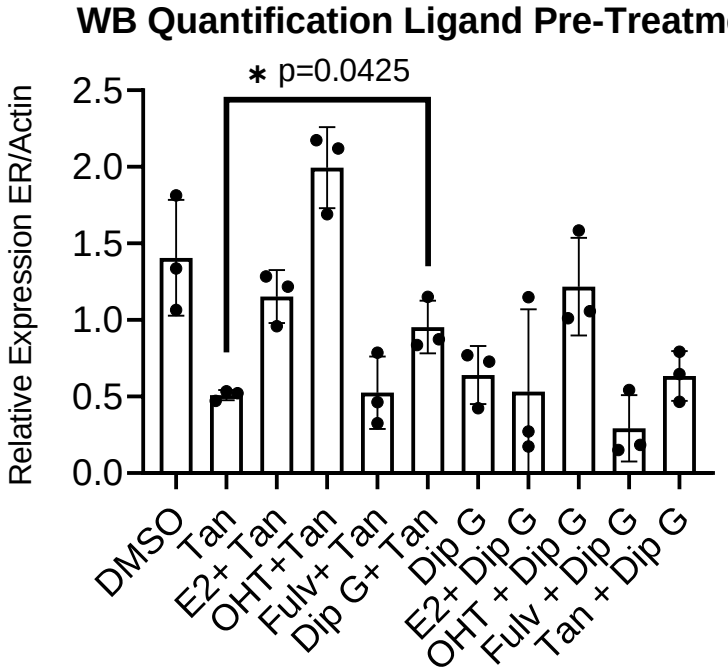
WB Quantification Ligand Pre-Treatment
∗ p=0.0425
Relative Expression ER/Actin
2.5
2.0
1.5
1.0
0.5
0.0
DMSO
Tan
E2+ Tan
OHT+Tan
Fulv+ Tan
Dip G+ Tan
Dip G
E2+ Dip G
OHT + Dip G
Fulv + Dip G
Tan + Dip G

Figure 2-25

(A) Western blot of ER levels in MCF7 cells treated with 10 μM deoxy-dip G, 1 μM tanespimycin or both compounds for 6 hours. MCF7 cells were hormone starved for 3 days prior to treatment. Actin was used as a loading control. Four independent experiments with four biological replicates (B) Quantification is shown as the mean ± SD. Individual biological replicates are plotted. Significance was determined using a Welch's t-test.

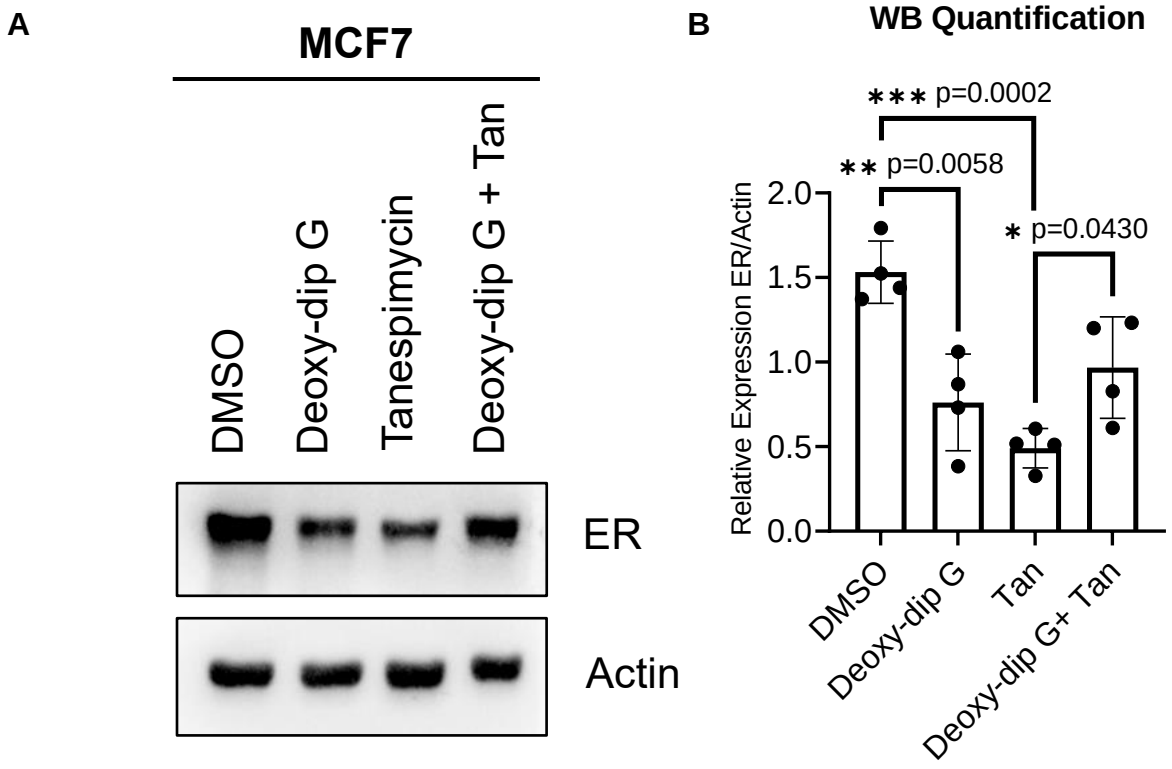

Figure 2-26

RT-qPCR analysis of HSP27, HSP40, HSP70, and HSP90 levels in MCF7 cells treated with DMSO, 10 μM dip G, 2 μM tanespimycin, or 40 μM novobiocin for 3 hours. Four independent experiments with 4 biological replicates and three technical replicates for each biological replicate, except for HSP70, which only has three independent experiments and three biological replicates. Graphed is the mean ± SD. Individual biological replicates are plotted. Significance was determined using an unpaired Welch's t-test.

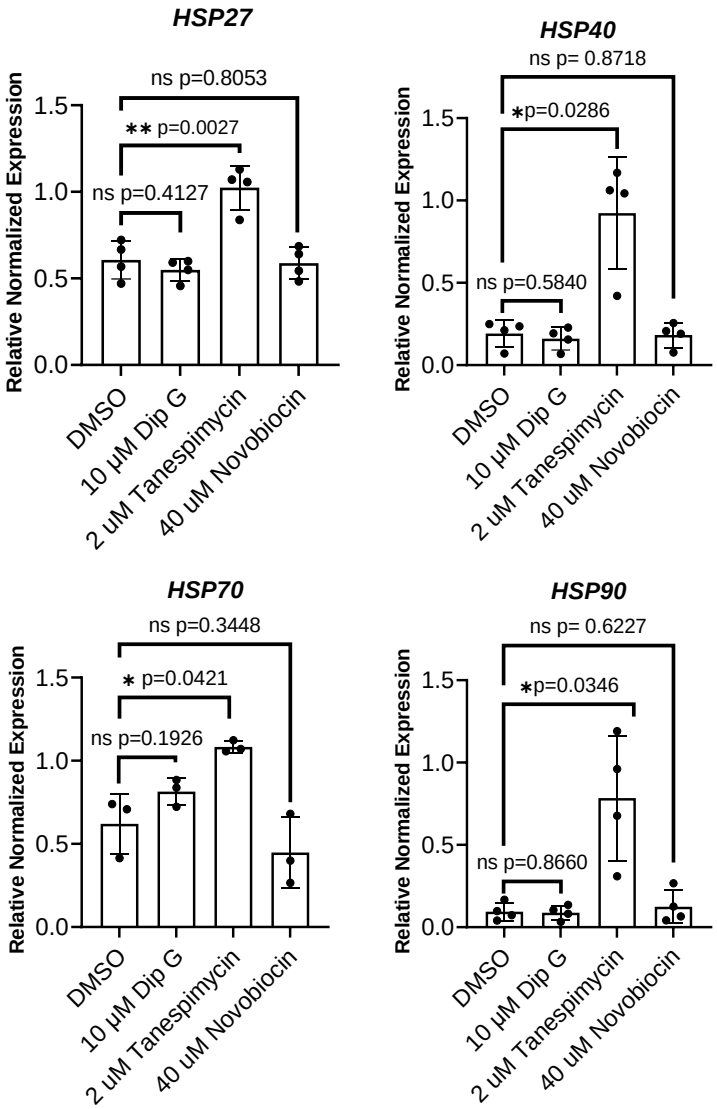

Figure 2-27

Western blot of ER levels in MCF7 cells treated with DMSO, 10 μM dip G, 1 μM tanespimycin, or a combination of both compounds for 6 hours. MCF7 cells were hormone starved for 3 days prior to treatment. Actin was used as a loading control.

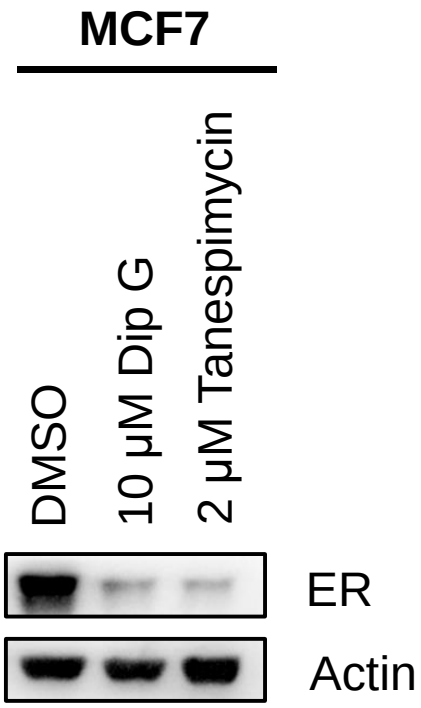

Figure 2-28

Volcano plot of proteins significantly downregulated (blue) and upregulated (red) in MCF7 cells treated with 2 μM Tanespimycin (top) or 10 μM dip G (bottom). Log_2 (fold change) is plotted on the x-axis and significance, or the $-log_{10}$(P-value) is plotted on the y-axis. Proteins not significantly changed are indicated in black.

A

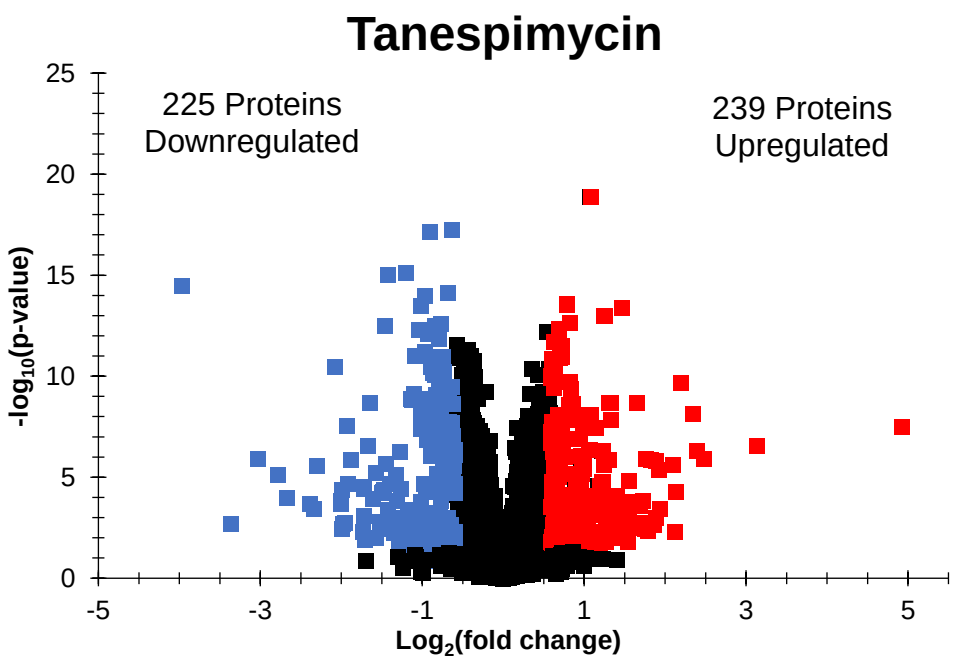

B

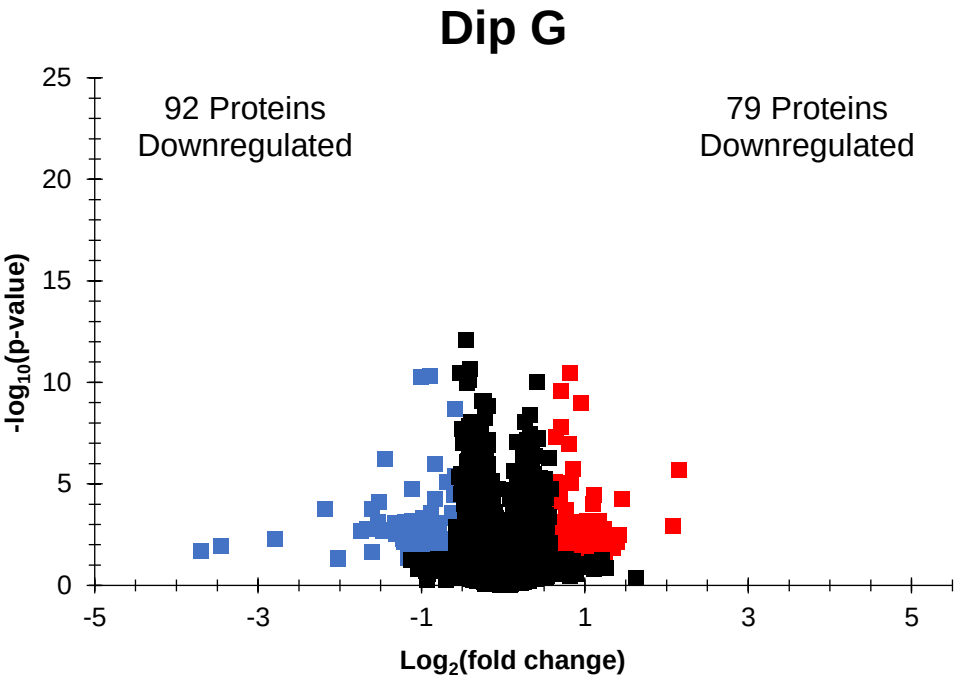

Figure 2-29

Venn diagrams comparing (A) proteins significantly upregulated and (B) significantly downregulated by both tanespimycin and dip G.

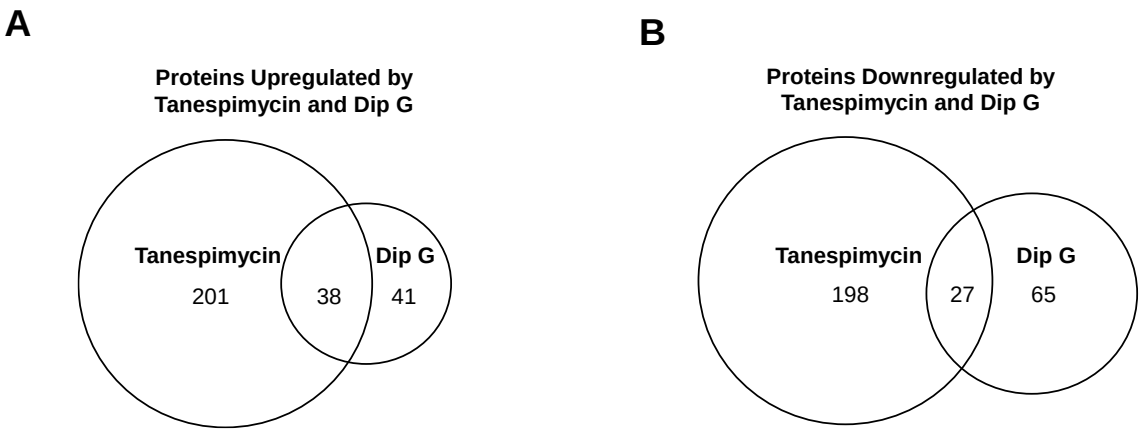

CHAPTER 3: Differential sensitivity to diptoindonesin G among models of endocrine resistance

Yidan Wang performed the RNAseq library preparation

Yidan Wang assisted with blood collection and oral gavage administration

Portions of this chapter were adapted from the following:

Donahue K, Xie H, Li M, Gao A, Ma M, Wang Y, Tipton R, Semanik N, Primeau T, Li S, Li L, Tang W, Xu W. Diptoindonesin G is a middle domain HSP90 modulator for cancer treatment. J Biol Chem. 2022 Nov 14:102700. doi: 10.1016/j.jbc.2022.102700. Epub ahead of print. PMID: 36395883.

Abstract

Our lab identified diptoindonesin G (dip G) as a novel HSP90 modulator that can promote degradation of HSP90 clients, including estrogen receptor α (ER), through the 26S proteasome by binding to the middle domain of HSP90. We hypothesized that because dip G can promote degradation of ER independently of the ligand-binding domain (LBD), it could be used therapeutically in the context of endocrine resistant breast cancer where ER is mutated in the LBD. We showed that treatment of ER mutant-expressing cells with dip G promoted degradation of wild type and mutant ER with similar efficacy, downregulated ER-regulated gene expression, and inhibited cell and patient-derived organoid proliferation. However, diptoindonesin G had no significant effect on breast tumor growth in patient derived xenograft mouse models, likely because therapeutic concentrations of dip G could not be reached in a mouse. Our data suggest that dip G circumvents some of the major obstacles associated with targeting mutant ER and may be developed as a new therapeutic avenue to treat many kinds of cancer, including endocrine resistant breast cancer. Medicinal chemistry and pharmacological optimization of dip G are required to develop dip G as a drug-like compound, particularly in the context of ER-positive breast cancer.

Introduction

Estrogen receptor α (ER)-positive tumors are associated with the most favorable prognosis, and ER expression predicts response to endocrine therapies. However, approximately 25% of patients with primary disease, and almost all patients with metastatic disease, will eventually develop resistance to these therapies[59]. One established mechanism of resistance in breast cancer patients treated with endocrine therapies is the development of hotspot missense mutations in the ligand-binding domain (LBD)[62–66]. *ESR1* LBD mutations result in a constitutively active receptor, and are associated with increased migratory capacity [62], and metastatic potential[67]. In addition, they have reduced ligand binding affinity, including to drugs that target the LBD, like fulvestrant, the only FDA-approved selective estrogen receptor degrader (SERD)[70–72]. Though fulvestrant has been shown to be effective in the metastatic setting, fulvestrant possesses dose-limiting pharmacological properties, such as low bioavailability, and must be administered intramuscularly[93,94,95,96]. Many new orally bioavailable SERDs are at various stages of clinical evaluation to directly antagonize mutant ER, but none is a pure antiestrogen like fulvestrant, and have mixed agonist and antagonist activity[103,104,106,110]. Therefore, there is unmet clinical need to develop mechanistically distinct treatment strategies that are insensitive to *ESR1* mutations, and do not rely on the ER LBD.

Diptoindonesin G (dip G) was originally reported by our group to be a modulator of the E3 ligase CHIP, and has been studied in the context of ER+ breast cancer[205,206], as well as in AML[207], triple negative breast cancer[208], and prostate cancer[209]. The anti-

cancer effects of dip G have also been observed in vivo in both triple negative breast cancer cell line MDA-MB-231-derived xenograft models[208], as well as castration-resistant prostate cancer 22Rv1-derived xenograft models[209].

This study focuses on determining dip G's potential clinical applications. In chapter 2, we show that dip G is not a CHIP modulator, as previously hypothesized[205]. Rather, dip G is an HSP90 modulator which binds to the middle domain of HSP90. Because dip G promotes ER degradation in an ER LBD- independent manner, we hypothesized that it could be used to target mutant ER. Unlike mainstay therapies that require binding to ER's LBD, dip G would be insensitive to *ESR1* mutations. We found that dip G promoted degradation of both wild type and mutant ER at similar efficacies. This resulted in subsequent inhibition of both ER-regulated gene expression and proliferation of breast cancer cell lines expressing mutant ER. In addition, we observed ER degradation, downregulation of ER target genes, as well as growth inhibition in ER-positive breast cancer patient derived xenograft organoids treated with dip G but did not observe any significant effects on tumor growth in vivo using patient-derived xenograft mouse models. Using a pan-cancer high throughput screen, we were able to identify additional cancer types that might respond favorably to dip G. Therefore, dip G represents a novel therapeutic avenue to treat many kinds of cancers, including endocrine-resistant breast cancer caused by ER ligand-binding domain mutations.

Results

Diptoindonesin G inhibits the Y537S ER mutant in vitro

Though many cancer models are sensitive to dip G, we hypothesized that dip G could be an effective therapy in the context of endocrine-resistant breast cancer, where mutations in the ligand-binding domain of ER reduce the efficacy of ER antagonists. Because dip G promotes ER degradation through HSP90 in a ligand-independent manner, we examined dip G's impact on ER Y537S degradation, transcriptional activity, and cell growth in MCF7 to test this hypothesis.

To quantitatively measure the ability of dip G to induce ER Y537S degradation, we treated MCF7 cells with a single allele knock-in of ER Y537S[221] with increasing concentrations of, fulvestrant, dip G, or tanespimycin for 24 hours. Heterozygous expression of both WT and Y537S ER recapitulates what is often observed in patients. ER levels were evaluated using an ER ELISA. Unlike in the WT ER context, where fulvestrant, dip G, and tanespimycin induced dose-dependent degradation of ER, ER Y537S protein was resistant to fulvestrant treatment, as observed by a plateau response (Fig. 3-1). Dip G and tanespimycin induced a dose-dependent decrease in ER Y537S protein, as previously observed in MCF7 WT. Treatment with 1 μM fulvestrant, 10 μM dip G, and 4 μM tanespimycin resulted in a 51.5%, 71.5%, and 68.4% reduction in ER, respectively, as compared to vehicle treatment. This is in contrast to the 64.8%, 72.8%, and 58.3% reduction, respectively, seen in WT ER-expressing MCF7 (Fig. 2-2), indicating that only the effects of fulvestrant are affected by mutant ER. However, in this experiment, we cannot distinguish between WT ER and ER Y537S, as we do not have

a mutant ER-specific antibody, and mutant ER-expression is heterozygous in this cell line.

Because we observed ER Y537S protein levels were decreased by dip G, we wanted to know whether a decrease in protein levels correlated to downregulation of ER Y537S protein's transcriptional activity. We performed RNA sequencing on T47D WT and T47D Y537S cells[66] treated with either DMSO or 10 uM dip G for 24 hours, followed by differential gene expression analysis and Gene Set Enrichment Analysis (GSEA). Hallmark gene sets "estrogen response early" and "estrogen response late" were significantly downregulated by dip G treatment (Fig. 3-2). Canonical ER target genes such as *GREB1, PGR, and MYC* were also significantly downregulated (Supplementary Table 4). Epithelial mesenchymal transition (EMT), which is consistent with the mutant's reported metastatic phenotype, was also downregulated. Glycolysis, mitotic spindle, and mTORC1 signaling, were also significantly downregulated, indicating that dip G also has putative effects on genes related to cancer cell metabolism, cell division, as well as growth factor receptors responsible for ligand-independent activation of ER.

We validated downregulation of several ER target genes including *GREB1*, *PGR*, and *MYC* in T47D and T47D Y537S cells treated with increasing concentrations of fulvestrant and 1 nM E2 or dip G with 1 nM E2 using RT-qPCR. In T47D WT cells, E2 upregulated *GREB1, PGR*, and *MYC* expression almost 3.8-fold, 2-fold, and 3.2-fold, respectively, compared to DMSO, and increasing concentrations of fulvestrant + 1 nM E2 and dip G + 1nM E2 resulted in a dose dependent decrease in *GREB1, PGR*, and *MYC* transcript (Fig. 3-3). In T47D Y537S cells, basal levels of *GREB1*, *PGR*, and *MYC*

were 1.5-2-fold higher than in T47D WT cells. E2 treatment only increased *GREB1*, *PGR, and MYC* transcript levels marginally compared to E2 treatment in T47D WT cells, consistent with the mutant receptor's constitutively active phenotype and reduced binding to E2. Increasing concentrations of dip G and 1 nM E2 resulted in a dose-dependent decrease in *GREB1*, *PGR*, and *MYC* expression (Fig. 3-3). We also confirmed these effects on *GREB1* using dip G and deoxy-dip G in MCF7 and MCF7 Y537S cells (Fig. 3-4, 3-5).

To test whether inhibition of cell growth correlated with the observed downregulation of ER protein and ER transcriptional activity, MCF7 and MCF7 Y537S cells were treated with increasing concentrations of fulvestrant or dip G in full medium, and cell number was counted for three days. We observed a dose-dependent decrease in cell number as the concentration of fulvestrant increased in WT MCF7 cells. ER Y537S cells were less responsive to fulvestrant treatment (Fig. 3-6). WT ER and ER Y537S cells respond almost identically to dip G treatment, as well as tanespimycin treatment, and this response is dose-dependent (Figure 3-6). Inhibition of cell growth is correlated to reduced ER protein levels, and ER transcriptional activity, indicating that dip G's antiproliferative effects may be mediated primarily through ER degradation in breast cancer cells. The inhibition of cell growth could be due to cell death, a decrease in cell proliferation, or both. Reports from our own lab, as well as others, have previously reported that dip G does not induce caspase-dependent apoptosis, necroptosis, or autophagic cell death, and induces cell cycle arrest at G2/M[207]. In the case of tanespimycin, inhibition of cell growth is not correlated to protein

downregulation, and additional effects other than ER degradation, such as downregulation of other protein clients, and induction of apoptosis might better explain tanespimycin's potent antiproliferative effects.

Diptoindonesin G inhibits patient-derived organoid growth and signaling

Given that dip G and tanespimycin inhibited 2D cell proliferation, we next examined whether dip G and tanespimycin could inhibit the growth of patient derived xenograft organoids (PDXOs). To test this, we used HCI-011 PDXOs, which were derived from the HCI-011 patient-derived xenograft (PDX), and express WT ER. The patient from which they were derived was refractory to treatment[222]. HCI-011 PDXOs were treated with DMSO, 10 μM dip G, 1 μM tanespimycin, or 1 μM fulvestrant for two weeks. Phase contrast microscopy showed that, in general, organoids in the treated groups were smaller than those in the DMSO-treated group (Fig. 3-7). In addition, dip G, tanespimycin, and fulvestrant all significantly decreased PDXO viability compared to DMSO treatment, as measured by MTS (Fig. 3-8). RT-qPCR analysis showed significant downregulation of ER target gene *GREB1* in response to dip G, and fulvestrant treatment, though tanespimycin had little effect on *GREB1* expression (Fig. 3-9). We also observed that dip G and fulvestrant treatment resulted in significant downregulation of ER protein in PDXOs, indicating that HCI-011 PDXOs rely heavily on ER for growth, and a decrease in viability correlates with ER degradation (Fig. 3-10). One explanation for why tanespimycin has marginal effects on ER target gene expression and ER protein levels in HCI-011 PDXOs compared to MCF7 2-D cultures is that tanespimycin has difficulty penetrating Matrigel. Another explanation is that in the

PDXO model, tanespimycin's anti-proliferative effects are not driven by downregulation of ER signaling, but primarily through degradation of other HSP90 client oncoproteins. It is also possible that this model is somewhat resistant to tanespimycin treatment.

Diptoindonesin G does not inhibit patient-derived xenograft growth and signaling

To determine whether the results observed in MCF7 and T47D cells, as well as HCI-011 PDXOs could be recapitulated in vivo in a WT ER-expressing model, 5-10-week-old NSG mice were implanted with estrogen pellets and orthotopically injected with HCI-011 PDX cells and randomized to treatment with vehicle, dip G or fulvestrant. Surprisingly, HCI-011 tumors were neither sensitive to fulvestrant, nor dip G, despite their WT ER status (Figure 3-11). To test whether dip G analog deoxy-dip G has effects on tumor growth, as well as assess the sensitivity of mutant ER to dip G and fulvestrant in vivo, PDX model HCI-013 EI, an estrogen independent subline of HCI-013, which expresses ER Y537S, was orthotopically injected into 5-10-week-old NSG mice that were not implanted with estrogen pellets. Mice were randomized to treatment with vehicle, deoxy-dip G, or fulvestrant. Contrary to what was expected, HCI-013 EI was exquisitely sensitive to fulvestrant treatment, despite expressing ER Y537S, which is known to be resistant to fulvestrant treatment. Deoxy-dip G had no significant effect on tumor growth compared to vehicle treatment (Figure 3-12). To measure ER degradation in HCI-013 EI tumors, we performed immunohistochemistry and stained for ER and Ki67 protein. Fulvestrant significantly decreased ER and Ki67 staining compared to vehicle, whereas deoxy-dip G had no significant effect on the expression of either protein compared to vehicle treatment (Figure 3-13). In NSG mice bearing parental HCI-

013 tumors and estrogen implants, we saw similar results, where only fulvestrant significantly decreased tumor volume compared to vehicle treatment (3-14).

To determine the optimal administration method for dip G, as well as determine the blood concentrations of dip G following each administration method, NSG mice were administered 50 mg/kg dip G by either subcutaneous injection, intraperitoneal injection, or oral gavage. Blood was collected prior to drug administration, and at 5, 30, and 60 min after drug administration. Dip G concentration was then measured using mass spectrometry. We found that subcutaneous and intraperitoneal injection resulted in a dip G concentration of 1.2 μM, the highest concentrations measured, at 5 min following dip G administration, and then quickly decreased, indicating that dip G is quickly metabolized. Almost no dip G could be detected following oral gavage treatment (Figure 3-15).

Many kinds of cancer are sensitive to diptoindonesin G and deoxy-diptoindonesin G

We used PRISM, a pan-cancer pooled screening developed by Broad Institute, to profile deoxy-dip G's effect on cell viability across 770 cancer cell lines, with the goal of identifying small molecules with a similar cytotoxicity profile previously determined using this platform, further informing about the mechanism of action of dip G and its analogs[223,224], as well as identifying additional cancer models that respond favorably to dip G treatment. Each cell line has a stably integrated DNA barcode, and is treated with compounds for five days. Bar codes are recovered and used to calculate viability and

relative cell line sensitivity. We found that many different tissue lineages were sensitive to deoxy-dip G, including bone, leukemia, lymphoma, rhabdoid and rhabdomyosarcoma lineages (Fig. 3-16). Though PRISM is an effective assay for quickly screening hundreds of cells lines at once to test for sensitivity to a compound of interest, it has difficulty predicting allosteric inhibitors, as well as sensitivity to very specific mutations. A summary of cell line sensitivity to deoxy-dipG is listed in Table 3-1.

Discussion

Dip G and deoxy-dip G elicited anti-proliferative effects, and could promote mutant ER degradation in ER+ breast cancer cells (Fig. 3-1). We also performed many in vivo studies using dip G and deoxy-dip G in several different models of ER+ breast cancer, including patient derived xenograft models (Fig. 3-11,12,14). However, we found that dip G and deoxy-dip G had no significant effect on tumor growth. One explanation for the discrepancy between our 2-D culture, organoid culture, and in vivo results is that therapeutic concentrations of dip G could not be reached in a mouse due to the poor pharmacological properties of dip G, such as bioavailability and stability. In addition, according to our PRISM results, ER+ breast cancer is not very sensitive to dip G. To circumvent these limitations, we instead utilized an organoid system derived from one of the PDXs used in our in vivo studies and treated them using our 2-D culture conditions (Fig. 3-8,9,10). Testing the effects of dip G in an ER Y537S-expressing PDXO model to complement our HCI-011 PDXO results warrants further investigation.

While dip G is not effective against ER+ breast cancer patient derived xenograft models, other groups have demonstrated dip G's anti-tumor effects in vivo. Fan et al

showed that xenografts of triple negative breast cancer cell line MDA-MB-231 were as sensitive to 7.5 mg/kg of dip G as to 10 mg/kg of paclitaxel. Both treatments significantly decreased tumor growth as well as the number of mice that developed lung metastases. In the group treated with 15 mg/kg of dip G, no lung metastases were detected[178]. Gao et al observed that xenografts of HL-60, an acute myeloid leukemia cell line, were also very sensitive to dip G. 10 mg/kg of dip G resulted in a similar significant decrease in tumor growth and tumor final weight as ATRA (a) compared to vehicle treatment[175]. Using androgen receptor slice variant 7 (ARv7)-expressing prostate cancer cell line 22Rv1-derived xenografts, Liu et al found that a combination of tanespimycin and dip G decreased tumor growth better than either single agent[176]. This is an interesting observation, as ARv7, like ER LBD mutants, has ligand-independent activity and does not associate with HSP90[225]. These results agree with our PRISM results, where in general, we found that leukemia lineages and triple negative breast cancer lineages were more sensitive to deoxy-dip G than the ER+ breast cancer lineage (Table 3-1).

Despite HCI-011 PDXOs being very sensitive to fulvestrant, no significant difference in tumor growth between vehicle and fulvestrant treatment in HCI-011 PDXs were observed. Differences in the tumor microenvironment might explain the differences in response, as PDXOs are cultured in medium supplemented with fetal bovine serum and growth factors which are not present in a mouse, and may affect drug response. Though usually PDXOs recapitulate the drug responses of the PDXs from which they are derived, this is not always the case. In addition, other groups have not only been able to confirm that HCI-011, which expresses WT ER, is not responsive to fulvestrant

in vivo, but also that HCI-013 is sensitive to fulvestrant, despite expressing ER Y537S, which agrees with our results[104], but disagrees with results from DeRose et al.[226]. In these models, ER mutational status alone does not fully explain sensitivity to fulvestrant, and other factors and driver proteins must be at play. Differences in histological subtype could explain differences in sensitivity to fulvestrant that are independent of ER mutational status, as HCI-011 is a model of intraductal carcinoma (IDC) while HCI-013 is a model of intralobular carcinoma (ILC)[227]. Testing the effects of dip G in an ER Y537S-expressing PDXO model to complement our HCI-011 PDXO results warrants further investigation.

Using HSP90 inhibitors to treat endocrine-resistant breast cancer has not been extensively explored. Toy *et al* treated MCF7 cells transfected with vector expressing HA-tagged wild-type ER or Y537S and D538G mutant ER with SNX2112, an N-terminal ATP binding site-targeting drug, at various doses for 3 hours[63]. Though WT ER levels were decreased in a dose-dependent manner, HSP90 inhibition did not affect the levels of Y537S and D538G mutant ER, indicating that HSP90 does not regulate mutant ER stability[63]. On the contrary, Yu *et al* found that ganetespib had cytotoxic effects in *ex vivo* cultured circulating tumor cells (CTCs) expressing *ESR1* mutations as a single agent, but also in combination with raloxifene and fulvestrant[228]. They also found that sensitivity to HSP90 inhibition was associated with mutant *ESR1* allele frequency[228]. Though the Y537S mutant resembles E2-bound ER in phenotype and structure, we found that ER mutant protein can be degraded in response to both dip G and tanespimycin treatment, indicating that the Y537S mutant, and perhaps other LBD

mutants, still associate and rely on HSP90. Because the conclusions of Toy *et al* conflict with the results from Yu *et al*, as well as our own results, where we found that efficacy of HSP90 inhibition is not affected by ER mutational status, further mechanistic studies are required to determine conclusively whether HSP90 associates with mutant ER, and whether this phenomenon holds true for other classes of N-terminal, as well as C-terminal-targeting HSP90 inhibitors. Establishing definitively whether HSP90 can interact with *ESR1* LBD mutants could open up a new class of drug for treatment of mutant-ER expressing tumors, and help better understand the biology of *ESR1* ligand-binding domain mutants.

This thesis furthers our understanding of ER degradation mechanisms and the biology of HSP90 inhibition, and proposes a new therapeutic strategy for treating endocrine-resistant breast cancer that has yet to be fully explored. Though this work was done using ER+ breast cancer cell lines, data from this thesis, as well as evidence from other groups, supports that dip G could be used even more effectively in other models of cancer.

Figure 3-1

ELISA assay of ER levels in MCF7 Y537S cells following treatment with (A) DMSO, 1, 10, 50, 100, and 1000 nM of fulvestrant, or (B) 0.1, 1, 5, 7.5, and 10 μM dip G or (C) 0, 0.25, 0.5, 1, 2, and 4 μM tanespimycin for 24 hours. MCF7 cells were hormone starved for 3 days prior to treatment. ER protein levels were normalized to either $1x10^7$ cells (fulvestrant and dip G) or total protein concentration (tanespimycin). Two independent experiments with three biological replicates and two technical replicates (fulvestrant and dip G). Three independent experiments with three biological replicates and two technical replicates (tanespimycin). Plotted are individual biological replicates and the mean ± SD.

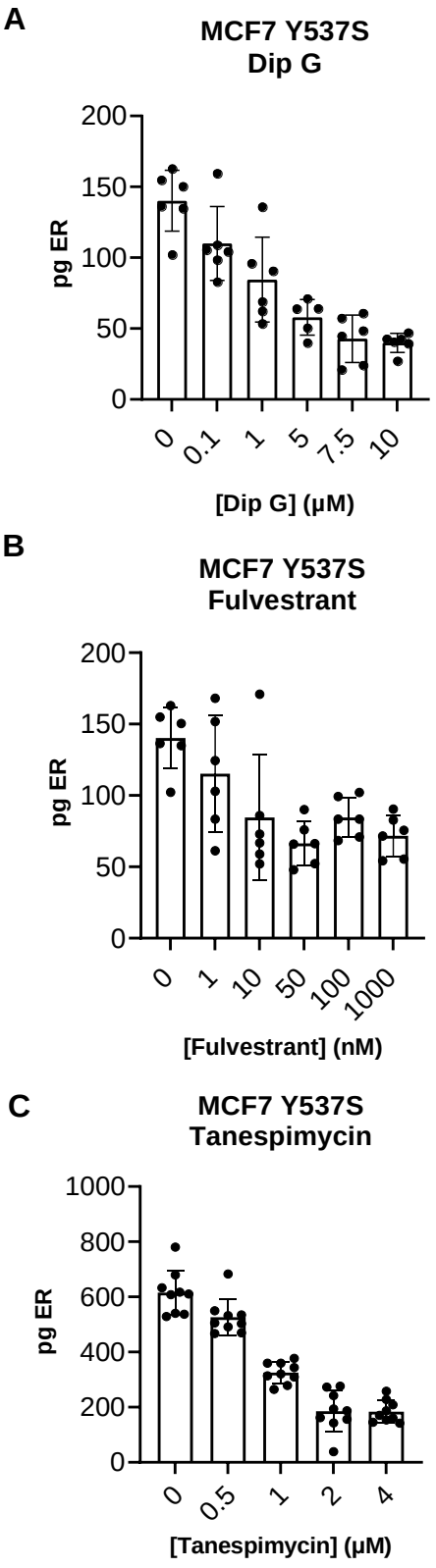
A
MCF7 Y537S
Dip G
pg ER
200
150
100
50
0
0
0.1
1
5
7.5
10
[Dip G] (μM)
B
MCF7 Y537S
Fulvestrant
pg ER
200
150
100
50
0
0
1
10
50
100
1000
[Fulvestrant] (nM)
C
MCF7 Y537S
Tanespimycin
pg ER
1000
800
600
400
200
0
0
0.5
1
2
4
[Tanespimycin] (μM)

Figure 3-2

(A) Hallmark gene set enrichment analysis of significantly changed gene sets (FDR < 25%, NES < -1.3 or NES > 1.3, NOM p-value < 0.05) from sequencing RNA from T47D and T47D Y537S cells treated with DMSO or 10 μM dip G for 24 hours. Enrichment plots for hallmark gene sets (B) estrogen response early and (C) estrogen response late showing significant downregulation of their respective gene sets.

A

Hallmark Gene Set	Enrichment Score (NES)
Estrogen Response Early	-1.38
Estrogen Response Late	-1.48
Epithelial Mesenchymal Transition	-1.43
Glycolysis	-1.33
Mitotic Spindle	-1.40
MTORC1 Signaling	-1.30

FDR <25%, NES <-1.30, NOM P-value <0.05

B

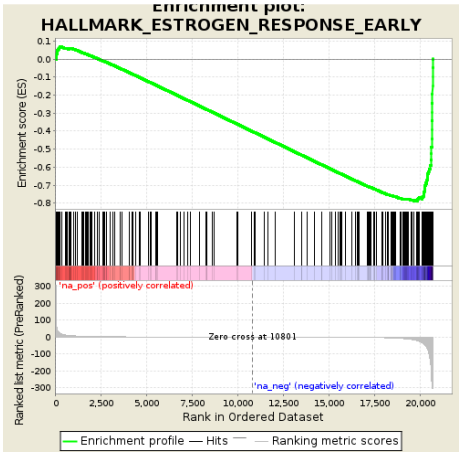

C

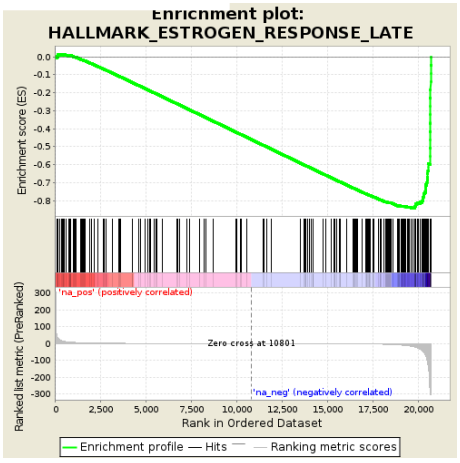

Figure 3-3

RT-qPCR analysis of ER target gene *GREB1* (A, B), *PGR* (C, D)*, and MYC* (E, F) expression in T47D (left) or T47D Y537S (right) cells treated with DMSO, 1 nM E2, or increasing concentrations of fulvestrant and 1 nM E2 or increasing concentrations of dip G and 1 nM E2 for 24 hours. Cells were hormone starved for 3 days prior to treatment. Expression was normalized to*18srRNA*. Two independent experiments with two biological replicates, and three technical replicates for each biological replicate. Plotted are individual biological replicates and the mean ± SD.

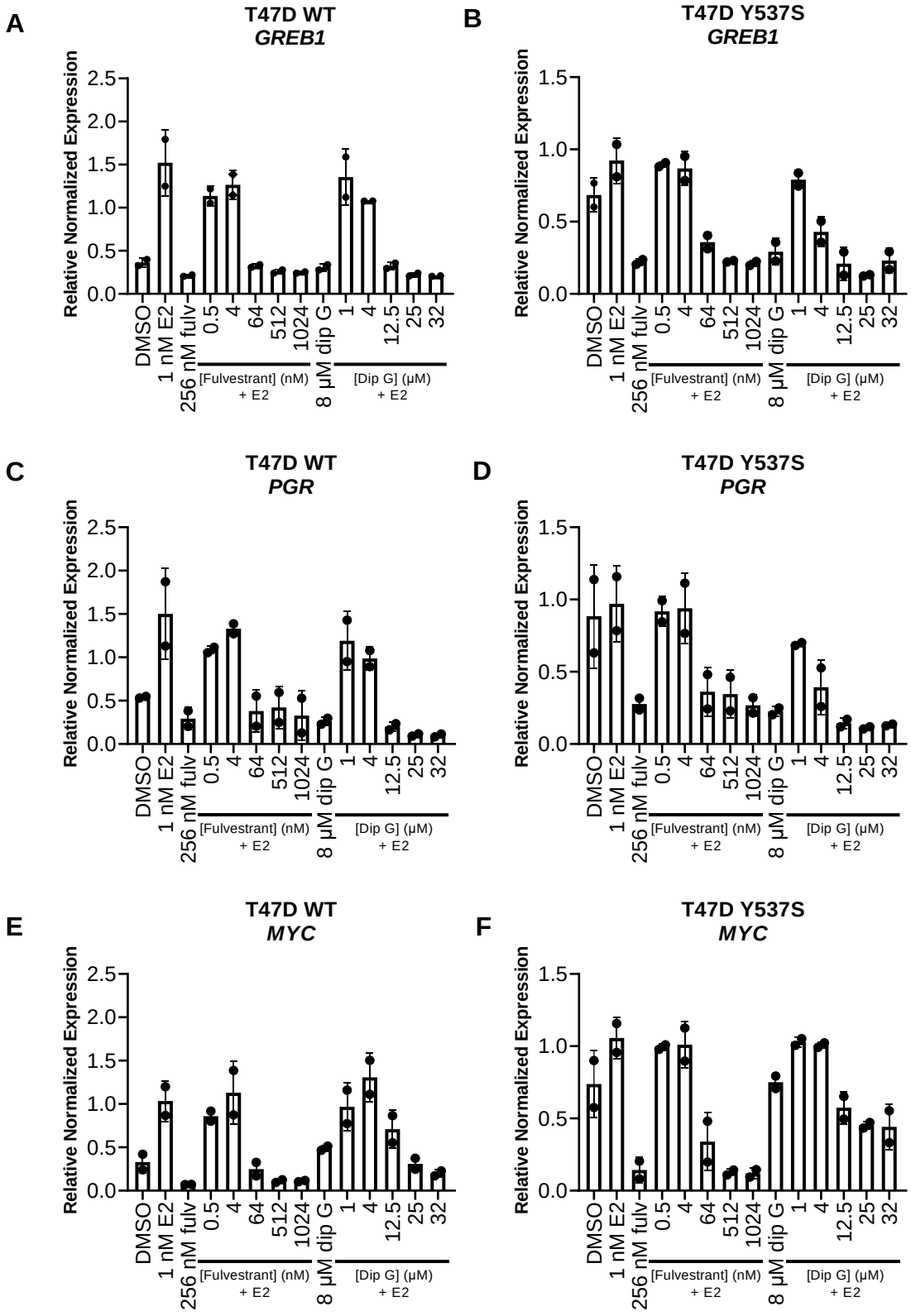
A
T47D WT
GREB1
B
T47D Y537S
GREB1
C
T47D WT
PGR
D
T47D Y537S
PGR
E
T47D WT
MYC
F
T47D Y537S
MYC
Relative Normalized Expression
DMSO
1 nM E2
256 nM fulv
0.5
4
64
512
1024
8 µM dip G
1
4
12.5
25
32
[Fulvestrant] (nM) + E2
[Dip G] (µM) + E2

Figure 3-4

RT-qPCR analysis of ER target gene *GREB1* expression in MCF7 (top) or MCF7 Y537S (bottom) cells treated with DMSO, 1 nM E2, or increasing concentrations of fulvestrant and 1 nM E2 (right) or dip G and 1 nM E2 (left) for 24 hours. Cells were hormone starved for 3 days prior to treatment. Expression was normalized to*18srRNA*. One independent experiment with one biological replicates, and three technical replicates for each biological replicate. Plotted is the mean ± SEM.

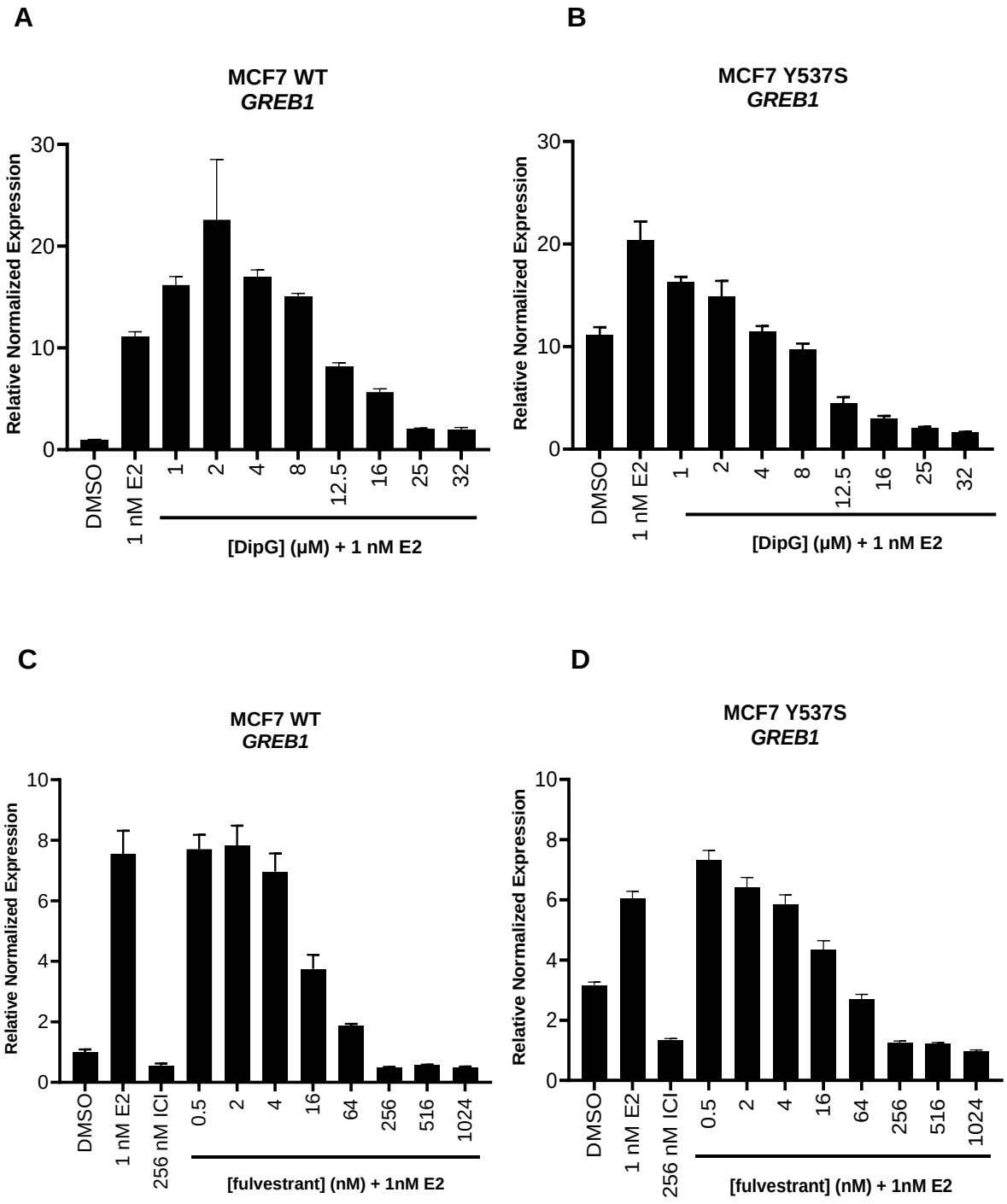
A
MCF7 WT
GREB1
Relative Normalized Expression
30
20
10
0
DMSO
1 nM E2
1
2
4
8
12.5
16
25
32
[DipG] (μM) + 1 nM E2
B
MCF7 Y537S
GREB1
Relative Normalized Expression
30
20
10
0
DMSO
1 nM E2
1
2
4
8
12.5
16
25
32
[DipG] (μM) + 1 nM E2
C
MCF7 WT
GREB1
Relative Normalized Expression
10
8
6
4
2
0
DMSO
1 nM E2
256 nM ICI
0.5
2
4
16
64
256
516
1024
[fulvestrant] (nM) + 1nM E2
D
MCF7 Y537S
GREB1
Relative Normalized Expression
10
8
6
4
2
0
DMSO
1 nM E2
256 nM ICI
0.5
2
4
16
64
256
516
1024
[fulvestrant] (nM) + 1nM E2

Figure 3-5

RT-qPCR analysis of ER target gene *GREB1* expression in (A) MCF7 WT (B) MCF7 Y537S (C) MCF7 D538G cells treated with DMSO, 1 nM E2, or increasing concentrations of fulvestrant and 1nM E2 or deoxy-dip G and 1 nM E2 for 24 hours. Cells were hormone starved for 3 days prior to treatment. Expression was normalized to *18srRNA*. One independent experiment with one biological replicate, and three technical replicates for each biological replicate. Plotted is the mean ± SEM.

A

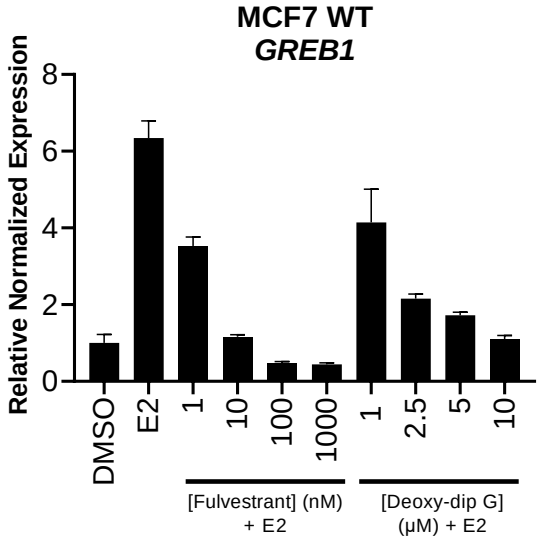
MCF7 WT
GREB1
Relative Normalized Expression
0
2
4
6
8
DMSO
E2
1
10
100
1000
1
2.5
5
10
[Fulvestrant] (nM) + E2
[Deoxy-dip G] (μM) + E2

B

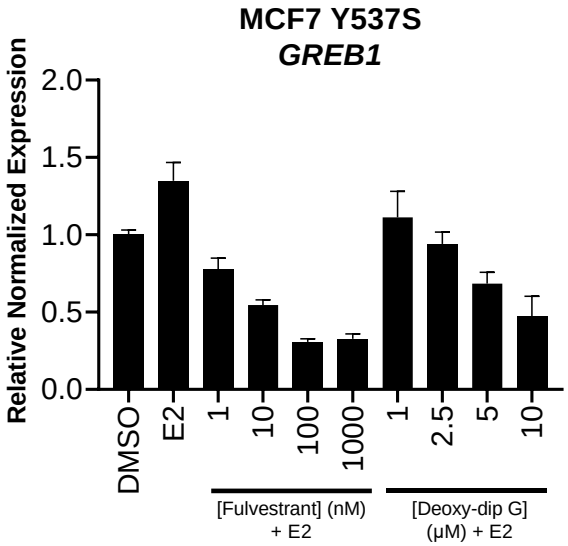
MCF7 Y537S
GREB1
Relative Normalized Expression
0.0
0.5
1.0
1.5
2.0
DMSO
E2
1
10
100
1000
1
2.5
5
10
[Fulvestrant] (nM) + E2
[Deoxy-dip G] (μM) + E2

C

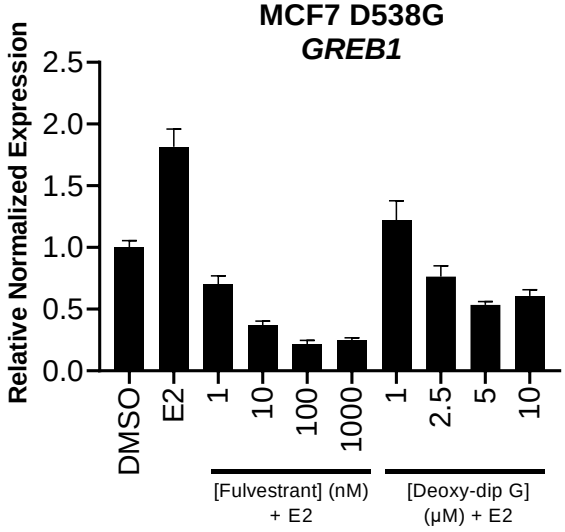
MCF7 D538G
GREB1
Relative Normalized Expression
0.0
0.5
1.0
1.5
2.0
2.5
DMSO
E2
1
10
100
1000
1
2.5
5
10
[Fulvestrant] (nM) + E2
[Deoxy-dip G] (μM) + E2

Figure 3-6

Cell counting data of MCF7 (pink) or MCF7 Y537S (blue) cells treated for three days with increasing concentrations of fulvestrant (0.25-512 nM) (top), dip G (0.5-16 μM) (middle), or tanespimycin (0.25-4 μM) (bottom) in full medium, using a BioTek Lionheart automated microscope. Shown are the number of cells present on the third and final day of treatment plotted in response to the log of the molar concentration of either fulvestrant, dip G, or tanespimycin.

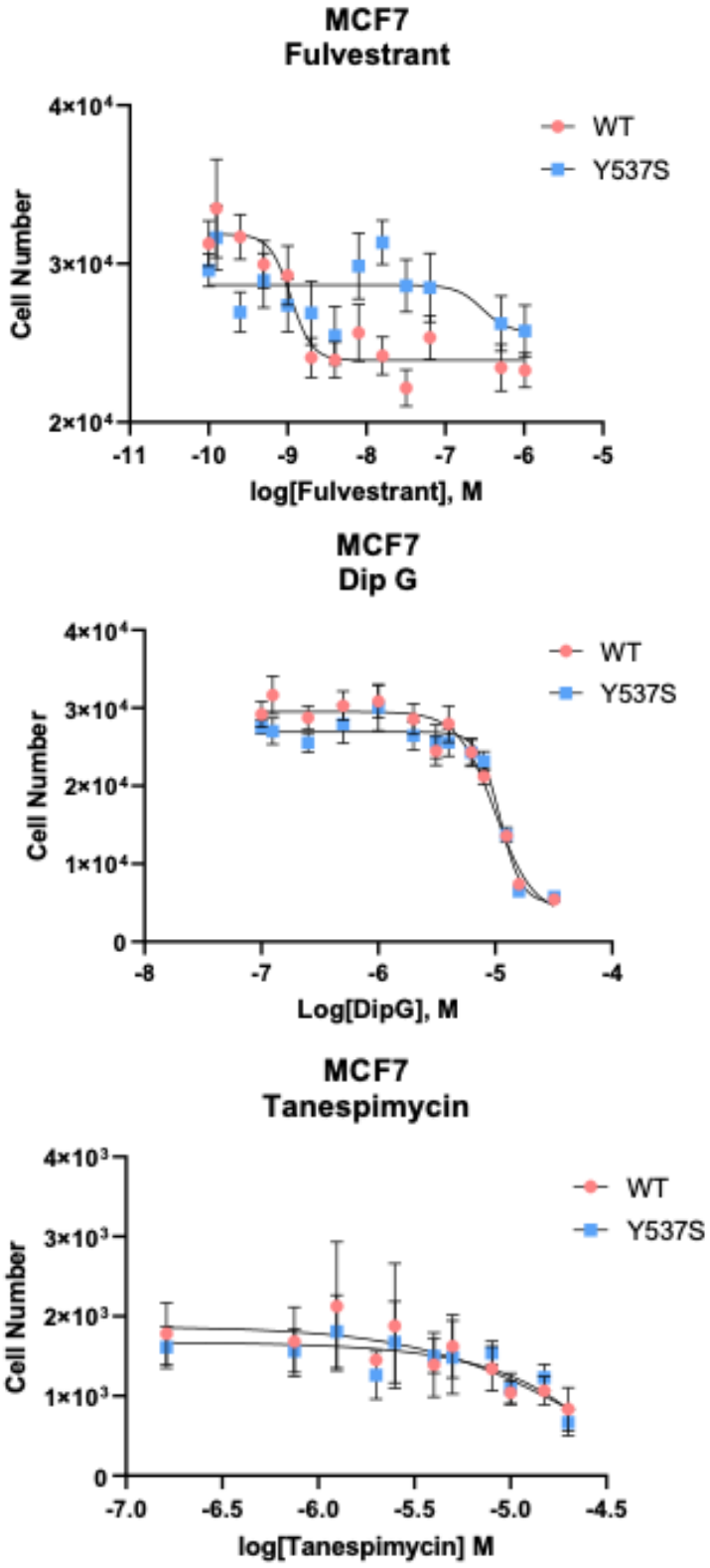
MCF7
Fulvestrant
Cell Number
4×10⁴
3×10⁴
2×10⁴
WT
Y537S
-11
-10
-9
-8
-7
-6
-5
log[Fulvestrant], M
MCF7
Dip G
Cell Number
4×10⁴
3×10⁴
2×10⁴
1×10⁴
0
WT
Y537S
-8
-7
-6
-5
-4
Log[DipG], M
MCF7
Tanespimycin
Cell Number
4×10³
3×10³
2×10³
1×10³
0
WT
Y537S
-7.0
-6.5
-6.0
-5.5
-5.0
-4.5
log[Tanespimycin] M

Figure 3-7

Brightfield microscopy images of HCI-011 PDX organoids treated for two weeks with DMSO, 10 µM dip G, 1 µM tanespimycin, or 1 µM fulvestrant in full medium. The scale bar corresponds to 1000 µm.

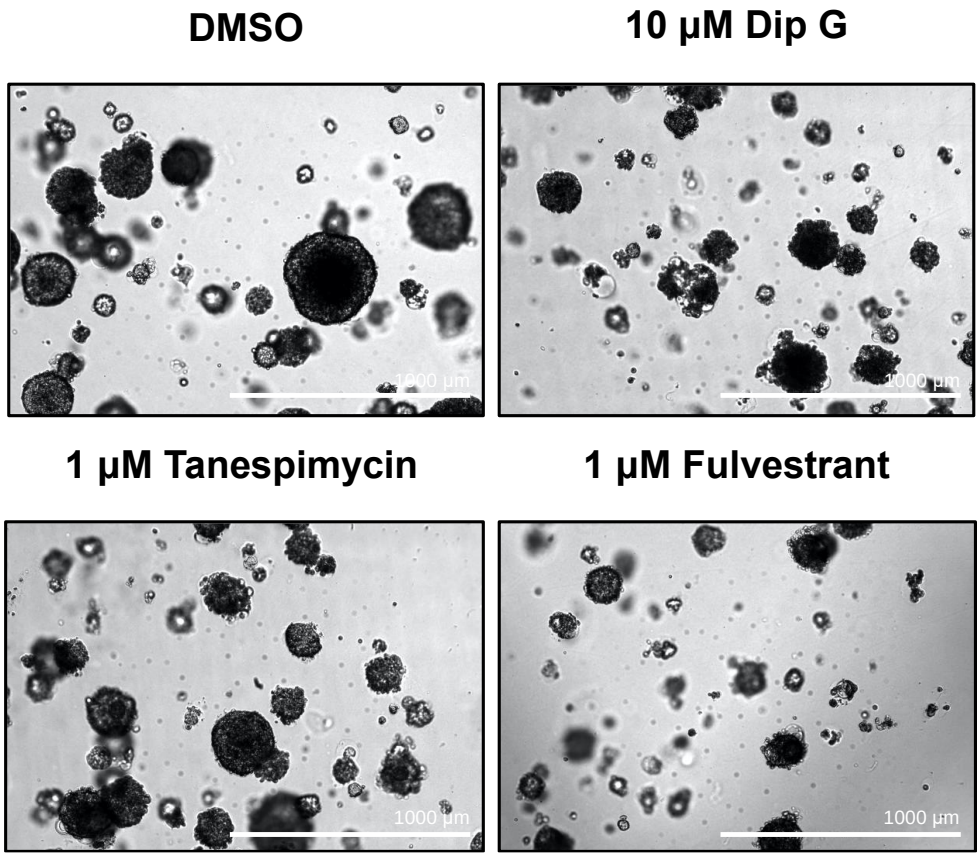

Figure 3-8

MTS assay of HCI-011 PDX organoids treated for two weeks with 10 μM dip G, 1 μM tanespimycin, or 1 μM fulvestrant in full medium. Three independent experiments with 9 biological replicates and three technical replicates for each biological replicate. Individual biological replicates are plotted. Significance was determined using an unpaired Mann-Whitney test.

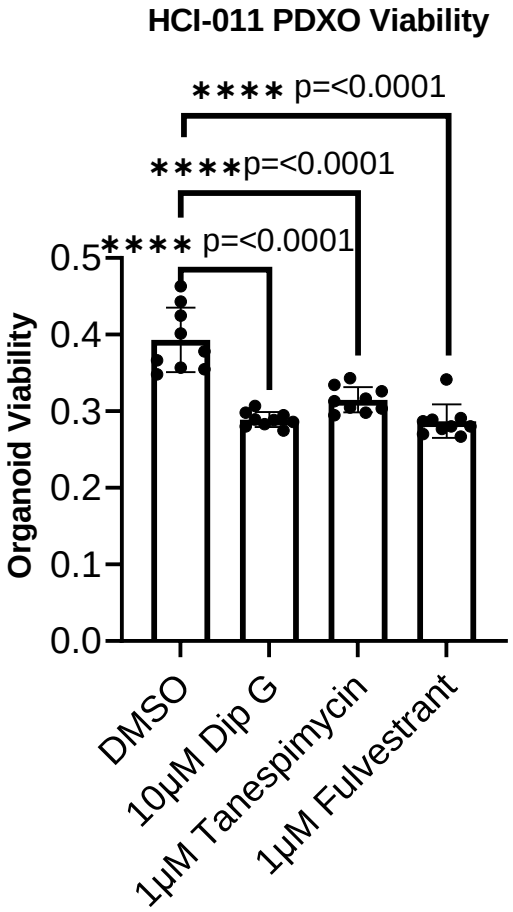

Figure 3-9

RT-qPCR analysis of ER target gene *GREB1* expression in HCI-011 PDXOs treated with DMSO, 10 μM dip G, 1μM tanespimycin, or 1μM fulvestrant for 72 hours. Expression was normalized to*18srRNA*. Four independent experiments with four biological replicates. Plotted are individual replicates and their mean ± SD. Significance was determined using an unpaired t-test with Welch's correction.

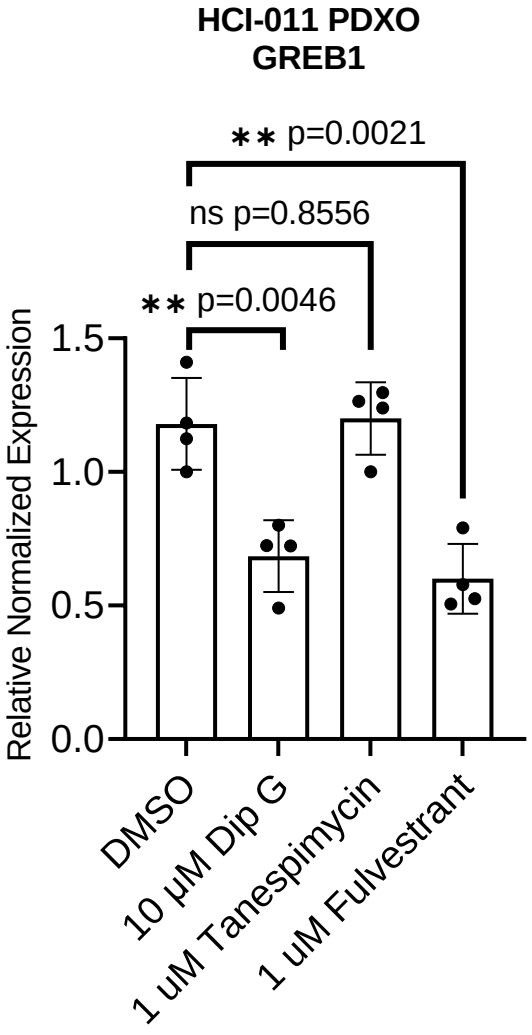

Figure 3-10

(A) Western blot of ER in HCI-011 PDXOs treated with DMSO, 10 μM dip G, 1 μM tanespimycin, or 1 μM fulvestrant in full medium for 3 days. Actin was used as a loading control. Four independent experiments with four biological replicates. One representative blot is shown. (B) Quantification of A. Plotted are individual biological replicates and their mean ± SD. Significance was determined using an unpaired Mann-Whitney test.

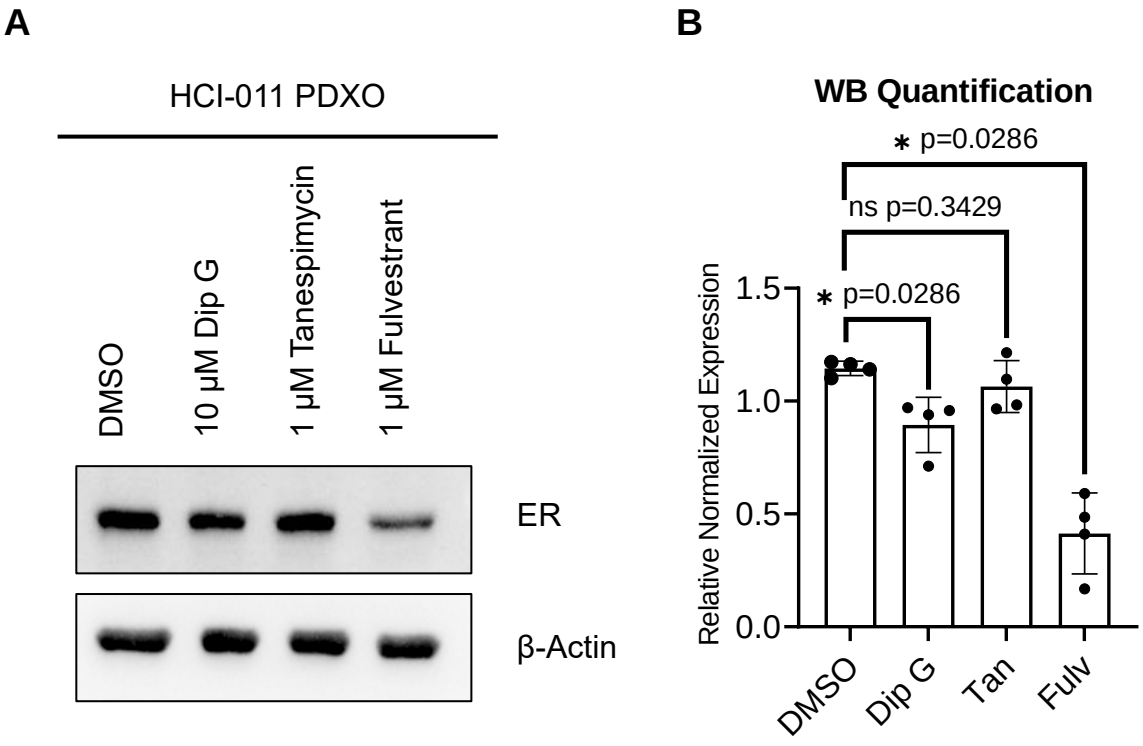

Figure 3-11

(A) Tumor growth curve over time and (B) final tumor weight of HCI-011 PDX tumors treated with 50 mg/kg dip G p.o. daily, 125 mg/kg fulvestrant s.c twice per week, and vehicle s.c. and p.o.. Half way through the study, drug doses were doubled for dip G and fulvestrant. Plotted is the mean ± SD. Significance was determined using an unpaired Mann-Whitney test.

A

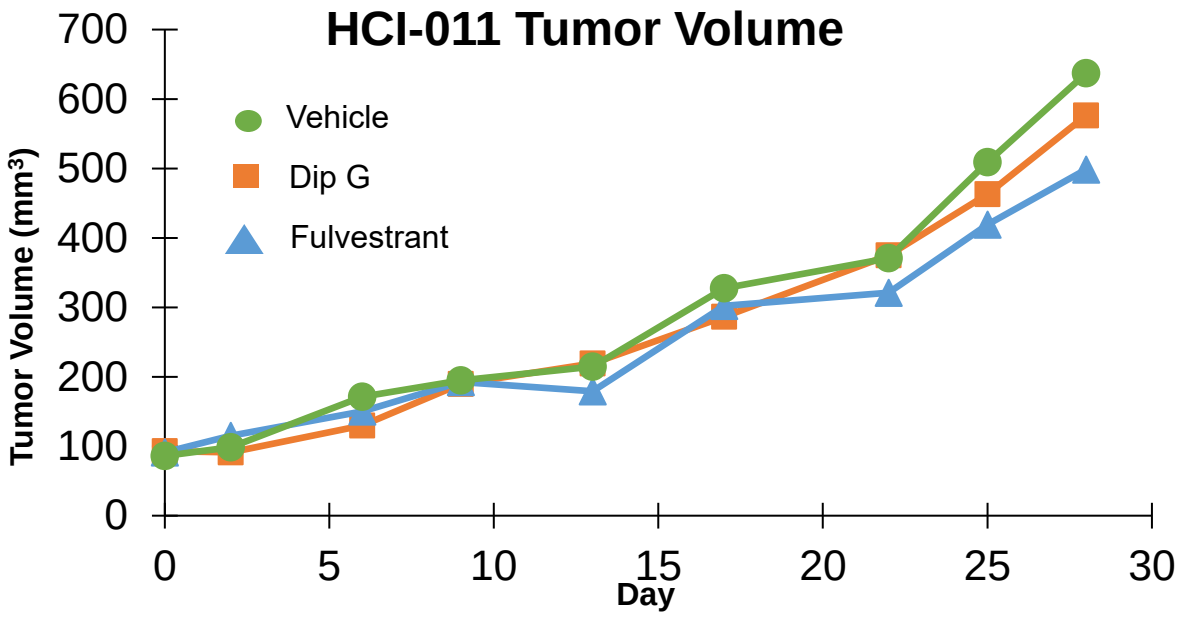
HCI-011 Tumor Volume
Vehicle
Dip G
Fulvestrant
Tumor Volume (mm³)
700
600
500
400
300
200
100
0
0
5
10
15
20
25
30
Day

B

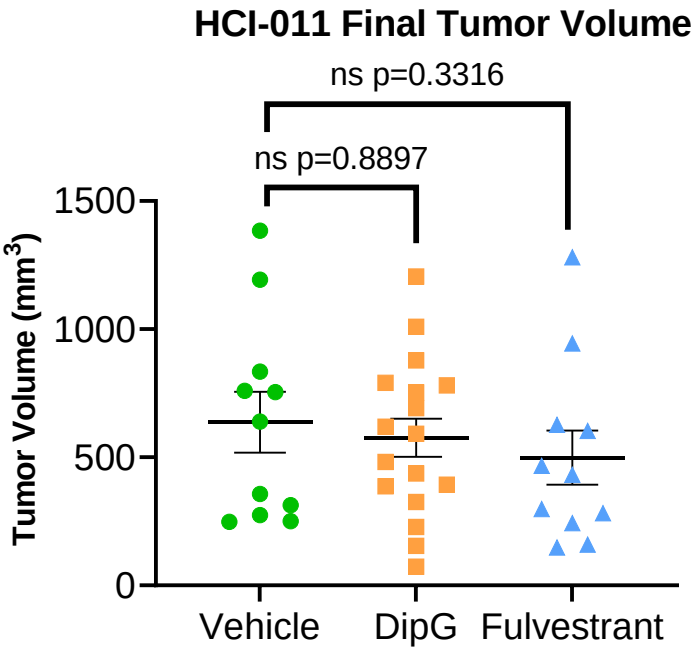
HCI-011 Final Tumor Volume
ns p=0.3316
ns p=0.8897
Tumor Volume (mm³)
1500
1000
500
0
Vehicle
DipG
Fulvestrant

Figure 3-12

(A) Tumor growth curve over time and (B) final tumor weight of HCI-013 EI PDX tumors implanted into 6-10 week old female NSG mice treated with 100mg/kg deoxy-dip G p.o. daily, 125 mg/kg fulvestrant s.c twice per week, and vehicle s.c. and p.o,.and (C) mouse body weight over time. Plotted is the mean ± SD. Significance was determined using an unpaired Mann-Whitney test.

A

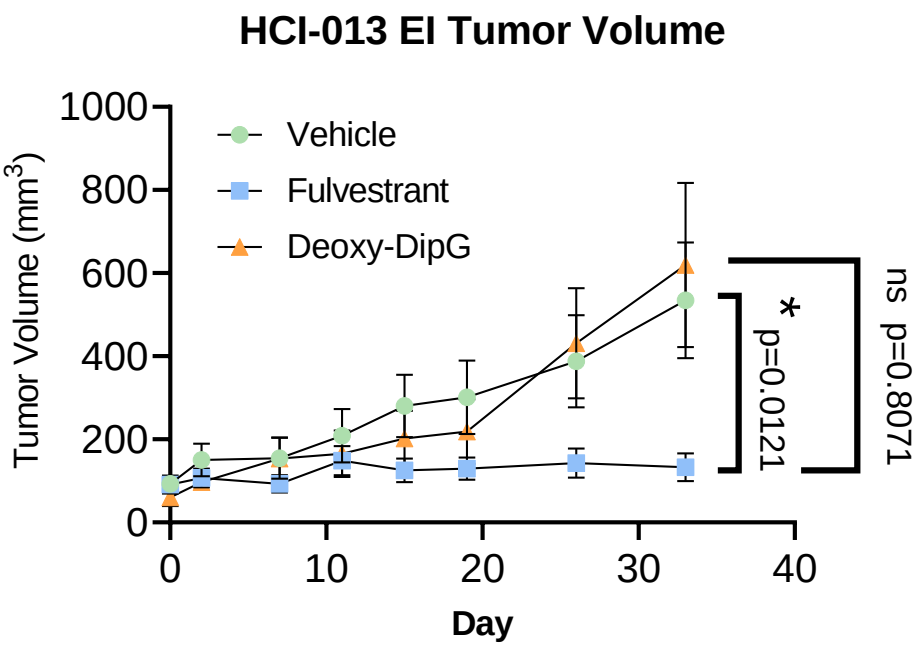
HCI-013 EI Tumor Volume
Tumor Volume (mm3)
1000
800
600
400
200
0
Vehicle
Fulvestrant
Deoxy-DipG
* p=0.0121
ns p=0.8071
0
10
20
30
40
Day

B

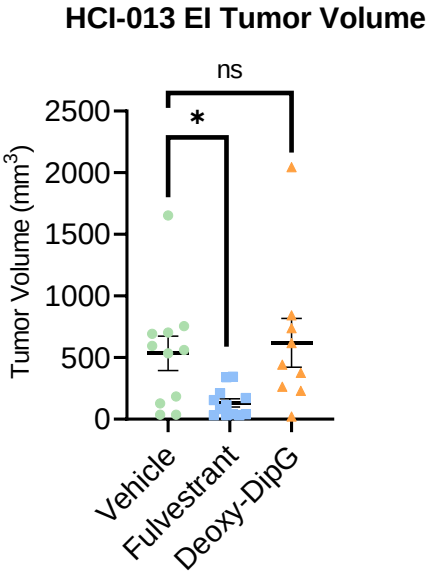
HCI-013 EI Tumor Volume
ns
*
Tumor Volume (mm3)
2500
2000
1500
1000
500
0
Vehicle
Fulvestrant
Deoxy-DipG

C

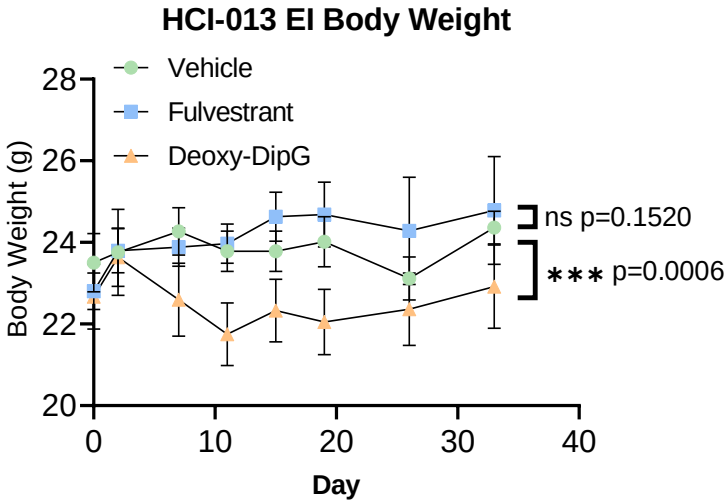
HCI-013 EI Body Weight
Vehicle
Fulvestrant
Deoxy-DipG
Body Weight (g)
28
26
24
22
20
ns p=0.1520
*** p=0.0006
0
10
20
30
40
Day

Figure 3-13

Immunohistochemistry staining of Ki67 (top) and ER (bottom) of HCI-013 EI tumors treated with fulvestrant (left), vehicle (middle), or deoxy-dip G (right)

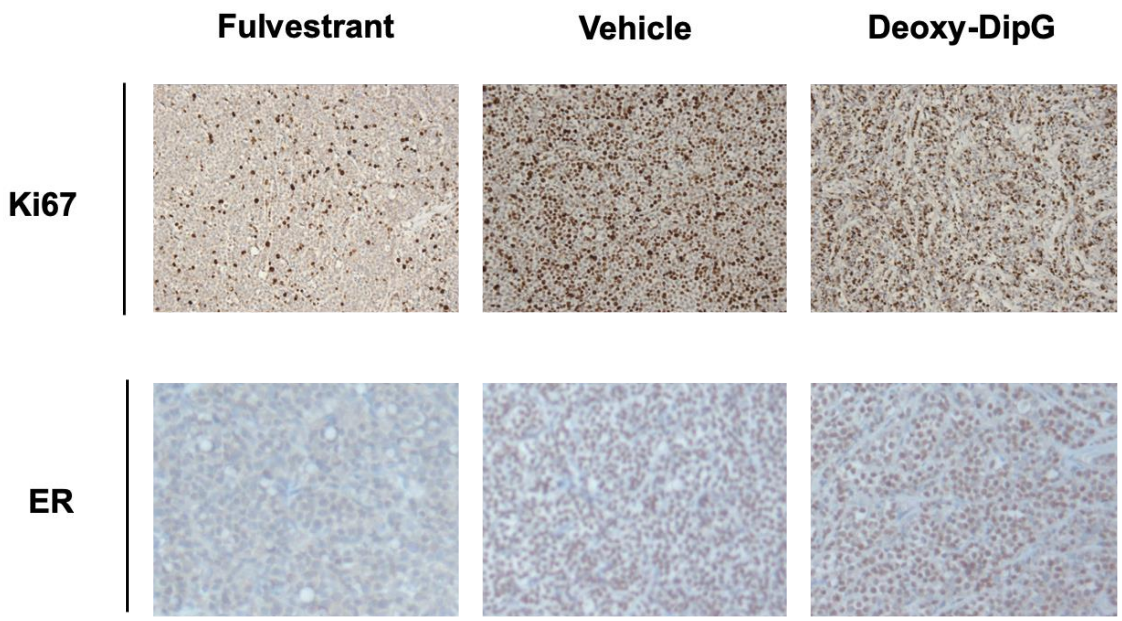

Figure 3-14

(A) Tumor growth curve over time and (B) final tumor weight of HCI-013 PDX tumors inplanted into 6-10 week old female NSG mice treated with 80 mg/kg deoxy-dip G p.o. daily, 250 mg/kg fulvestrant s.c twice per week, and vehicle s.c. and p.o,.and (C) mouse body weight over time. Plotted is the mean ± SD. Significance was determined using an unpaired Mann-Whitney test.

A

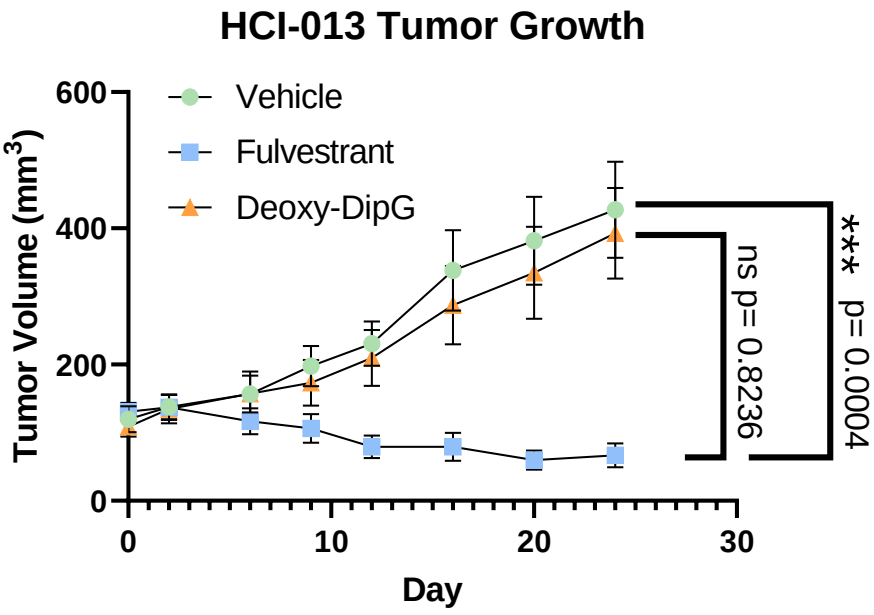
HCI-013 Tumor Growth
Vehicle
Fulvestrant
Deoxy-DipG
Tumor Volume (mm3)
600
400
200
0
0
10
20
30
Day
ns p=0.8236
*** p= 0.0004

B

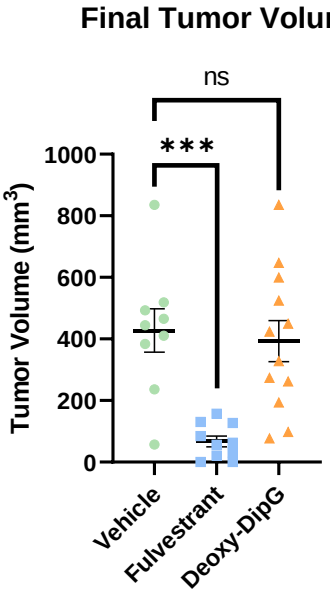
Final Tumor Volume
ns
***
Tumor Volume (mm3)
1000
800
600
400
200
0
Vehicle
Fulvestrant
Deoxy-DipG

C

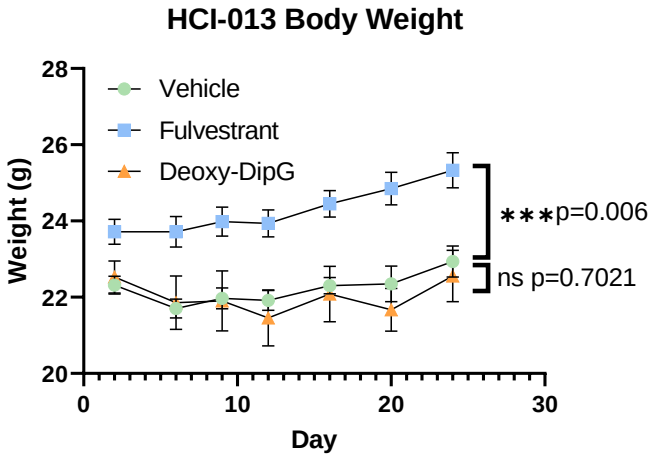
HCI-013 Body Weight
Vehicle
Fulvestrant
Deoxy-DipG
Weight (g)
28
26
24
22
20
0
10
20
30
Day
***p=0.006
ns p=0.7021

Figure 3-15

Concentration of dip G in the serum of mice following administration of 50 mg/kg dip G by either subcutaneous injection (S.C), intraperitoneal injection (I.P.), or oral gavage (O.G.). Blood was collected prior to drug administration, and 5, 30, and 60 min after drug administration. Dip G concentration was measured using mass spectrometry. Plotted is the mean ± SD.

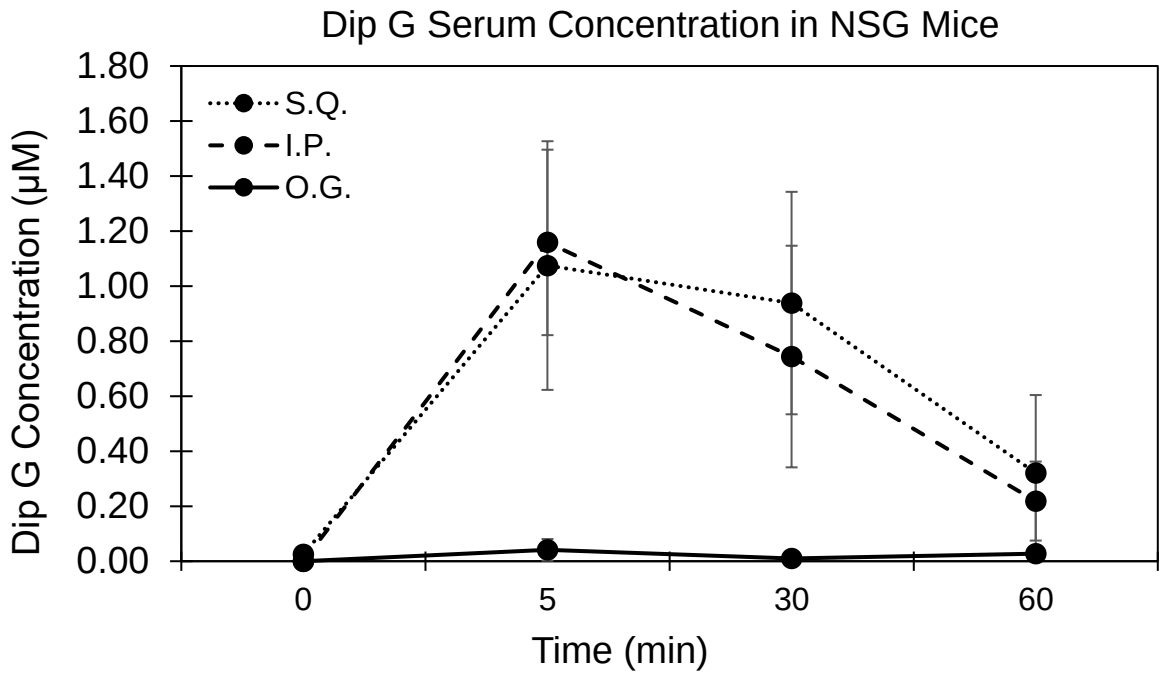

Figure 3-16

Area under the curve (AUC) plots of the sensitivity of different cancer cell line lineages to deoxy-dip G using the PRISM assay. In each of the figures, each individual dot represents a single cell line. The black dashed line represents the mean computed over all cell lines and the red dashed line represents the mean computed over cell lines within a primary disease area.

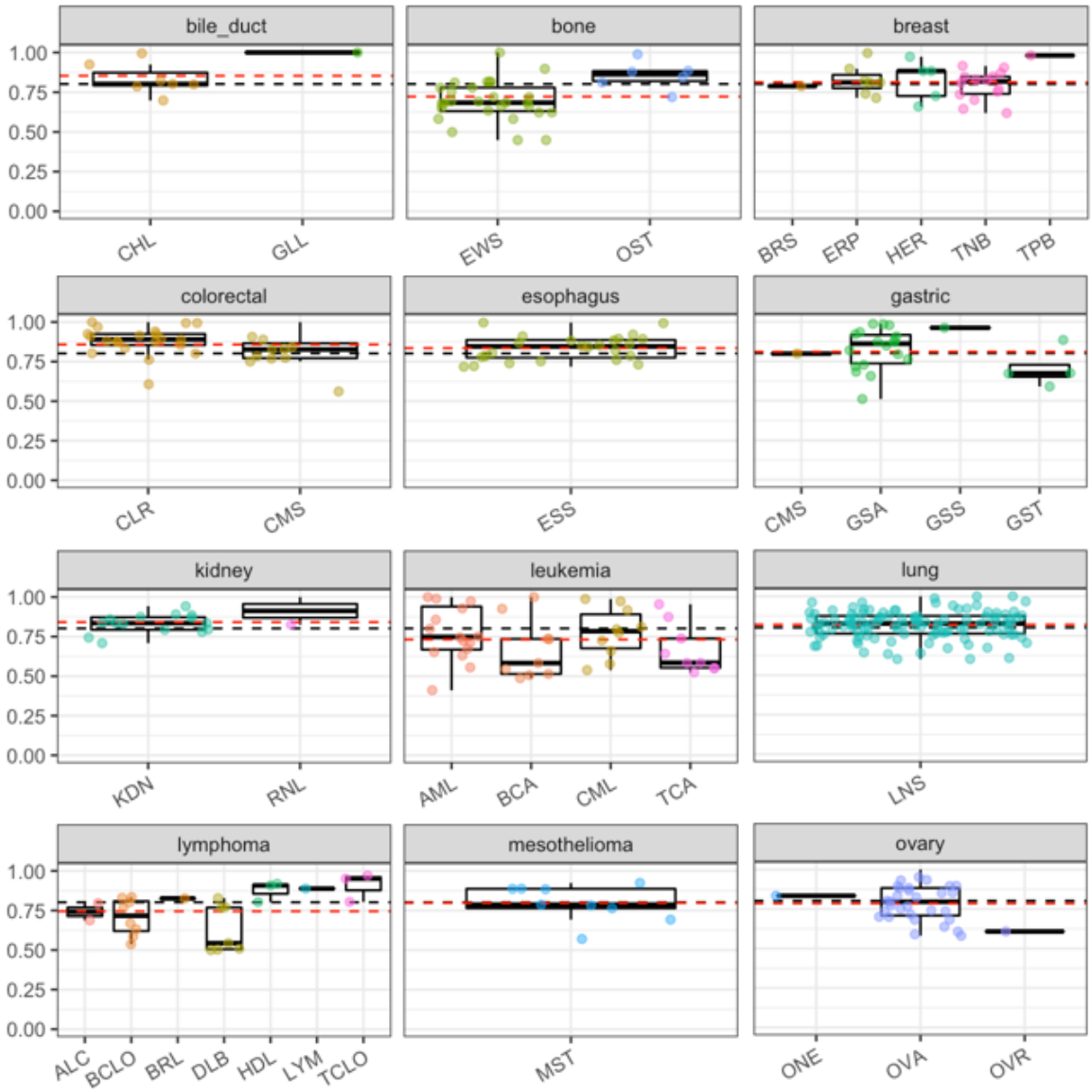

Table 3-1

Summary of the most sensitive cell lines in the PRISM data set.

Lineage	Cell Line	IC_{50} (μM)
AML (Promyelocytic)	NB4	0.07
AML	MOLM13	0.39
Ewing Sarcoma	TC32	0.44
Ewing Sarcoma	TC205	0.53
B-cell ALL	SEM	0.57
Rhabdoid	DL	0.68
B-cell ALL	RCHACV	0.69
DLBCL	NUDHL	0.7
DLBCL	OCILY19	0.78
T-cell ALL	MOLT16	0.81
B-cell ALL	KOPN8	0.85
B-cell ALL	JM1	0.97
Rhabdomyosarcoma	TE617T	1
DLBCL	SUDHL8	1
Gastric adenocarcinoma	2313287	1.03
T-cell ALL	P12 Ichikawa	1.04
Uterus Endometrium	JHUEM2	1.08
CML	EM2	1.08
Rhabdoid	KD	1.12
DLBCL	DOHH2	1.13
T-cell ALL	RPMI8402	1.18
CML	CMLT1	1.24
AML	OCIAML5	1.33
CML	BV173	1.34
Rhabdoid	A204	1.4
Urinary Tract	UBLC1	1.52
Ovary Adenocarcinoma	ONCODG1	1.6
Liver	JHH4	1.62
Lung small cell	NCIH1048	1.69
B-cell lymphoma	JVM3	1.72
Ovary Adenocarcinoma	A2780	1.74
Glioma	A1207	1.81

Lineage	Cell Line	IC_{50} (μM)
TNBC	DU4475	1.82
Melanoma	A375	1.92
Mesothelioma	MSTO211H	1.94
Ovary Adenocarcinoma	OC316	2.03
Ewing Sarcoma	RDES	2.05
AML	U937	2.16
Pancreas	HUPT4	2.18
B-cell lymphoma	MC116	2.31
Lung NSC	A427	2.35
Ovary Adenocarcinoma	TOV21G	2.55
Gastric	LMSU	2.57
Uterus Endometrium	AN3CA	2.57
AML	SKNO1	2.73
Ewing Sarcoma	CBAGPN	2.73
Rhabdoid	G402	2.86
Ewing Sarcoma	SKES1	2.91
Rhamdoid	BT12	2.93
Rhabdoid	MON	2.99
Melanoma	COLO783	3.21
Glioma	U251MG	3.26
Colorectal	LS513	3.35
Ovary Adenocarcinoma	OAW42	3.44
Lung NSC	HCC1588	3.73
Ovary Adenocarcinoma	IGROV1	4.17
Lung NSC	NCIH1792	4.2
TNBC	MDA-MB-231	4.56
Breast	MCF7	6.51
Breast	T47D	12.81
Prostate	22RV1	12.96

CHAPTER 4 Discussion and Future Directions

Conclusions

ER positive breast cancer remains a challenging disease to manage, despite advances in understanding and treating breast cancer. Most mortality is related to metastatic disease and the development of resistance to mainstay therapies. One recently established mechanism of resistance is caused by *ESR1* ligand binding domain hot spot mutations. However, effective therapeutic strategies to target mutant ER remain elusive as mutations in the ligand binding domain have reduced binding affinity to endocrine therapies, rendering them less effective. New orally bioavailable SERDs are being developed to overcome the shortcomings of aromatase inhibitors, fulvestrant, and tamoxifen, but have their own shortcomings, and have thus far have been unsuccessful in the clinic. Modulating molecular chaperones and E3 ligases that control ER stability could be a promising ligand-binding domain-independent approach to circumvent endocrine resistance. However, the efficacy of HSP90 inhibitors and E3 ligase modulators in mutant ER-expressing breast cancer requires additional investigation.

This thesis expands on the work originally published by Zhao et al. where CHIP was hypothesized as dip G's bona fide target. We now have a clearer and more nuanced understanding of dip G's mechanism. We demonstrated that dip G is a middle domain modulator of HSP90. Though CHIP appears to be an important E3 ligase that is recruited to promote degradation of mature ER in response to HSP90 inhibition, and geldanamycin has been shown to stimulate the interaction between CHIP and ER[33], CHIP does not play an exclusive role in regulating the turnover of HSP90 client

signaling proteins. We expect that in other cell lines, the necessity of CHIP will depend on the expression profile of other E3 ligases that also regulate client protein degradation in response to HSP90 inhibition or modulation. We demonstrated that CHIP was not required for dip G-mediated ER degradation through establishing CHIP KO cell lines using CRISPR-cas9. To our knowledge, our cell line is the first CHIP KO cell line in breast cancer cells, and can be used to better understand mechanisms regulating protein degradation in breast cancer. The constructs we made could easily be used to knock out CHIP in other cancer models, and may be of particular interest to the neurodegeneration field.

Fluorescence polarization assays showed that dip G fluorescent analog deoxy-dip G binds directly to HSP90 (K_d = 0.31 ± 0.06 μM) with an affinity comparable to geldanamycin, an amino-terminal HSP90 inhibitor (K_d = 0.51 ± 0.17 μM) (Fig. 2-19, 2-20). Deoxy-dip G could neither be competed off by N-terminal inhibitors (geldanamycin and radicicol), nor C-terminal inhibitors (GTP and novobiocin) (Fig. 2-21). This supports that dip G is a middle domain modulator, as it neither competitively binds to the N-terminus, nor C-terminus. In addition, using purified recombinant HSP90 fragments, we found that deoxy-dip G binds to the fragment corresponding to the middle domain with a higher affinity (K_d=0.13 μM ± 0.002 μM) than to the fragments encoding the N-terminus (K_d = 13.77 ± 0.17 μM) and C-terminus (K_d = 8.01 ± 1.80 μM) (Fig. 2-13).

Dip G and deoxy-dip G elicited anti-proliferative effects, and could promote mutant ER degradation in 2-D models of ER+ breast cancer (Fig. 3-1), but had no significant effect on the growth of patient derived xenograft models (Fig. 3-11,12,14).

One explanation for the discrepancy between our 2-D culture, and in vivo results is that therapeutic concentrations of dip G could not be reached in a mouse due to the poor pharmacological properties of dip G, such as bioavailability and stability. In addition, according to our PRISM results, ER+ breast cancer is not very sensitive to dip G. To circumvent these limitations, we instead utilized an organoid system derived from one of the PDXs used in our in vivo studies and treated them using our 2-D culture conditions (Fig. 3-8,9,10). Testing the effects of dip G in an ER Y537S-expressing PDXO model to complement our HCI-011 PDXO results warrants further investigation.

Our study is one of the first to study to explore HSP90 modulation in breast cancer with ligand-binding domain mutations. Two other groups have explored this, with conflicting results. One study concluded that HSP90 inhibition is not affected by ER mutational status [63]. Though WT ER levels were decreased in a dose-dependent manner, HSP90 inhibition did not affect the levels of Y537S and D538G mutant ER, indicating that HSP90 does not regulate mutant ER stability[63], while the other group concluded that HSP90 inhibition is affected by ER mutation status[228]. Further mechanistic studies are required to determine conclusively whether HSP90 associates with mutant ER, and whether this phenomenon holds true for other classes of N-terminal, as well as C-terminal-targeting HSP90 inhibitors. Establishing definitively whether HSP90 can interact with *ESR1* LBD mutants could open up a new class of drug for treatment of mutant-ER expressing tumors.

This thesis proposes a new therapeutic strategy for treating endocrine-resistant breast cancer and furthers our understanding of ER degradation mechanisms and the

biology of HSP90 modulation. Though this work was done using ER+ breast cancer cell lines, there is strong rationale to use dip G in other cancer models.

Future Directions

What specific residues does dip G target in the HSP90 middle domain?

By fluorescence polarization, we determined that dip G binds to the middle domain of HSP90 with higher affinity than the N or C-domains using purified HSP90 protein fragments. The middle domain fragments correspond to AA 272-617 of HSP90 α. However, using our experimental strategy, we are not able to further resolve what specific residues in this region are essential for dip G binding. To further understand dip G's mechanism of action, the specific residues on the HSP90 M-domain could be determined by co-crystalizing dip G with full length HSP90 or the HSP90 M-domain. To validate that the residues found via examining the crystal structure of HSP90 and dip G are bona fide targets of dip G, a series of mutations could be introduced into the residues identified. Mutations that abolish binding of dip G to HSP90, as measured by fluorescence polarization assays could be considered dip G's targets.

Is dip G an isoform-selective modulator or pan HSP90 modulator?

HSP90 has four human isoforms. HSP90 α and HSP90 β are primarily cytosolic. HSP90 α is the major inducible form, and HSP90 β is the minor constitutive form. TRAP1 is a mitochondria-specific isoform, and GRP94 is an endoplasmic reticulum-specific isoform. Finding isoform-selective HSP90 inhibitors has become an active area of research in the last decade. Many groups attribute the failure of HSP90 inhibitors in

the clinic to their pan-inhibitory effects. Identifying isoform-selective molecules is of great interest as they have the potential to have fewer deleterious side effects in patients, as well as to be used as probes to better understand the biology of individual isoforms, which is not well understood, as well as their contributions to disease progression. Relying on genetic knock out models alone is difficult, as HSP90 β knock out results in embryonic lethality in mice, and is an essential gene for cancer cells.

Thus far, designing probes that distinguish between isoforms, especially between the two cytosolic isoforms HSP90 α and HSP90 β, has been especially challenging as their N-terminal domains share > 95% sequence identity. Most studies on HSP90 are actually carried out on a mixture of the two cytosolic forms. Based on our fluorescence polarization experiments, we determined that dip G binds to full length HSP90 α and the middle domain of HSP90 α. However, we have not tested binding to other human HSP90 isoforms such as HSP90 β, TRAP1, or GRP94, and we do not know whether dip G has isoform specificity or is a pan HSP90 inhibitor. Using CLICK chemistry, followed by mass spectrometry to probe the dip G interactome, we found that alkyne dip G could pulldown both HSP90 α and HSP90 β, but not TRAP1 and GRP94, indicating that perhaps dip G only targets cytosolic HSP90 isoforms. To determine definitively whether dip G has isoform selectivity, we could use the lysates from our CLICK chemistry experiment to probe for all HSP90 isoforms by western blot. Detecting these proteins in our pulldown lysates would indicate that they interact with dip G. This could then be validated using purified proteins and deoxy-dip G using fluorescence polarization assays, as was performed for HSP90 α. If dip G has isoform selectivity, it could be used

as a probe to help dissect the distinct cellular roles of the HSP90 isoforms, and would explain why dip G does not induce heat shock response.

Improving dip G's potency using medicinal chemistry and SAR

As discussed in Chapter 3, dip G and deoxy-dip G had no significant effect on tumor growth in vivo. One strategy to improve dip G's in vivo potency is to perform additional medicinal chemistry and structure activity relationship analysis. Previously, we found the rotatable phenol group on the A-ring of dip G is indispensable for dip G's ability to promote ER degradation (Fig. 4-1)[206].

Currently the IC_{50} for deoxy-dip G, our most robust analog in terms of stability and ability to promote ER degradation in MCF7, is 6.51 μM, based on results from PRISM (Chapter 3). Deoxy-dip G does not have the dispensable -OH on the A-ring. Treating MCF7 cells with additional dip G analogs and measuring ER degradation identified YZ-017 (Fig. 4-2). YZ-017 has a phenylacetate group on the E ring of dip G (Fig. 4-3). We found that the addition of the phenylacetate group improves ER degradation compared to the parental compound and deoxy-dip G, where ER degradation is being used as a proxy to measure HSP90 inhibition. Further modifications based on this analog could be made to improve ER degradation. Testing using WB has been laborious and time intensive, and the results are qualitative and sometimes not reproducible. Instead, a new library of analogs could be tested rapidly using MCF7 stably expressing Hi-BiT-tagged ER, where cells can be grown in 96 well plates, and ER degradation can be measured with the addition of "LgBiT" after cell lysis.

Binding of LgBiT to Hi-BiT produces a luminescent signal which can be measured quantitatively in an antibody-free manner using a Nano-Glo luciferase assay. Hits from this assay could be used in subsequent fluorescence polarization assays to measure analog binding to HSP90.

Testing dip G in other cancer and disease models

Dip G's anti-cancer effects have now been demonstrated in several cancer models, including triple negative breast cancer, prostate cancer, and hematological malignancies, HER2+ breast cancer (unpublished results from Ang Gao), and ER + breast cancer. Based on work from others characterizing dip G's anti-cancer effects, as well as our own results from PRISM (Chapter 3), we hypothesize that dip G could have applications in many cancer types, particularly those that have been demonstrated to sensitive to HSP90 perturbation (HSP90 knock out or knock down), as well as cancers addicted to HSP90 client proteins. According to Depmap, lineages that are exquisitely sensitive to HSP90 perturbation include blood, B-cell, Ewing sarcoma, and acute lymphocytic leukemia (ALL) lineages. Our PRISM data agrees with the Depmap perturbation data, as cell lines most affected by perturbation of HSP90 are also sensitive to deoxy-dip G. In particular, we found that NB4, an acute myeloid leukemia (AML) cell line, was the most sensitive cell line tested, with an IC_{50} of 70 nM out of over 700 cell line screened (Table 3-1). The second most sensitive cell line, MOLM13, is also an AML cell line, with an IC_{50} of 390 nM. Ewing's sarcoma cell lines TC32, and TC205 were also quite sensitive, with IC50s of 440 nM and 530 nM, respectively (Table 3-1). By comparison, we found that deoxy-dipG's IC_{50} in MCF7 was 6.51 μM, indicating that

there is strong rationale to test dip G in AML and Ewing's sarcoma (Table 3-1). In AML, dip G would likely not require further optimization, as cell lines in this lineage have sensitivity to dip G in the nanomolar range. In the promyelocytic subtype of AML, all trans retinoic acid (ATRA) and arsenic trioxide are extremely effective. However, Meyer et al. was able to show that in cell line models of APL that were resistant to ATRA, tanespimycin could still induce apoptosis, indicating that HSP90 inhibition could be used in treatment-refractory acute promyelocytic leukemia (APL)[229]. Testing diptoindonesin G in this context could yield similar results. The standard of care for Ewing sarcoma includes chemotherapy and radiation therapy and/or surgery. There are currently no approved targeted therapies or immunotherapies, and the five-year survival rate for all SEER stages is 61%. Treatment with HSP90 inhibitors, such as PU-H71 alone and in combination with bortezomib, resulted in promising pre-clinical results. Testing dip G in this disease context would likely yield positive results in a field that needs new therapeutic strategies, as well as a better understanding of the disease's biology.

Beyond cancer, dip G could potentially be used therapeutically in the neurodegeneration field. The pathology of many neurodegenerative diseases, like Alzheimer's, Parkinson's, Huntington's diseases and spinal-bulbar muscular atrophy (SBMA), are characterized by accumulation of misfolded proteins, such as α-synuclein, Tau, or polyglumatine (polyQ) expansion of Huntington and androgen receptor (AR)[230,231]. Interestingly, α-synuclein[232], tau[233], Huntington[234], and AR[235] are all known HSP90 clients. Selectively eliminating these misfolding aggregates by inhibiting or modulating HSP90 could have beneficial therapeutic effects, and there has been

increasing interest in using HSP90 inhibitors in this disease context. However, whether protein aggregates are causal or correlative with neuronal dysfunction remains controversial[230]. Indeed, HSP90 inhibitors have been shown to have neuroprotective effects in Huntington's disease, Parkinson's, and taupathies[231], and decrease levels of Tau in vitro and in vivo[236]. Silencing HSP90 has been shown to reduce levels of polyQ-expanded Huntington protein[234]. In addition, polyQ-expanded AR has been implicated in SBMA, and HSP90 inhibitors tanespimycin and alvespimycin were shown to promote polyQ AR degradation in human neuroblastoma cell line SH-SY5Y[237]. Like for cancer, HSP90 inhibitors have not yet been approved in neurodegenerative diseases, as similar toxicity issues have been observed in clinical trials. Because dip G does not induce heat shock response, and has been shown to downregulate some HSP90 client proteins, it could have an advantage over N-terminal inhibitors in this disease context.

Figure 4-1

Model of the working hypothesis. (A) Dip G promotes ER degradation through the 26S proteasome. CHIP is not required for dip G-mediated ER degradation. HSP90 is required for dip G-mediated ER degradation, and Y537S mutants are sensitive to dip G and HSP90i, but not fulvestrant. (B) Dip G binds to HSP90 via the middle domain, whereas tanespimycin binds to the N-terminus and novobiocin binds to the C-terminus.

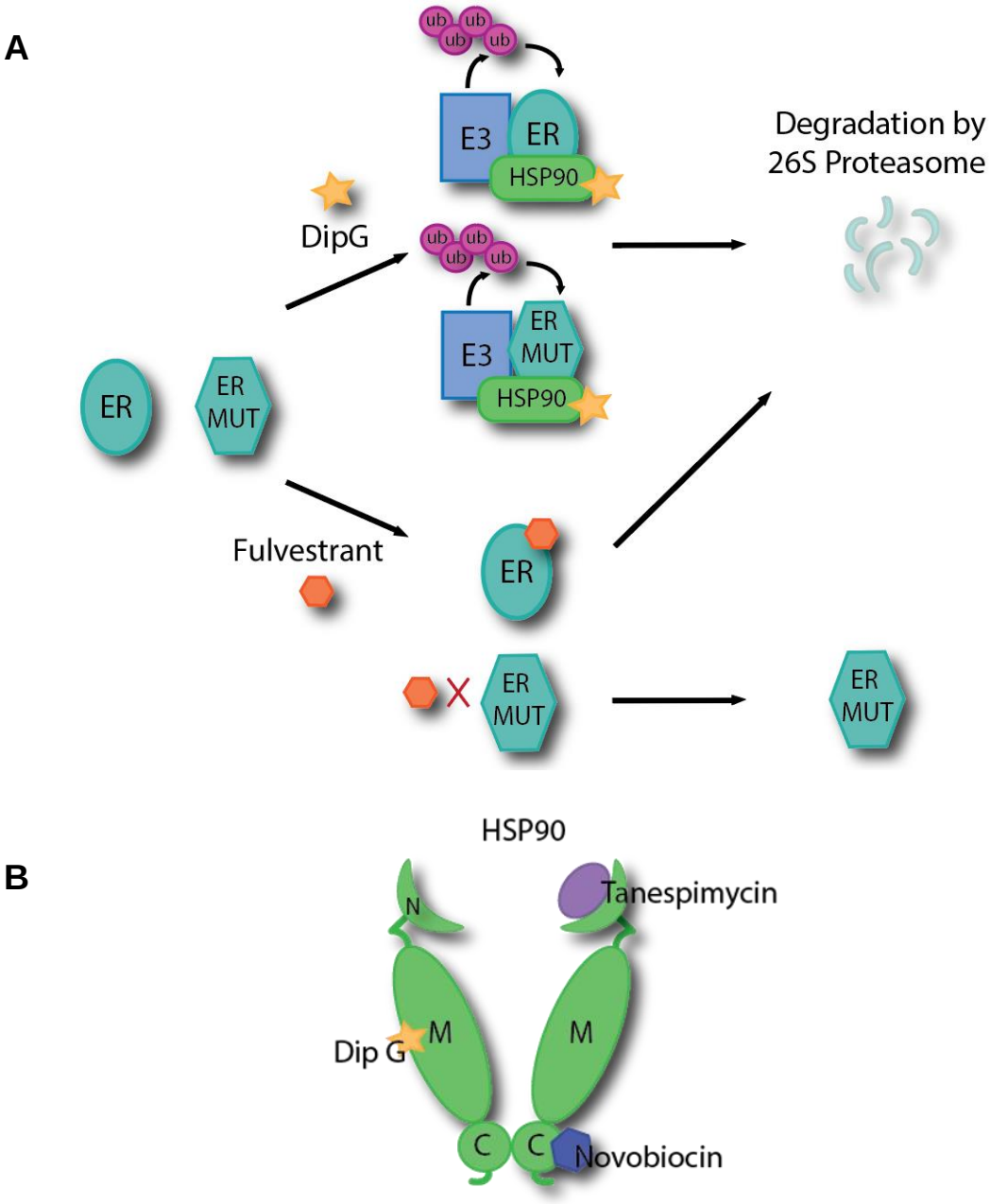

Figure 4-2

Summary of diptoindonesin G structure-relationship analysis.

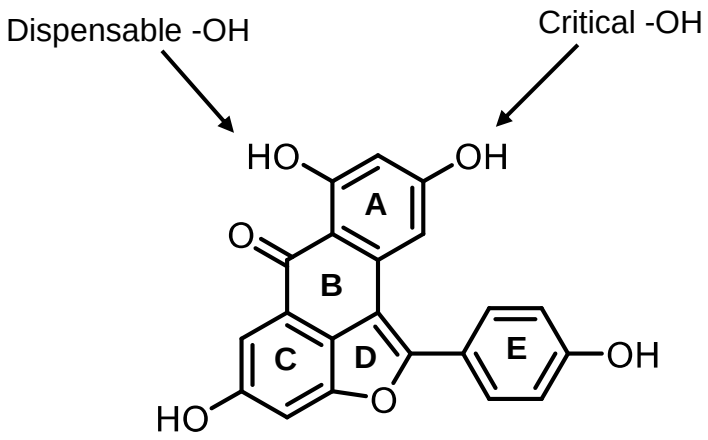

Figure 4-3

MCF7 cells were hormone starved for three days and treated with the following compounds for 24 hours, and ER levels were measured by western blot.

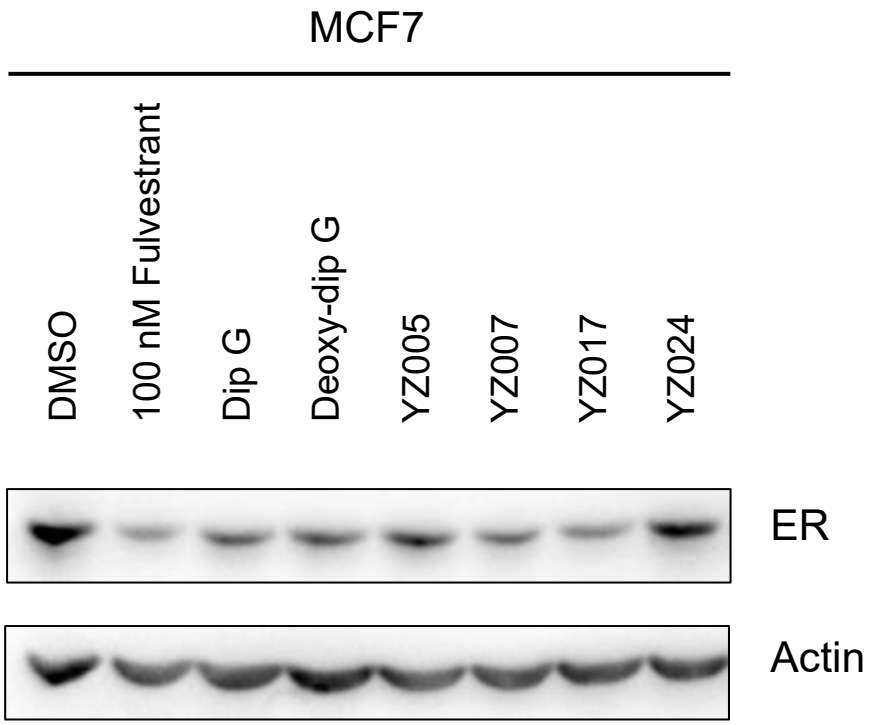

Figure 4-4

Structures of diptoindonesin G analogs tested in Figure 4-3

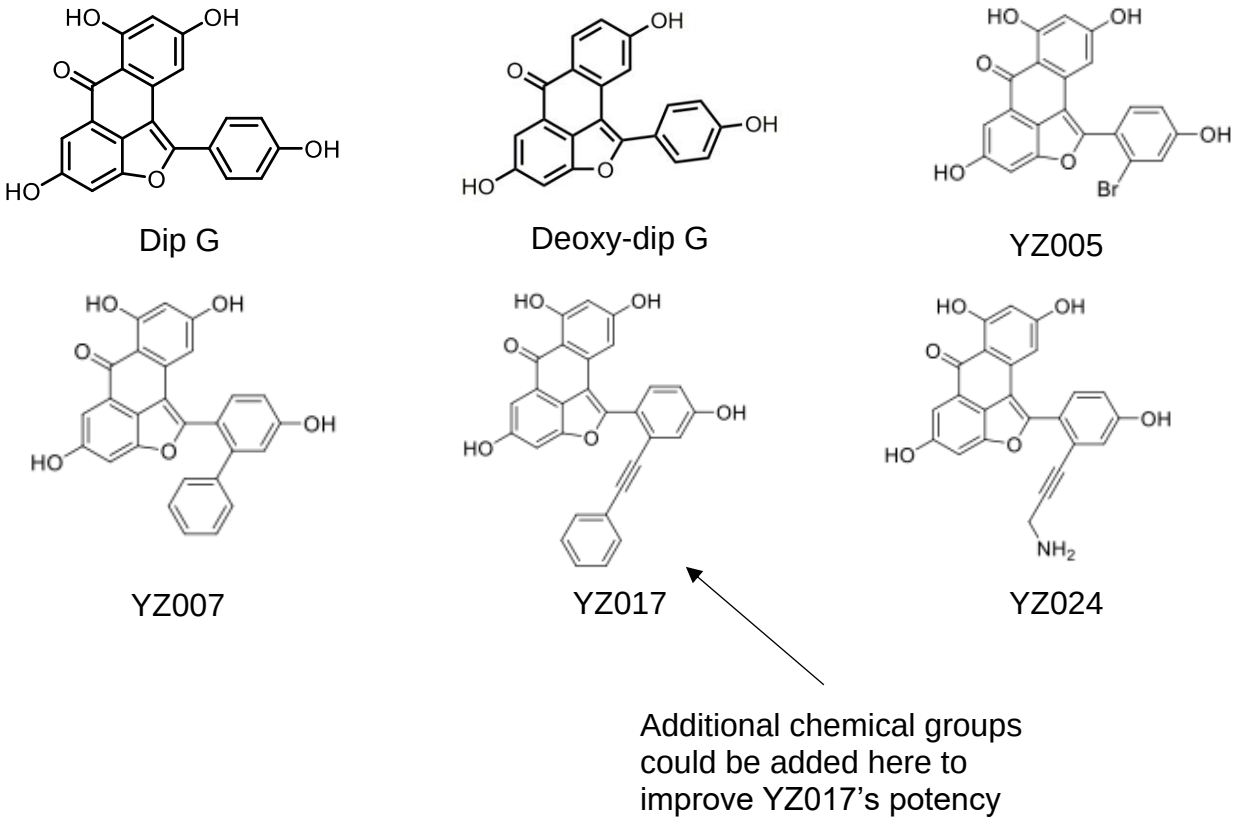

CHAPTER 5

Materials and Methods

Materials and Methods

2-D Cell Culture

MCF7, LCC-2, and BT474 cells were all purchased from the American Type Culture Collection (ATCC). MCF7 WT and MCF7 Y537S cells were provided by Dr. Ben Ho Park. T47D WT and T47D Y537S cells were provided by Dr. Shunqiang Li. All MCF7 cell lines were maintained in DMEM supplemented with 10% fetal bovine serum (FBS) (Gibco, Gaithersburg, MD) and 1% penicillin-streptomycin. T47D cell lines were maintained in RPMI 1640 supplemented with 10% FBS, 1% penicillin-streptomycin, 1% HEPES, 1% L-glutamine, and 1% sodium pyruvate. For subculturing and all experiments, MCF7 and T47D cell lines were all seeded in full medium. The following day, cells were washed with DPBS and medium was changed to phenol red-free equivalents of the culture conditions described above with the substitution of 5% 6X charcoal-stripped FBS. MCF7 and T47D cells were hormone starved for 3 days prior to using in experiments, unless otherwise noted. All cells were cultured at 37°C in a humidified incubator at 5% CO_2.

Generation of CHIP and AR KO Cell Lines

To generate the MCF7 CHIP KO cell lines, a guide RNA specifically targeting exon 2 of *STUB1* was designed and ligated into CRISPR/Cas9/eGFP plasmid PX458 (Addgene, #48138)[211]. For the MCF7 and MCF7 Y537S AR KO cell lines, a guide RNA specifically targeting exon 2 of AR was designed and ligated into CRISPR/Cas9/eGFP plasmid PX458 (Addgene, #48138)[211]. Primer sequences are listed in Table 5-2. Cells were

transfected using Mirus LT1 transfection reagent according to the manufacturer's instructions. 48 hours following transfection, cells were sorted using a BD FACSAria cell sorter at the UW Carbone Cancer Center Flow Cytometry Laboratory, selecting only cells expressing high levels of GFP. Sorted cells were seeded as single cells into 96 well plates, and were allowed to form colonies. Medium was refreshed every week. Colonies were allowed to grow for about 1 month prior to being expanded and screened individually by western blot.

Western Blot

SDS-PAGE gels were transferred to nitrocellulose membranes using a BioRad Turbo Blot. Blots were blocked with 5% nonfat milk in phosphate-buffered saline with 0.1% tween 20 (PBST) for 1-2 hours at room temperature on a shaker, and then incubated with primary antibodies diluted in 5% non-fat milk in PBST at 4°C overnight on a rotator. Blots were washed for 30 min in PBST and then incubated with a goat anti-rabbit and goat anti-mouse horse radish peroxidase-labeled secondary antibodies diluted in 5% non-fat milk in PBST for 1-2 hours at room temperature. Blots were washed once for 30 minutes on a shaker in PSBT and incubated with SuperSignal West Pico ECL (Thermo Fisher Scientific, Waltham, MA) prepared according to the manufacturer's instructions. Blots were exposed using a BioRad ChemiDoc. All antibodies used for western blot are listed in Table 5-1.

Sanger Sequencing

Primers used to confirm AR knockout are listed in Table 5-2. Cells were harvested using trypsin and washed twice with cold DPBS. Genomic DNA was extracted using the ENZA Tissue DNA kit according to the manufacturer's instructions. The extracted genomic DNA was used for PCR. For each 25 µL reaction, the following was included: 2.5 µL 10X Taq buffer (New England Biosystems), 0.5 µL 10 mM dNTPs, 0.5 µL 10 µM forward and reverse primers, 1 µL template DNA, 0.125 µL of Taq (produced and purified in the Xu lab) and 19.875 µL of nuclease free water. The following cycling conditions were used: 95°C for 4 min, 39 cycles of 95°C for 30 s, 58°C for 30s, 72 °C for 30s, followed by 72°C for 5 min and a 4°C hold. 15 uL of PCR product was run on a 1% agarose gel to confirm amplification and size of the PCR product. The QIAquick PCR Purification Kit was used to clean up the PCR products prior to sequencing according to the manufacturer's instructions. The PCR product was used for Sanger sequencing. Each 20 uL sequencing reaction contained 10 uL of template, 3 uL of Big Dye buffer, 2 uL of Big Dye, and 2 uL of androgen receptor forward primer. The following cycling conditions were used: 95°C for 4 min, 39 cycles of 95°C for 30 s, 58°C for 30s, 72 °C for 30s, followed by 72°C for 5 min and a 4°C hold. The sequencing reactions were cleaned up using Mag beads according to the manufacturer's instructions. Reactions were sent to the UW Madison Biotechnology Center for sequencing.

Mass spectrometry for Proteomics

Protein extraction and trypsin digestion

The lysis buffer containing 8M urea and protease and phosphatase inhibitors were added into biological samples at a 1:10 (w/v) ratio. Samples were placed on ice and sonicated 1 min with a 3-s interval at amplitude 25%. Then the lysate was reduced with 10 mM dithiothreitol (DTT) at 37°C for 1 h, and alkylated with 20mM iodoacetamide at room temperature in the dark for an additional 15 min. BCA assay (Thermo Fisher) was performed to determine the proteins concentration and around 100 µg of protein was then digested using trypsin at an enzyme to protein ratio of 1:100 (w/w) at 37 °C overnight. Digested peptides were desalted using C18 cartridges (Waters) and dried in SpeedVac. The concentrations of peptide mixture were measured by peptide assay (Thermo Fisher). Samples were lyophilized and stored at -80 °C.

LC-MS/MS analysis

The liquid chromatography-tandem mass spectrometry (LC-MS/MS) analysis was performed on a Q Exactive HF mass spectrometer (Thermo Fisher) coupled to a nanoflow high-performance liquid chromatography (HPLC) (Dionex UltiMate 3000 UPLC system, Thermo Fisher) with a nanoelectrospray ion source (Thermo Fisher). Peptides were reconstituted in 0.1% formic acid (FA) and about 0.5 µg of peptides were loaded onto a 75 µm x 15 cm self-fabricated column packing with 1.7 µm Ethylene Bridged Hybrid packing materials (130 Å, Waters). A 126-min linear gradient of 3–45% Mobile Phase B (buffer A, 0.1% FA in water; buffer B, 0.1% FA in ACN) at a flow rate of 0.3 ul/min. The MS analysis was performed in a data-dependent manner using an Orbitrap mass analyzer. For a full mass spectrometry survey scan, the automatic gain control (AGC) value was 1e5, and the scan ranged from 300 to 2,000 m/z at a resolution of 60,000, with

a maximum injection time of 100 ms. For the MS2 scan, up to 15 of the most intense precursor ions from a survey scan were selected for MS/MS and detected by the Orbitrap at a mass resolution of 15,000 at m/z 400. Only spectra with a charge state of 2–6 were selected for fragmentation by higher-energy collision dissociation (HCD) with normalized collision energy (NCE) of 30%. The AGC for MS/MS was set to 8e3, with maximum ion injection times of 100ms. Dynamic exclusion time was 30 s, and the isolation window of the precursors was 1.4 Th.

Label-free based MS quantification for proteins

MaxQuant (version 1.5.3.8) with the integrated Andromeda search engine was used for database searching and protein identification and quantification. The false discovery rate (FDR) was controlled below 1% at both peptide and protein level. The tandem mass spectra were searched against the human UniProt database (version 20200219, 20,193 sequences). A reverse database for the decoy search was generated automatically in MaxQuant. Trypsin was selected as the enzyme in specificity, and a minimum number of seven amino acids were required for peptide identification. For label-free protein quantification (LFQ), the MaxQuant LFQ algorithm was enabled to quantitate the MS signals, and the proteins' intensities were represented in LFQ intensity. Cysteine carbamidomethylation was set as the fixed modification, and methionine oxidation, as well as protein N-terminal acetylation, were set as the variable modifications. The first search mass tolerance was set as 20 ppm, and the main search peptide tolerance was 4.5 ppm. The FDR of the peptide-spectrum matches (PSMs) and proteins were set to less than 1%.

ELISA

Cells were seeded in 6 cm dishes in full medium. Following hormone starvation, cells were treated with drug (see related figures for drug treatments and concentrations) for 24 hours. Cells were trypsinized and collected. ELISA was performed using an R&D Systems Human Total ER alpha/NR3A1 DuoSet IC ELISA following the manufacturer's instructions.

CLICK Chemistry and Streptavidin Pull Down

BT474 cells were treated with DMSO as control or 20 μM alkyne dip G for 1 hour. Cells were UV crosslinked (365nM) for 20 minutes, and then then lysed in cold Dulbecco's phosphate buffered saline (DPBS) spiked with a protease inhibitor cocktail using a sonicator (3s on, 3s off, 20 cycle, 30% amplitute). Then gel-based analysis of crosslinked proteins in cells and labeling were performed as described below:

Gel-based analysis of crosslinked proteins in cells (with TAMRA)

Proteomes from treated cells were diluted to 1 mg/mL. To each sample (50 mL), 6 mL of a freshly prepared ''click'' reagent mixture containing 0.1mM tris (benzyltriazolylmethyl)amine (TBTA) (3 mL/sample, 1.7 mM in 1:4 DMSO:t-ButOH), 1 mM CuSO4 (1 mL/sample, 50 mM in H2O), 25 mM tetramethylrhodamine (TAMRA) azide (1 mL/sample, 1.25 mM in DMSO), and freshly prepared 1 mM tris(2-carboxyethyl)phosphine HCl (TCEP) (1 mL/sample, 50 mM in H_2O) was added to conjugate the fluorophore to probe-labeled proteins. Upon addition of the click mixture, each reaction was immediately mixed by vortexing and then allowed to react at ambient

temperature for 1 hr before quenching the reactions with SDS loading buffer (4X stock, 17 mL). Proteins (25 mg total protein loaded per gel lane) were resolved using SDS-PAGE (10% acrylamide) and visualized by in-gel fluorescence on a Bio-Rad ChemiDoc MP flatbed fluorescence scanner. Gel fluorescence and imaging was processed using Image Lab (v 5.2.1) software.

Preparation of labeled proteome for MS-based analysis (with biotin beads)

Profiling experiments were adapted from methods previously reported (Niphakis et al., 2015). To the combined mixture of heavy and light soluble proteomes (1.5 mg) in 1 mL DPBS, a mixture of TBTA (60 mL/sample, 1.7mMin 1:4 DMSO:t-BuOH), CuSO4 (20 mL/sample, 50mM in H2O), TCEP (20 mL/sample, 50mM in DPBS) and Biotin-N3 (10 mL/sample, 10mM in DMSO) was added and each sample was rotated at room temperature. After 1 hr, the mixture was transferred to a 15 mL falcon tube and a cold 4:1 mixture (2.5 mL) of methanol (MeOH)/chloroform (CHCl3) was added followed by cold PBS (1 mL) on ice. The resulting cloudy mixture was centrifuged (5,000 x g, 10 min, 4°C) to fractionate the protein interphase from the organic and aqueous solvent layers. After washing the protein disc carefully with cold 1:1 MeOH:CHCl3 followed by sonication in cold 4:1 MeOH:CHCl3 (3 mL) to ensure click reagents were efficiently removed, the remaining precipitate was pelleted by centrifugation (5,000 x g, 10 min, 4C). The pellet was aspirated and resuspended in a freshly-prepared solution of proteomics-grade urea (500 mL, 6 M in DPBS) containing 10 mL of 10% SDS and then dissolved by sonication. Disulfides were reduced by adding 50 mL of a 1:1 mixture containing TCEP (200 mM in DPBS) preneutralized with potassium carbonate (600 mM

in DPBS) for 30 min at 37°C. Reduced thiols were then alkylated by addition of iodoacetamide (400mM in DPBS) for 30 min at ambient temperature protected from light. To each solution, 130 mL of 10% SDS (in DPBS) was added and then diluted to 0.2% SDS with DPBS (5.5 mL) and incubated with pre-equilibrated streptavidin agarose resin (100 mL 1:1 slurry, Pierce) for 1.5 hr at ambient temperature on a rotator. The streptavidin beads were collected by centrifugation (1,400 x g, 1–2 min) and sequentially washed with 0.2% SDS in DPBS (135 mL), detergent-free DPBS (235 mL), and water (235 mL) to remove unbound protein, excess detergent, and small molecules. The resin was transferred to a Protein LoBind tube (Eppendorf) and bound proteins were digested on-bead overnight at 37°C in 200 mL total volume containing sequencing grade porcine trypsin (2 mg, Promega) in the presence of urea (2M in DPBS) and CaCl2 (1 mM). The proteolyzed supernatant was transferred to a fresh Protein LoBind tube, acidified with formic acid (5% final) and stored at –20°C until analyzed as described above.

Fluorescence polarization

To measure binding to full length HSP90, as well as HSP90 fragments, deoxy-dip G (final concentration of 1μM) was mixed with a serially diluted concentrations of protein in In Black Nunc™ 384-Shallow Well Standard Height Polypropylene Microplates (Catalog Number: 267461) in 50 mM HEPES, 75 mM NaCl, 0.01% Triton X-100, pH 7.4. with a final assay volume of 20μL. After mixing, the plate was incubated at room temperature for 20 minutes. The polarization signals (mP) were acquired by PHERAstar FS Plate Reader (FP 485-520-520nM Optic module). The data was processed, K_d and IC_{50} was

calculated using GraphPad 6.0. The competition assays, were performed as described for the binding assays to HSP90, but competing protein concentrations were kept constant and competed with serially diluted competitor. The radicicol competition assay, as well as the HSP90 α-deoxy-dip G binding results and HSP90 M-deoxy-dip G binding assays were carried out in 150 mM KCl instead of 75 mM NaCl.

HSP90 fragment expression and purification

Purified GST-HSP90 N (9-236) (Addgene #22481), GST-HSP90 M (272-617) (Addgene #22482) and GST-HSP90 C (626-732) (Addgene #22483) plasmids were transformed into BL21 cells and used to inoculate a 5 mL starter cultures in LB with ampicillin grown overnight at 37°C in a shaker. The following day, the starter cultures were used to inoculate 500 mL LB with ampicillin which were grown at 37°C in a shaker. When the OD600 nM reached 0.8-1, cultures were treated with 1M IPTG (1:500), and were placed in a shaker overnight at room temperature. The following day, cultures were spun down at 4°C at 13,000 rpm. The supernatant was decanted, and the pellets were stored at -20°C until use. The pellet was thawed on ice, and sonicated (30 s on 30 s off 50% amplitude for 5 min) in 15 mL of lysis buffer (25 mM TRIS pH 7.5, 1 mM EDTA, 157 mM NaCl, 1% Triton X-100, and protease inhibitor cocktail) on ice. Lysate was spun down at 13,000 rpm at 4°C for 20 min. 500 uL of Glutathione Agarose Resin (Pierce) was washed once with 10 mL of lysis buffer, and loaded with lysate supernatant and incubated on a rotator overnight at 4°C. Beads were washed with 10 mL of wash buffer I (25 mM TRIS pH 7.5, 2 mM EDTA, 500 mM NaCl, 0.5% NP-40, and protease inhibitor cocktail) and then 10 mL of wash buffer II (53 mM TRIS pH 8, 1 mM EDTA, 157 mM

NaCl, 10% glycerol, and protease inhibitor cocktail). Beads were then washed twice with 12 mL of thrombin cleavage buffer. The beads were transferred to microcentrifuge tubes and spun down at 2,000 rpm for 20 seconds. The supernatant was removed, and the beads were resuspended in 2X the bead volume of thrombin cleavage buffer (2.5 mM TRIS pH 8, 3mM NaCl, 6.25 μM $CaCl_2$, 4 μM DTT). 2 units of thrombin enzyme (Novogen) was added/100 uL of beads. The tubes were incubated on a rotator at room temperature for 30 minutes. The tubes were then spun down at 2,000 rpm for 20 seconds and transferred to a new tube (elution 1). An addition 2X the bead volume of thrombin cleavage buffer was added, and incubated on a rotator for 5 minutes. The tubes were spun down at 2,000 rpm for 20 seconds and the supernatant was transferred to a new tube (elution 2).

Coomassie Blue Staining

SDS-PAGE gel was removed from the electrophoresis chamber and placed in enough Coomassie Blue G-250 solution (prepared in 50% methanol, 10% acetic acid) to cover the gel. Gel was stained for 5 min. Stain was discarded, and the gel was rinsed with distilled water to remove residual stain, and destained with destaining solution (40% methanol, 10% acetic acid) for 20 minutes. Destaining solution was removed, and gel was destained in distilled water overnight.

PRISM

The PRISM assay was performed as previously described[223].

RNA sequencing

RNA was extracted from T47D WT and T47D Y537S cell pellets using the Omega ENZA Total RNA Extraction Kit following the manufacturer's instructions. RNA sequencing libraries were prepared using the Illumina TruSeq RNA Library Prep Kit v2 following the manufacturer's instructions. Each library was sequenced in single read mode, 1 x 50 bp, using the HiSeq4000 platform. Sequencing reads were aligned to human genome (hg38 assembly) using STAR[238]. Read counts were performed using HTSeq[239]. Differentially expressed genes were identified by DESeq2[240]. Genes that were changed at least 1.5-fold change and had an adjusted p-value < 0.05 were considered significant. Gene Set Enrichment Analysis (GSEA)[241,242] was performed by taking the total detected genes with $p < 0.05$ in the T47D Y537S dip G treatment vs T47D Y537S DMSO treatment and were analyzed by GSEA using hallmark gene sets.

RT-qPCR

Total cellular RNA was extracted from cell lines and organoids using the Omega ENZA Total RNA Kit according to the manufacturer's instructions. 1 µg of RNA was reverse transcribed using Superscript II RT (Invitrogen, Carlsbad, CA). Quantitative PCR was performed using SYBR Green Master Mix (Roche Scientific, Basel, Switzerland) per the manufacturer's instructions (including cycling parameters), and a BioRad CFX96 instrument (BioRad, Hercules, CA). The Cq values obtained for the genes of interest were then normalized to the Cq values of *18srRNA*. See Table 5-2 for primer sequences.

Cell counting

3×10^3 cells/well were seeded in 100 µL of medium, according to the cell line's culture conditions, in 96-well plates. The next day, 100 µL of 2X concentrated drugs diluted in medium were added to each well. Drugs and medium were refreshed every day for three days. Cells were imaged and counted every day on a BioTek Lion Heart FX Automated microscope at 37°C.

3-D organoid culture

Organoids were cultured as previously described. Briefly, organoids were embedded in matrigel domes in a multi-well plate. For a 96-well plate, 30-40 uL of Matrigel and organoids was used. For a 24-well plate, 40 uL of Matrigel and organoids was used. Plates were flipped and incubated for 30 min at 37°C to allow Matrigel to solidify and reduce the number of organoids growing on plastic. Following the 30 min incubation, medium was added. Organoids were maintained in advanced DMEM supplemented with 5% FBS, 1% penicillin streptomycin, HEPES, Glutamax, gentamycin, 10 ng/ml human EGF, 1 ug/ml hydrocortisone, 100 ng/ml FGF2, 1 mM NAC (N-Acetyl-L-cysteine), and fresh 10 uM Y-27632. Media was exchanged every 3-4 days. Mature cultures were passaged using cell recovery solution according to the manufacturer's instructions, followed by dissociation in TrypLE for 10-15 min at 37°C, with occasional shaking, to dissociate organoids into single cells and smaller organoids.

MTS

Organoids were seeded and cultured as described above. The next day, organoids were treated with drugs. Drugs and medium were refreshed every day for two weeks.

MTS reagent was prepared and added based on the manufacturer's instructions (Promega, Madison, WI)

Tumor Xenograft Experiments

All animal work was performed in accordance with protocols approved by the Institutional Animal Care and Use Committee of the University of Wisconsin-Madison. 5-10-week-old female NSG mice were used for xenograft experiments. HCI-011 and HCI-013 and HCI-013 EI PDX models[179] were generous gifts from Dr. Alana Welm (University of Utah). Fresh PDX tumor tissue ~2-5 mm^3 in size was minced and passed through an 18g needle, followed by a 20g needle in PBS to produce a cell suspension. An equal volume of Matrigel (Corning) (1:1) was added to the PBS and cell suspension mixture, and subcutaneously injected into the mammary fat pads of the mice, and allowed to form visible tumors. For HCI-011 tumors, mice were implanted with beeswax estrogen pellets which were prepared as previously described[226] a few days prior to the study. For HCI-013 EI tumors, no estrogen pellet was implanted due to the estrogen-independent behavior of this PDX. When the tumors reached ~100 mm^3 in size, after approximately 3-4 weeks, mice were randomized to treatment with one of the following treatments: 1) 50 mg/kg of dip G or 100mg/kg of deoxy-dip G, depending on the study, in a 0.4% NaCl and PEG400 solution, administered by oral gavage daily 2) 125 mg/kg of fulvestrant in DMSO and corn oil administered twice a week by subcutaneous injection 3) both dip G and fulvestrant vehicle, administered as described for their

respective drugs. Tumor size was measured twice a week using calipers. Tumor volume was calculated using the following formula: $V = [\text{length} \times (\text{width})^2]/2$.

Immunohistochemistry

Immunohistochemistry was performed with formalin-fixed-paraffin-embedded tumor tissue samples. Tissues were de-paraffinized and rehydrated in three changes of xylenes, followed by decreasing concentrations of ethanol (100%, 95%, and 70%), and finally two changes of water. Antigen retrieval was performed by heating slides at 90-100°C for 20 minutes in 10 mM citrate buffer pH 6. Slides were blocked with Peroxidazed 1 (Biocare Medical) for 5 minutes, washed in phosphate buffered saline (PBS) + 0.1% tween 20 (PBS-T), and then blocked using 2% bovine serum albumin and 5% normal goat serum (Thermo) in PBS for one hour. Slides were incubated with avadin for 15 minutes (Biocare Medical, Pacheco, CA), washed in PBS-T, and then incubated with biotin for 15 minutes and washed in PBS-T. Slides were then incubated with the following antibodies overnight at 4°C in a humidified chamber: ER α (Santa Cruz Biotechnology F-10) (1:100). Ki67 (Proteintech 27309-1-AP) (1:5000). Secondary biotin labeled IgG (4 + biotinylated goat anti-rabbit/mouse IgG, Biocare Medical) incubation was performed at room temperature for 15 min, followed by a 15 min incubation with Streptavidin-HRP (Biocare Medical) at room temperature. Finally, slides were stained with 3,3'-diaminobenzidine (DAB) for 30 seconds to 2 minutes, and counterstained with hematoxylin (Sigma).

Western Blot Quantification

Quantification was performed using Fiji (Image J) for ER and actin. Bands were selected using the square tool. The first band for either ER or actinwas selected using control + 1. Subsequent bands were selected using control + 2. Image type was changed to 8-bit and background was subtracted (default settings). Control + 3 was used to examine curves of the blot band intensity. The line tool was used to confine curves that did not have defined tails. The magic wand tool was used to calculate the area under the curves. Relative expression was calculated by dividing the area of the ER band over the area of the corresponding actin band. Only experiments with at least three independent experiments and three biological replicates were quantified.

ACI Rat Experiments

All animal work was performed in accordance with protocols approved by the Institutional Animal Care and Use Committee at the University of Wisconsin-Madison. 20 eight- week- old female rats were included in this study. All rats were born on 05/30/17. 10 rats received a subcutaneous E2 implant, five received a subcutaneous empty implant as a control, and five rats did not receive an implant. Following implant implantation, rats were randomized to either vehicle (0.4% NaCl and PEG400 solution) or 50 mg/kg of deoxy-dip G treatment by oral gavage. Animals were sacrificed seven days after starting drug treatment. Uteri and pituitary glands were harvested and weighed. Paraffin embedding, mammary gland sectioning, and H&E staining was performed at the UWCCC Experimental Animal Pathology lab.

Measuring the concentration of dip G in mouse serum

All animal work was performed in accordance with protocols approved by the Institutional Animal Care and Use Committee at the University of Wisconsin-Madison. Nine female NSG mice (three mice for each administration method) were dosed with 50 mg/kg dip G, prepared as described above for the tumor xenograft experiments, at T=0 by either oral gavage, subcutaneous injection, or intraperitoneal injection. Mice were lanced, and blood was collected at either T= 0 (no treatment), 5, 30, or 60 minutes after drug administration. Each time point was collected on a different day. Samples were spun down for 30 seconds at 1,200 rpm to remove blood from the tube side walls. After collection, samples were placed in a 37°C water bath. Blood was allowed to coagulate for ~90 minutes. Samples were transferred from the 1.5 mL Eppendorf collection tubes to BD micotainer SST gel tubes. Samples were placed in centrifuge for 10 minutes and spun down at 2,000g. The resulting supernatant was then transferred to 0.5 mL microcentrifuge tubes and stored at -80° C and sent to the Analytical Instrumentation Center at the University of Wisconsin-Madison for tandem mass spectrometry analysis.

Statistical and other analyses

Biological replicates from at least 3 independent experiments were used to perform statistical analyses. The number of technical and biological replicates, as well as independent experiments is listed in each figure legend. A Shapiro-Wilk test was performed to determine whether data follow a normal (Gaussian) distribution. To determine whether the difference between the two means is significant for data that follow a normal distribution, a parametric unpaired t-test with Welch’s correction was

performed. For data that do not follow a normal distribution, a non-parametric Mann-Whitney test was used. Exact p-values are listed in each figure or figure legend. A p-value > 0.05 is considered significant. For RNA-seq, significantly up or down-regulated genes are defined as genes that are changed at least 1.5-fold and have a p-value > 0.05 with a false discovery rate less than 25%. For proteomics data, significantly up or down-regulated proteins are defined as those that are changed at least 1.5-fold and have a p-value > 0.05. Fluorescence polarization curves were analyzed using the [inhibitor] vs. response (three parameters) least squares fit nonlinear regression model in GraphPad Prism.

Table 5- 1

Antibodies			
Antibody Name	Vendor	Catalog Number	Dilution
Mouse Monoclonal Estrogen Receptor Alpha F-10	Santa Cruz Biotechnology	CAT# sc-8002	1:2,000
Rabbit polyclonal C-terminus of HSC-70 Interacting Protein H-231	Santa Cruz Biotechnology	CAT# sc-66830	1:1,000
C-terminus of HSC-70 Interacting Protein	Thermo	CAT# PA1-015	1:1,000
Monoclonal Anti-β-Actin antibody produced in mouse	Sigma	CAT# A5441	1:5,000
Rabbit polyclonal HSP 90α/β Antibody (H-114)	Santa Cruz Biotechnology	CAT# sc-7947	1:1,000
Ubiquitin (P4D1)	Santa Cruz Biotechnology	CAT# sc-8017	1:1,000
Rabbit monoclonal MDM2	Cell Signaling Technology	CAT# 86934S	1:500
HER2	Cell Signaling Technology	CAT# 2165S	1:1,000
E6AP	Invitrogen	CAT# 703785	1:1,000
Androgen Receptor (D6F11)	Cell Signaling Technology	CAT# 5153	1:1,000
Ki67	Proteintech	CAT# 27309-1-AP	1:5,000
Anti-mouse secondary (H+L)	Jackson ImmunoResearch	CAT# 115-035-062	1:5,000
Anti-rabbit secondary (H+L)	Jackson ImmunoResearch	CAT# 111-035-144	1:5,000

Table 5-2

Primers	
Gene	Primer Sequence
18srRNA Forward	TAGTAGCGACGGGCGGTGTG
18srRNA Reverse	CAGCCACCCGAGATTGAGCA
GREB1 Forward	GTGGTAGCCGAGTGGACAAT
GREB1 Reverse	ATTTGTTTCCAGCCCTCCTT
PGR Forward	GGCCAGCAGTCCTGCAACAGTC
PGR Reverse	CCCAAGCTTGTCCGCAGCCTT
HSP27 Forward	AAGCTAGCCACGCAGTCCAA
HSP27 Reverse	CGACTCGAAGGTGACTGGGA
HSP40 Forward	GGACTATGGACTCTTTCAAAGG
HSP40 Reverse	GTAATCAGAAGCAAAGACCC
HSP70 Forward	ATGTCGGTGGTGGGCATAGA
HSP70 Reverse	ACAGCGACGTAGCAGCTCT
HSP90 Forward	GAAATCTGTAGAACCCAAATTTCAA
HSP90 Reverse	TCTTTGGATACCTAATGCGACA
Androgen Receptor Forward	TTGCCTATTTCTGCCATTCA
Androgen Receptor Reverse	GAAGACCTTGCAGCTTCCAC
CHIP KO gRNA Forward	AAACACTGCCGGCGCGCCCTGGAGC
CHIP KO gRNA Reverse	CACCGCTCCAGGGCGCGCCGGCAGT
AR KO gRNA Forward	CACCGATCAGGCAGGTCTTCTGGGG
AR KO gRNA Reverse	AAACCCCCAGAAGACCTGCCTGATC

Table 5-3

Recombinant DNA		
Construct Name	Source	Catalog Number
PX458	Ran et al., 2013	Addgene #48138
GST-HSP90 N	Fontana et al., 2002	Addgene #22481
GST-HSP90	Fontana et al., 2002	Addgene #22482
GST-HSP90 C	Fontana et al., 2002	Addgene #22483
PX458 CHIP KO	This thesis	N/A
PX548 AR KO	This thesis	N/A

Table 5-4

Reagents		
Reagent Name	Vendor	Catalog Number
Glutathione Agarose Resin	Pierce	CAT# 16101
Novagen Thrombin, Restriction Grade	Sigma	CAT# 69671-3
Superscript II RT	Thermo Fisher	CAT# 18064014
Matrigel	Corning	CAT# 354230
Bortezomib	Cayman	CAT# 13697
Human EGF	VWR	CAT# 10787-468
Human FGF2	Fisher	CAT# 50-161-3806
Hydrocortisone	Sigma	CAT# H4001-5G
NAC (N-Acetyl-L-cysteine)	Sigma	CAT# A7250-10G
ROCK inhibitor (Y-27632)	Thermo Fisher	CAT# NC1300641
Avidin-Biotin Kit	Biocare Medical	CAT# AB972
Normal Goat Serum	Thermo	CAT# 31872
4+ biotinylated goat anti-rabbit/mouse IgG	Biocare Medical	CAT#GR602H/GM601H
4+ Streptavadin HRP	Biocare Medical	CAT# HP604
Betazoid DAB Chromogen Kit	Biocare Medical	CAT# BDB2004
Peroxidazed 1	Biocare Medical	CAT# PX968

Table 5-5

Commercial Assays		
Assay Name	Vendor	Catalog Number
Human Total ER alpha/NR3A1 DuoSet IC ELISA	R&D Systems	CAT# DY355-05
Maxima SYBR Green/Rox qPCR Master Mix 2X	Fisher	CAT# FERK0223
TruSeq RNA Library Prep Kit v2	Illumina	CAT# RS-122-2001
MTS	Promega	CAT# G3580
Cell Recovery Solution	Corning	CAT# 354253
Transit LT1	Mirus	CAT# MIR2306
Omega ENZA Total Kit I	Omega Bio-Tek	CAT# R6834-01
Omega ENZA Tissue DNA Kit	Omega Bio-Tek	CAT # D3396
QIAquick PCR Purification Kit	Qiagen	CAT # 28104

Table 5-6

Software and Algorithms		
Software	Source	Link
RNA STAR	Dobin et al., 2013	https://bioinformaticshome.com/tools/rna-seq/descriptions/STAR.html
HTSeq	Anders et al., 2014	https://bioinformaticshome.com/tools/rna-seq/descriptions/HTSeq.html
DESeq2	Love et al. 2014	https://bioconductor.riken.jp/packages/3.2/bioc/html/DESeq2.html
GSEA (Gene Set Enrichment Analysis)	Subramanian et al. (2005)	https://www.gsea-msigdb.org/gsea/index.jsp
	Mootha et al. (2003)	

Table 5-7

Deposited data		
Data	Source	Accession
Raw and analyzed RNAseq data	This thesis	GEO GSE205716
Raw proteomics data	This thesis	Proteome Xchange # PXD035398
Human reference genome NCBI build 38 (GRCh38.p10)	Genome Reference Consortium	http://www.ncbi.nlm.nih.gov/projects/genome/assembly/grc/human/

APPENDIX A: Development of AR Knock Out Cells

Estrogen receptor is not the only steroid hormone receptor that contributes to ER+ breast cancer carcinogenesis. Androgen receptor is widely expressed in ER+ disease. However, the role of AR in breast cancer is complex. In ER+ breast cancer, AR signaling antagonizes ER signaling. However, overexpression of AR in ER+ breast cancer also induced resistance to tamoxifen. In addition, a high AR:ER ratio, as determined by IHC staining correlates with poor disease-free survival in women treated with tamoxifen. In triple negative breast cancer, AR can drive tumor progression. Androgen receptor is also an HSP90 client whose stability is regulated by CHIP. In addition, enzalutamide and tamoxifen can inhibit ER+ AR+ tamoxifen-resistant xenografts better than either drug alone, indicating that both ER and AR are both driving proliferation in some tumors. To further resolve the role of AR in ER+ breast cancer, particularly in the context of ER mutant-expressing breast cancer, knocked out AR in both MCF7 WT cells and MCF7 Y537S cells. Knock out of AR was confirmed by both western blot and sanger sequencing (Fig. A-1-7)

Figure A-1

Western blot measuring AR levels in both parent cells as well as AR knock out clones.

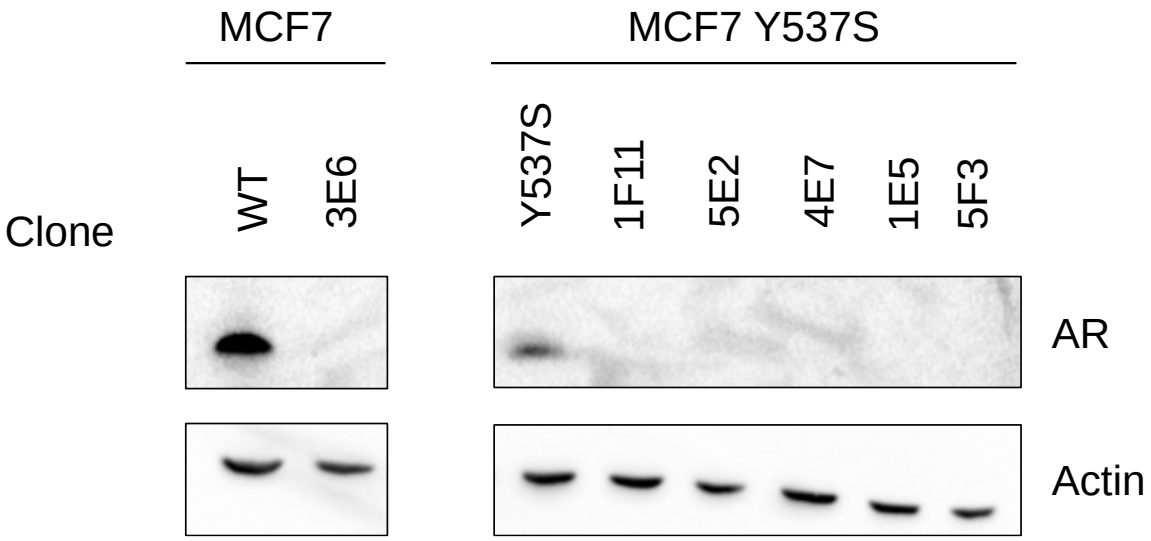

Figure A-2

Sanger sequencing verification of parental Parental WT cells. Sequences were aligned to the corresponding full-length AR sequence to see single nucleotide deletions.

Parental MCF7 WT

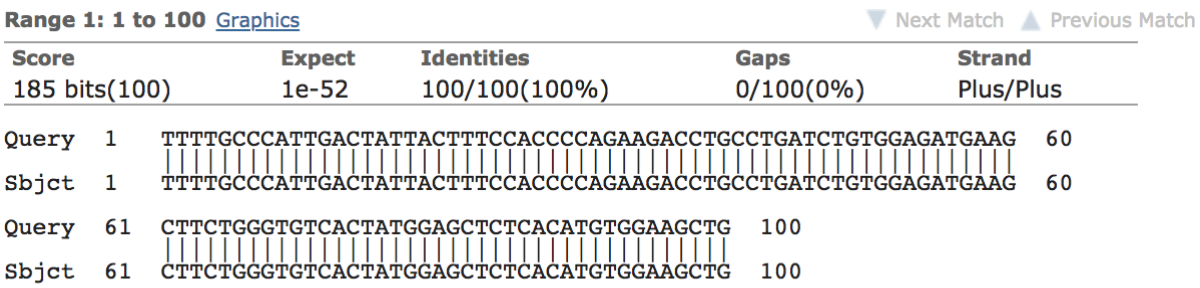

Figure A-3

Sanger sequencing verification of WT AR KO clone 3E6. (Top) Sequences were aligned to the corresponding full-length AR sequence to see single nucleotide deletions. (Bottom) Sequencing base calls near insertion or deletion.

Clone 3E6

Sequence ID: Query_7709 **Length:** 100 **Number of Matches:** 1

Range 1: 1 to 100 Graphics ▼ Next Match ▲ Previous Match

Score	Expect	Identities	Gaps	Strand
152 bits(82)	1e-42	95/100(95%)	5/100(5%)	Plus/Plus

```
Query  1   TTTTGCCCATTGACTATTACTTT-----CCAGAAGACCTGCCTGATCTGTGGAGATGAAG  55
           |||||||||||||||||||||||     ||||||||||||||||||||||||||||||||
Sbjct  1   TTTTGCCCATTGACTATTACTTTCCACCCCAGAAGACCTGCCTGATCTGTGGAGATGAAG  60

Query  56  CTTCTGGGTGTCACTATGGAGCTCTCACATGTGGAAGCTG  95
           |||||||||||||||||||||||||||||||||||||||
Sbjct  61  CTTCTGGGTGTCACTATGGAGCTCTCACATGTGGAAGCTG  100
```

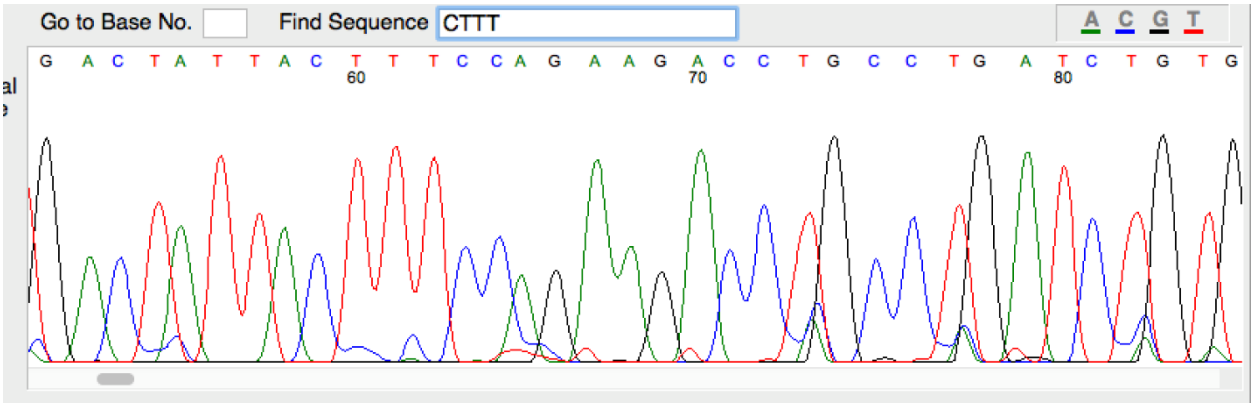

Figure A-4

Sanger sequencing verification of parental MCF7 Y537S. Sequences were aligned to the corresponding full-length AR sequence to see single nucleotide deletions.

Parental MCF7 Y537S

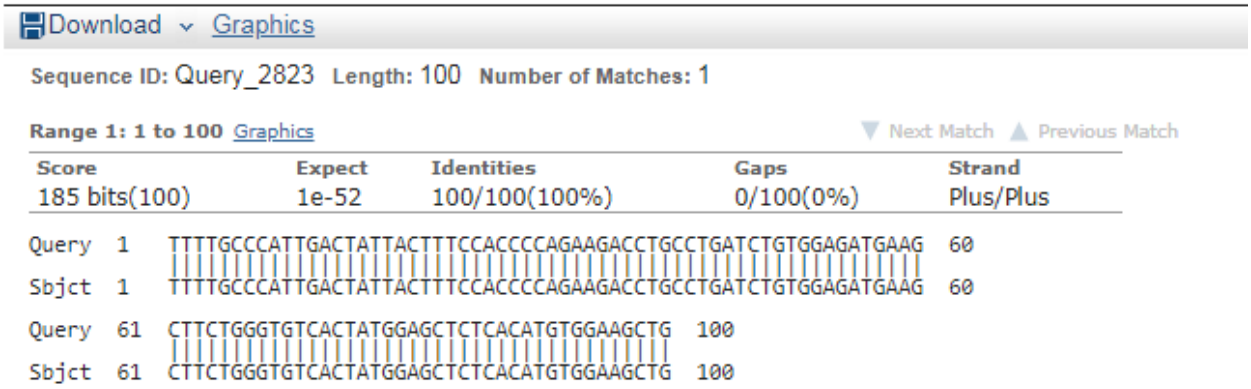

Figure A-5

Sanger sequencing verification of MCF7 Y537S AR KO clone 1F11. (Top) Sequences were aligned to the corresponding full-length AR sequence to see single nucleotide deletions. (Bottom) Sequencing base calls near insertion or deletion.

Clone 1F11

Figure A-6

Sanger sequencing verification of MCF7 Y537S AR KO clone 5E2. (Top) Sequences were aligned to the corresponding full-length AR sequence to see single nucleotide deletions. (Bottom) Sequencing base calls near insertion or deletion.

5E2

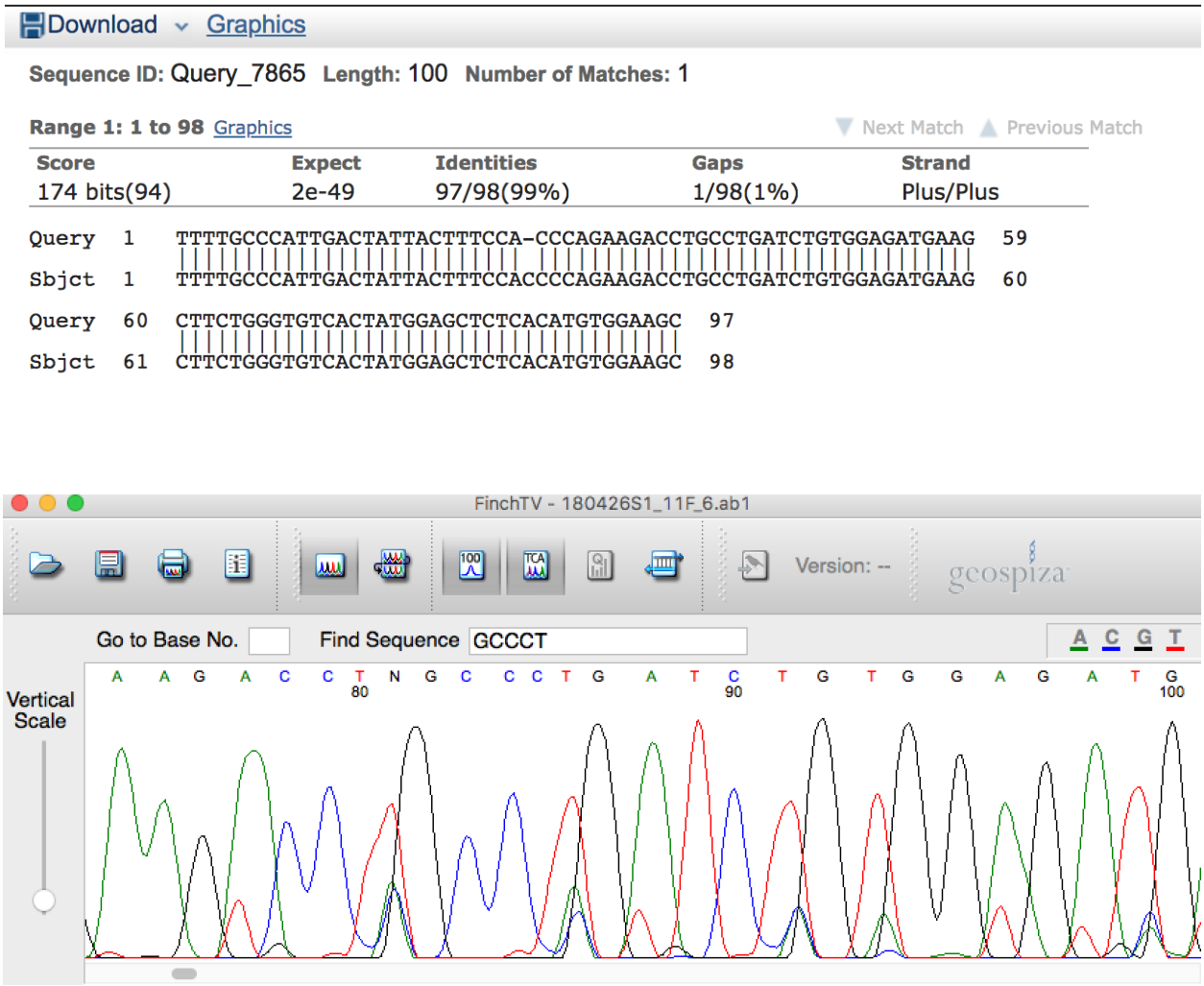

Figure A-7

Sanger sequencing verification of MCF7 Y537S AR KO clone 4E7. (Top) Sequences were aligned to the corresponding full-length AR sequence to see single nucleotide deletions. (Bottom) Sequencing base calls near insertion or deletion.

4E7

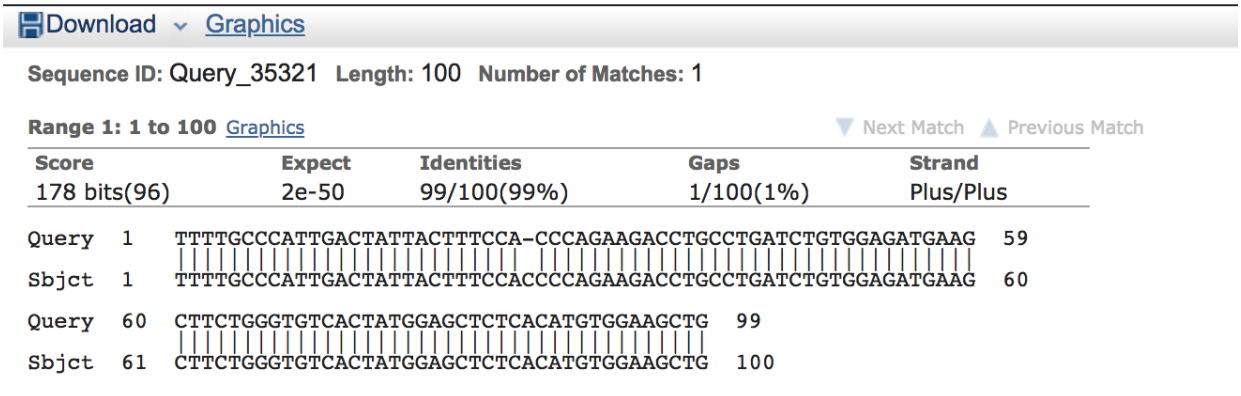

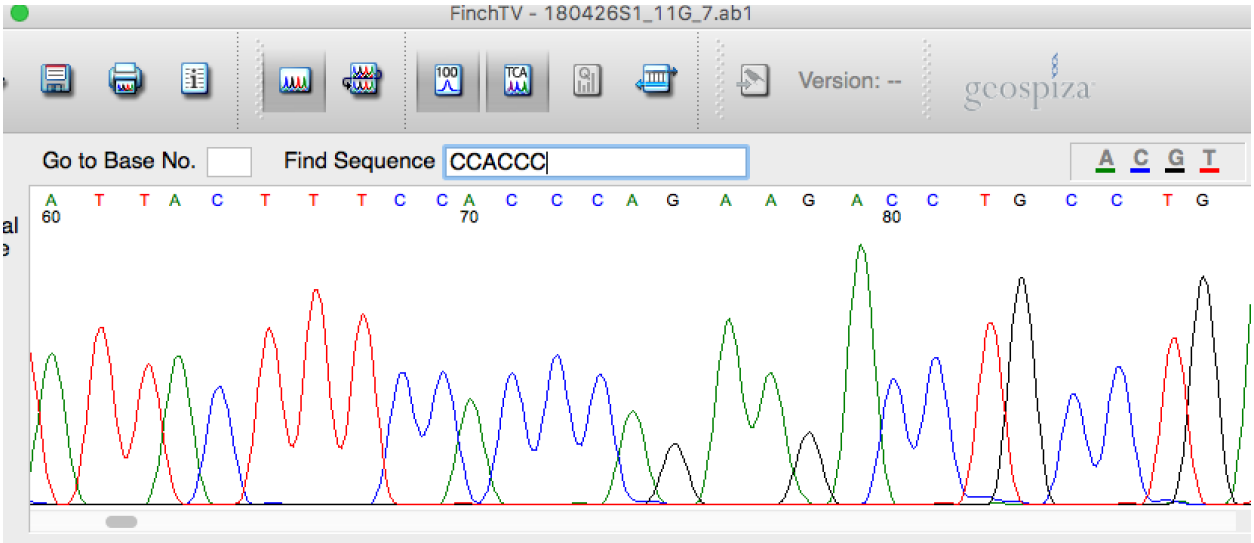

Figure A-6

Sanger sequencing verification of MCF7 Y537S AR KO clone 1E5. (Top) Sequences were aligned to the corresponding full-length AR sequence to see large insertion.

1E5

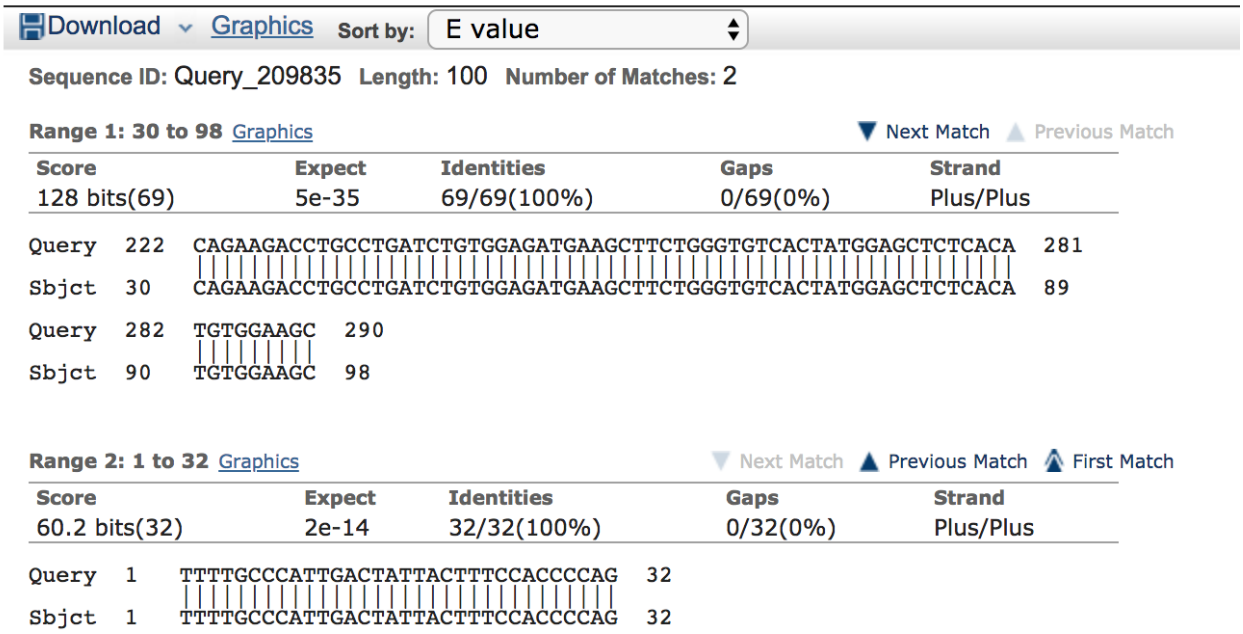

Figure A-7

Sanger sequencing verification of MCF7 Y537S AR KO clone 5F3. (Top) Sequences were aligned to the corresponding full-length AR sequence to see single nucleotide deletions.

5F3

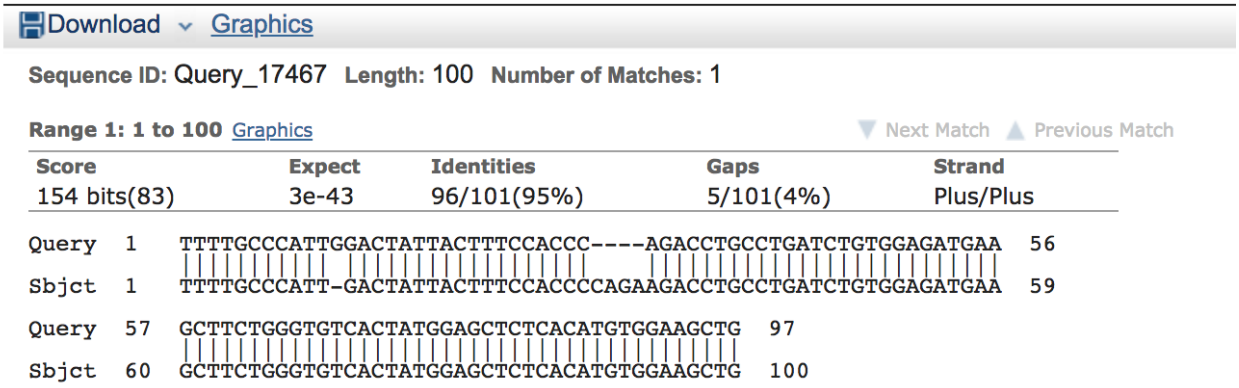

APPENDIX B: Cellular and molecular effects of deoxy-dip G on susceptibility to estradiol-dependent hyperplasia development in the ACI rat model

Aaron Chack and Kirsten Dennison performed all animal handling, husbandry, drug treatments, and assisted with necropsies

Yidan Wang assisted with rat handling, drug treatments, and necropsies

The Experimental Animal Pathology Lab at UW Carbone Cancer Center Histology performed all histology work, including tissue embedding, sectioning, and H&E staining

Reza Karim performed all FLIM analysis

Introduction

To further study the biological effects of diptoindonesin G (dip G) as a drug for treatment of breast cancer we performed a study in collaboration with the Shull lab using ACI Rats. The Shull lab has previous used the ACI rat as a model to study the mechanisms through which estrogens contribute to mammary cancer development, as well as identify genetic determinants of susceptibility to mammary cancer. Unlike other strains, such as BN, which are relatively resistant to 17β-estradiol (E2)-induced mammary cancer, female ACI rats develop mammary carcinomas cancers that express estrogen receptor α (ER), as well as progesterone receptor. These carcinomas are also dependent on E2 for continued growth and survival. Development of mammary cancer in E2-treated ACI rats is dramatically inhibited by concurrent treatment with tamoxifen, indicating a requirement for one or more ER-mediated mechanisms in tumor development, and making them a relevant animal model for ER-positive breast cancer.

Changes in cellular metabolism are a hallmark of cancer development and progression. It is well known that cancer cells alter their utilization of different fuels compared to normal cells throughout tumorigenesis, tumor progression, and metastasis. In particular, tumors will selectively use aerobic glycolysis over oxidative phosphorylation at the cost of 32 molecules of ATP. Metabolic cofactors nicotinamide adenine dinucleotide (NADH) and flavin adenine dinucleotide (FAD) autofluorescence lifetime and intensity can be captured and measured in the same field of view to determine changes in metabolism.

We wanted to see what effects dip G analog deoxy-dip G treatment might have on susceptibility to E2-dependent hyperplasia development in the ACI rat model. We hypothesize that deoxy-dip G decreases susceptibility to E2-dependent hyperplasia development, as well as E2-induced metabolic changes. To measure the cellular and molecular effects of deoxy-dip G, we used several experimental approaches:

1. Fluorescence lifetime imaging microscopy to measure metabolic changes in response to E2 and deoxy-dip G treatment might have on cellular metabolism.

2. H&E to perform histological analyses to determine whether deoxy-dip G can counter act the effects of E2 driven hyperplasia development

Results

20 eight- week- old female rats were included in this study. All rats were born on 05/30/17. 10 rats received a subcutaneous E2 implant, five received a subcutaneous empty implant as a control, and five rats did not receive an implant. Rats were treated with either vehicle or deoxy-dip G by oral gavage. Five rats in the subcutaneous estrogen implant group were treated with deoxy-dip G by oral gavage, five rats in the subcutaneous empty implant group were treated with vehicle by oral gavage, and five rats from the no implant group were treated with deoxy-dip G by oral gavage (Figure B-1). All rats survived to the final endpoint.

After sacrifice, mammary glands from six rats, two from the vehicle oral gavage and empty implant group (vehicle), two from the E2 implant and deoxy-dip G oral gavage groups (E2+ deoxy-dip G), one from the E2 implant (E2) group, and one from the deoxy-dip G oral gavage (deoxy-dip G) group, were immediately taken for fluorescence lifetime imaging microscopy (FLIM), performed in collaboration with Reza Karim from the Skala lab, to see if any differences in cellular metabolism could be observed between the four treatment groups (Fig. B-1). For each rat (three/day), three fields of view were taken. The ROI was defined in ImageJ, and included the mammary duct epithelial cells, and excluded adipocytes (Fig. B-2). We found that the redox ratio for the E2 rat was very high, and the E2+ deoxy-dip G rats had a lower redox ratio than the E2-treated rat. We also found that vehicle-treated rats and deoxy-dip G-treated rats had lower redox ratios compared to the E2+ deoxy-dip G-treated and E2-treated rats. However, there is such a large variation in the redox ratios from the three fields of view

for the E2 treatment condition, and the differences in redox ratios between the different treatment groups does not reach statistical significance (Fig. B-3). As a result, it is hard to draw any conclusions from this data. This variation may be due to the small sample size from each mammary gland. This variation may also be due to one field of view being a true outlier, with no significant differences in redox ratio between all of the conditions.

To determine what effects deoxy-dip G may have on the mammary gland epithelial cells and mammary gland architecture, and whether deoxy-dip G treatment could counteract the oncogenic effects of E2 treatment, mammary gland tissue collected from all 20 rats, including the tissue used for FLIM (26 slides total) were formalin fixed, embedded in paraffin, sectioned to 5 μM, mounted on slides, and stained with H &E. In the vehicle-treated condition, epithelial cells in the ducts are stained purple, and they are nicely organized around the duct (Fig. B-4A)

However, in the E2-treated rat the luminal epithelium exhibited a rapid increase in epithelial density. The ductal epithelial cells are no longer organized around the ducts, and are proliferating rapidly, and may be exhibiting lobular alveolar hyperplasia. The cells are still considered normal, but there is evidence of E2-dependent proliferation. There also appears to be an increase in the collagenous stroma surrounding the epithelial cells (Fig. B-4B). The deoxy-dip G-treated rat tissue resembles the control tissue in that there is very little collagen, and the cells are well organized around the mammary ducts (Fig. B-4C). The E2+ deoxy-dip G rat mammary gland appears to have a phenotype very similar to the E2 treated tissue, where the

epithelial cells lining the ducts are not well organized, and are proliferating rapidly (Fig. B-4D). There also appears to be collagen around the ducts. Finally, after initial inspection on my own, I showed all of my slides to a pathologist, Dr. Ruth Sullivan. The treatment conditions for the slides were blinded. She was able to separate the slides into E2 treated and non-E2 treated. However, she could not distinguish between the E2 and E2 + deoxy-dip G treated rats, nor could she distinguish between the control and deoxy-dip G rats. One explanation for why Dr. Sullivan could not distinguish between the E2 and E2+ deoxy-dip G, nor the control and deoxy-dip G rats, is due to the length of the study. Seven days was long enough to see E2 dependent growth, but perhaps was not long enough to see any changes induced by deoxy-dip G. In addition, the changes caused by deoxy-dip G may be too subtle to be seen with the naked eye, and a more quantitative approach is necessary to really distinguish between the treatment groups. Interestingly, the slides could be further separated into secretory and non-secretory groups, though the secretory and non-secretory groupings did not segregate based on treatment conditions (Table B-1). However, for the most part, in non-E2 treated, appears that treatment with dip G prevents secretion, which makes sense because E2 is critical in development and these rats were very young. As a result, there may be an age-based hormonal effect. Cell degeneration was observed as well, mostly due to sample handling.

To further examine whether deoxy-dip G treatment could counteract the oncogenic effects of E2 treatment, we measured uteri and pituitary gland weight from the necropsied rats. These tissues are very hormone-sensitive, and are known to

enlarge in response to E2 treatment. Surprisingly, we found that E2 treatment did not significantly increase uterus weight compared to vehicle treatment. One explanation is that the rats were treated long enough to see some hyperplasia develop, but not long enough where the uteri would significantly increase in weight. On the other hand, E2 treatment significantly increase pituitary gland weight, whereas deoxy-dip G did not, indicating that deoxy-dip G does not have estrogenic effects on the pituitary gland. However, deoxy-dip G could not counteract the growth-promoting effects of E2, and there was no significant difference between the E2-treated pituitary weights and the E2 and deoxy-dip G-treated pituitary weights.

Discussion

The goal of this study was to determine whether deoxy-dip G could counteract E2-induced hyperplasia, uterotrophy, and metabolic changes. We were able to see E2-induced hyperplasia quite clearly, as well as E2-induced pituitary gland growth, we did not see any E2-induced uterotrophic effects, nor did we observe any E2-induced metabolic changes, making it difficult to interpret the results of this study, as well as determine what effect, if any, deoxy-dip G had. However, based on these results, it is unlikely deoxy-dip G has estrogenic properties, unlike E2, and most SERMs and SERDs. Lengthening the duration of treatment of both E2 and deoxy-dip G could help resolve issues faced in this study. The significance of the secretory and non-secretory phenotype is not clear.

Figure B-1

Summary of study design. 20 rats were randomized to four treatment groups. 10 rats were implanted with a subcutaneous estrogen implant. 5 rats were implanted with an empty implant. 5 rats did not receive an implant. Half of the rats implanted with an E2 implant were treated with deoxy-dip G by oral gavage daily. The empty implant group was treated with vehicle by oral gavage daily. The group with no implant was treated with deoxy-dip G by oral gavage daily. After 7 days of treatment, the rats were sacrificed, and 6 rats had their mammary glands collected for FLIM analysis. Two rats were in the empty implant vehicle group, two were in the deoxy-dip G subcutaneous estrogen implant group, one was from the empty implant deoxy-dip G group, and one was from the subcutaneous estrogen implant group.

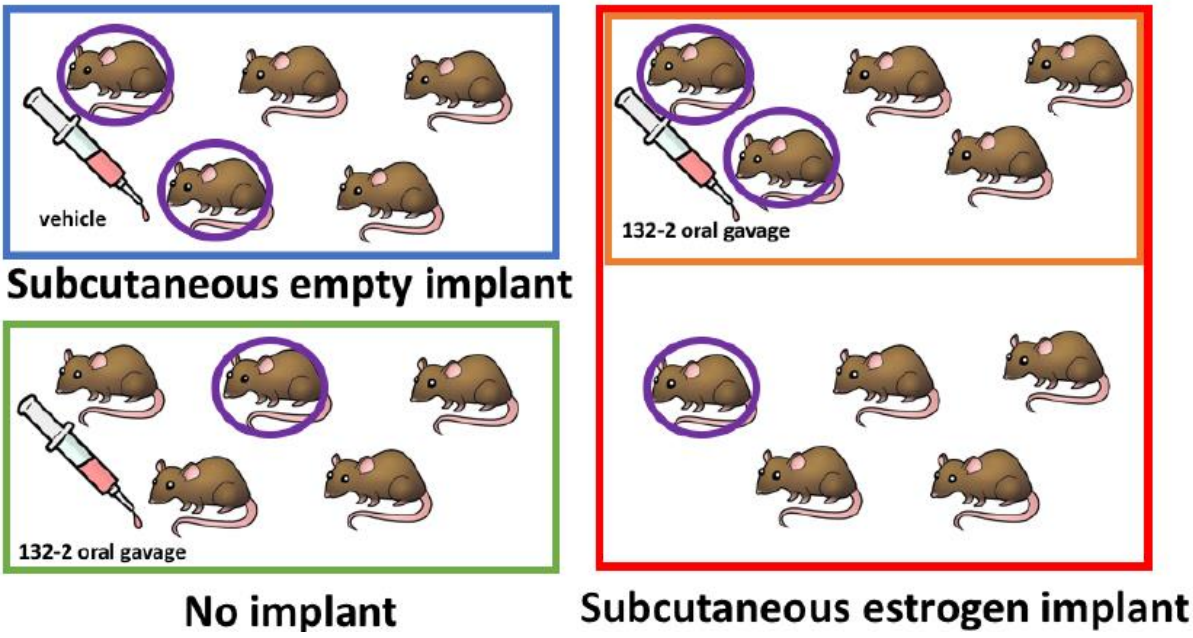

Figure B-2

Multiphoton FLIM of excised mammary glands from ACI rats treated with vehicle, E2, deoxy-dip G, or E2+ deoxy-dip G from A) day 1 or B) day 2. Each condition had three fields of view, except for the E2+deoxy-dip G condition on day 1.

A

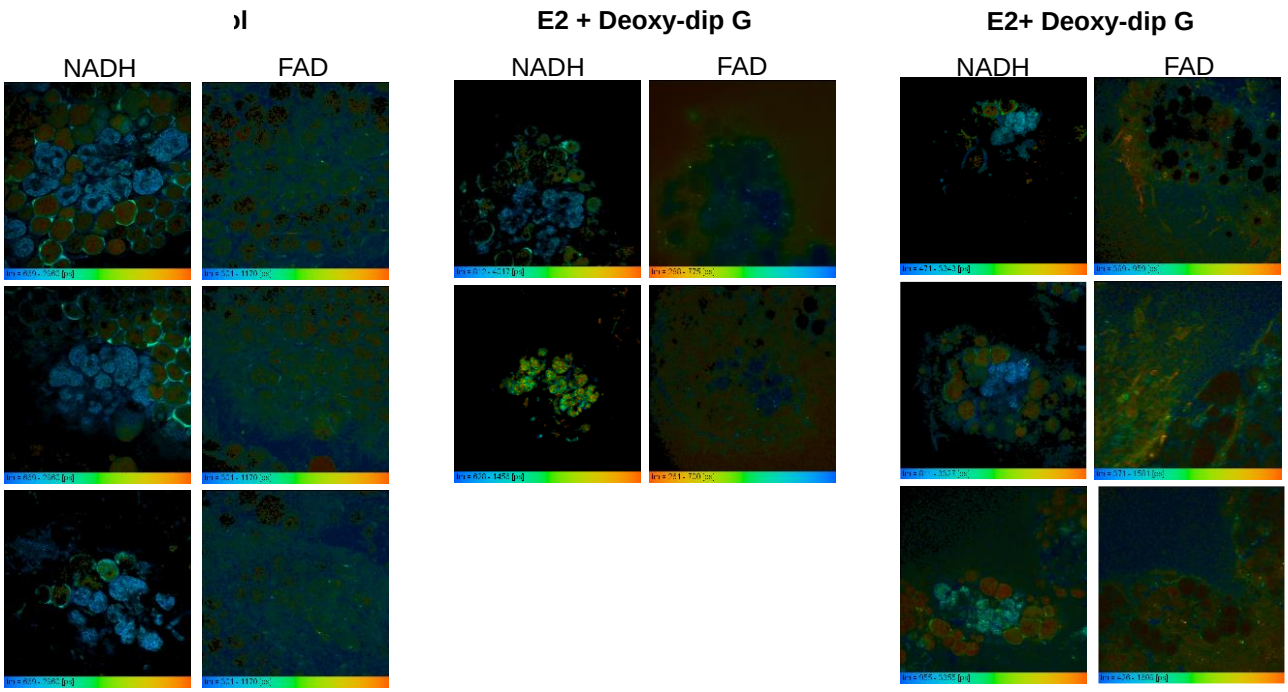
›l
NADH
FAD
E2 + Deoxy-dip G
NADH
FAD
E2+ Deoxy-dip G
NADH
FAD

B

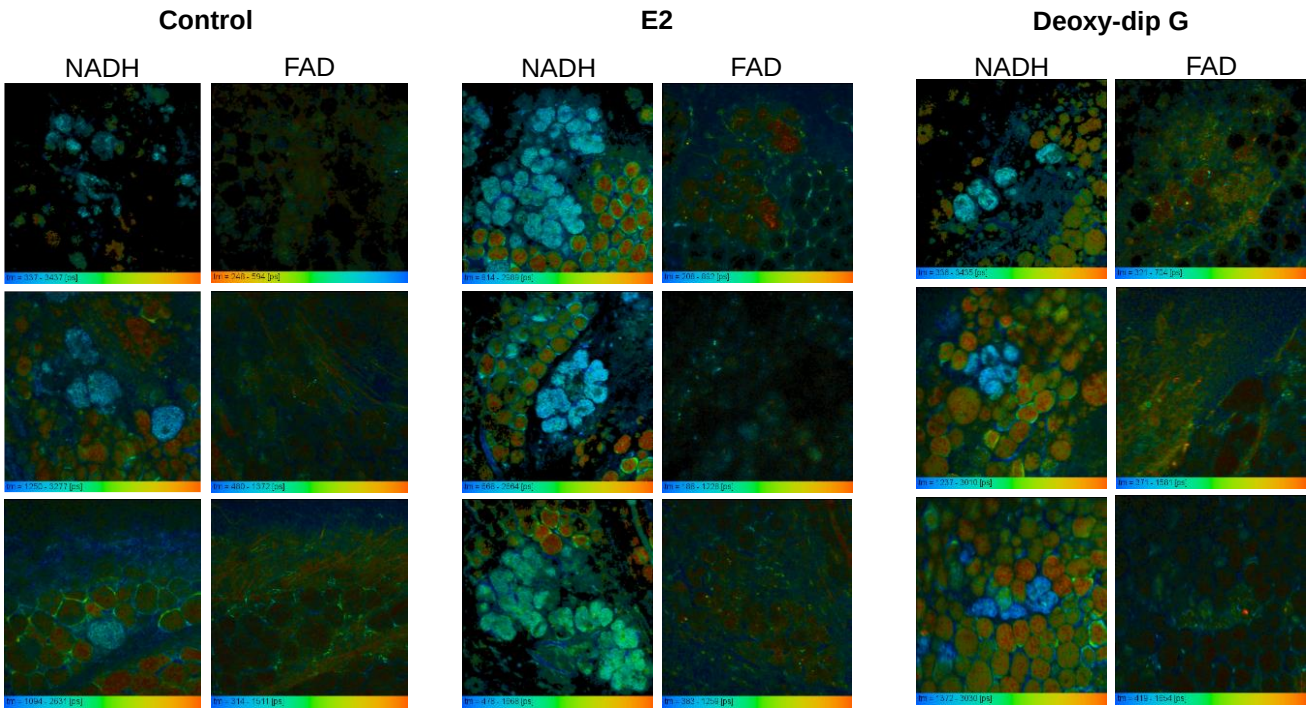
Control
NADH
FAD
E2
NADH
FAD
Deoxy-dip G
NADH
FAD

Figure B-3

The average of the redox ratios for all fields of view for each mammary gland from the six rats used for FLIM. Redox ratios (NADH/FAD) are calculated from Figure B-2. Significance was determined using an unpaired Mann-Whitney test.

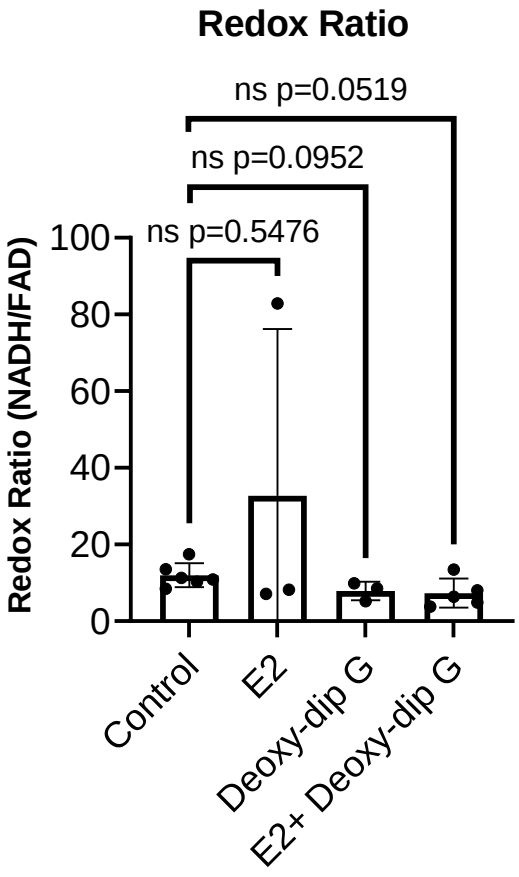

Figure B-4

Representative H&E brightfield staining images of ACI rat mammary glands for each treatment condition taken at 40X objective.

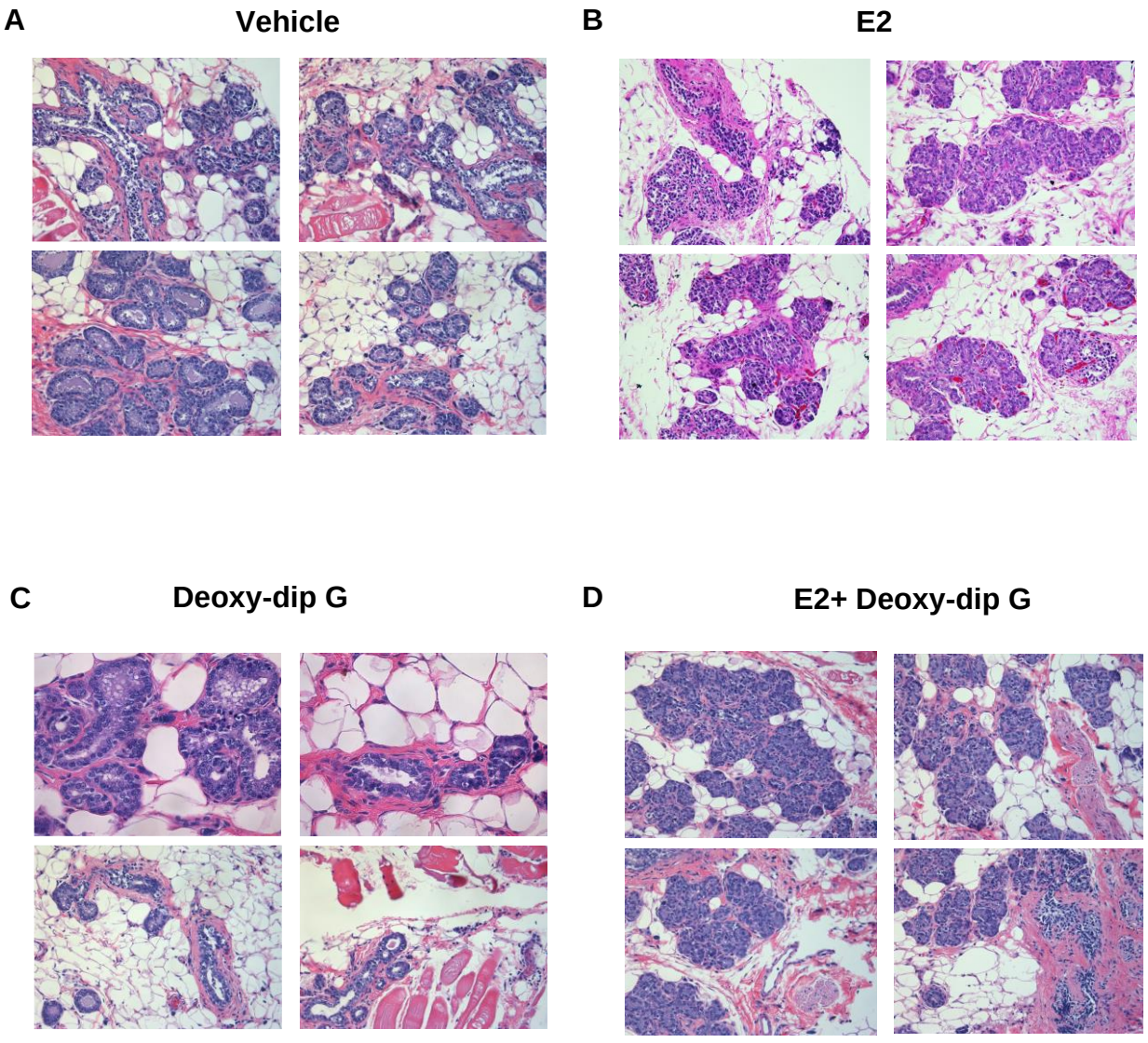

Figure B-5

(A) Uterus weight of ACI rats treated with vehicle, E2, deoxy-dip G, or E2 and deoxy-dip G at time of necropsy. Significance was determined using an unpaired Mann-Whitney test. (B) Pituitary weight of ACI rats treated with vehicle, E2, deoxy-dip G, or E2 and deoxy-dip G at time of necropsy. Significance was determined using an unpaired Welch's t-test.

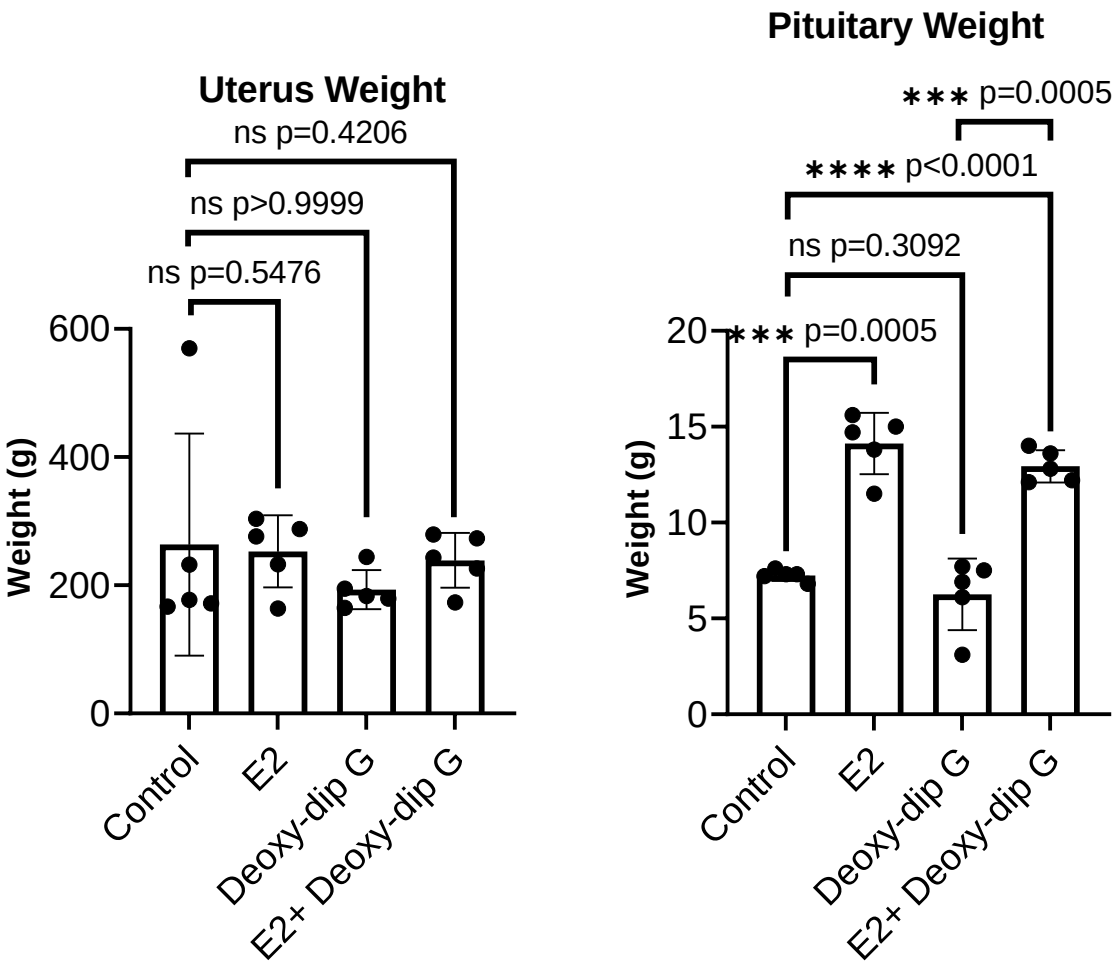

Table B-1

Summary of rat IDs and treatment conditions, as well as pathological classification.

Rat ID	**Treatment Condition**
No E2 Treatment	
Non-secretory	
22168	Vehicle
22184	Deoxy-dip G
22182	Deoxy-dip G
22185	Deoxy-dip G
22186	Deoxy-dip G
Secretory	
22169	Control
22183	Deoxy-dip G
22167	Control
22166	Control
22176	Control
E2-treated	
Secretory	
22180	E2
Non-secretory	
22170	E2+ deoxy-dip G
22172	E2+ deoxy-dip G
22173	E2 + deoxy-dip G
22174	E2 + deoxy-dip G
22179	E2
22177	E2
In-Between	
22178	E2
22175	E2+ deoxy-dip G
22181	E2

References

1. Siegel, R. L., Miller, K. D. & Jemal, A. Cancer statistics, 2019. *CA Cancer J Clin* (2019) doi:10.3322/caac.21551.

2. ALLEN, E. & DOISY, E. A. AN OVARIAN HORMONE: PRELIMINARY REPORT ON ITS LOCALIZATION, EXTRACTION AND PARTIAL PURIFICATION, AND ACTION IN TEST ANIMALS. *J Am Med Assoc* **81**, 819–821 (1923).

3. Jensen, E. v. & Jordan, V. C. The estrogen receptor: A model for molecular medicine. *Clinical Cancer Research* Preprint at (2003).

4. Jensen, E. v., Jacobson, H. I., Walf, A. A. & Frye, C. A. Estrogen action: A historic perspective on the implications of considering alternative approaches. *Physiol Behav* (2010) doi:10.1016/j.physbeh.2009.08.013.

5. Green, S. *et al.* Cloning of the human oestrogen receptor cDNA. *J Steroid Biochem* (1986) doi:10.1016/0022-4731(86)90035-X.

6. Walter, P. *et al.* Cloning of the human estrogen receptor cDNA. *Proc Natl Acad Sci U S A* (1985) doi:10.1073/pnas.82.23.7889.

7. Beatson, G. T. On the Treatment of Inoperable Cases of Carcinoma of the Mamma: Suggestions for a New Method of Treatment, with Illustrative Cases. *Trans Med Chir Soc Edinb* **15**, 153–179 (1896).

8. Tora, L. *et al.* The human estrogen receptor has two independent nonacidic transcriptional activation functions. *Cell* (1989) doi:10.1016/0092-8674(89)90031-7.

9. Lees, J. A., Fawell, S. E. & Parker, M. G. Identification of two transactlvation domains in the mouse oestrogen receptor. *Nucleic Acids Res* (1989) doi:10.1093/nar/17.14.5477.

10. Peng, Y. *et al.* A Metastable Contact and Structural Disorder in the Estrogen Receptor Transactivation Domain. *Structure* **27**, 229-240.e4 (2019).

11. Ali, S., Metzger, D., Bornert, J. M. & Chambon, P. Modulation of transcriptional activation by ligand-dependent phosphorylation of the human oestrogen receptor A/B region. *EMBO Journal* (1993) doi:10.1002/j.1460-2075.1993.tb05756.x.

12. Chen, D. *et al.* Activation of estrogen receptor α by S118 phosphorylation involves a ligand-dependent interaction with TFIIH and participation of CDK7. *Mol Cell* (2000) doi:10.1016/S1097-2765(05)00004-3.

13. Arnold, S. F., Obourn, J. D., Jaffe, H. & Notides, A. C. Phosphorylation of the human estrogen receptor by mitogen-activated protein kinase and casein kinase II: Consequence on DNA binding. *J Steroid Biochem Mol Biol* **55**, 163–172 (1995).

14. Bunone, G., Briand, P. A., Miksicek, R. J. & Picard, D. Activation of the unliganded estrogen receptor by EGF involves the MAP kinase pathway and direct phosphorylation. *EMBO J* **15**, 2174–2183 (1996).

15. Kato, S. *et al.* Activation of the Estrogen Receptor Through Phosphorylation by Mitogen-Activated Protein Kinase. *Science (1979)* **270**, 1491 LP – 1494 (1995).

16. Green, S., Kumar, V., Theulaz, I., Wahli, W. & Chambon, P. The N-terminal DNA-binding 'zinc finger' of the oestrogen and glucocorticoid receptors determines target gene specificity. *EMBO J* (1988) doi:10.1002/j.1460-2075.1988.tb03168.x.

17. Mader, S., Kumar, V., de Verneuil, H. & Chambon, P. Three amino acids of the oestrogen receptor are essential to its ability to distinguish an oestrogen from a glucocorticoid-responsive element. *Nature* (1989) doi:10.1038/338271a0.

18. Umesono, K. & Evans, R. M. Determinants of target gene specificity for steroid/thyroid hormone receptors. *Cell* (1989) doi:10.1016/0092-8674(89)90051-2.

19. Zwart, W. *et al.* The hinge region of the human estrogen receptor determines functional synergy between AF-1 and AF-2 in the quantitative response to estradiol and tamoxifen. *J Cell Sci* (2010) doi:10.1242/jcs.061135.

20. Wang, C. *et al.* Direct Acetylation of the Estrogen Receptor α Hinge Region by p300 Regulates Transactivation and Hormone Sensitivity. *Journal of Biological Chemistry* (2001) doi:10.1074/jbc.M100800200.

21. Sentis, S., le Romancer, M., Bianchin, C., Rostan, M. C. & Corbo, L. Sumoylation of the estrogen receptor β hinge region regulates its transcriptional activity. *Molecular Endocrinology* (2005) doi:10.1210/me.2005-0042.

22. Berry, N. B., Fan, M. & Nephew, K. P. Estrogen receptor-α hinge-region lysines 302 and 303 regulate receptor degradation by the proteasome. *Molecular Endocrinology* (2008) doi:10.1210/me.2007-0449.

23. Mader, S., Chambon, P. & White, J. H. Defining a minimal estrogen receptor DNA binding domain. *Nucleic Acids Res* (1993) doi:10.1093/nar/21.5.1125.

24. Shiau, A. K. *et al.* The structural basis of estrogen receptor/coactivator recognition and the antagonism of this interaction by tamoxifen. *Cell* (1998) doi:10.1016/S0092-8674(00)81717-1.

25. Evans, R. M. The steroid and thyroid hormone receptor superfamily. *Science (1979)* (1988) doi:10.1126/science.3283939.

26. Devin-Leclerc, J. *et al.* Interaction and dissociation by ligands of estrogen receptor and Hsp90: The antiestrogen RU 58668 induces a protein synthesis-dependent clustering of the receptor in the cytoplasm. *Molecular Endocrinology* (1998) doi:10.1210/mend.12.6.0121.

27. Powell, E., Wang, Y., Shapiro, D. J. & Xu, W. Differential requirements of Hsp90 and DNA for the formation of estrogen receptor homodimers and heterodimers. *Journal of Biological Chemistry* (2010) doi:10.1074/jbc.M110.104356.

28. Kumar, V. & Chambon, P. The estrogen receptor binds tightly to its responsive element as a ligand-induced homodimer. *Cell* (1988) doi:10.1016/0092-8674(88)90017-7.

29. Klein-Hitpaß, L., Schorpp, M., Wagner, U. & Ryffel, G. U. An estrogen-responsive element derived from the 5′ flanking region of the Xenopus vitellogenin A2 gene functions in transfected human cells. *Cell* (1986) doi:10.1016/0092-8674(86)90705-1.

30. Klinge, C. M., Jernigan, S. C., Smith, S. L., Tyulmenkov, V. v. & Kulakosky, P. C. Estrogen response element sequence impacts the conformation and transcriptional activity of estrogen receptor α. *Mol Cell Endocrinol* (2001) doi:10.1016/S0303-7207(01)00382-3.

31. Heery, D. M., Kalkhoven, E., Hoare, S. & Parker, M. G. A signature motif in transcriptional co-activators mediates binding to nuclear receptors. *Nature* (1997) doi:10.1038/42750.

32. Valley, C. C., Solodin, N. M., Powers, G. L., Ellison, S. J. & Alarid, E. T. Temporal variation in estrogen receptor-α protein turnover in the presence of estrogen. *J Mol Endocrinol* (2008) doi:10.1677/JME-07-0067.

33. Fan, M., Park, A. & Nephew, K. P. CHIP (carboxyl terminus of Hsc70-interacting protein) promotes basal and geldanamycin-induced degradation of estrogen receptor-α. *Molecular Endocrinology* (2005) doi:10.1210/me.2005-0111.

34. Wijayaratne, A. L. & McDonnell, D. P. The Human Estrogen Receptor-α is a Ubiquitinated Protein Whose Stability is Affected Differentially by Agonists, Antagonists, and Selective Estrogen Receptor Modulators. *Journal of Biological Chemistry* (2001) doi:10.1074/jbc.M101097200.

35. Kushner, P. J. *et al.* Estrogen receptor pathways to AP-1. in *Journal of Steroid Biochemistry and Molecular Biology* (2000). doi:10.1016/S0960-0760(00)00108-4.

36. Safe, S. Transcriptional activation of genes by 17β-estradiol through estrogen receptor-Sp1 interactions. *Vitamins and Hormones* Preprint at https://doi.org/10.1016/s0083-6729(01)62006-5 (2001).

37. McKay, L. I. & Cidlowski, J. A. Molecular Control of Immune/Inflammatory Responses: Interactions Between Nuclear Factor-κB and Steroid Receptor-Signaling Pathways. *Endocr Rev* **20**, 435–459 (1999).

38. Nettles, K. W. *et al.* NFkappaB selectivity of estrogen receptor ligands revealed by comparative crystallographic analyses. *Cell* (1998) doi:10.1016/j.mrfmmm.2005.02.028.

39. Chen, D. *et al.* Phosphorylation of human estrogen receptor α at serine 118 by two distinct signal transduction pathways revealed by phosphorylation-specific antisera. *Oncogene* (2002) doi:10.1038/sj.onc.1205420.

40. Font de Mora, J. & Brown, M. AIB1 Is a Conduit for Kinase-Mediated Growth Factor Signaling to the Estrogen Receptor. *Mol Cell Biol* (2000) doi:10.1128/mcb.20.14.5041-5047.2000.

41. Levin, E. R. Plasma membrane estrogen receptors. *Trends in Endocrinology and Metabolism* Preprint at https://doi.org/10.1016/j.tem.2009.06.009 (2009).

42. Halsted, W. S. I. The Results of Operations for the Cure of Cancer of the Breast Performed at the Johns Hopkins Hospital from June, 1889, to January, 1894. *Ann Surg* **20**, 497–555 (1894).

43. Boyd, S. Sixty-Eighth Annual Meeting of the British Medical Association. *Br Med J* **2**, 1161 LP – 1187 (1900).

44. Toft, D. & Gorski, J. A receptor molecule for estrogens: isolation from the rat uterus and preliminary characterization. *Proc Natl Acad Sci U S A* (1966) doi:10.1073/pnas.55.6.1574.

45. Greene, G. L. *et al.* Sequence and expression of human estrogen receptor complementary DNA. *Science (1979)* **231**, 1150–1154 (1986).

46. Jensen, E. v., Block, G. E., Smith, S., Kyser, K. & DeSombre, E. R. Estrogen receptors and breast cancer response to adrenalectomy. *Natl Cancer Inst Monogr* (1971).

47. Greene, G. L., Sobel, N. B., King, W. J. & Jensen, E. v. Immunochemical studies of estrogen receptors. *J Steroid Biochem* (1984) doi:10.1016/0022-4731(84)90188-2.

48. King, W. J., DeSombre, E. R., Jensen, E. v. & Greene, G. L. Comparison of Immunocytochemical and Steroid-binding Assays for Estrogen Receptor in Human Breast Tumors. *Cancer Res* (1985) doi:10.1007/978-1-4684-5242-6_24.

49. Harper, M. J. & Walpole, A. L. Mode of action of I.C.I. 46,474 in preventing implantation in rats. *J Endocrinol* (1967) doi:10.1677/joe.0.0370083.

50. Skidmore, J., Walpole, A. L. & Woodburn, J. Effect of some triphenylethylenes on oestradiol binding in vitro to macromolecules from uterus and anterior pituitary. *J Endocrinol* (1972) doi:10.1677/joe.0.0520289.

51. Jordan, V. C. Prolonged antioestrogenic activity of ICI 46,474 in the ovariectomized mouse. *J Reprod Fertil* (1975) doi:10.1530/jrf.0.0420251.

52. Jordan, V. C. & Koerner, S. Tamoxifen (ICI 46,474) and the human carcinoma 8S oestrogen receptor. *European Journal of Cancer (1965)* Preprint at https://doi.org/10.1016/0014-2964(75)90119-X (1975).

53. Jordan, V. C. Effect of tamoxifen (ICI 46,474) on initiation and growth of DMBA-induced rat mammary carcinomata. *European Journal of Cancer (1965)* (1976) doi:10.1016/0014-2964(76)90030-X.

54. Sakamoto, T. *et al.* Estrogen receptor-mediated effects of tamoxifen on human endometrial cancer cells. *Mol Cell Endocrinol* **192**, 93–104 (2002).

55. McInerney, E. M. & Katzenellenbogen, B. S. Different regions in activation function-1 of the human estrogen receptor required for antiestrogen- and estradiol-dependent transcription activation. *Journal of Biological Chemistry* (1996) doi:10.1074/jbc.271.39.24172.

56. Liu, H., Lee, E. S., de Los Reyes, A., Zapf, J. W. & Jordan, V. C. Silencing and reactivation of the selective estrogen receptor modulator-estrogen receptor α complex. *Cancer Res* (2001).

57. Long, X. & Nephew, K. P. Fulvestrant (ICI 182,780)-dependent interacting proteins mediate immobilization and degradation of estrogen receptor-α. *Journal of Biological Chemistry* (2006) doi:10.1074/jbc.M510809200.

58. Sherr, C. J., Beach, D. & Shapiro, G. I. Targeting CDK4 and CDK6: From discovery to therapy. *Cancer Discovery* Preprint at https://doi.org/10.1158/2159-8290.CD-15-0894 (2016).

59. Jeselsohn, R., Buchwalter, G., de Angelis, C., Brown, M. & Schiff, R. ESR1 mutations-a mechanism for acquired endocrine resistance in breast cancer. *Nature Reviews Clinical Oncology* Preprint at https://doi.org/10.1038/nrclinonc.2015.117 (2015).

60. Musgrove, E. A. & Sutherland, R. L. Biological determinants of endocrine resistance in breast cancer. *Nature Reviews Cancer* Preprint at https://doi.org/10.1038/nrc2713 (2009).

61. Osborne, C. K. & Schiff, R. Mechanisms of endocrine resistance in breast cancer. *Annu Rev Med* (2011) doi:10.1146/annurev-med-070909-182917.

62. Merenbakh-Lamin, K. *et al.* D538G mutation in estrogen receptor-α: A novel mechanism for acquired endocrine resistance in breast cancer. *Cancer Res* (2013) doi:10.1158/0008-5472.CAN-13-1197.

63. Toy, W. *et al.* ESR1 ligand-binding domain mutations in hormone-resistant breast cancer. *Nat Genet* (2013) doi:10.1038/ng.2822.

64. Robinson, D. R. *et al.* Activating ESR1 mutations in hormone-resistant metastatic breast cancer. *Nat Genet* (2013) doi:10.1038/ng.2823.

65. Jeselsohn, R. *et al.* Emergence of Constitutively Active Estrogen Receptor-α Mutations in Pretreated Advanced Estrogen Receptor–Positive Breast Cancer. *Clinical Cancer Research* **20**, 1757 LP – 1767 (2014).

66. Li, S. *et al.* Endocrine-Therapy-Resistant ESR1 Variants Revealed by Genomic Characterization of Breast-Cancer-Derived Xenografts. *Cell Rep* (2013) doi:10.1016/j.celrep.2013.08.022.

67. Jeselsohn, R. *et al.* Allele-Specific Chromatin Recruitment and Therapeutic Vulnerabilities of ESR1 Activating Mutations. *Cancer Cell* (2018) doi:10.1016/j.ccell.2018.01.004.

68. Chandarlapaty, S. *et al.* Prevalence of ESR1 Mutations in Cell-Free DNA and Outcomes in Metastatic Breast Cancer: A Secondary Analysis of the BOLERO-2 Clinical Trial. *JAMA Oncol* (2016) doi:10.1001/jamaoncol.2016.1279.

69. Spoerke, J. M. *et al.* Heterogeneity and clinical significance of ESR1 mutations in ER-positive metastatic breast cancer patients receiving fulvestrant. *Nat Commun* (2016) doi:10.1038/ncomms11579.

70. Fanning, S. W. *et al.* Estrogen receptor alpha somatic mutations Y537S and D538G confer breast cancer endocrine resistance by stabilizing the activating function-2 binding conformation. *Elife* (2016) doi:10.7554/eLife.12792.

71. Zhao, Y. *et al.* Structurally novel antiestrogens elicit differential responses from constitutively active mutant estrogen receptors in breast cancer cells and tumors. *Cancer Res* (2017) doi:10.1158/0008-5472.CAN-17-1265.

72. Katzenellenbogen, J. A., Mayne, C. G., Katzenellenbogen, B. S., Greene, G. L. & Chandarlapaty, S. Structural underpinnings of oestrogen receptor mutations in endocrine therapy resistance. *Nat Rev Cancer* **18**, 377–388 (2018).

73. Toy, W. *et al.* Activating ESR1 mutations differentially affect the efficacy of ER antagonists. *Cancer Discov* (2017) doi:10.1158/2159-8290.CD-15-1523.

74. Fuqua, S. A. W. *et al.* A Hypersensitive Estrogen Receptor-α Mutation in Premalignant Breast Lesions. *Cancer Res* **60**, 4026 LP – 4029 (2000).

75. Brzozowski, A. M. *et al.* Molecular basis of agonism and antagonism in the oestrogen receptor. *Nature* (1997) doi:10.1038/39645.

76. Martin, L. A. *et al.* Discovery of naturally occurring ESR1 mutations in breast cancer cell lines modelling endocrine resistance. *Nat Commun* (2017) doi:10.1038/s41467-017-01864-y.

77. Fuqua, S. A. W. *et al.* Abstract S4-02: The Y537S ESR1 mutation is a dominant driver of distant ER-positive breast cancer metastasis. *Cancer Res* **77**, S4-02 LP-S4-02 (2017).

78. Gates, L. A. *et al.* Proteomic profiling identifies key coactivators utilized by mutant ERα proteins as potential new therapeutic targets. *Oncogene* (2018) doi:10.1038/s41388-018-0284-2.

79. Fu, X. *et al.* FOXA1 upregulation promotes enhancer and transcriptional reprogramming in endocrine-resistant breast cancer. *Proc Natl Acad Sci U S A* (2019) doi:10.1073/pnas.1911584116.

80. Harrod, A. *et al.* Genomic modelling of the ESR1 Y537S mutation for evaluating function and new therapeutic approaches for metastatic breast cancer. *Oncogene* (2017) doi:10.1038/onc.2016.382.

81. Andreano, K. J. *et al.* The dysregulated pharmacology of clinically relevant ESR1 mutants is normalized by ligand-activated WT receptor. *Mol Cancer Ther* (2020) doi:10.1158/1535-7163.mct-19-1148.

82. Helzer, K. T. *et al.* The Phosphorylated Estrogen Receptor α (ER) Cistrome Identifies a Subset of Active Enhancers Enriched for Direct ER-DNA Binding and the Transcription Factor GRHL2. *Mol Cell Biol* (2018) doi:10.1128/mcb.00417-18.

83. Rajbhandari, P. *et al.* Pin1 modulates ERα levels in breast cancer through inhibition of phosphorylation-dependent ubiquitination and degradation. *Oncogene* (2014) doi:10.1038/onc.2013.78.

84. Jia, S. *et al.* Clinically Observed Estrogen Receptor Alpha Mutations within the Ligand-Binding Domain Confer Distinguishable Phenotypes. *Oncology (Switzerland)* (2018) doi:10.1159/000485510.

85. Sun, J., Zhou, W., Kaliappan, K., Nawaz, Z. & Slingerland, J. M. ERα phosphorylation at Y537 by Src triggers E6-AP-ERα binding, ERα ubiquitylation, promoter occupancy, and target gene expression. *Molecular Endocrinology* (2012) doi:10.1210/me.2012-1140.

86. O'leary, B. *et al.* The genetic landscape and clonal evolution of breast cancer resistance to palbociclib plus fulvestrant in the PALOMA-3 trial. *Cancer Discov* (2018) doi:10.1158/2159-8290.CD-18-0264.

87. Schiavon, G. *et al.* Analysis of ESR1 mutation in circulating tumor DNA demonstrates evolution during therapy for metastatic breast cancer. *Sci Transl Med* (2015) doi:10.1126/scitranslmed.aac7551.

88. Zhang, K. *et al.* Clinical value of circulating ESR1 mutations for patients with metastatic breast cancer: A meta-analysis. *Cancer Management and Research* Preprint at https://doi.org/10.2147/CMAR.S173193 (2018).

89. Najim, O. *et al.* The association between type of endocrine therapy and development of estrogen receptor-1 mutation(s) in patients with hormone-sensitive advanced breast cancer: A systematic review and meta-analysis of randomized and non-randomized trials. *Biochimica et Biophysica Acta - Reviews on Cancer* Preprint at https://doi.org/10.1016/j.bbcan.2019.188315 (2019).

90. de Santo, I., McCartney, A., Malorni, L., Migliaccio, I. & di Leo, A. The emerging role of esr1 mutations in luminal breast cancer as a prognostic and predictive biomarker of response to endocrine therapy. *Cancers* Preprint at https://doi.org/10.3390/cancers11121894 (2019).

91. Linden, H. M., Peterson, L. M. & Fowler, A. M. Clinical Potential of Estrogen and Progesterone Receptor Imaging. *PET Clin* **13**, 415–422 (2018).

92. Kumar, M. *et al.* 18F-fluoroestradiol PET imaging of activating estrogen receptor-a mutations in breast cancer. *Journal of Nuclear Medicine* (2019) doi:10.2967/jnumed.118.224667.

93. Wardell, S. E. *et al.* Pharmacokinetic and pharmacodynamic analysis of fulvestrant in preclinical models of breast cancer to assess the importance of its estrogen receptor-α degrader activity in antitumor efficacy. *Breast Cancer Res Treat* (2020) doi:10.1007/s10549-019-05454-y.

94. van Kruchten, M. *et al.* Measuring residual estrogen receptor availability during fulvestrant therapy in patients with metastatic breast cancer. *Cancer Discov* (2015) doi:10.1158/2159-8290.CD-14-0697.

95. Robertson, J. F. R. Fulvestrant (Faslodex®)—How to Make a Good Drug Better. *Oncologist* (2007) doi:10.1634/theoncologist.12-7-774.

96. Robertson, J. F. R. & Harrison, M. Fulvestrant: Pharmacokinetics and pharmacology. *Br J Cancer* (2004) doi:10.1038/sj.bjc.6601630.

97. Laine, M. *et al.* Abstract PD7-09: Lasofoxifene decreases breast cancer lung and liver metastasis in a mammary intraductal (MIND) xenograft model of mutant ERα+ breast cancer. in (2019). doi:10.1158/1538-7445.sabcs18-pd7-09.

98. Wardell, S. E., Nelson, E. R., Chao, C. A. & McDonnell, D. P. Bazedoxifene exhibits antiestrogenic activity in animal models of tamoxifen-resistant breast cancer: Implications for treatment of advanced disease. *Clinical Cancer Research* (2013) doi:10.1158/1078-0432.CCR-12-3771.

99. Tikoo, D. & Gupta, M. Duavee: a tissue-selective estrogen complex for menopausal symptoms and prevention of osteoporosis. *Int J Basic Clin Pharmacol* (2015) doi:10.5455/2319-2003.ijbcp20150425.

100. Lewis-Wambi, J. S. *et al.* The selective estrogen receptor modulator bazedoxifene inhibits hormone-independent breast cancer cell growth and down-regulates estrogen receptor α and cyclin D1. *Mol Pharmacol* (2011) doi:10.1124/mol.111.072249.

101. Komm, B. S. *et al.* Bazedoxifene acetate: A selective estrogen receptor modulator with improved selectivity. *Endocrinology* (2005) doi:10.1210/en.2005-0030.

102. Fanning, S. W. *et al.* The SERM/SERD bazedoxifene disrupts ESR1 helix 12 to overcome acquired hormone resistance in breast cancer cells. *Elife* (2018) doi:10.7554/eLife.37161.

103. Guan, J. *et al.* Therapeutic Ligands Antagonize Estrogen Receptor Function by Impairing Its Mobility. *Cell* (2019) doi:10.1016/j.cell.2019.06.026.

104. Weir, H. M. *et al.* AZD9496: An oral estrogen receptor inhibitor that blocks the growth of ER-positive and ESR1-mutant breast tumors in preclinical models. *Cancer Res* (2016) doi:10.1158/0008-5472.CAN-15-2357.

105. Joseph, J. D. *et al.* The selective estrogen receptor downregulator GDC-0810 is efficacious in diverse models of ER+ breast cancer. *Elife* (2016) doi:10.7554/eLife.15828.

106. Lai, A. *et al.* Identification of GDC-0810 (ARN-810), an Orally Bioavailable Selective Estrogen Receptor Degrader (SERD) that Demonstrates Robust Activity in Tamoxifen-Resistant Breast Cancer Xenografts. *J Med Chem* (2015) doi:10.1021/acs.jmedchem.5b00054.

107. Nardone, A. *et al.* The oral selective oestrogen receptor degrader (SERD) AZD9496 is comparable to fulvestrant in antagonising ER and circumventing endocrine resistance. *Br J Cancer* (2019) doi:10.1038/s41416-018-0354-9.

108. Metcalfe, C. *et al.* Abstract P5-04-07: GDC-9545: A novel ER antagonist and clinical candidate that combines desirable mechanistic and pre-clinical DMPK attributes. in (2019). doi:10.1158/1538-7445.sabcs18-p5-04-07.

109. Bardia, A. *et al.* EMERALD: Phase III trial of elacestrant (RAD1901) vs endocrine therapy for previously treated ER+ advanced breast cancer. *Future Oncology* Preprint at https://doi.org/10.2217/fon-2019-0370 (2019).

110. Bihani, T. *et al.* Elacestrant (RAD1901), a Selective Estrogen Receptor Degrader (SERD), has antitumor activity in multiple ER+ breast cancer patient-derived xenograft models. *Clinical Cancer Research* (2017) doi:10.1158/1078-0432.CCR-16-2561.

111. Patel, H. K. *et al.* Elacestrant (RAD1901) exhibits anti-tumor activity in multiple ER+ breast cancer models resistant to CDK4/6 inhibitors. *Breast Cancer Research* (2019) doi:10.1186/s13058-019-1230-0.

112. Wardell, S. E., Nelson, E. R., Chao, C. A., Alley, H. M. & McDonnell, D. P. Evaluation of the pharmacological activities of RAD1901, a selective estrogen receptor degrader. *Endocr Relat Cancer* (2015) doi:10.1530/ERC-15-0287.

113. Lu, Y. *et al.* Design and Synthesis of Basic Selective Estrogen Receptor Degraders for Endocrine Therapy Resistant Breast Cancer. *J Med Chem* (2019) doi:10.1021/acs.jmedchem.9b01580.

114. Sreekumar, S. *et al.* Differential regulation and targeting of estrogen receptor α turnover in invasive lobular breast carcinoma. *Endocrinology* (2020) doi:10.1210/endocr/bqaa109.

115. Wardell, S. E., Marks, J. R. & McDonnell, D. P. The turnover of estrogen receptor α by the selective estrogen receptor degrader (SERD) fulvestrant is a saturable process that is not required for antagonist efficacy. *Biochem Pharmacol* (2011) doi:10.1016/j.bcp.2011.03.031.

116. Puyang, X. *et al.* Discovery of selective estrogen receptor covalent antagonists for the treatment of ERαWT and ERαMUT breast cancer. *Cancer Discov* (2018) doi:10.1158/2159-8290.CD-17-1229.

117. Hamilton, E. P. *et al.* Phase I dose escalation of H3B-6545, a first-in-class highly Selective ERα Covalent Antagonist (SERCA), in women with ER-positive, HER2-negative breast cancer (HR+ BC). *Journal of Clinical Oncology* **37**, 1059 (2019).

118. Rioux, N. *et al.* Nonclinical pharmacokinetics and in vitro metabolism of H3B-6545, a novel selective ERα covalent antagonist (SERCA). *Cancer Chemother Pharmacol* (2019) doi:10.1007/s00280-018-3716-3.

119. Fribbens, C. *et al.* Plasma ESR1 Mutations and the treatment of estrogen receptor-Positive advanced breast cancer. *Journal of Clinical Oncology* (2016) doi:10.1200/JCO.2016.67.3061.

120. Wardell, S. E. *et al.* Efficacy of SERD/SERM Hybrid-CDK4/6 Inhibitor Combinations in Models of Endocrine Therapy-Resistant Breast Cancer. *Clinical Cancer Research* (2015) doi:10.1158/1078-0432.CCR-15-0360.

121. Gelsomino, L. *et al.* ESR1 mutations affect anti-proliferative responses to tamoxifen through enhanced cross-talk with IGF signaling. *Breast Cancer Res Treat* (2016) doi:10.1007/s10549-016-3829-5.

122. Li, Z. *et al.* Upregulation of IRS1 enhances IGF1 response in Y537S and D538G ESR1 mutant breast cancer cells. *Endocrinology* (2018) doi:10.1210/en.2017-00693.

123. Nayar, U. *et al.* Acquired HER2 mutations in ER + metastatic breast cancer confer resistance to estrogen receptor–directed therapies. *Nature Genetics* Preprint at https://doi.org/10.1038/s41588-018-0287-5 (2019).

124. Mao, P. *et al.* Acquired FGFR and FGF alterations confer resistance to estrogen receptor (ER) targeted therapy in ER+ metastatic breast cancer. *bioRxiv* 605436 (2019) doi:10.1101/605436.

125. Tateishi, Y. *et al.* Ligand-dependent switching of ubiquitin-proteasome pathways for estrogen receptor. *EMBO Journal* (2004) doi:10.1038/sj.emboj.7600472.

126. Trepel, J., Mollapour, M., Giaccone, G. & Neckers, L. Targeting the dynamic HSP90 complex in cancer. *Nature Reviews Cancer* Preprint at https://doi.org/10.1038/nrc2887 (2010).

127. Lai, B. T., Chin, N. W., Stanek, A. E., Keh, W. & Lanks, K. W. Quantitation and intracellular localization of the 85K heat shock protein by using monoclonal and polyclonal antibodies. *Mol Cell Biol* **4**, 2802 LP – 2810 (1984).

128. Morano, K. A., Santoro, N., Koch, K. A. & Thiele, D. J. A trans -Activation Domain in Yeast Heat Shock Transcription Factor Is Essential for Cell Cycle Progression during Stress . *Mol Cell Biol* **19**, (1999).

129. Borkovich, K. A., Farrelly, F. W., Finkelstein, D. B., Taulien, J. & Lindquist, S. hsp82 is an essential protein that is required in higher concentrations for growth of cells at higher temperatures. *Mol Cell Biol* **9**, (1989).

130. Nakai, A. & Ishikawa, T. Cell cycle transition under stress conditions controlled by vertebrate heat shock factors. *EMBO Journal* **20**, (2001).

131. Hoter, A., El-Sabban, M. E. & Naim, H. Y. The HSP90 family: Structure, regulation, function, and implications in health and disease. *International Journal of Molecular Sciences* vol. 19 Preprint at https://doi.org/10.3390/ijms19092560 (2018).

132. Grad, I. *et al.* The Hsp90 Cochaperone p23 Is Essential for Perinatal Survival. *Mol Cell Biol* **26**, (2006).

133. Voss, A. K., Thomas, T. & Gruss, P. Mice lacking HSP90β fail to develop a placental labyrinth. *Development* **127**, (2000).

134. Roe, S. M. *et al.* The Mechanism of Hsp90 Regulation by the Protein Kinase-Specific Cochaperone p50cdc37. *Cell* **116**, (2004).

135. Prodromou, C. *et al.* Identification and structural characterization of the ATP/ADP-binding site in the Hsp90 molecular chaperone. *Cell* **90**, 65–75 (1997).

136. Stebbins, C. E. *et al.* Crystal structure of an Hsp90-geldanamycin complex: Targeting of a protein chaperone by an antitumor agent. *Cell* **89**, 239–250 (1997).

137. Meyer, P. *et al.* Structural basis for recruitment of the ATPase activator Aha1 to the Hsp90 chaperone machinery. *EMBO Journal* **23**, (2004).

138. Mercier, R. *et al.* The conserved NxNNWHW motif in Aha-type co-chaperones modulates the kinetics of Hsp90 ATPase stimulation. *Nat Commun* **10**, (2019).

139. Marcu, M. G., Chadli, A., Bouhouche, I., Catelli, M. & Neckers, L. M. The heat shock protein 90 antagonist novobiocin interacts with a previously unrecognized

ATP-binding domain in the carboxyl terminus of the chaperone. *Journal of Biological Chemistry* **275**, (2000).

140. Allan, R. K., Mok, D., Ward, B. K. & Ratajczak, T. Modulation of Chaperone Function and Cochaperone Interaction by Novobiocin in the C-terminal Domain of Hsp90. *Journal of Biological Chemistry* **281**, (2006).

141. Obermann, W. M. J., Sondermann, H., Russo, A. A., Pavletich, N. P. & Hartl, F. U. In vivo Function of Hsp90 Is Dependent on ATP Binding and ATP Hydrolysis . *Journal of Cell Biology* **143**, 901–910 (1998).

142. Panaretou, B. *et al.* ATP binding and hydrolysis are essential to the function of the Hsp90 molecular chaperone in vivo. *EMBO J* **17**, 4829–4836 (1998).

143. Grenert, J. P., Johnson, B. D. & Toft, D. O. The importance of ATP binding and hydrolysis by Hsp90 in formation and function of protein heterocomplexes. *Journal of Biological Chemistry* **274**, 17525–17533 (1999).

144. Patricia Hernández, M., Sullivan, W. P. & Toft, D. O. The assembly and intermolecular properties of the hsp70-Hop-hsp90 molecular chaperone complex. *Journal of Biological Chemistry* (2002) doi:10.1074/jbc.M206566200.

145. Jolly, C. & Morimoto, R. I. Role of the heat shock response and molecular chaperones in oncogenesis and cell death. *Journal of the National Cancer Institute* vol. 92 Preprint at https://doi.org/10.1093/jnci/92.19.1564 (2000).

146. McCollum, A. K., TenEyck, C. J., Sauer, B. M., Toft, D. O. & Erlichman, C. Up-regulation of heat shock protein 27 induces resistance to 17-allylamino-demethoxygeldanamycin through a glutathione-mediated mechanism. *Cancer Res* (2006) doi:10.1158/0008-5472.CAN-06-1629.

147. Clarke, P. A. *et al.* Gene expression profiling of human colon cancer cells following inhibition of signal transduction by 17-allylamino-17-demethoxygeldanamycin, an inhibitor of the hsp90 molecular chaperone. *Oncogene* (2000) doi:10.1038/sj.onc.1203753.

148. Erlichman, C. Tanespimycin: The opportunities and challenges of targeting heat shock protein 90. *Expert Opinion on Investigational Drugs* Preprint at https://doi.org/10.1517/13543780902953699 (2009).

149. Kiang, J. G. & Tsokos, G. C. Heat shock protein 70 kDa: Molecular biology, biochemistry, and physiology. *Pharmacology and Therapeutics* vol. 80 Preprint at https://doi.org/10.1016/S0163-7258(98)00028-X (1998).

150. Neckers, L. *et al.* Methods to validate Hsp90 inhibitor specificity, to identify off-target effects, and to rethink approaches for further clinical development. *Cell Stress Chaperones* **23**, (2018).

151. Yano, M., Naito, Z., Tanaka, S. & Asano, G. Expression and roles of heat shock proteins in human breast cancer. *Japanese Journal of Cancer Research* **87**, (1996).

152. Yano, M. *et al.* Expression of hsp90 and cyclin D1 in human breast cancer. *Cancer Lett* **137**, (1999).

153. Pick, E. *et al.* High HSP90 expression is associated with decreased survival in breast cancer. *Cancer Res* **67**, (2007).

154. Zou, M. *et al.* Evolutionarily conserved dual lysine motif determines the non-chaperone function of secreted Hsp90alpha in tumour progression. *Oncogene* **36**, (2017).

155. Tang, X. *et al.* Heterogeneous Responses and Isoform Compensation Dim the Therapeutic Window of Hsp90 ATP-Binding Inhibitors in Cancer. *Mol Cell Biol* **42**, (2022).

156. Kamal, A. *et al.* A high-affinity conformation of Hsp90 confers tumour selectivity on Hsp90 inhibitors. *Nature* (2003) doi:10.1038/nature01913.

157. Linja, M. J. *et al.* Amplification and overexpression of androgen receptor gene in hormone-refractory prostate cancer. *Cancer Res* **61**, (2001).

158. Carlsson, J. *et al.* HER2 expression in breast cancer primary tumours and corresponding metastases. Original data and literature review. *British Journal of Cancer* vol. 90 Preprint at https://doi.org/10.1038/sj.bjc.6601881 (2004).

159. Heisey, R. M. & Putnam, A. R. Herbicidal Effects of Geldanamycin and Nigericin, Antibiotics from Streptomyces Hygroscopicus. *J Nat Prod* **49**, (1986).

160. Bagatell, R. *et al.* Destabilization of steroid receptors by heat shock protein 90-binding drugs: A ligand-independent approach to hormonal therapy of breast cancer. *Clinical Cancer Research* (2001).

161. Supko, J. G., Hickman, R. L., Grever, M. R. & Malspeis, L. Preclinical pharmacologic evaluation of geldanamycin as an antitumor agent. *Cancer Chemother Pharmacol* **36**, (1995).

162. Samuni, Y. *et al.* Reactive oxygen species mediate hepatotoxicity induced by the Hsp90 inhibitor geldanamycin and its analogs. *Free Radic Biol Med* **48**, (2010).

163. Delmotte, P. & Delmotte-Plaquee, J. A New Antifungal Substance of Fungal Origin. *Nature* **171**, (1953).

164. Roe, S. M. *et al.* Structural basis for inhibition of the Hsp90 molecular chaperone by the antitumor antibiotics radicicol and geldanamycin. *J Med Chem* (1999) doi:10.1021/jm980403y.

165. Schulte, T. W. *et al.* Interaction of radicicol with members of the heat shock protein 90 family of molecular chaperones. *Molecular Endocrinology* **13**, (1999).

166. Moulin, E., Zoete, V., Barluenga, S., Karplus, M. & Winssinger, N. Design, synthesis, and biological evaluation of HSP90 inhibitors based on conformational analysis of radicicol and its analogues. *J Am Chem Soc* **127**, (2005).

167. Ying, W. *et al.* Ganetespib, a unique triazolone-containing Hsp90 inhibitor, exhibits potent antitumor activity and a superior safety profile for cancer therapy. *Mol Cancer Ther* (2012) doi:10.1158/1535-7163.MCT-11-0755.

168. Shimamura, T. *et al.* Ganetespib (STA-9090), a nongeldanamycin HSP90 inhibitor, has potent antitumor activity in in vitro and in vivo models of non-small cell lung cancer. *Clinical Cancer Research* **18**, (2012).

169. Chiosis, G. *et al.* A small molecule designed to bind to the adenine nucleotide pocket of Hsp90 causes Her2 degradation and the growth arrest and differentiation of breast cancer cells. *Chem Biol* **8**, (2001).

170. Caldas-Lopes, E. *et al.* Hsp90 inhibitor PU-H71, a multimodal inhibitor of malignancy, induces complete responses in triple-negative breast cancer models. *Proc Natl Acad Sci U S A* **106**, (2009).

171. Zhang, H. *et al.* BIIB021, a synthetic Hsp90 inhibitor, has broad application against tumors with acquired multidrug resistance. *Int J Cancer* **126**, (2010).

172. Lundgren, K. *et al.* BIIB021, an orally available, fully synthetic small-molecule inhibitor of the heat shock protein Hsp90. *Mol Cancer Ther* **8**, (2009).

173. Hong, D. S. *et al.* Phase I study of BIIB028, a selective heat shock protein 90 inhibitor, in patients with refractory metastatic or locally advanced solid tumors. *Clinical Cancer Research* **19**, (2013).

174. Corral Jaime, J. *et al.* The HALO study: A phase I-II of the oral HSP90 inhibitor Debio0932 in combination with SOC in first- and second-line therapy of advanced NSCLC. *Journal of Clinical Oncology* **32**, (2014).

175. Ohkubo, S. *et al.* TAS-116, a highly selective inhibitor of heat shock protein 90α and β, demonstrates potent antitumor activity and minimal ocular toxicity in preclinical models. *Mol Cancer Ther* **14**, (2015).

176. Yim, K. H. *et al.* Gambogic acid identifies an isoform-specific druggable pocket in the middle domain of Hsp90β. *Proc Natl Acad Sci U S A* **113**, (2016).

177. James, A. *et al.* 610 IN VIVO EFFICACY OF KU-174, A C-TERMINAL INHIBITOR OF HSP90 IN A PC3 XENOGRAFT MODEL. *Journal of Urology* **185**, (2011).

178. Palermo, C. M., Westlake, C. A. & Gasiewicz, T. A. Epigallocatechin gallate inhibits aryl hydrocarbon receptor gene transcription through an indirect mechanism involving binding to a 90 kDa heat shock protein. *Biochemistry* **44**, (2005).

179. Li, Y. *et al.* (-)-Epigallocatechin-3-gallate inhibits Hsp90 function by impairing Hsp90 association with cochaperones in pancreatic cancer cell line mia paca-2. *Mol Pharm* **6**, (2009).

180. Donnelly, A. & Blagg, B. Novobiocin and Additional Inhibitors of the Hsp90 C-Terminal Nucleotide- binding Pocket. *Curr Med Chem* (2008) doi:10.2174/092986708786242895.

181. Li, D. *et al.* Natural Product Kongensin A is a Non-Canonical HSP90 Inhibitor that Blocks RIP3-dependent Necroptosis. *Cell Chem Biol* (2016) doi:10.1016/j.chembiol.2015.08.018.

182. Zhang, F. Z., Ho, D. H. H. & Wong, R. H. F. Triptolide, a HSP90 middle domain inhibitor, induces apoptosis in triple manner. *Oncotarget* **9**, (2018).

183. Zhang, Y. *et al.* Sulphoxythiocarbamates modify cysteine residues in HSP90 causing degradation of client proteins and inhibition of cancer cell proliferation. *Br J Cancer* **110**, (2014).

184. Powers, M. v., Clarke, P. A. & Workman, P. Dual Targeting of HSC70 and HSP72 Inhibits HSP90 Function and Induces Tumor-Specific Apoptosis. *Cancer Cell* **14**, (2008).

185. Benchekroun, M. N., Schneider, E., Safa, A. R., Townsend, A. J. & Sinha, B. K. Mechanisms of resistance to ansamycin antibiotics in human breast cancer cell lines. *Mol Pharmacol* **46**, (1994).

186. Gaspar, N. *et al.* Acquired resistance to 17-Allylamino-17-Demethoxygeldanamycin (17-A AG, Tanespimycin) in glioblastoma cells. *Cancer Res* **69**, (2009).

187. Landmann, H. *et al.* UDP glucuronosyltransferase 1A expression levels determine the response of colorectal cancer cells to the heat shock protein 90 inhibitor ganetespib. *Cell Death Dis* **5**, (2014).

188. Zhou, W. & Slingerland, J. M. Links between oestrogen receptor activation and proteolysis: Relevance to hormone-regulated cancer therapy. *Nature Reviews Cancer* Preprint at https://doi.org/10.1038/nrc3622 (2014).

189. Deng, L., Meng, T., Chen, L., Wei, W. & Wang, P. The role of ubiquitination in tumorigenesis and targeted drug discovery. *Signal Transduction and Targeted Therapy* Preprint at https://doi.org/10.1038/s41392-020-0107-0 (2020).

190. Saji, S. *et al.* MDM2 enhances the function of estrogen receptor in human breast cancer cells. *Biochem Biophys Res Commun* (2001) doi:10.1006/bbrc.2001.4339.

191. Hashizume, R. *et al.* The RING Heterodimer BRCA1-BARD1 Is a Ubiquitin Ligase Inactivated by a Breast Cancer-derived Mutation. *Journal of Biological Chemistry* (2001) doi:10.1074/jbc.C000881200.

192. Eakin, C. M., MacCoss, M. J., Finney, G. L. & Klevit, R. E. Estrogen receptor α is a putative substrate for the BRCA1 ubiquitin ligase. *Proc Natl Acad Sci U S A* (2007) doi:10.1073/pnas.0610887104.

193. Ito, T. *et al.* Identification of a primary target of thalidomide teratogenicity. *Science (1979)* (2010) doi:10.1126/science.1177319.

194. Singhal, S. *et al.* Antitumor activity of thalidomide in refractory multiple myeloma. *New England Journal of Medicine* (1999) doi:10.1056/NEJM199911183412102.

195. Gandhi, A. K. *et al.* Immunomodulatory agents lenalidomide and pomalidomide co-stimulate T cells by inducing degradation of T cell repressors Ikaros and Aiolos

via modulation of the E3 ubiquitin ligase complex CRL4CRBN. *Br J Haematol* (2014) doi:10.1111/bjh.12708.

196. Hansen, J. D. *et al.* Discovery of CRBN E3 Ligase Modulator CC-92480 for the Treatment of Relapsed and Refractory Multiple Myeloma. *J Med Chem* **63**, 6648–6676 (2020).

197. Flanagan, J. *et al.* Abstract P5-04-18: ARV-471, an oral estrogen receptor PROTAC degrader for breast cancer. in (2019). doi:10.1158/1538-7445.sabcs18-p5-04-18.

198. Gonzalez, T. L. *et al.* Targeted degradation of activating estrogen receptor α ligand-binding domain mutations in human breast cancer. *Breast Cancer Res Treat* (2020) doi:10.1007/s10549-020-05564-y.

199. Roberts, B. L. *et al.* Two-Stage Strategy for Development of Proteolysis Targeting Chimeras and its Application for Estrogen Receptor Degraders. *ACS Chem Biol* (2020) doi:10.1021/acschembio.0c00140.

200. Catelli, M. G. *et al.* The common 90-kd protein component of non-transformed '8S' steroid receptors is a heat-shock protein. *EMBO J* **4**, 3131–3135 (1985).

201. Pratt, W. B. & Toft, D. O. Steroid Receptor Interactions with Heat Shock Protein and Immunophilin Chaperones*. *Endocr Rev* **18**, 306–360 (1997).

202. Egorin, M. J. *et al.* Metabolism of 17-(allylamino)-17-demethoxygeldanamycin (NSC 330507) by murine and human hepatic preparations. *Cancer Res* (1998).

203. Chiosis, G. *et al.* 17AAG: Low target binding affinity and potent cell activity - Finding an explanation. *Mol Cancer Ther* (2003).

204. Bhatt, S., Xiao, Z., Meng, Z. & Katzenellenbogen, B. S. Phosphorylation by p38 Mitogen-Activated Protein Kinase Promotes Estrogen Receptor Turnover and Functional Activity via the SCFSkp2 Proteasomal Complex. *Mol Cell Biol* (2012) doi:10.1128/mcb.06561-11.

205. Zhao, Z. *et al.* Reciprocal Regulation of ERα and ERβ Stability and Activity by Diptoindonesin G. *Chem Biol* (2015) doi:10.1016/j.chembiol.2015.10.011.

206. Liu, J. T. *et al.* Total synthesis of diptoindonesin G and its analogues as selective modulators of estrogen receptors. *Org Biomol Chem* (2016) doi:10.1039/c6ob01657j.

207. Gao, J. *et al.* Diptoindonesin G promotes ERK-mediated nuclear translocation of p-STAT1 (Ser727) and cell differentiation in AML cells. *Cell Death Dis* (2017) doi:10.1038/cddis.2017.159.

208. Fan, M. *et al.* Triggering a switch from basal- to luminal-like breast cancer subtype by the small-molecule diptoindonesin G via induction of GABARAPL1. *Cell Death Dis* (2020) doi:10.1038/s41419-020-02878-z.

209. Fengyi Mao, Yifan Kong, Jinghui Liu, Xiongjian Rao, Chaohao Li, Kristine Donahue, Yanquan Zhang, Katelyn Jones, Qiongsi Zhang, Wei Xu, X. L.

Diptoindonesin G antagonizes AR signaling and enhances the efficacy of anti-androgen therapy in prostate cancer. *Prostate* (2022).

210. Briinner, N. *et al.* MCF7/LCC2: A 4-Hydroxytamoxifeii Resistant Human Breast Cancer Variant That Retains Sensitivity to the Steroidal Antiestrogen ICI 182,780. *Cancer Res* (1993).

211. Ran, F. A. *et al.* Genome engineering using the CRISPR-Cas9 system. *Nat Protoc* (2013) doi:10.1038/nprot.2013.143.

212. Roe, S. M. *et al.* Structural basis for inhibition of the Hsp90 molecular chaperone by the antitumor antibiotics radicicol and geldanamycin. *J Med Chem* (1999) doi:10.1021/jm980403y.

213. Soti, C., Vermes, Á., Haystead, T. A. J. & Csermely, P. Comparative analysis of the ATP-binding sites of Hsp90 by nucleotide affinity cleavage: A distinct nucleotide specificity of the C-terminal ATP-binding site. *Eur J Biochem* **270**, (2003).

214. Fontana, J. *et al.* Domain mapping studies reveal that the M domain of hsp90 serves as a molecular scaffold to regulate Akt-dependent phosphorylation of endothelial nitric oxide synthase and NO release. *Circ Res* (2002) doi:10.1161/01.RES.0000016837.26733.BE.

215. Modi, S. *et al.* Combination of trastuzumab and tanespimycin (17-AAG, KOS-953) is safe and active in trastuzumab-refractory HER-2-overexpressing breast cancer: A phase I dose-escalation study. *Journal of Clinical Oncology* **25**, (2007).

216. Burlison, J. A. *et al.* Development of novobiocin analogues that manifest anti-proliferative activity against several cancer cell lines. *Journal of Organic Chemistry* (2008) doi:10.1021/jo702191a.

217. Morishima, Y. *et al.* CHIP deletion reveals functional redundancy of E3 ligases in promoting degradation of both signaling proteins and expanded glutamine proteins. *Hum Mol Genet* (2008) doi:10.1093/hmg/ddn296.

218. Yu, Y. *et al.* Withaferin A targets heat shock protein 90 in pancreatic cancer cells. *Biochem Pharmacol* (2010) doi:10.1016/j.bcp.2009.09.017.

219. Li, N. *et al.* Discovery of Novel Celastrol Derivatives as Hsp90-Cdc37 Interaction Disruptors with Antitumor Activity. *J Med Chem* (2019) doi:10.1021/acs.jmedchem.9b01290.

220. Hadden, M. K., Galam, L., Gestwicki, J. E., Matts, R. L. & Blagg, B. S. J. Derrubone, an inhibitor of the Hsp90 protein folding machinery. *J Nat Prod* (2007) doi:10.1021/np070190s.

221. Bahreini, A. *et al.* Mutation site and context dependent effects of ESR1 mutation in genome-edited breast cancer cell models. *Breast Cancer Research* (2017) doi:10.1186/s13058-017-0851-4.

222. Guillen, K. P. *et al.* A human breast cancer-derived xenograft and organoid platform for drug discovery and precision oncology. *Nat Cancer* **3**, (2022).

223. Corsello, S. M. *et al.* Discovering the anticancer potential of non-oncology drugs by systematic viability profiling. *Nat Cancer* (2020) doi:10.1038/s43018-019-0018-6.

224. Yu, C. *et al.* High-throughput identification of genotype-specific cancer vulnerabilities in mixtures of barcoded tumor cell lines. *Nat Biotechnol* (2016) doi:10.1038/nbt.3460.

225. Gillis, J. L. *et al.* Constitutively-active androgen receptor variants function independently of the HSP90 chaperone but do not confer resistance to HSP90 inhibitors. *Oncotarget* **4**, (2013).

226. DeRose, Y. S. *et al.* Patient-derived models of human breast cancer: Protocols for in vitro and in vivo applications in tumor biology and translational medicine. *Curr Protoc Pharmacol* (2013) doi:10.1002/0471141755.ph1423s60.

227. Sikora, M. J. *et al.* Invasive lobular carcinoma cell lines are characterized by unique estrogen-mediated gene expression patterns and altered tamoxifen response. *Cancer Res* (2014) doi:10.1158/0008-5472.CAN-13-2779.

228. Yu, M. *et al.* Ex vivo culture of circulating breast tumor cells for individualized testing of drug susceptibility. *Science (1979)* (2014) doi:10.1126/science.1253533.

229. Meyer, P. N., Roychowdhury, S., Kini, A. R. & Alkan, S. HSP90 inhibitor 17AAG causes apoptosis in ATRA-resistant acute promyelocytic leukemia cells. *Leuk Res* **32**, (2008).

230. Muchowski, P. J. & Wacker, J. L. Modulation of neurodegeneration by molecular chaperones. *Nature Reviews Neuroscience* vol. 6 Preprint at https://doi.org/10.1038/nrn1587 (2005).

231. Reis, S. D., Pinho, B. R. & Oliveira, J. M. A. Modulation of Molecular Chaperones in Huntington's Disease and Other Polyglutamine Disorders. *Molecular Neurobiology* vol. 54 Preprint at https://doi.org/10.1007/s12035-016-0120-z (2017).

232. Daturpalli, S., Waudby, C. A., Meehan, S. & Jackson, S. E. Hsp90 inhibits α-synuclein aggregation by interacting with soluble oligomers. *J Mol Biol* **425**, (2013).

233. Dickey, C. A. *et al.* The high-affinity HSP90-CHIP complex recognizes and selectively degrades phosphorylated tau client proteins. *Journal of Clinical Investigation* **117**, (2007).

234. Baldo, B. *et al.* A screen for enhancers of clearance identifies huntingtin as a heat shock protein 90 (Hsp90) client protein. *Journal of Biological Chemistry* **287**, (2012).

235. Solit, D. B. *et al.* 17-Allylamino-17-demethoxygeldanamycin induces the degradation of androgen receptor and HER-2/neu and inhibits the growth of prostate cancer xenografts. *Clinical Cancer Research* **8**, (2002).

236. Luo, W. *et al.* Roles of heat-shock protein 90 in maintaining and facilitating the neurodegenerative phenotype in tauopathies. *Proc Natl Acad Sci U S A* **104**, (2007).

237. Tokui, K. *et al.* 17-DMAG ameliorates polyglutamine-mediated motor neuron degeneration through well-preserved proteasome function in an SBMA model mouse. *Hum Mol Genet* **18**, (2009).

238. Dobin, A. *et al.* STAR: Ultrafast universal RNA-seq aligner. *Bioinformatics* **29**, (2013).

239. Anders, S., Pyl, P. T. & Huber, W. HTSeq-A Python framework to work with high-throughput sequencing data. *Bioinformatics* **31**, (2015).

240. Love, M. I., Huber, W. & Anders, S. Moderated estimation of fold change and dispersion for RNA-seq data with DESeq2. *Genome Biol* **15**, (2014).

241. Mootha, V. K. *et al.* Reply to 'Statistical concerns about the GSEA procedure'. *Nat Genet* **36**, 663–663 (2004).

242. Subramanian, A. *et al.* Gene set enrichment analysis: A knowledge-based approach for interpreting genome-wide expression profiles. *Proc Natl Acad Sci U S A* **102**, (2005).